Regulation of Dopamine Synthesis and Accumulation in Rat Brain through G protein-independent Mechanisms

Sally Hamdon

Universitat Autònoma de Barcelona

Regulation of Dopamine Synthesis and Accumulation in Rat Brain through G protein-independent Mechanisms

Author

Sally Hamdon

Directors

Carles Gil Giró, Ph.D.
Jordi Ortiz de Pablo, Ph.D.

A thesis submitted in partial fulfillment of the requirements for the

Ph.D. degree

In

Biochemistry, Molecular Biology and Biomedicine

Ph.D. thesis
2023

Science knows no country, because knowledge belongs to humanity,
and is the torch which illuminates the world.
-Louis Pasteur

Acknowledgements

First and foremost, I would like to express my sincere gratitude to my esteemed supervisors, Jordi Ortiz de Pablo and Carles Gil Giró. You gave me the opportunity to be part of a great team during my Masters and Ph.D., and your guidance, support, insightful comments and unceasing ideas helped me tremendously at all times in my research and writing of this thesis.

Second, I would like to thank the committee members, Enrique Claro Izaguirre, Jesús Giraldo Arjonilla and Lydia Giménez Llort for your advice and discussion that always shed new perspective on my results and guided me to improve them.

I am also very grateful to former team members Mohammad Yusof Omar and Pol Fernandez, as their work was an essential contribution to my research. And to Susana Benítez for her invaluable technical assistance with HPLC-EC, as well as to all faculty members in the Biochemistry and Molecular Biology department, especially the Proteomics laboratory.

To my late father, your memory will forever be a blessing, and I hope I have made you proud.

Words cannot describe my appreciation for my husband´s constant support and understanding, whom I would not have been able to succeed without.

A special and endless thanks goes to my mother, who equipped me with the necessary knowledge and skills to tackle life´s obstacles and inspired me to pursue an academic career.

And to my brother, you may be younger, but you have always cared for me like a big brother and for that, I immensely thank you.

Abstract

The ability of G protein coupled receptors such as D_2 receptors to heterodimerize and generate novel signaling complexes has demonstrated the tremendous potential of these receptors to access diverse signaling cascades, and to modulate the nature of the transduced signal. D_2 receptor signaling has become widely appreciated to be more complex than simply changes in cAMP levels, and biased agonists that are able to exclusively modulate the β-arrestin pathway of D_2 receptors present a promising pharmacological tool. GSK3β, a downstream target of β-arrestin, has been implicated in a plurality of pathologies, including mental disorders and neurodegenerative diseases. However, the tools available to assess D_2-arrestin-GSK3 signaling are limited. In this study, the reliability of several commercial antibodies against D_2 receptors and β-arrestin were tested and found to be partly unspecific. Using HPLC and fresh rat brain striatal minces *ex vivo*, I also showed that the β-arrestin biased D_2 receptor agonist UNC9994 dramatically decreases dopamine accumulation. It was also found that the GSKβ inhibitor CHIR99021 decreases dopamine accumulation and synthesis by indirectly inhibiting Tyrosine hydroxylase (TH), the rate limiting enzyme in brain dopamine biosynthesis. I used two other GSKβ inhibitors, SB216763 and lithium, which were found to be much less effective in modulating dopamine dynamics due to absence of GSK3β action on TH, suggesting an alternative mechanism of action of CHIR99021 other than solely GSK3 inhibition. CHIR99021 also affected dopamine storage in a similar manner to Tetrabenazine, a VMAT2 inhibitor prescribed for Huntington´s disease. Mass spectrometry analysis of an immunoprecipitated TH sample revealed a novel phosphorylation site, Threonine 30. And finally, although largely considered to be a cytosolic enzyme, I observed higher TH activity in the mitochondria as compared to the cytosol. These results show a contribution of β-arrestin biased agonism to dopamine metabolism, and that CHIR99021 can lead to dopamine decrease in brain striatum through vesicle storage-related TH inactivation, opening the possibility of its use in dopamine-related disorders, and shows off-target effects to be considered in future clinical trials.

Resumen

La capacidad de los receptores acoplados a proteínas G, como los D_2 (D_2R), para heterodimerizarse y generar nuevos complejos de señalización ha demostrado su gran potencial para acceder a diversas cascadas de señalización y modular la señal transducida. La señalización del D_2R se reconoce como más compleja que simples cambios en los niveles de cAMP, y los agonistas sesgados que pueden modular exclusivamente la vía de la β-arrestina de los D_2R son una herramienta farmacológica prometedora. GSK3β, una quinasa señalizadora de la β-arrestina, se ha implicado en una pluralidad de patologías, trastornos mentales y enfermedades neurodegenerativas incluidas. Sin embargo, las herramientas disponibles para examinar la señalización D_2R-arrestina-GSK3 son limitadas. En la presente tesis se probó la fiabilidad de varios anticuerpos contra los D_2R y la β-arrestina y se encontró que eran inespecíficos y no aptos para su uso con garantías. Utilizando HPLC y miniprismas de estriado de cerebro de rata fresco *ex vivo*, también observé que el agonista del D_2R sesgado para β-arrestina UNC9994 reduce drásticamente la acumulación de dopamina. También se encontró que el inhibidor de GSKβ CHIR99021 disminuye la acumulación y síntesis de dopamina al inhibir indirectamente la tirosina hidroxilasa (TH). Usé otros dos inhibidores de GSKβ, SB216763 y litio, que resultaron ser mucho menos efectivos en la modulación de la dinámica de la dopamina debido a la ausencia de acción de GSK3β en TH, lo que sugiere un mecanismo de acción alternativo de CHIR99021 que no sea únicamente la inhibición de GSK3. CHIR99021 también afectó el almacenamiento de dopamina de manera similar a la tetrabenazina, un inhibidor de VMAT2 usado en la enfermedad de Huntington. El análisis por espectrometría de masas de una muestra de TH inmunoprecipitada reveló un sitio de fosforilación nuevo, la treonina 30. Y finalmente, aunque en gran medida se considera como una enzima citosólica, observé una mayor actividad de TH en las mitocondrias en comparación con el citosol. Estos resultados muestran una contribución del agonismo sesgado de la β-arrestina en el metabolismo de la dopamina, y que CHIR99021 puede conducir a una disminución de la dopamina en el cuerpo estriado del cerebro a través de una inactivación de la TH relacionada con el almacenamiento vesicular, lo que abre la posibilidad de su uso en trastornos relacionados con la dopamina y muestra efectos "off-target" a considerar en futuros ensayos clínicos.

Resum

La capacitat dels receptors acoblats a proteïnes G, com els receptors D_2 (D_2R), per a heterodimeritzar i generar nous complexos de senyalització ha demostrat el seu enorme potencial per a accedir a diverses cascades de senyalització i modular la naturalesa del senyal transduït. La senyalització del receptor D_2 es reconeix com més complexa que simples canvis en els nivells de cAMP, i els agonistes esbiaixats que poden modular exclusivament la via de la β-arrestina dels receptors D_2 són una eina farmacològica prometedora. GSK3β, una quinasa senyalitzadora de la β-arrestina, s'ha implicat en una pluralitat de patologies, trastorns mentals i malalties neurodegeneratives incloses. Malgrat això, les eines disponibles per examinar la senyalització D_2R-arrestina-GSK3 són limitades. En la presentat tesi es va provar la fiabilitat de diversos anticossos comercials contra els receptors D_2 i la β-arrestina i es va trobar que eren inespecífics i no aptes per al seu ús amb garanties. Utilitzant HPLC i miniprismes d'estriat de cervell de rata fresc *ex vivo*, també demostro que l'agonista del receptor D_2 esbiaixat per a β-arrestina UNC9994 redueix dràsticament l'acumulació de dopamina. També es va trobar que l'inhibidor de GSKβ CHIR99021 disminueix l'acumulació i síntesi de dopamina en inhibir de forma indirecta la tirosina hidroxilasa (TH), l'enzim limitant de la ruta de síntesi de dopamina en el cervell. Vaig usar altres dos inhibidors de GSKβ, SB216763 i liti, que van resultar ser molt menys efectius en la modulació de la dinàmica de la dopamina a causa de l'absència d'acció de GSK3β en TH, la qual cosa suggereix un mecanisme d'acció alternatiu de CHIR99021 que no sigui únicament la inhibició de GSK3. CHIR99021 també afecta l'emmagatzematge de dopamina de manera similar a la tetrabenazina, un inhibidor de VMAT2 utilitzat en la malaltia de Huntington. L'anàlisi d'espectrometria de masses d'una mostra de TH immunoprecipitada va revelar un lloc de fosforilació nou, la treonina 30. I finalment, encara que en gran manera es considera que és un enzim citosòlic, vaig observar una major activitat de TH en els mitocondris en comparació amb el citosol. Aquests resultats mostren una contribucio de l'agonisme esbiaixat de la β-arrestina en el metabolisme de la dopamina, i que CHIR99021 pot conduir a una disminució de la dopamina en el cos estriat del cervell a través de una inactivació de la TH relacionada amb l'emmagatzemament vesicular, la qual cosa obre la possibilitat del seu ús en trastorns relacionats amb la dopamina i mostra efectes "off-target" a considerar en futurs assajos clínics.

Abbreviations

AADC	Aromatic-L-amino-acid decarboxylase
AC	Adenyl cyclase
ADHD	Attention deficit hyperactivity disorder
APD	Antipsychotic drug
BH_4	Tetrahydrobiopterin
cAMP	Cyclic AMP
COMT	Catecol-O-methyl transferase
D_2R	D_2 receptor
DA	Dopamine
DAT	Dopamine transporter
DDA	Data dependent acquisition
DOPAC	3,4-dihydroxyphenylacetic acid
DOPAL	3,4-dihydroxyphenylacetaldehyde
DOPET	3,4-dihydroxyphenylethanol
DSM	Statistical Manual of Mental Disorders
EPS	Extrapyramidal side effects
ERK	Extracellular signal-regulated kinase
GABA	Gamma-aminobutyric acid
GDP	Guanosine diphosphate
GPCR	G protein coupled receptor
GPe	External segment of the Globus pallidus
GPi	Internal segment of the Globus pallidus
GTP	Guanosine triphosphate
HD	Huntington's disease
HPLC-EC	High performance liquid chromatography with electrochemical detection
HPLC-UV	High performance liquid chromatography with ultraviolet detection
ICD	International Classification of Diseases
LB	Lewy body
LC-MS	Liquid chromatography-mass spectrometry
L-DOPA	L-dihydroxyphenylalanine
MAO	Monoamine oxidase

MSN	Medium spiny neuron
PD	Parkinson’s disease
PSMs	Peptide spectrum matches
pS	Phosphoserine
pT	Phosphothreonine
Ser	Serine
SN	Substantia nigra
SNC	Substantia nigra pars compacta
SNR	Substantia nigra pars reticulata
STN	Subthalamic nucleus
TD	Tardive dyskinesia
TBZ	Tetrabenazine
TH	Tyrosine hydroxylase
Thr30	Threonine 30
VMAT2	Vesicular monoamine transporter 2
VTA	Ventral tegmental area

Table of contents

Introduction

1. Dopamine (DA)

Dopamine (DA) was designated simply as a precursor of norepinephrine for a long time, but was later shown to be an independent neurotransmitter in the brain. Since then, it has been recognized as a major catecholamine in the central nervous system (Meiser et al., 2013). 3-hydroxytyramine (dopamine) is derived from the amino acid tyrosine and possesses a key role in the regulation of motor neurons, spatial memory function, motivation, arousal, reward and pleasure, as well as in lactation, sexual behavior and nausea. Alterations in DA neurotransmission are involved, directly or indirectly, in several brain dysfunctions, making the DA system the focus of abundant research. For example, degeneration of DA neurons in the substantia nigra contributes to the pathogenesis of Parkinson's disease, which is treated with DA receptor agonists or with the DA precursor L-DOPA, in order to compensate for the lack of endogenously produced DA (Klein et al., 2019). On the other hand, imbalances in the limbic DA pathways are thought to contribute to psychotic disorders such as schizophrenia (Patel et al., 2014), where DA receptor antagonists are considered clinically important in the management of this disease (Klein et al., 2019). Unfortunately, all these drugs have multiple side effects, linked primarily to their action on the DA system.

Preliminary research on the localization of catecholamine-containing neurons identified 12 neuronal groups, designated as A1–A12 in the rat brain, while subsequent studies found five more cell groups, A13–A17. The A8, A9, and A10 are the main DA cell groups and they coincide with the retrorubral field (RRF), the substantia nigra (SN), and the ventral tegmental area (VTA), respectively (Fu et al., 2011).

2. Anatomy and neurophysiology of dopamine and related pathways

2.1 Anatomy

Since the focus of my experimental design for this thesis is the rat brain striatum, I would like to briefly explore the anatomy and neurophysiology of the striatum in the brain. The striatum is a cluster of neurons (depicted as a nucleus) found in the basal ganglia, a neuronal circuit necessary for voluntary movement control. The striatum is made up of three nuclei: caudate, putamen, and ventral striatum, which contains the nucleus accumbens.

Striatal nerve fibers arrive from three major sources: cortex, midbrain and thalamus. The striatum receives inputs from different elements of the reward circuit. These include striato-nigral midbrain cells, amygdala, orbitofrontal cortex, and anterior cingulate cortex (Báez-Mendoza & Schultz, 2013). It is also worth to mention that the striatum receives the densest DA innervation and contains the highest concentration of DA receptors in the brain (Cabello et al., 2009). A 3D representation of the striatum can be found at https://bbp.epfl.ch/nexus/cell-atlas/.

2.2 Neurophysiology

The striatum possesses two main efferent pathways. The direct pathway composes of axons of medium spiny neuron (MSN) expressing D_1 receptors that mainly project to GABAergic neurons in the substantia nigra pars reticulata (SNR). The indirect pathway is formed from the MSN that express D_2 receptors which mostly target the external segment of the globus pallidus (GPe). GABAergic neurons that are in GPe project to SNR and the internal segment of the globus pallidus (GPi), making the SNR and the GPi the output nuclei of the basal ganglia (Báez-Mendoza & Schultz, 2013).

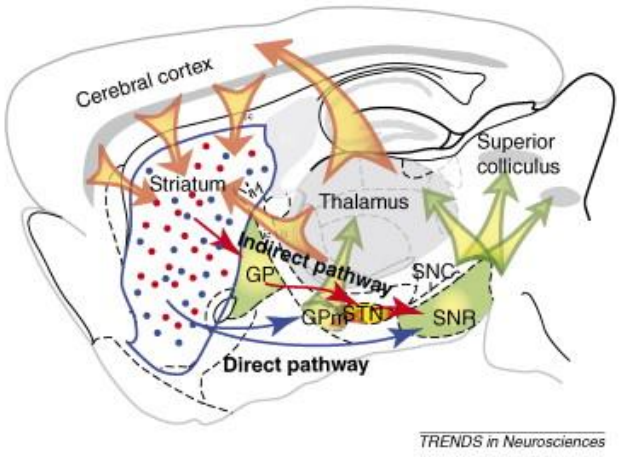

Figure 1. The direct and indirect pathways of the basal ganglia (Surmeier et al., 2007). Abbreviations: SNC, substantia nigra pars compacta; SNR, substantia nigra pars reticulata; STN, subthalamic nucleus. Neurons in the cerebral cortex (orange arrows) and thalamus (green arrows) project excitatory, glutamatergic inputs to medium spiny neurons, contributing to both the direct (blue dots) and the indirect pathway (red dots). The direct Striatonigral pathway medium spiny neurons project directly to neurons of the SNR and internal segment of the GPi, while the indirect striatopallidal pathway medium spiny neurons project axons to the external segment of the GPe or entopeduncular nucleus in rodents. Finally, GPe project to the interface nuclei (SNR and GPi) and to the STN.

The main cell type in the striatum is the MSN, which release γ-amino butyric acid (GABA) at their synaptic terminals. Other cell types include cholinergic and fast-firing GABAergic interneurons. Cholinergic interneuron activity is closely related to reward-predicting stimuli and reward and punishment, suggesting that these neurons may play a role in learning. Functionally, striatal neurons (MSN) exhibit motor and reward responses as well. Abundant evidence led to the hypothesis that striatal activity forms a "limbic-motor" interface (Báez-Mendoza & Schultz, 2013).

3. Dopamine synthesis

DA is synthesized by the hydroxylation of the amino acid L-tyrosine to L-dihydroxyphenylalanine (L-DOPA) by the enzyme tyrosine hydroxylase (TH-EC 1.14.16.2), followed by the decarboxylation of L-DOPA by aromatic-L-amino-acid decarboxylase (AADC-EC 4.1.1.28) (Figure 2). The source of tyrosine is dietary protein (and phenylalanine) and is then transported from the blood into the brain (Meiser et al., 2013). TH is considered to be the rate-limiting enzyme in the pathway because it determines the overall rate of DA and norepinephrine formation (Daubner et al., 2011).

High DA levels within the nerve terminal activate a negative feedback inhibition, inhibiting TH. TH also exhibits substrate inhibition phenomenon, which controls synthesis and DA levels despite large fluctuations in tyrosine due to meals (Best et al., 2009; Reed et al., 2010). We can therefore say that there are several mechanisms that enable dopaminergic neurons to control their rate of neurotransmitter formation (Daubner et al., 2011). Following synthesis, DA is transported into synaptic vesicles for subsequent release. A vesicular monoamine transporter, also known as VMAT2, is used to transport neurotransmitter molecules from the cytoplasm of the cell to the interior of the synaptic vesicles (Figure 2).

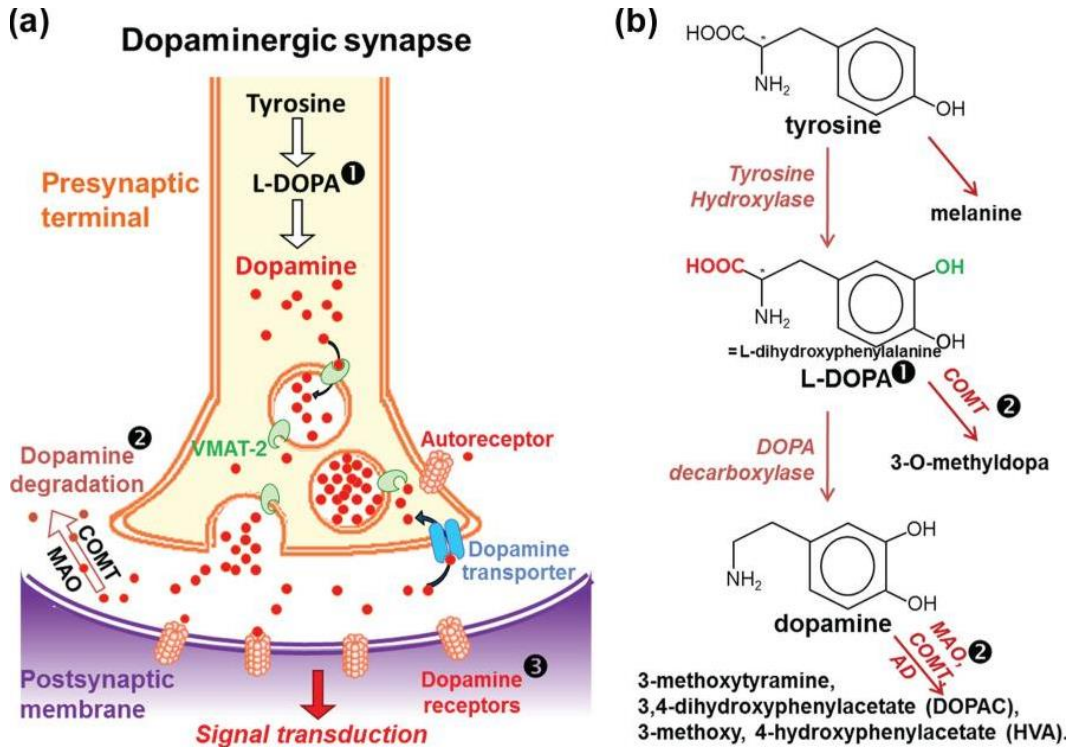

Figure 2. Dopaminergic synapse and DA metabolism. (Jones et al., 2013). **(b)** Tyrosine is transformed into L-DOPA by the enzyme TH in the presynaptic terminal of dopaminergic neurons, which is then transformed to DA by the action of DOPA decarboxylase. **(a)** DA is then uptaken into vesicles by the vesicular monoamine transporter 2 (VMAT2), and, following its release, DA binds to DA receptors on the pre- and postsynaptic membrane, leading to the transduction of the signal. (a,b) DA is finally either recycled by reuptake *via* the DA transporter, or catabolized by the action of 3 enzymes; monoamine oxidase (MAO), cathecol-*O*-methyl transferase (COMT) and aldehyde dehydrogenase (AD).

4. Tyrosine hydroxylase (TH)

Tyrosine hydroxylase (TH-tyrosine 3-monooxygenase) is the rate limiting enzyme in the biosynthesis of brain DA (as well as adrenaline and noradrenaline) by catalyzing the conversion of the amino acid L-tyrosine to the precursor of DA, L-DOPA (Figure 3). These catechol monoamines aid in several brain functions, such as motor control, emotion, reward, biorhythms and learning. Mutations in the TH gene are associated with different diseases such as congenital TH deficiency (THD), L-Dopa responsive dystonia (DRD), infantile parkinsonism and severe encephalopathy. In addition, striatal TH deficiency is a hallmark of Parkinson's disease (Bueno-Carrasco et al., 2022). Therefore, TH, as the slowest enzyme in the pathway, is of great interest in many fields of biomedical research.

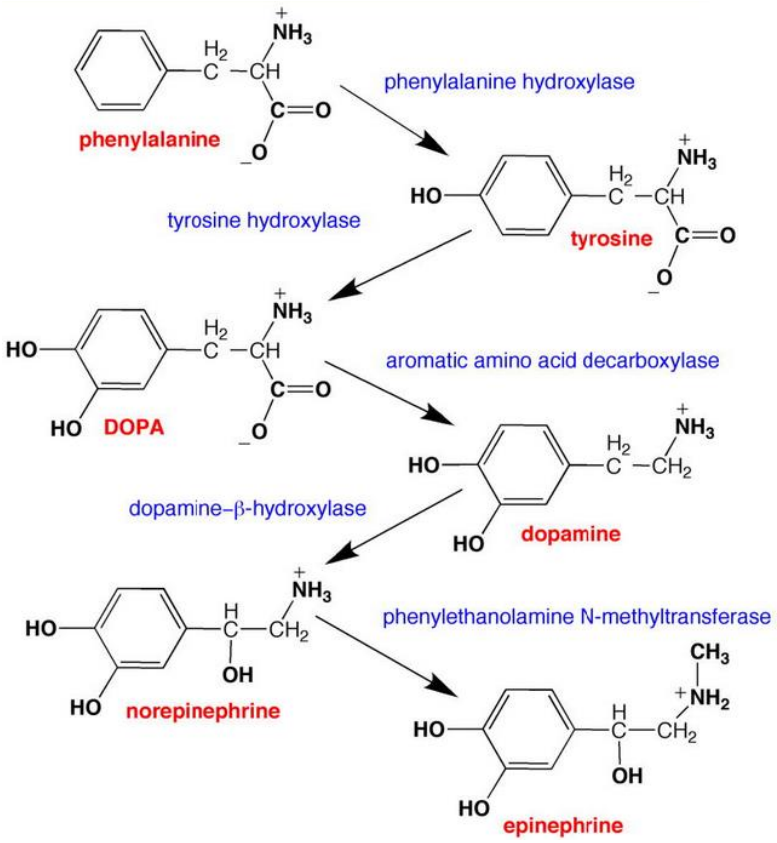

Figure 3. The biosynthetic pathway of catecholamine neurotransmitters (Daubner et al., 2011). Phenylalanine is converted to tyrosine by phenylalanine hydroxylase, tyrosine is hydroxylated to L-DOPA by TH. DA is made from L-DOPA by aromatic amino acid decarboxylase. Finally, DA could also be hydroxylated to norepinephrine by dopamine-β-hydroxylase, which could also be methylated to epinephrine by phenylethanolamine N-methyltransferase. TH is the rate-limiting enzyme of this pathway.

TH is a member of the aromatic amino acid hydroxylases family which also includes phenylalanine hydroxylase and tryptophan hydroxylase. As their name suggests, these enzymes perform hydroxylation of the aromatic ring of an amino acid using molecular oxygen (O_2), iron (Fe^{2+}) and tetrahydrobiopterin (BH_4) as a cofactor. The iron atom is kept in place in the active site cleft by two histidine residues and a glutamate residue, and the ferrous state is imperative to carry out catalysis (Daubner et al., 2011).

4.1 TH protein structure

In terms of its three-dimensional structure, TH has a multi-domain structure, consisting of an amino-terminal regulatory domain of varying size from 100–150 amino acid residues, followed by a catalytic domain of about 330 residues, and a coiled-coil domain at the carboxyl terminus of about 20 amino acids (Daubner et al., 2011). TH forms

tetramers with a molecular mass of about 240 kDa, and the subunits interact through two distinct oligomerization interfaces, forming a dimer of dimers (Szigetvari et al., 2019).

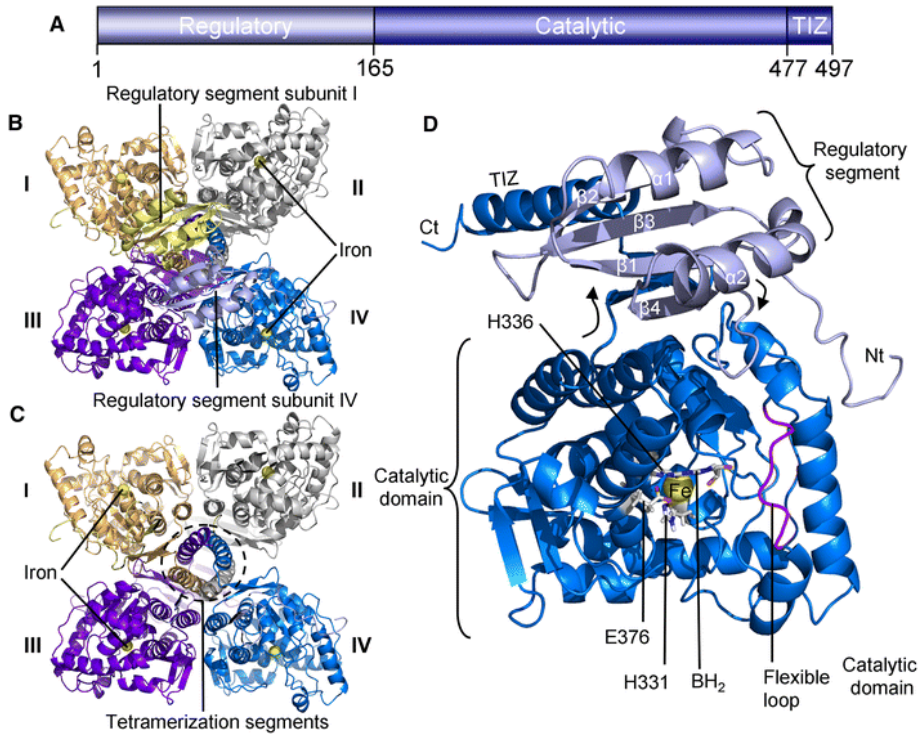

Figure 4. Molecular models of the structure of TH (Tekin et al., 2014). **A)** Linear structure and size of the monomeric human tyrosine hydroxylase. **B)** Molecular model of tetrameric rat TH (depicted I–IV) showing two of the four regulatory segments, with the other two regulatory domains hidden in the back. **C)** Same view as b with representation of the tetramerization domains in a colored coded manner to match the catalytic domains. **D)** The active site of rat monomeric TH, which contains iron and BH_4. His331, His336, and Glu376, (which all bind iron), as well as iron and BH_4, are represented as sticks. Ct: carboxyterminus, Nt: amino-terminus, TIZ: tetramerization segment.

4.2 TH activity

Although the regulatory domain of TH mostly lies above and to the side of the opening to the active site, a short portion lies across it and possibly obstructs access to the active site. Phosphorylation moves the regulatory domain out of the opening of the active site, and dephosphorylation by a phosphatase returns it to its closed position (Bueno-Carrasco et al., 2022; Daubner et al., 2011) (Figure 5A).

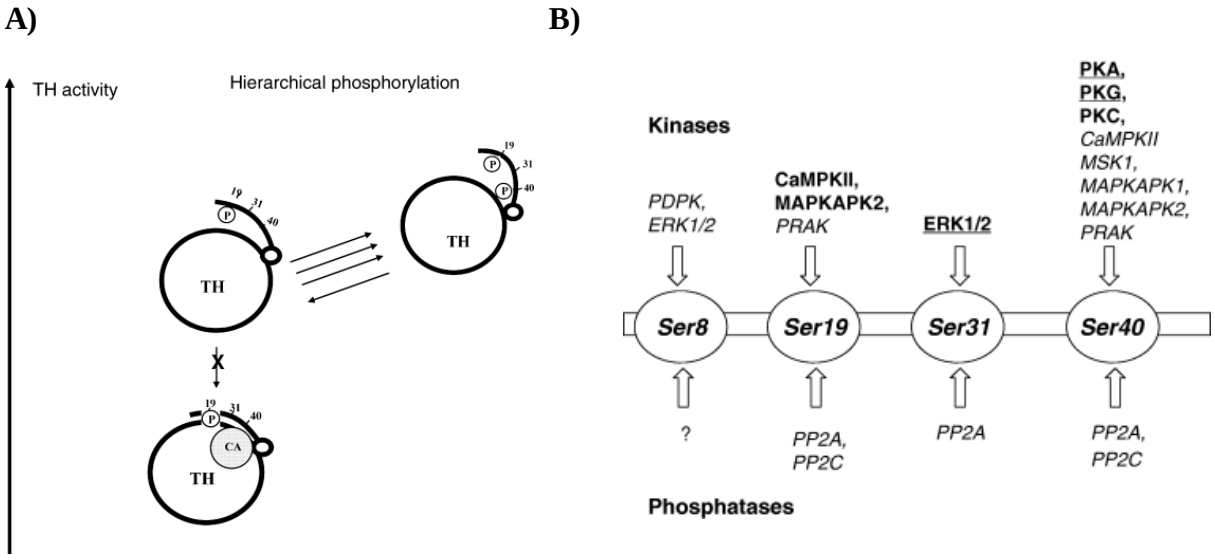

Figure 5. TH activity (Dunkley et al., 2004). **A)** A theoretical representation of the activation by hierarchical phosphorylation of serine residues in the regulatory domain of TH. It is not known if hierarchical phosphorylation of Ser40 can also occur with catecholamine (CA)-bound TH. **B)** A graphical summary of the protein kinases that react with the serine residues of the regulatory domain of TH.

Enzymatic activity has shown that it can be accelerated by increases in TH phosphorylation. Distinct protein kinases can induce TH phosphorylation at Serine 19 (Ser19), Serine 31 (Ser31) and Serine 40 (Ser40). TH is also phosphorylated at Serine 8 (Ser8) and Threonine 8 (Thr8) in human TH, however this phosphorylation site has yet to be investigated or linked to modulating TH activity. In regards to the other sites, Ser19 phosphorylation has been suggested to be catalyzed by Ca^{2+}/calmodulin-dependent protein kinase II. Extracellular signal-regulated kinases (ERK1 and ERK2) stimulate TH phosphorylation at Ser31, while cyclic adenosine monophosphate (cAMP)-dependent protein kinase (PK) phosphorylates TH at Ser40. Some other kinases are also mentioned in Figure 5B. Dephosphorylation, on the other hand, is mediated by protein phosphatase 2A (PP2A) and protein phosphatase PP2C (Dunkley et al., 2004).

5. Dopamine storage

The Vesicular Monoamine Transporter (VMAT) was identified in rats as the key mediator of monoamine uptake into intracellular vesicles, followed by the discovery of both isoforms (VMAT1 and VMAT2) later on. Neuroendocrine cells mainly express VMAT1, whereas VMAT2 (encoded by the SLC 18A2 gene) is expressed in neurons of the central, peripheral, and enteric nervous systems.

The VMAT2 is primarily found in small synaptic vesicles in the central nervous system. VMAT2 synaptic vesicle localization within presynaptic terminals plays a vital role in monoamine uptake. In the case of DA, following its synthesis, it is incorporated and stored into synaptic vesicles by the action of VMAT2.

VMAT2 acts as a stoichiometric antiporter, transporting two H^+ ions out of a synaptic vesicle and one monoamine molecule into a vesicle (Figure 6). VMAT2 transport activity is dependent on high intravesicular H^+ concentration, which in turn is dependent on ATPase activity (German et al., 2015).

The following compounds directly or indirectly interact with VMAT2 (German et al., 2015):

1. Tetrabenazine (TBZ): a VMAT2 inhibitor that stops amine transport into synaptic vesicles. It was originally of therapeutic interest due to its antipsychotic properties and was prescribed for the treatment of hyperkinetic disorders including chorea associated with Huntington's disease, and Tourette's syndrome because of its dopamine-depleting properties (Eiden & Weihe, 2011). This results in secondary symptoms including gastrointestinal distress, depression, and fatigue.
2. Methamphetamine and methylphenidate: treatment with methamphetamine decreases striatal VMAT2 activity acutely, presumed to be a result of redistribution of VMAT2 protein within nerve terminals (Hanson et al., 2009). Amphetamine-related drugs may function as weak bases, therefore disrupting the synaptic vesicle pH and contributing to VMAT2 dysfunction. On the other hand, methylphenidate, a DA reuptake inhibitor, increases VMAT2 immunoreactivity and function through D_1 and D_2 receptor–mediated mechanisms (German et al., 2015).

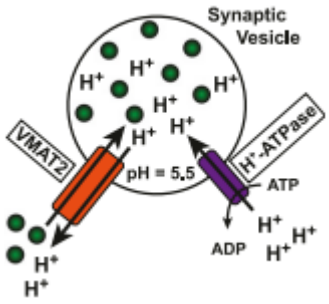

Figure 6. VMAT2 transports DA into synaptic vesicles from the cytoplasmic space, which is facilitated by H+ -ATPase (German et al., 2015).

6. Dopamine release

Following its release, DA can bind to and activate both presynpatic and postsynaptic DA receptors. As DA disperses away from the synapse, it is taken back up into dopaminergic terminals via the perisynaptically localized DAT and subsequently repackaged into synaptic vesicles or degraded. Extracellular reuptake, first specified for norepinephrine, was initially characterized as the primary mechanism for catecholamine synaptic clearance and signal termination. Even though previous studies have specified that DAT influences the duration and extent of presynaptic and postsynaptic DA receptor signaling, recent modeling data suggest that dispersion of DA away from the terminal and dilution within the extracellular space, rather than uptake through the DAT, may be the presiding factors governing the extent and duration of DA signaling. On the other hand, the perisynaptically localized DAT may regulate the kinetics and volume of extrasynaptic DA dispersion, rather than the DA content within individual synapses (German et al., 2015).

7. Dopamine transporter

As previously discussed, DA can be recycled and reused following its release mainly via perisynaptically localized DAT to transport DA against its concentration gradient from the synaptic cleft back to the dopaminergic terminals. This process is dependent on extracellular Na^+ and Cl^- concentrations with the binding of two Na^+ ions and one Cl^- ion for every DA molecule, causing a conformational change from outward-facing to inward-facing and therefore generating a complex transport-associated current. DAT shifts back to its original conformation with the release of DA and ions into the cytoplasm (Figure 7). Psychostimulants such as cocaine, methylphenidate and amphetamine exhibit their actions on DAT by prolonging the duration of DA action on its receptors. On the other hand, impairment of DAT is implicated with ADHD and depression, and has even been correlated with drug abuse and their reinforcing properties (German et al., 2015).

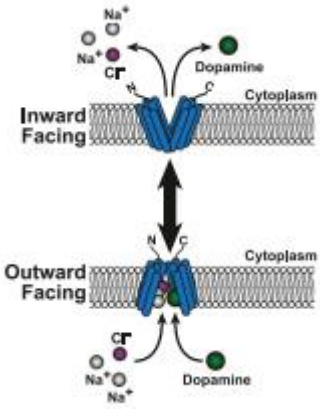

Figure 7. The change in shape of DAT from outward-facing to inward-facing to facilitate the movement of DA from the extracellular to cytoplasmic space (German et al., 2015).

8. Dopamine metabolism

Synaptic vesicles are emptied into the synaptic cleft, as previously mentioned, when dopaminergic neurons are excited. This allows DA to interact with the postsynaptic DA receptors or regulatory presynaptic DA autoreceptors. I also previously mentioned that extracellular DA has to be removed from the synaptic cleft in order to cease signaling. This is done via recycling after reuptake by dopaminergic neurons or through degradation by COMT.

DAT is responsible for neuronal reuptake which is then proceeded by sequestration into the synaptic storage vesicles by VMAT2 or metabolism by MAO. DA which has leaked from synaptic vesicles into the cytosol undergoes oxidative deamination by MAO which produces hydrogen peroxide and the reactive aldehyde 3,4-dihydroxyphenylacetaldehyde (DOPAL). DOPAL is then either reduced to the corresponding alcohol 3,4-dihydroxyphenylethanol (DOPET) by alcohol dehydrogenase (ADH) or further oxidized to the carboxylic acid 3,4-dihydroxyphenylacetic acid (DOPAC) by aldehyde dehydrogenase (ALDH), although, under normal conditions, the latter is more likely (Delcambre et al., 2016). COMT, on the other hand, is located in glial cells and neuronal membranes (Chen et al., 2011) and degrades DA by methylating its 3'-hydroxyl group of the catechol ring to yield 3-methoxytyramine, which is further metabolized by MAO to form 3-methoxy-4-hydroxy-phenylacetaldehyde (Delcambre et al., 2016). It is worth to mention that MAO exists as two isoforms, MAO-A and MAO-B, with different pH optima and sensitivity to heat inactivation, and with greater MAO-B activity in basal ganglia (Youdim & Bakhle, 2006). Both DOPAC and 3-methoxy-4-hydroxy-

phenylacetaldehyde can be subsequently metabolized to form homovanillic acid, by COMT and ALDH, respectively (Delcambre et al., 2016). Details of this overall DA metabolism pathway in the brain is illustrated in Figure 8.

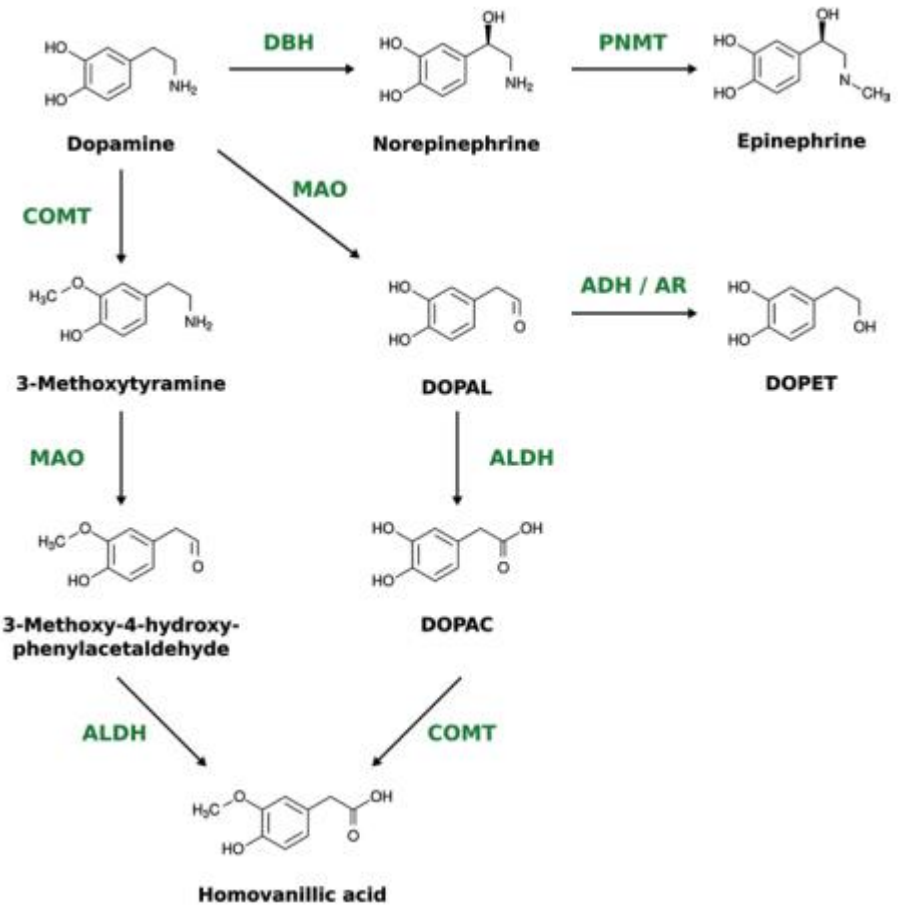

Figure 8. Brain DA metabolism pathway (Delcambre et al., 2016). Abbreviations: MAO; monoamine oxidase, COMT; catechol-O-methyl transferase, ALDH; aldehyde dehydrogenase, AR; aldose reductase, DOPAL; 3,4-dihydroxy-phenylacetaldehyde, DOPAC; 3,4-dihydroxy-phenylacetic acid, DOPET; 3,4-dihydroxyphenylethanol.

9. Dopamine receptors

In 1972 DA receptors were discovered and it was also indicated that DA stimulates adenylyl cyclase (AC) activity. Further pharmacological studies showed that DA has several binding sites, giving rise to 2 types of DA receptors: one which is positively coupled to AC and the other is negatively coupled to AC. The subsequent classification of DA receptors was also into 2 families, D_1-like receptors and D_2-like receptors, based

on pharmacologic properties and the ability to regulate cAMP generation (Mishra et al., 2018), as shown in Figure 9.

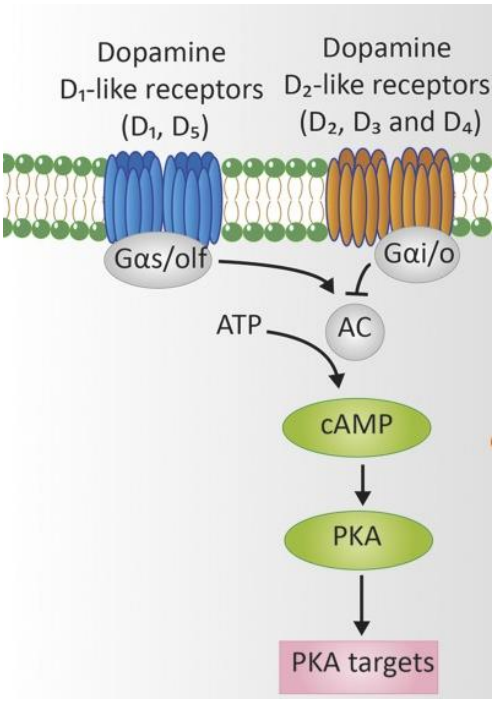

Figure 9. Classification of DA receptors into D_1-like receptors and D_2-like receptors based on their signaling action on AC (Osinga et al., 2017).

DA receptors are GPCRs (Osinga et al., 2017) and their relative density in the human central nervous system is $D_1 > D_2 > D_3 > D_5 > D_4$. The region of expression in the brain, mechanism of action, behavioural functions, and the selective agonists and antagonists of the subtypes of DA receptors are described in Table 1, adapted from (Mishra et al., 2018). DA receptor agonists and antagonists are used to alleviate symptoms associated with diseases and conditions such as hyperprolactinemia, PD, schizophrenia, Tourette syndrome, attention deficit hyperactivity disorder, and Huntington´s disease that are contributed by a dysfunction of DA neurotransmission (Mishra et al., 2018).

Receptors	*Location*	*Type*	*Mechanism*	*Function*	*Selective agonist*	*Selective antagonist*
D_1	Striatum, nucleus accumbens. olfactory bulb, amygdala hippocampus, substantia nigra hypothalamus, frontal cortex	Gs-coupled	Increased intracellular level of cAMP by activating adenyl cyclase	Locomotion, learning and memory, attention, impulse control, sleep, regulation of renal function	SKF-38393 SKF-81297 Fenoldopam (SKF-82526)	SCH-23390 SCH-39166 SKF-83566 Flupentixol
D_5	Cortex, substantia nigra, hypothalamus	Gs-coupled	Adenyl cyclase↑	Cognition, attention, decision making, motor learning, renin secretion	—	—
D_2	Striatum, VTA olfactory bulb, cerebral cortex	Gi-coupled	Adenyl cyclase↓	Locomotion, learning and memory, attention, sleep, reproductive behaviour	Bromocriptine Pergolide Cabergoline Ropinirole Aripiprazole (partial agonist)	Haloperidol Raclopride Sulpiride Spiperone Risperidone
D_3	Striatum, islands of Calleja, cortex	Gi-coupled	Adenyl cyclase↓	Locomotion, cognition, attention, impulse control, sleep, regulation of food intake	7-OH-DPAT Pramipexole Rotigotine PD-128907 Apomorphine, Bromocriptine (partial agonists)	Nafadotride Sulpiride GR-218231 SB277011A NGB-2904 PG-01037 ABT-127
D_4	Frontal cortex, amygdala, hypothalamus, nucleus accumbens	Gi-coupled	Adenyl cyclase↓	Cognition, impulse control, attention, sleep, reproductive behavior	A-412997 ABT-670 PD-168077	A-381393 FAUC213 L-745870 L-750667 Loxapine

Table 1. **DA receptor classification, localization, and their functions.** Adapted from (Mishra et al., 2018) and https://www.guidetopharmacology.org/GRAC/FamilyDisplayForward?familyId=20

Another difference between D_1 and D_2-like family receptors is the availability of introns in their coding sequence, where the D_1-like family receptors do not contain introns, while the D_2-like family receptors contain several introns in their sequence. This structure results in the generation of two major D_2-like family receptor variants, D_2S (D_2-short) and D_2L (D_2-long) with an extra 29 amino acids in the latter (Usiello et al., 2000). While the D_2S variant is mostly expressed presynaptically and is involved in autoreceptor function, the D_2L is expressed at postsynaptic dendrites. Since the scope of this thesis is focused on D_2 receptors, as they play an important role in the treatment of DA-related neurological disorders, I will now focus and elaborate on the regulation and functional action at the presynaptic terminals of the D_2-like family, specifically the D_2-like autoreceptor (D_2R). There are several mechanisms involved in the regulation of D_2R at the presynaptic terminals, the major one being regulating DA release from axon terminals. This regulation involves the inhibition of voltage-gated calcium channel, which allows Ca^{2+} to enter and therefore trigger DA release and hyperpolarization. This occurs via voltage-dependent K^+ channels (Kv1.2) or the activation of GIRK (G protein-coupled inwardly-rectifying potassium channel), which is mediated through G-protein $\beta\gamma$ inhibition. Since the amount of DA-mediated signaling at post-synaptic receptors is dependent on the amount of DA accumulated in the synaptic cleft, extracellular DA clearance is therefore primarily determined by DAT reuptake. This brings us to the second mechanism of action of D_2R in regulating DA neurotransmission: altering DAT-mediated DA reuptake. The third mechanism, in turn, is decreasing DA synthesis. This involves down-regulation on TH activity via inhibition of AC, which naturally leads to the reduction of cAMP-protein kinase A, and a subsequent feedback inhibition of DA at the presynaptic terminals (Ford, 2014). These overall mechanisms by which D_2R regulates DA transmission at the presynaptic terminals are illustrated in Figure 10. In addition to these three regulatory mechanisms, one study also shows that D_2R activation may also regulate and increase the reuptake of DA into synaptic vesicles via VMAT2, leading to changes in extracellular DA *in vivo* (Truong et al., 2004). And lastly, the absence of D_2R has been shown to elevate both DA synthesis and release (Ford, 2014). All this evidence supports the important role of D_2R in regulating dopaminergic neurotransmission and in regulating the activity of DA neurons, making them an important pharmacological target for the treatment of a variety of psychiatric diseases.

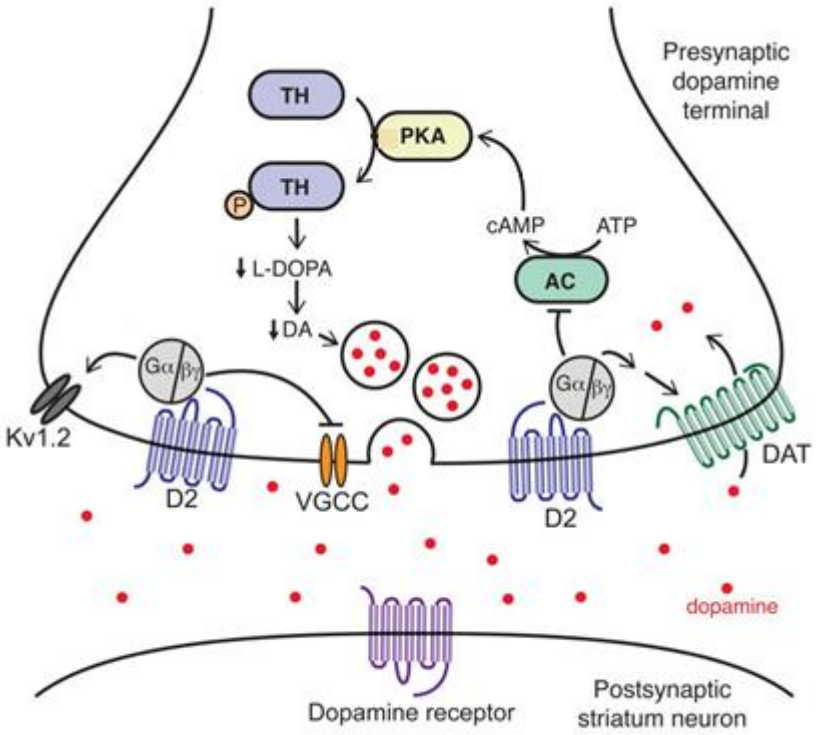

Figure 10. D_2R signaling mechanisms and regulation of DA transmission at presynaptic dopaminergic terminals. Adapted from (Ford, 2014).

10. G protein coupled receptors

G protein coupled receptors (GPCRs), also knows as 7-TM receptors, or the heptahelical receptors, are the largest family of membrane proteins which transduce extracellular stimuli into intracellular signals (Hu et al., 2017). They are characterized by the presence of seven membrane-spanning α-helical segments separated by alternating intracellular and extracellular loop regions. Several stimuli such as light, neurotransmitters, odorants, biogenic amines, lipids, proteins, amino acids, hormones, nucleotides, chemokines and many others, can trigger different responses from GPCRs through a variety of intracellular signaling pathways (Palczewski et al., 2000; Rosenbaum et al., 2009). Over 800 different GPCRs interact with 16 Gα proteins which are comprised of 4 families, $G\alpha_i$, $G\alpha_s$, $G\alpha_q$, and $G\alpha_{12/13}$ (Voss & Müller, 2022). $G\alpha_s$ and $G\alpha_i$ depict stimulatory or inhibitory effects on the enzyme adenylyl cyclase, respectively. $G\alpha_q$ activates phosphoinositide-dependent phospholipase C (PLC), while $G\alpha_{12/13}$ subunits signal to small G protein-dependent pathways (Chakravorty & Assmann, 2018).

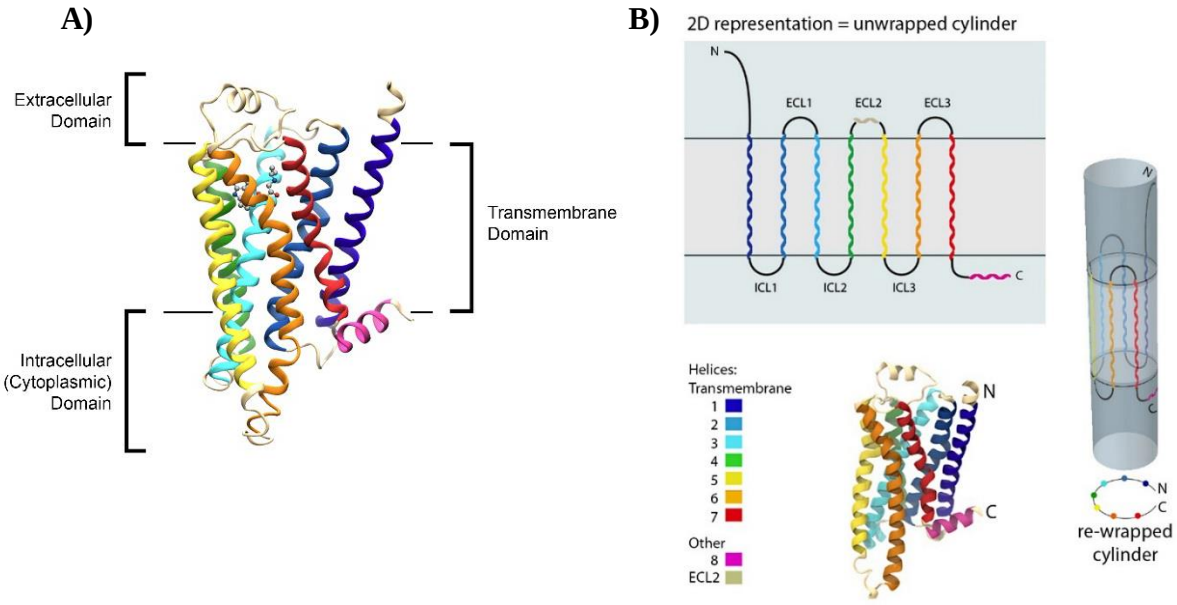

Figure 11. GPCRs structure (Sojka et al., 2017). **A)** GPCRs are composed of extracellular, transmembrane, and intracellular domains. Lines represent membrane hydrophobic core boundaries. **B)** Two-dimensional representation and three-dimensional cylindrical shape of GPCRs.

There are 6 different GPCR classes, labeled A to F:

Class A is known as the "rhodopsin-like family" and is the largest group because it accounts for around 80% of GPCRs. It includes hormones, neurotransmitters, and light receptors. Structurally, class A GPCRs have seven TM helices, and the C terminal tail is characterized by the eighth helix and a palmitoylated cysteine.

Class B, or the "secretin receptor family", consists of around 70 receptors and have seven TM helices. They have a long N-terminal domain of around 120 residues which are stabilized by disulfide bonds.

Class C are also characterized by seven TM helices and a large extracellular N-terminal domain with approximately 600 residues. They include the metabotropic glutamate family, GABA receptors, calcium-sensing receptors, and taste receptors. This domain is shaped like a clam and is connected to the TM helix 1 by a cysteine-rich loop.

Class D contains the fungal mating pheromone receptors, **class E** contains the cAMP receptors, and **class F** contains the frizzled/smoothened receptors. The amino acid sequences of classes D-F also contain seven TM helices that have hydrophobic domains.

The "GRAFS" system has also been proposed as another classification system of GPCRs based on the phylogenetic tree of approximately 800 human GPCR sequences. This system is composed of five main families; Glutamate (G), Rhodopsin (R), Adhesion (A), Frizzled/Taste2 (F), and Secretin (S). The main difference between the GRAFS system and the A-F system is the further sub-division of class B into the Secretin family and the Adhesion family in the GRAFS System. This is due to a preliminary finding that the evolutionary history of these two families is distinct from each other (Hu et al., 2017).

11. Heterodimerization

Previously, GPCRs were believed to exist in monomeric or homodimeric forms. More recently, however, an increasing amount of research has verified the formation of heterodimers or higher-order heterooligomers among GPCRs *in vivo* as well as *in vitro* with many GPCR heterodimers being regarded as 'novel receptors'. This is due to the fact that heterodimerization results in ligand binding affinities, signal transduction cascades, receptor internalization and/or desensitization processes that are distinct from those of the corresponding monomers or homodimers. All of this suggests that GPCR heterodimers present as promising targets for new drug development (Marshall & Foord, 2010; Satake & Sakai, 2008).

12. G protein versus β-arrestin signaling

As previously mentioned, GPCR signaling provides multiple means of communication between cells. It has been demonstrated that different ligands induce either G protein dependent or G protein independent signaling of GPCR via β-arrestins, possibly giving rise to functional selectivity (Violin & Lefkowitz, 2007).

12.1 G proteins

G proteins are derived from 35 genes, 16 encoding Gα subunits, 5 Gβ and 14 Gγ (Milligan & Kostenis, 2006). GPCR signaling induces coupling of the G protein to a liganded receptor. When a GPCR is inactive, Gα is bound to Gβγ dimer and GDP. Activation occurs through the binding of an agonist and therefore starting G protein mediated signaling. Next, the exchange of guanosine diphosphate (GDP) for guanosine triphosphate (GTP) associated with the Gα subunit occurs. Therefore, conformational changes takes place in the activated GPCR as a result of the exchange of GTP for GDP

on the Gα subunit, leading to a dissociation of Gβγ dimer from Gα and thus activates multiple molecules of G proteins (Figure 12). These activated Gα and Gβγ proteins in turn bind to various effectors and therefore switch it either on or off in different systems, and subsequently pass the signal to different kinds of second messengers. This is when intrinsic GTPase activity of Gα hydrolyzes the bound GTP back to GDP and hence inactivates the G proteins cascade. GTPase activity of the Gα subunits may also be regulated by effectors, as well as RGS proteins, which are regulators of G proteins signaling. It is also possible for effector enzymes such as adenylyl cyclases to regulate the activation of G proteins by receptors (Tuteja, 2009).

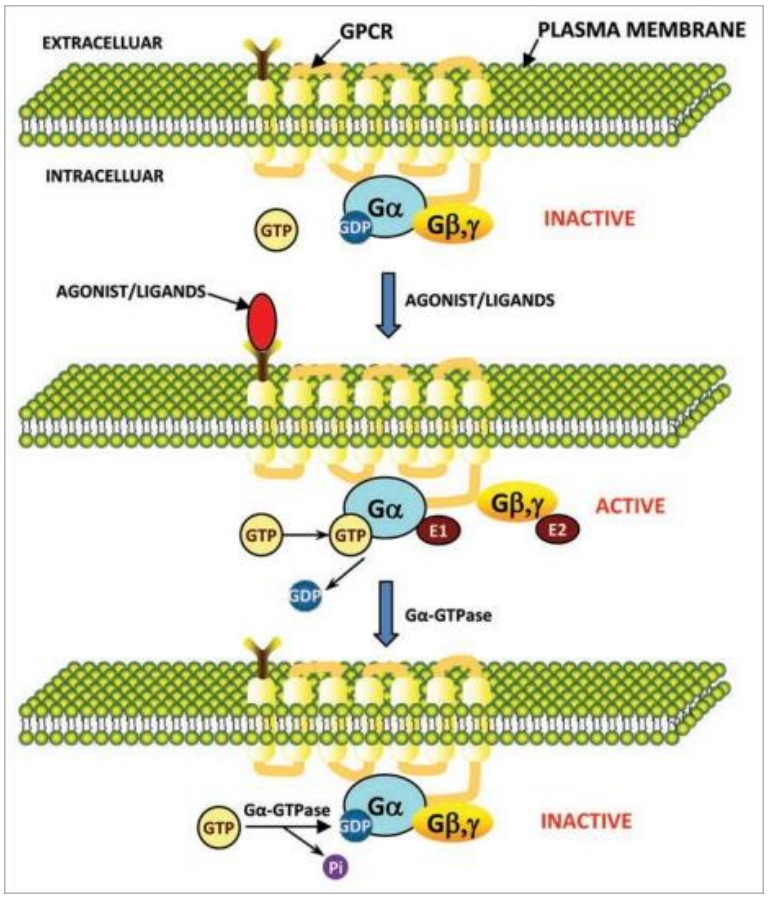

Figure 12. The regulatory cycle of G proteins (Tuteja, 2009).

These effector molecules include calcium, potassium channels, adenylyl cyclase, phospholipases and protein kinases. It was hypothesized that the βγ dimer acts as a negative regulator and can block activation of adenylyl cyclase. But this hypothesis was later changed when it was found that the βγ subunit could activate the muscarinic K^+ channel and positively regulate effectors. Eventually, the βγ subunit was shown to be

a positive regulator of other effectors such as adenylyl cyclase, phospholipase C-β (PLC-β), phospholipase A_2 (PLA_2), phosphoinositide 3-kinase (PI3-kinase), and β-adrenergic receptor kinase. It was also found that Gβγ can activate Gα subunit. It is therefore clear that several effectors are regulated by both α and βγ subunits (Tuteja, 2009).

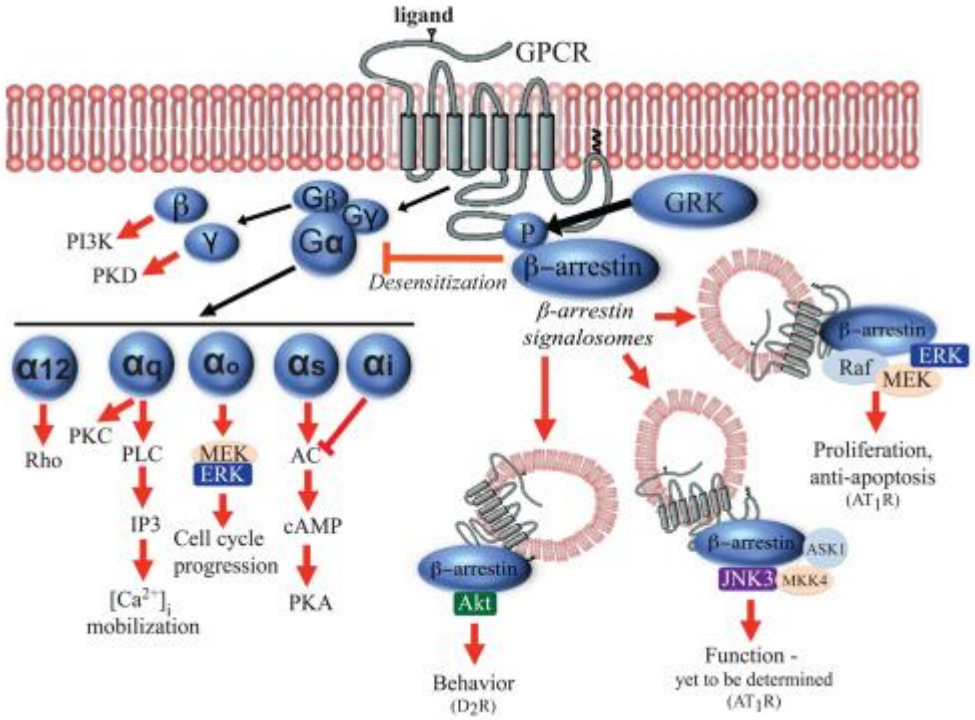

Figure 13. Examples of GPCR downstream signaling through G protein and β-arrestin signaling pathways. Once an agonist binds to a GPCR, both G proteins (Gα12, Gαq/11, Gαi/o, Gαs, Gβ and Gγ subunits) and β-arrestin are activated which sets off a variety of distinct downstream signaling pathways. For example, stimulation of Gβ subunit can activate PI3Kγ, whereas Gγ subunit can activate PKD and Gα12 can activate Rho kinase signaling pathways. Gαq activates PLC/IP3 and therefore can induce the mobilization of calcium from intracellular, whereas Gαo induces cell cycle progression by activating the MEK/ERK pathway, and Gαs proteins activate PKA by promoting AC. β-arrestin recruitment occurs as a result of GPCR phosphorylation by GRK, which subsequently desensitizes G protein signaling, mediates receptor trafficking to endosomes, and activates β-arrestin-dependent signaling (Bologna et al., 2017).

12.2 β-arrestin

β-arrestins 1 and 2 are negative regulators of GPCR signaling through G proteins. β-arrestins translocate to the cell membrane and bind to the agonist-occupied receptors when a GPCR is phosphorylated by GPCR kinases (GRKs). This causes desensitization through the uncoupling of these receptors from G proteins and therefore promoting their internalization. However, accumulating reports have indicated that β-arrestins function as

scaffold proteins that interact with several cytoplasmic proteins and link GPCRs to intracellular signaling pathways, including MAPK cascades. Evidence also shows that β-arrestins translocate from the cytoplasm to the nucleus as a response to activation of some GPCRs and associate with transcription cofactors such as p300 and cAMP-response element-binding protein (CREB) at the promoters of target genes to promote transcription. They also play important roles in cell growth, apoptosis and modulation of immune functions through indirect regulation of transcription. They do this by interacting with regulators of transcription factors, such as IκBα and MDM2, in the cytoplasm (Ma & Pei, 2007).

The coupling framework of GPCRs is highly shared across their family in which agonist activation leads to the coupling of heterotrimeric G proteins. Even though typical and natural agonists induce both G protein and β-arrestin coupling to these receptors, there is a new concept referred to as biased agonism, whereby ligands are designed to promote preferential coupling to only one of these transducers leading to biased signaling (Rajagopal et al., 2010; Smith et al., 2018). This phenomenon provides therapeutic potential for minimizing the side effects associated with conventional GPCR-targeting drugs (Violin & Lefkowitz, 2007). However, the question remains to what extent these ligands are actually biased. There are some examples in the literature of 7-TM receptors, which display absence of functional G protein coupling but presence of agonist-induced β-arrestin recruitment (Bachelerie et al., 2014; Nibbs & Graham, 2013; Van Lith et al., 2009). Nonetheless, there is little to no information on their comprehensive G protein-coupling profile, GRK dependence, β-arrestin conformational signatures, and downstream signaling.

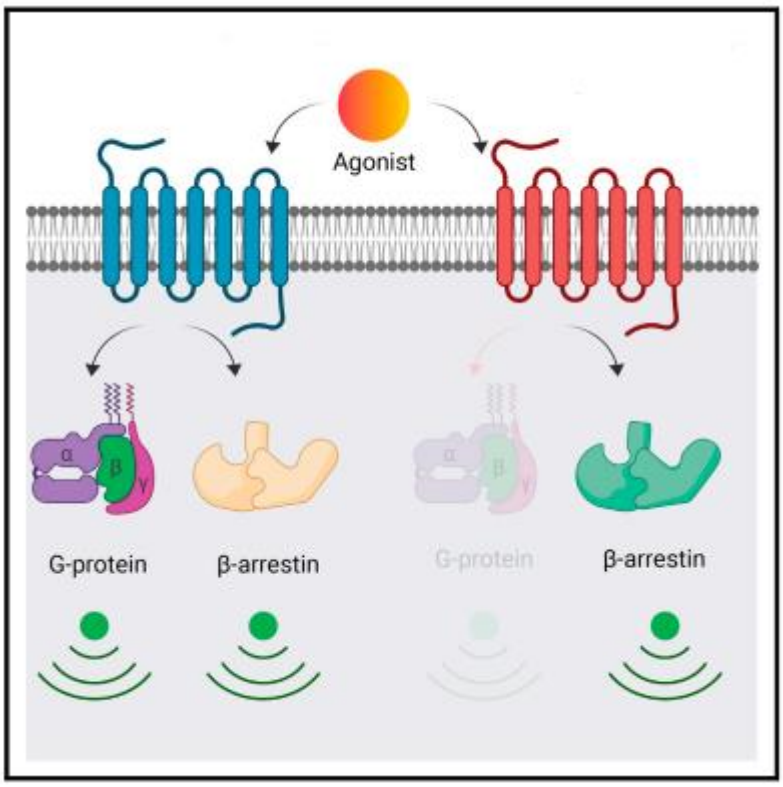

Figure 14. A graphical representation of both signaling pathways possible from 7-TM receptors. An agonist could be biased to the GPCR-activating β-arrestins (Pandey et al., 2021).

13. β-arrestin signaling to Glycogen synthase kinase 3

Glycogen synthase kinase 3 (GSK3) is a highly conserved protein serine/threonine kinase that plays a key role in a wide variety of cellular processes associated with coordinating catabolic and anabolic pathways, as well as regulating cellular fate and cell growth. When GSK3 phosphorylates its target, it typically inhibits the activity of the substrate, and, therefore, the signaling pathway. Thus, it is possible to describe GSK3 as a suppressor of hormone/growth factor-induced signaling cascades. One example is inhibiting insulin signaling through the phosphorylation of glycogen synthase, which leads to inhibition of glycogen synthesis, while phosphorylating the insulin receptor substrates, IRS-1/IRS-2, inhibits insulin receptor tyrosine kinase activity. The second important pathway is the canonical Wnt signaling pathway, which is inhibited by GSK3 through phosphorylation of β-catenin, destabilizing the protein and subsequently leads to degradation in the proteasome. GSK3 also phosphorylates a wide range of transcription factors including Nuclear Factor of Activated T-Cells (NFAT), heat shock factor-1, cAMP response element binding protein (CREB), and nuclear factor-kappa B (NF-κB), to inhibit gene expression. GSK3 possesses a unique property, which is that, unlike most protein kinases,

it is active under basal conditions and is inhibited when cells are stimulated. It is also worth to mention that GSK3 has a very broad range of substrates, including an estimated number of over 500 substrates, as well as 100 "physiological substrates" which are related to diverse cellular functions (Rippin & Eldar-Finkelman, 2021).

GSK3 activation has been linked to GPCR binding of ligands (Wu & Pan, 2010), and it is a downstream target of the β-arrestin signaling pathway, as seen in Figure 15, which is why it was a principal target in the scope of this thesis.

GSK3 has two isoforms, GSK3α and GSK3β which are nearly identical, but they have different C-terminal sequences and GSK3α contains a large glycine-rich N-terminal region that is not present in GSK3β. In regards to the brain, GSK3α is found in the hippocampus, cerebral cortex, striatum, and cerebellum, whereas GSK3β is expressed in nearly all brain regions (Rippin & Eldar-Finkelman, 2021). GSK3 has largely been considered a cytoplasmic protein, however it is also found in the mitochondria and nucleus. In GPCRs, D_2 receptor activation leads to cAMP production regulation. β-arrestin then brings Akt and GSK3 into close proximity to protein PP2A, which dephosphorylates Akt to deactivate it and dephosphorylates GSK3 to activate it (Beaulieu et al., 2009). GSK3 then promotes the formation of this β-arrestin-2/Akt/PP2A complex, thereby providing a mechanism for GSK3 to promote its own activation. It was also found that GSK3 is also inhibited by lithium, a widely accepted mood stabilizer used to treat bipolar disorder (Klein & Melton, 1996; O'Brien et al., 2011). This finding implicated GSK3 as a principal target of mood behavior and psychiatric disorders, which has been supported by numerous studies that suggest that hyperactivity of GSK3 is a contributing factor to progressive neurodegenerative and psychiatric conditions, while inhibition of GSK3 may be therapeutic (Rippin & Eldar-Finkelman, 2021).

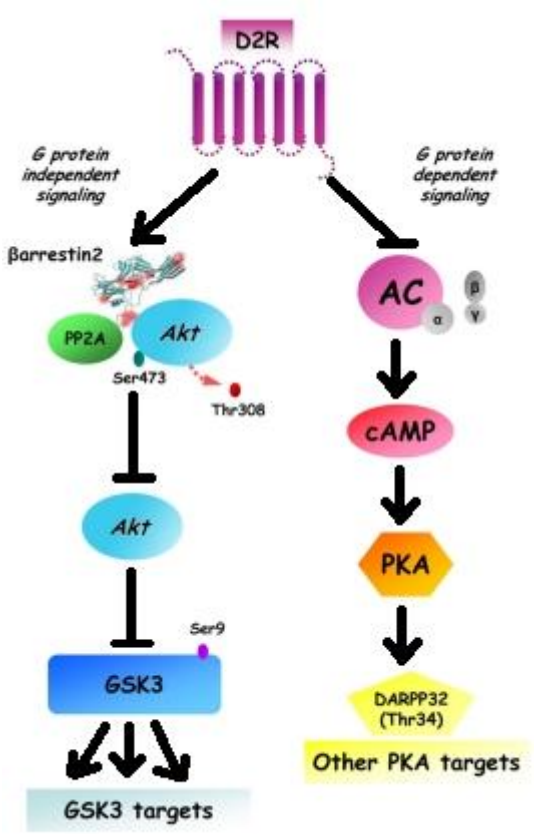

Figure 15. β-arrestin downstream signaling to GSK3. D_2R activation leads to both classical G protein mediated signaling, as well as the formation of complexes of signaling molecules that are associated together by β-arrestins. In the specific case of striatal D_2R, β-arrestin 2 is able to enhance the interaction between Akt and PP2A, ultimately resulting in Akt inactivation and increased activation of GSK3. Adapted from (Beaulieu et al., 2011).

14. Dopamine-related disorders

DA plays a vital role in several aspects of the body, including the modulation of behavior and cognition, voluntary movement, motivation, punishment and reward, inhibition of prolactin production, sleep, dreaming, mood, attention, working memory and learning (Juárez Olguín et al., 2016). Dysfunctional dopaminergic neurons have been implicated in several neurological disorders. I would like to give an overview of the pathophysiology of some of these disorders, which include Parkinson's disease, Huntington's disease, ADHD, and Schizophrenia, and the mechanisms of action of the drugs used for treatments.

14.1 Parkinson´s Disease

Parkinson's disease (PD) is a progressive neurodegenerative movement disorder which affects nearly 1% of the population over the age of 60. Symptoms include bradykinesia, tremor, rigidity, and sometimes mental disturbances (Tysnes & Storstein, 2017). These symptoms arise as a result of extreme degeneration of dopaminergic neurons in the SNC. However, neuropathology suggests that the SNC is involved later toward the middle stages of the disease (Braak et al., 2003). In fact, the earliest changes can be observed in the medulla oblongata and olfactory bulb (Braak stages 1 and 2) and this is when patients are pre-symptomatic (Braak et al., 2006). After that, the changes are spread into the substantia nigra areas of the midbrain and basal forebrain (Braak stages 3 and 4). This is when the illness most likely becomes symptomatic and clinically manifests. It finally goes to stages 5 and 6, when the lesions appear in the neocortex. The pathological hallmarks of PD are Lewy bodies (LBs), which are round eosinophilic intracytoplasmic proteinaceous inclusions of the protein α-synuclein (Simon et al., 2021).

There is no cure for PD at the moment, and the present treatments aim to alleviate symptoms. Since symptoms are related to the depletion of DA, treatments were therefore aimed at increasing DA levels. Several drugs and compounds have been approved for the treatment of PD, which are based on their mechanism of action on DA and can therefore be classified into dopaminergic and nondopaminergic. They can then be subclassified (Saba et al., 2022) according to the following table:

	Dopaminergic				**Nondopaminergic**	
Subclassification	Levodopa	Dopaminergic agonists	MAO-B inhibitors	COMT inhibitors	Amantadine	Anti-cholinergics
Mechanism	DA precursor that crosses the blood-brain barrier and is converted to DA	Act directly on striatal DA receptors with preferential affinity for D_2 receptors and do not depend on DA-converting enzymes to work	Increase extracellular DA levels in the striatum	Decrease the metabolism of levodopa by increasing its supply to the central nervous system	Increasing the DA release and inhibition on N-methyl-D-aspartate (NMDA) receptors	Blocking acetylcholine receptors and aim to reestablish the balance between dopaminergic deficits and striatal cholinergic excess in PD
Examples	-	bromocriptine, pramipexole, rotigotine	selegiline, rasagiline, safinamide	entacapone	-	trihexyphenidyl, benztropine, orphenadrine, procyclidine, biperiden

Table 2. Classification of treatments used in PD.

14.2 Huntington's Disease

Huntington's disease (HD) is an inherited disorder with a worldwide service-based prevalence of 2.71 per 100,000, a mean age of onset of between 30 and 50 years, and a mean duration of 17-20 years (Pringsheim et al., 2012). The disease is characterized by degeneration of the caudate and putamen in the corpus striatum and loss of efferent medium spiny neurons (MSNs). The gene responsible for HD is called HTT which encodes a 350 kDa ubiquitously expressed protein called huntingtin. The mutation that causes the disease is an abnormal expansion of a tract of uninterrupted CAG trinucleotide repeats, which is a codon for glutamine. The mutation leads to an abnormally expanded polyglutamine tract in the protein huntingtin (Jimenez-Sanchez et al., 2017).

The typical motor changes are involuntary, unwanted movements which start in the fingers, toes, and small facial muscles and eventually spread to all other muscles. Choreatic movements are present at all times that the patient is awake, and this is known as the hyperkinetic phase. It is followed by a hypokinetic phase, which is characterized by akinesia (difficulty in starting movements), and bradykinesia (slowness of movement) and an extreme hesitation in embarking on a movement.

Prior to the motor symptoms, patients offer suffer from a wide variety of psychiatric symptoms, such as apathy, depression, low self-esteem, feelings of guilt and anxiety, obsessions and compulsions, psychosis and dementia. The typical drugs for treating hyperkinesia, or chorea, are typical or atypical neuroleptics (DA receptor blocking) and tetrabenazine (DA depleting). Clozapine and olanzapine are examples of the atypical neuroleptics used. Their side effects include weight increase, while the side effects of tetrabanzine are more severe such as depression and sedation. However, the efficacy of tetrabenazine is better established (Roos, 2010).

14.3 Attention Deficit Hyperactivity Disorder

Attention deficit hyperactivity disorder (ADHD), also called hyperkinetic disorder by The World Health Organization (WHO), is characterized by pervasive and impairing symptoms of inattention, hyperactivity, as well as impulsivity. There is a lack of consensus among the literature reviews about its worldwide prevalence, ranging from as low as 1% to as high as nearly 20% among school-age children (Polanczyk et al., 2007).

The neural pathways underlying the deficits of ADHD are mostly the frontal-subcortical catecholamine networks, more precisely, the nigrostriatal DA pathway projecting from the substantia nigra to the basal ganglia (caudate nucleus and putamen), as well as the mesolimbic and the mesocortical DA pathways (Engert & Pruessner, 2008) and the noradrenergic pathway (Del Campo et al., 2011). The inattention and hyperactivity associated with the disease and that begin in childhood most often cause impairment to school performance, intellectual functioning, and later on to social skills, driving, and occupational functioning in adults (Biederman & Faraone, 2005). The exact cause that contributes to the development of ADHD is still unknown, although it has been hypothesized that there is a complex association between genetic factors and environmental risks. A dysfunction of the transporter DAT has also been suggested to cause ADHD, which is supported by evidence from DAT knockout mouse that exhibits symptoms of hyperactivity and deficits in inhibitory behavior (Gainetdinov, 2008). Moreover, among different DA receptor subtypes, it has also been indicated that the impairments affect mostly D_4 and D_5 receptor subtypes (Banaschewski et al., 2010).

The main treatments for ADHD are the stimulant drugs methylphenidate and amphetamine, which are believed to enhance neurotransmission of DA and norepinephrine. Despite many decades of clinical use, stimulant drugs have been controversial because of concerns that they might cause tics, substance abuse, addiction, as well as delaying growth (Biederman & Faraone, 2005). Some research even suggests that stimulants could cause heart problems and psychiatric symptoms. Other medications that may be effective in treating ADHD are Atomoxetine and antidepressants, however they have an increased risk of suicidal thinking in children and teenagers (https://www.mayoclinic.org/diseases-conditions/adhd/diagnosis-treatment/drc-20350895).

14.4 Schizophrenia

Schizophrenia is a chronic mental disorder caused by abnormalities in neurotransmission. The onset of the disease can occur as early as the age of 20, more common for men at this age, while women tend to experience their first episode in their early 30's (Patel et al., 2014). Because it starts early in life and chronically progresses, this accounts for its high prevalence (7.2/1000) but low incidence (15.2/100 000). While genes (a wide array of them) and family history account for most of the cases of schizophrenia, certain

environmental factors and drug abuse have recently risen as other contributing factors, making schizophrenia a multifactorial disorder (Picchioni & Murray, 2008).

Schizophrenia is characterized by relapse episodes of psychosis. Since no biological marker for schizophrenia has been found so far, the diagnosis of the illness is based on the assessment of the several symptoms, as was proposed by Eugen Bleuler, which were printed in the first edition of the Diagnostic and Statistical Manual of Mental Disorders (DSM-I) (Ashok et al., 2012). In addition to the diagnosis, this assessment also makes suggestions for treatment, and has been continuously updated on the basis of new findings, with the latest edition, the fifth (DSM-V), published in 2013.

The theory of schizophrenia has changed from its initial conception to the recent comparisons in the DSM-V and ICD-11 (International Classification of Diseases-11), which are based on the evaluation of the current ICD and DSM, the available scientific evidence, and the consensus reached by their developers. There are conceptualization changes (diagnostic criteria and specifiers) of ICD-11 schizophrenia with respect to those of DSM-V, and they are based on the scientific literature published in Medline, Scopus and Scielo until July 2019 and the information on the WHO and APA websites (Valle, 2020). The different aspects are grouped according to Table 3, also adapted from Valle (2020).

The more classical way to characterize the symptoms of schizophrenia is to divide them into two categories: positive and negative. Positive symptoms include lack of insight, hallucinations, delusions and thought disorder, while negative symptoms include social withdrawal, social neglect, loss of motivation and speech deficiency. Cognitive disturbances also often accompany the disorder. The common subtypes of schizophrenia according to DSM-IV are paranoid, simple, catatonic and hebephrenic, and they differ according to the most prominent symptoms (Picchioni & Murray, 2008).

Aspects	DSM-V	ICD-11
Name of chapter	Schizophrenia spectrum and other psychotic disorders	Schizophrenia and other primary psychiatric disorders
Duration of psychotic symptoms	Symptoms of the disorder persist for at least 6 months	Psychotic symptoms for at least 1 month
Functionality criteria	Level of functioning at work, interpersonal or self-care level, is well below the premorbid level	Does not include functionality criteria
Symptom specifier	Hallucinations, delusions, disorganised course, abnormal psychomotor behaviour, negative symptoms, cognitive impairment, depression mania	Positive symptoms, negative symptoms, depressive symptoms, manic symptoms, psychomotor symptoms, cognitive impairments

Table 3. Diagnostic criteria and specifiers of ICD-11 schizophrenia with respect to those of DSM-V (Valle 2020).

It has become common knowledge that schizophrenia is mainly associated to DA over activation, and post-mortem studies have revealed that the affinity of these D_2Rs is elevated in the striata (Seeman, 2011). Extensive research on the topic has shown great support for the original DA hypothesis, which states that psychotic episodes of schizophrenia are a result of hyperactive DA transmission (Howes & Kapur, 2009). Four dopaminergic pathways are involved in the pathophysiology of schizophrenia, shown in Figure 16. It must be stressed, however, that dopaminergic changes can account for certain symptoms but are insufficient to explain the etiology of the disorder. Other theories center on either an excess or a deficiency of serotonin and glutamate, and less extensively on an imbalance in aspartate, glycine, and gamma-aminobutyric acid (GABA) (Patel et al., 2014).

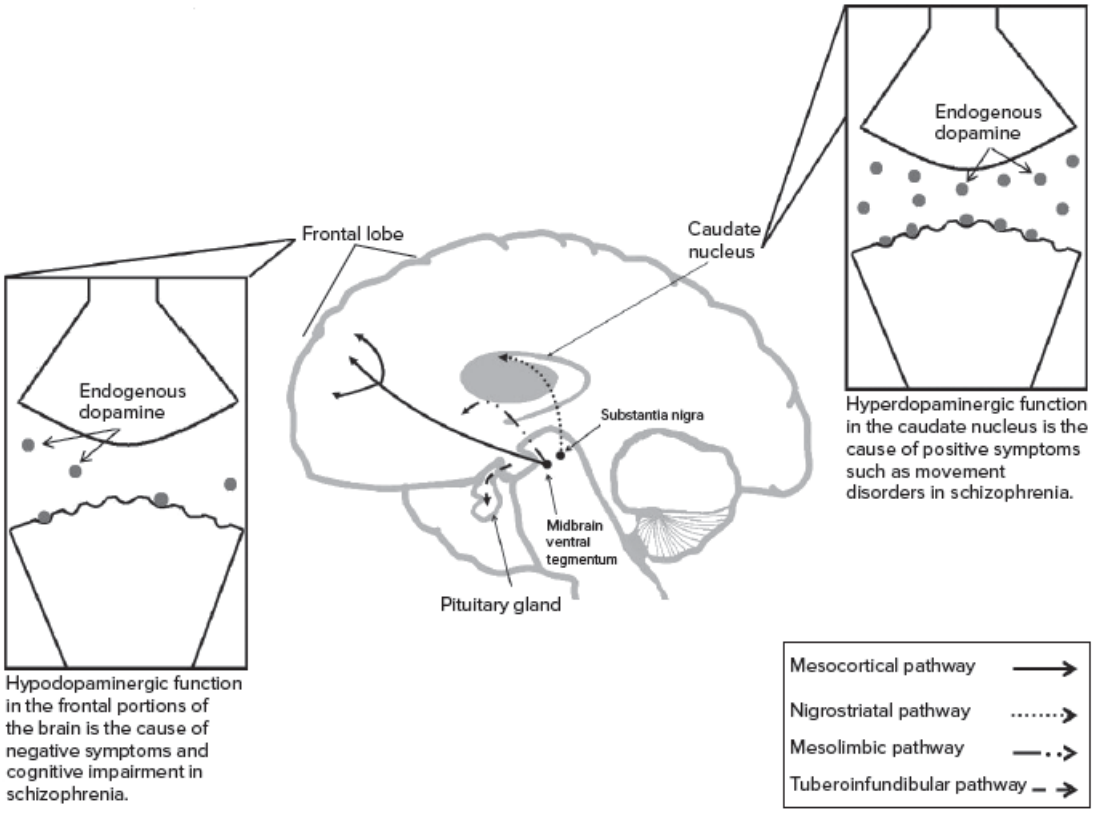

Figure 16. The Pathophysiology of Schizophrenia. Four dopaminergic pathways are implicated with the symptoms of schizophrenia. Low DA levels in the nigrostriatal pathway, which extends from the SN to the caudate nucleus, are thought to affect the extrapyramidal system, leading to motor symptoms. On the other hand, excess DA in the mesolimbic pathway, which originates from the VTA to limbic areas, may play a role in the positive symptoms of schizophrenia. Negative symptoms and cognitive deficits could be a result of low DA levels in the mesocortical pathway, projecting from the VTA to the cortex. The tuberoinfundibular pathway projects from the hypothalamus to the pituitary gland. A decrease of DA in the tuberoinfundibular pathway, extending from the hypothalamus to the pituitary gland, causes elevated prolactin levels and, subsequently, galactorrhea, amenorrhea, and reduced libido (Patel et al., 2014).

Like most psychotic disorders, schizophrenia remains to be incurable. Its positive symptoms can be decreased with the use of antipsychotics, the majority of which, however, possess at least one adverse effect as a potential liability (Picchioni & Murray, 2008).

15. Antipsychotic drugs

Antipsychotic drugs (APDs) aid in the management of hallucinations and delusions in patients with neuropsychiatric disorders, particularly schizophrenia and bipolar disorder, however they vary in efficacy and side effects, as well as mechanism of action. APDs are prescribed in the treatment of many other disorders, most commonly treatment-resistant

depression, dementia, obsessive-compulsive disorder, aggression, autism spectrum disorders, pervasive developmental disorder, and sleep disorders, but psychotic disorders remain to be their main indication. APDs are classified into two main classes known as typical and atypical. Some specialists believe there have been no advances in the treatment of schizophrenia since 1952 when chlorpromazine was discovered (except for the discovery of clozapine, the prototypical atypical APD). Another way to sort the APDs is into two generations, with clozapine marking the beginning of the second generation APDs. A third classification is pharmacologic, based on the ability to bind to D_2 receptors as a mechanism of action of chlorpromazine-like drugs to distinguish them from clozapine and related drugs. For example, clozapine's mechanism of action involves more potent blockade of 5-HT2A (serotonin) instead of D_2 receptors in addition to other non–D_2 DA receptor–mediated actions. The fourth classification is functional based on the ability to cause extrapyramidal side effects (EPS). At clinically effective doses, the side effect profile of the typical APD, such as chlorpromazine, differs from that of the atypical APD, such as clozapine. Atypical APDs have a lower incidence of EPS at the same usual clinical dosages of both (Meltzer, 2013).

The most serious side effects from typical APDs include lifelong tardive dyskinesia (TD) and the rare but fatal neuroleptic malignant syndrome. The side effects of chlorpromazine and its relatives are linked to their antipsychotic mechanism of action, specifically blockade of D_2 receptors in the limbic region of the brain, which occur at higher D_2 receptor occupancy rates. D_2 receptor blockade also causes elevated plasma prolactin, which is under tonic inhibition by D_2 receptors in the anterior pituitary gland. Hyperprolactinemia can cause galactorrhea and gynecomastia, and can be related to dysphoria, osteoporosis, and breast cancer (Meltzer, 2013).

Even though atypical APDs have a lower incidence of EPS, they may still cause some secondary side effects such as weight gain, type II diabetes mellitus, hyperlipidemia, QTc interval prolongation, myocarditis, sexual side effects and cataract (Uçok & Gaebel, 2008). Such adverse events have been linked to high D_2 occupancy levels. Obviously, there is a relevance of antipsychotic doses on D_2 occupancy, and a threshold of 65% receptor occupancy is needed in order to observe a clinical response. However, occupancy levels higher than this are associated with a much higher risk of side effects and no therapeutic advantage (Kapur, 2000).

Objectives

The overall aim of this thesis was to further investigate how D_2 receptor signaling affects dopamine metabolism in the brain. Thus, we focused on two specific objectives:

The first objective was to establish experimental conditions to look for heterodimerization of D_2R with other G protein coupled receptors.

The second objective was to assess if signaling of D_2R through β-arrestin/GSK3, regulates DA content through TH modulation by phosphorylation or interaction with protein partners.

Both objectives were sought for in rat brain tissue. For the first objective, we assessed the reliability of antibodies as a necessary step to detect the proteins involved. For the second objective, we had additional techniques, such as mass spectrometry and functional assays. A relevant functional assay used in this thesis was developed by the group during the course of this thesis, and is named "dopamine accumulation". It is described in Section 2.4 in Methodology and in (González-Sepúlveda et al., 2022).

Methodology

1. Materials

1.1 Chemicals used with HPLC experiments

Natrium hydrogen carbonate ($NaHCO_3$), potassium dihydrogen phosphate (KH_2PO_4), and magnesium sulfate heptahydrate ($MgSO_4.7H_2O$) were obtained from Merck Biosciences, Darmstadt, Germany. Sodium disulphite ($Na_2S_2O_5$) and D-(+)-glucose anhydrous were purchased from Panreac Quimica S.A.U., Spain. Perchloric acid 70% and triethylamine (TEA) were obtained from Fluka Biochemika, Buchs. Sodium chloride (NaCl) was purchased from Scharlau S.L., Spain and octane-1-sulphonic acid sodium salt ($CH_3(CH_2)7SO_3.Na$), HPLC grade was obtained from Romil Ltd, Cambridge, UK. Methanol and acetonitrile, both with ultra-gradient HPLC grade were from J.T. Baker, Netherlands. Optiphase 'Hisafe'-III liquid scintillation cocktail was purchased from Perkin-Elmer, MA, USA. Other chemicals include l-ascorbic acid, calcium chloride dihydrate 99% ($CaCl_2.2H_2O$), potassium chloride (KCl), sodium phosphate monobasic monohydrate 98% ($Na_2H_2PO_4$), ethylenediaminetetraacetic acid disodium salt dihydrate 99-101% (EDTA), DA hydrochloride, dimethyl sulfoxide 99.5% (DMSO), citric acid ($C_6H_8O_7$), and trichloroacetic acid 99% (TCA), were purchased from Sigma-Aldrich, Steinheim, Germany.

1.2 Drugs and kits

CHIR99021 HCl (CT99021), SB216763, tetrabenazine (TBZ), (-)-quinpirole hydrochloride and PD98059 were obtained from Tocris Bioscience, UK. LiCl was obtained from Sigma-Aldrich. UNC9994 was from Axon Medchem. 3-hydroxybenzylhydrazine dihydrochloride (NSD-1015) was from Sigma-Aldrich, Steinheim, Germany. The peptides mimicking phosphorylated TH sequences were from ProteoGenix (France).

IP and coIP were performed with the ThermoFisher Pierce Classic Magnetic IP/coIP Kit (ref 88804) and BCA assay with the Thermo Fisher Pierce BCA Protein Assay kit (ref 23225).

1.3 Preparation of Krebs-Ringer buffer

Krebs-Ringer buffer was composed of 120 mM NaCl, 0.8 mM KCl, 2.6 mM $CaCl_2$, 0.67 mM $MgSO_4$, 1.2 mM KH_2PO_4, 27.5 mM $NaHCO_3$, 10 mM D-(+)-glucose anhydrous. For preparing the buffer, half of the chemicals (potassium chloride, sodium chloride, potassium dihydrogen phosphate and magnesium sulfate heptahydrate) were dissolved in Milli-Q water and prepared earlier, and the rest of the chemicals (calcium chloride dehydrate, sodium hydrogen carbonate and D-(+)-glucose anhydrous), were added into the solution right before the experiments were performed. The buffer was also saturated with 95% O_2/5% CO_2 (carbogen) and the pH was adjusted to 7.4 with a diluted NaOH solution.

1.4 Mobile phases used in the HPLC system

Preparation of the mobile phase for the quantification of [^{3}H]-DA synthesis

The mobile phase used for the determination of [^{3}H]-DA synthesis with HPLC-UV is an ion-pair mobile phase with the following composition: 100 mM sodium phosphate monobasic monohydrate and 0.75 mM octane-1-sulphonic acid sodium salt dissolved in Milli-Q water. The pH was adjusted to pH 4.5 with a diluted hydrochloric acid solution. The mobile phase solution was then filtered, degassed, and 15% (v/v) methanol was added into the solution prior to the analysis.

Preparation of the mobile phase for the quantification of DA, DOPAC and L-DOPA concentrations

The mobile phase used for the determination of endogenous DA, DOPAC and L-DOPA with HPLC-EC is an ion-pair mobile phase with the following composition: 0.055 M citric acid, 0.063 mM ethylenediaminetetraacetic acid disodium salt dihydrate and 1.217 mM octane-1-sulphonic acid sodium salt dissolved in Milli-Q water. The pH was adjusted to pH 7.2 with a diluted triethylamine solution. The mobile phase solution was then filtered, degassed and 0.5% (vol/vol) acetonitrile was added into the solution prior to the analysis.

1.5 Antibodies used in Western blot

Primary Antibody	Dilution	Source	Supplier
pS8 Tyrosine Hydroxylase	1:1000/1:500	Rabbit	Invitrogen (PA538344)
pS19 Tyrosine Hydroxylase	1:500	Rabbit	Invitrogen (PA538240)
pS31 Tyrosine Hydroxylase	1:500	Rabbit	Millipore (AB5423)
pS40 Tyrosine Hydroxylase	1:1000/1:500	Rabbit	Millipore (AB5953)
Tyrosine Hydroxylase	1:1000	Mouse	Millipore (MAB5280)
β-catenin	1:1000	Mouse	Transduction Labs (BD610154)
pS33S37Thr41 β-catenin	1:1000	Rabbit	Invitrogen (PA567518)
α-synuclein	1:1000	Mouse	BD TransD Labs (610786)
TOM-20	1:1000	Rabbit	Santa Cruz (sc-11415)
ERK 1/2	1:1000	Mouse	Cell Signal (4695)
pERK 1/2	1:1000	Rabbit	Cell Signal (9101)
Tyrosine Hydroxylase	1:1000	Sheep	Millipore (1542)
Alomone D_2	1:1000	Rabbit	Alomone Labs (ADR002)
Abcam D_2	1:1000	Goat	Abcam (AB30743)
β-arrestin	1:1000	Rabbit	Thermo (PA1730)
Actin	1:1000	Mouse	Sigma (A1978)
GAPDH	1:1000	Mouse	Abgent (AM1020b)

Table 4. List of primary antibodies used in the Western Blots. In the Primary Antibody column, **p** means phosphorylated.

Secondary Antibody	Dilution	Source	Supplier
IRDye 680RD Anti-rabbit IgG	1:10000	Donkey	LiCor (92668073)
IRDye 800CW Anti-mouse IgG	1:10000	Donkey	LiCor (92632212)
HRP-conjugated Anti-mouse	1:2000	Goat	BioRad (1721011)
HRP-conjugated Anti-rabbit	1:2000	Goat	Invitrogen (31460)
HRP-conjugated Anti-sheep	1:2000	Donkey	Thermo (A16041)
Biotin-conjugated Anti-rabbit	1:1250	Chicken	Abcam (AB6828-1)
Biotin-conjugated Anti-Goat	1:1250	Donkey	Jackson (705065147)

Table 5. List of secondary antibodies used in Western Blot and immunostaining.

Methods

2.1 Immunostaining

Slices from rat or mouse brains that had been fixed by immersion and cryoprotected were washed with PBS and antigen retrieval was performed with citrate buffer pH 6 (tri-sodium citrate dihydrate-SIGMA 71405) at 80°C for 40 minutes followed by 20 minutes at room temperature. After washing, 1% sodium borohydrate (SIGMA 452882) was added to block autofluorescence. Slices were washed with PBS-T and unspecific binding was blocked with 5% BSA in PBS-T followed by incubation with the primary antibody diluted in 2.5% BSA in PBS-T at 4°C overnight with rotation. Following washing, slices were incubated with the secondary antibody diluted in the same primary antibody buffer for 90 minutes at room temperature. After that, slices were washed and incubated with Streptavidin Alexa followed by counterstaining with Hoescht 33258. Finally, slices were washed and mounted on slides.

2.2 Striatal tissue preparations for HPLC

Animals were euthanized in accordance with the Ethics Committee for Human and Animal Research (Universitat Autònoma de Barcelona), and in compliance with the guidelines established by the Ethical Committee for the use of Laboratory Animals in Spain (53/2013) and European Communities Council Directive 1986 (86/609/EEC). The experimental protocol is as previously described (González-Sepúlveda et al., 2013; Ma et al., 2015), which is that, naive Sprague-Dawley rats of both sexes (only 8% female due to their lower weight) (Charles River, France), aged 8-10 weeks with the weight between 0.25-0.35 kg, were euthanized via carbon dioxide asphyxiation in the animal service of Universitat Autònoma de Barcelona. Brains were immediately removed and chilled in ice-cold Krebs-Ringer buffer (composition and preparation in Materials). Next, striatal tissue (dorsal/medial from both hemisphere) dissection and mincing was performed using the McIlwain tissue chopper (The Mickle Laboratory Engineering Co., Surrey, UK), with an approximate cube shape of 0.3 x 0.3 mm/side. Brain dissection and mincing was done at a 4ºC chamber. Tissue minces were then reimmersed in ice-cold Krebs-Ringer buffer followed by centrifugation (1000 rpm, 1 min, 3 times) to remove cell debris. Striatal tissue from a single rat yielded up to 30 aliquots of 25 µl (0.3-0.7 mg protein each) corresponding to 24 incubation samples and 6 blank samples inside 2ml polypropylene

tubes containing 225 µl of Krebs-Ringer buffer and different treatments. Blank samples are controls (without drugs) that are kept on ice for the duration of the incubation period and therefore correspond to basal levels of the assay. This method is illustrated in Figure 17.

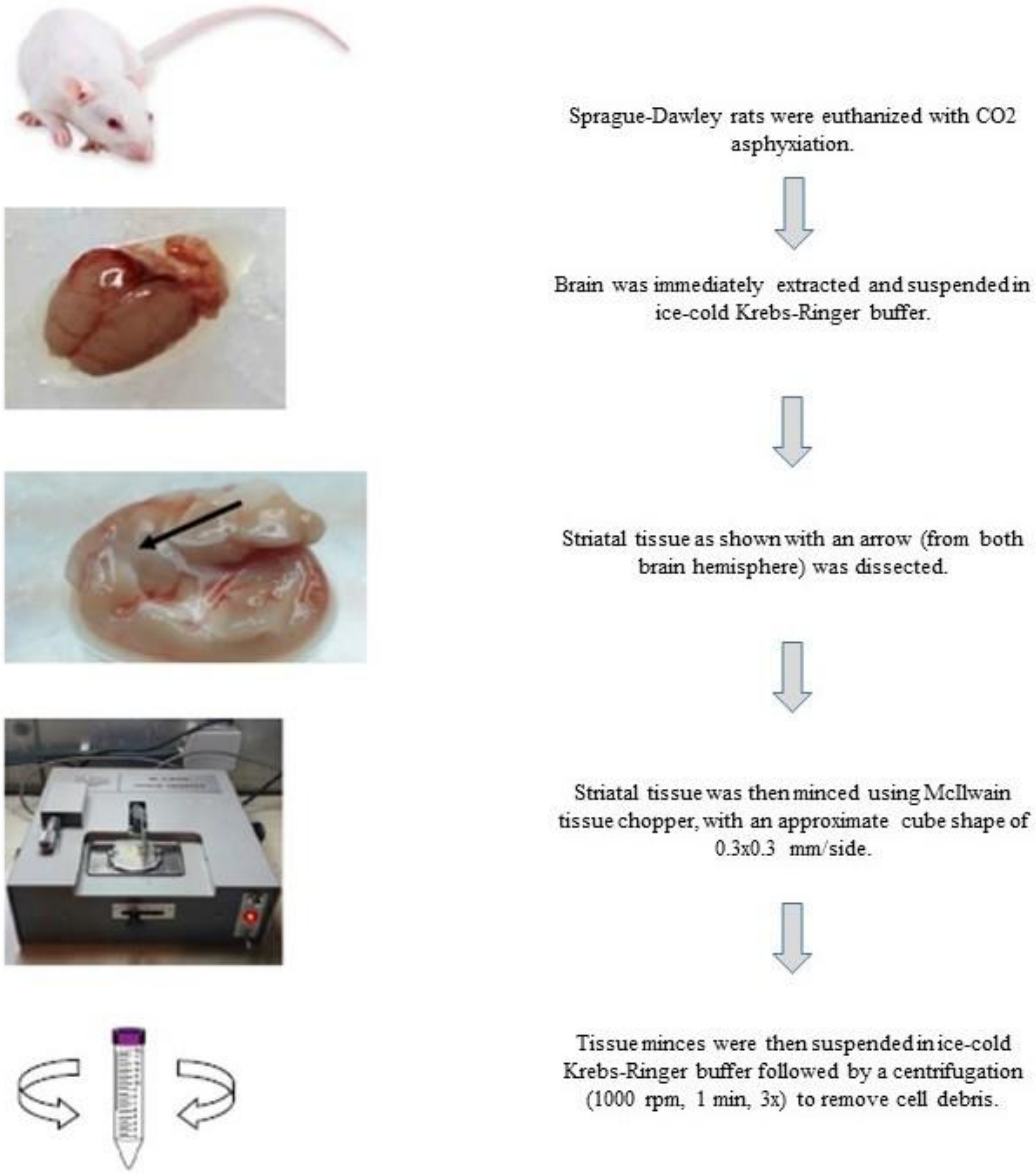

Figure 17. Overall steps for striatal tissue preparations.

2.3 Determination of newly synthesized DA ([^{3}H]-DA synthesis)

How the HPLC system works

The HPLC system is a technique used for the purification and separation of a mixture into its respective components. The HPLC is mainly composed of an injector, a pump, a column (stationary phase) and a liquid form of a mobile phase (solvent), as illustrated in Figure 19. It is usually connected with a detector to visualize, identify and quantify each component in the compound. Each component is visualized as a peak with its concentration quantified based on the area under the curve. The HPLC system relies on the pump to control and pressurize the liquid form of the mobile phase, which carries the injected sample through a column consisting of an adsorbent (e.g., silica-C18 in a reverse-phase column) to separate each component from the mixtures depending on the degree of interaction with the adsorbent particles. The composition and the pH of the mobile phase along with the flow rate, which can be controlled via the pump, play important roles to regulate the retention time for an analyte.

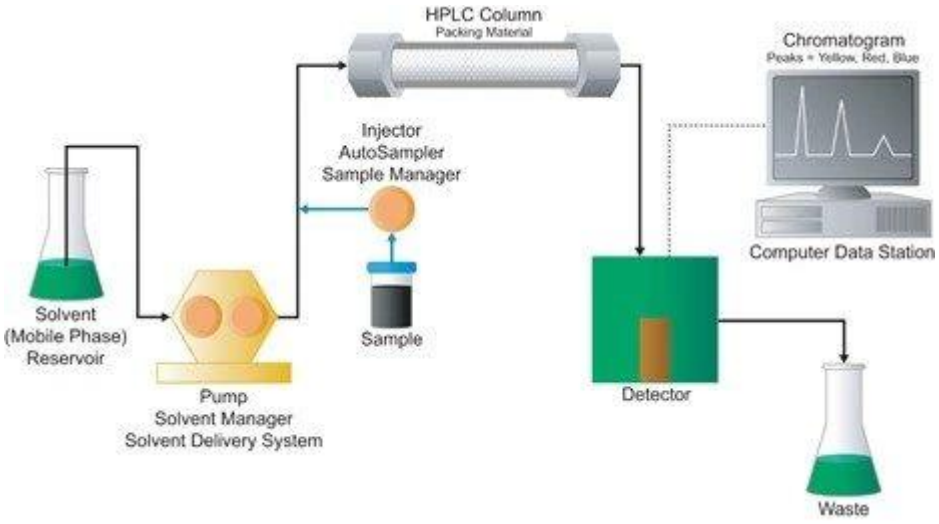

Figure 18. The HPLC system. Image is extracted from https://www.waters.com/content/dam/waters/en/figures/primers/hplc/primer_e_lcsystem.jpeg.82.620.resize/img.jpeg

[^{3}H]-L-tyrosine purification using high-performance liquid chromatography with UV detector (HPLC-UV)

Radio-labeled [^{3}H]-L-tyrosine ([^{3}H]-Tyr), 40–60 Ci/mmol was regularly purified before use to maintain a high degree of purity after storage due to its 1–3% degradation rate per month. The HPLC system used for this purification consisted of a reverse-phase C18 column (Tracer Extrasil ODS2, 5 μm particle size, 25 x 0.46 cm; Teknokroma, Spain) equipped with a UV detector set at 285 nm and a mobile phase as described above with a flow rate of 1.0 ml/min. Tyrosine was eluted for 9–10 min using these conditions. 0.4 mCi of [^{3}H]-Tyr was injected into the HPLC per purification and all tyrosine fractions (1.5–1.8 ml) were collected. 3-5 μl of [^{3}H]-Tyr fraction was mixed with optiphase 'Hisafe'-III liquid scintillation cocktail in a scintillation vial, and [^{3}H]-Tyr was quantified with a liquid scintillation counter (Perkin Elmer Tri-Carb 2810TR, USA) which determines the concentration of [^{3}H]-Tyr against an external standard calibration curve of non-radiolabeled tyrosine (MY Omar, PhD thesis).

Sample incubation for the determination of [^{3}H]-DA synthesis and drug treatment

Striatal tissue samples were incubated for 2 hours at 37°C, 400 rpm with 15s/10s of agitation/interval in an Eppendorf Thermomixer Comfort (5 Prime, Inc., Boulder, CO) under a constant carbogen atmosphere. Radio-labeled [^{3}H]-Tyr was added with a final concentration of 0.10 μM to all the samples during the final 10-min of incubation to synthesize [^{3}H]-DA. The experiment was stopped by the addition of deproteinizing solution which contains the following composition: 7% w/v TCA, 32.2 nmol l-ascorbic acid and 25 nmol DA hydrochloride as an internal standard. As for the blank samples, the deproteinizing solution was added before [^{3}H]-Tyr and they were kept on ice throughout the experiment. Samples were then homogenized using Dynatech/Sonic Dismembrator (Dynatech Labs, Chantilly, VA) and an aliquot was taken for protein quantification using Pierce BCA protein assay (Thermo Scientific, IL, USA), to adjust the variability of tissue contents in each sample. Samples were finally centrifuged (12,000 rpm, 10 min, 4°C), and supernatants were recovered. [^{3}H]-DA was analyzed by HPLC-UV. [^{3}H]-DA formed during the incubation reaction was separated from [^{3}H]-tyrosine by HPLC purification by a modification of previous procedures used in our laboratory for other neurotransmitters (Ortiz et al., 2000). This experiment was performed by MY Omar from our laboratory as he specializes in HPLC-UV.

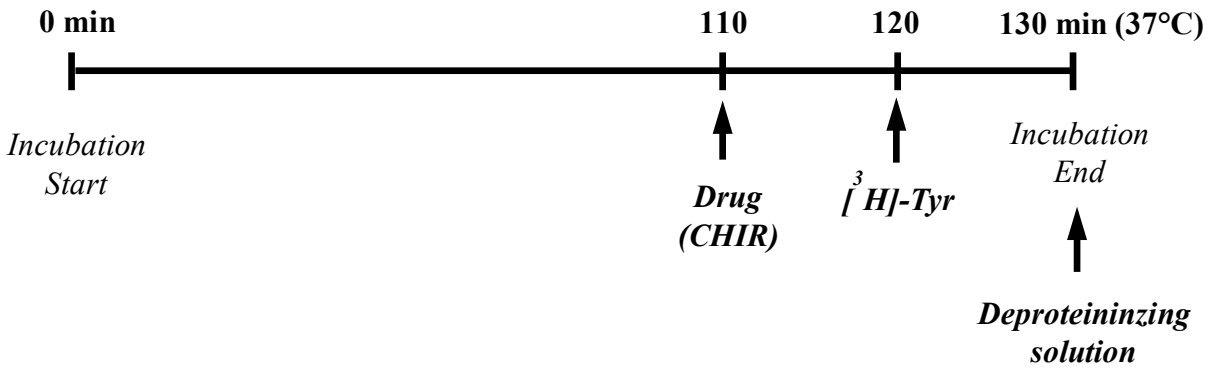

Figure 19 . Experimental design of drug incubation time for the determination of [^{3}H]-DA synthesis illustrated in a timeline.

[^{3}H]-DA analysis with HPLC-UV

Our chromatographic system consists of a reverse-phase C18 column (Tracer Extrasil ODS2, 5 μm particle size, 25 x 0.46 cm; Teknokroma, Spain) with an ion-pair mobile phase prepared as in Materials. The flow rate was always 1.0 ml/min. The HPLC system´s UV detector was set at 285 nm and detected DA as an internal standard since endogenous DA cannot be detected by the UV detector due to its low sensitivity. Internal standard recovery was quantified in each sample (internal/external standard peak area). Fractions of DA were collected in scintillation vials, mixed with optiphase 'Hisafe'-III liquid scintillation cocktail, and [^{3}H]-DA was then quantified with a liquid scintillation counter (Perkin Elmer Tri-Carb 2810TR, USA). Results were recorded as disintegration per min (DPM) and corrected with the following variables: (1) DA internal standard recovery, (2) DPM counts in blank samples, and (3) amount of protein in each incubated tube. Results were expressed as a percentage with respect to control samples run in the same experiment.

2.4 Determination of endogenous DA, DOPAC and L-DOPA concentrations

During the course of this thesis, we developed a method in our laboratory for measuring endogenous DA (as well as DOPAC and L-DOPA) accumulation *ex vivo* using a simple experimental method and HPLC. Endogenous DA accumulated spontaneously in *ex vivo* incubated striatal brain samples during a 2 hour period in the absence of release. This spontaneous accumulation allows us to model brain DA dynamics in brain tissue under the influence of treatments used in Parkinson's disease, Huntington's disease, ADHD and

schizophrenia. Neurotransmitter storage before release is relevant for the pharmacological treatments of these disorders as it can tonically modulate chemical communications between neurons. We explained this phenomenon as a transient disinhibition of TH until vesicles are filled with newly synthesized DA (González-Sepúlveda et al., 2022).

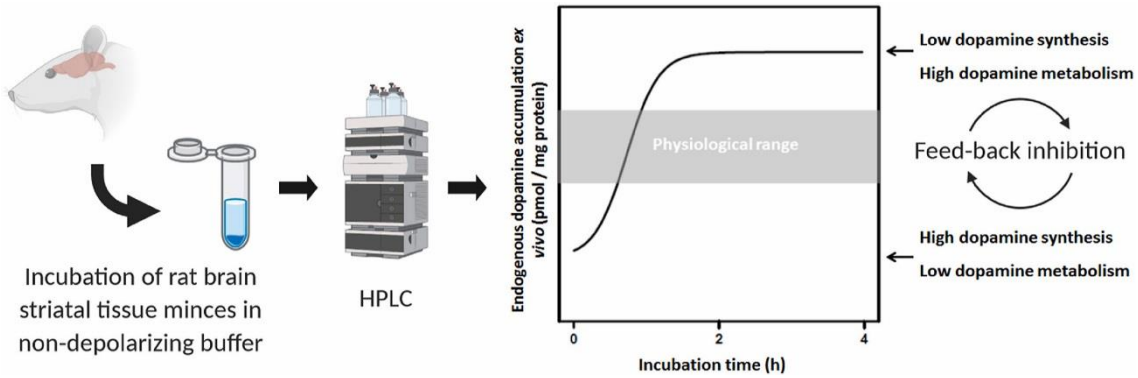

Figure 20. Our method for measuring DA accumulation using HPLC-EC.

Drug treatments and sample incubations for endogenous DA, DOPAC and L-DOPA accumulation

For determination of endogenous DA, DOPAC and L-DOPA concentrations, the method previously explained was used to prepare striatal tissue minces. The incubation was stopped by the addition of 10 volumes (w/v) deproteinizing solution of 0.25 M perchloric acid containing 0.25 mM EDTA and 0.1 mM $Na_2S_2O_5$. To demonstrate basal values in the samples, the deproteinizing solution was added at the beginning of sample preparations to non-incubated samples and they were kept on ice throughout the experiments. During a 120-min incubation, for example, a typical 3.6-fold increase of endogenous DA occurs vs basal values, thought to reflect new DA formation and storage without release in non-depolarizing conditions (González-Sepúlveda et al, 2022). Thus, we have termed this increase "spontaneous DA accumulation" in our group however for the scope of this thesis, I shall refer to it as "endogenous DA accumulation" as I will also quantify exogenous DA stored (see next section). All samples were then homogenized by 5 second sonications using Dynatech/Sonic Dismembrator (Dynatech Labs, Chantilly, VA). An aliquot was taken for protein quantifications using Pierce BCA protein assay (Thermo Scientific, IL, USA), to quantify the amount of tissue per sample tube and adjust the variability between samples. Samples were then centrifuged (13,000 rpm, 5 min, 4°C),

supernatants recovered, and concentrations of DA, DOPAC and L-DOPA were quantified using high-performance liquid chromatography with an electrochemical detector (HPLC-EC).

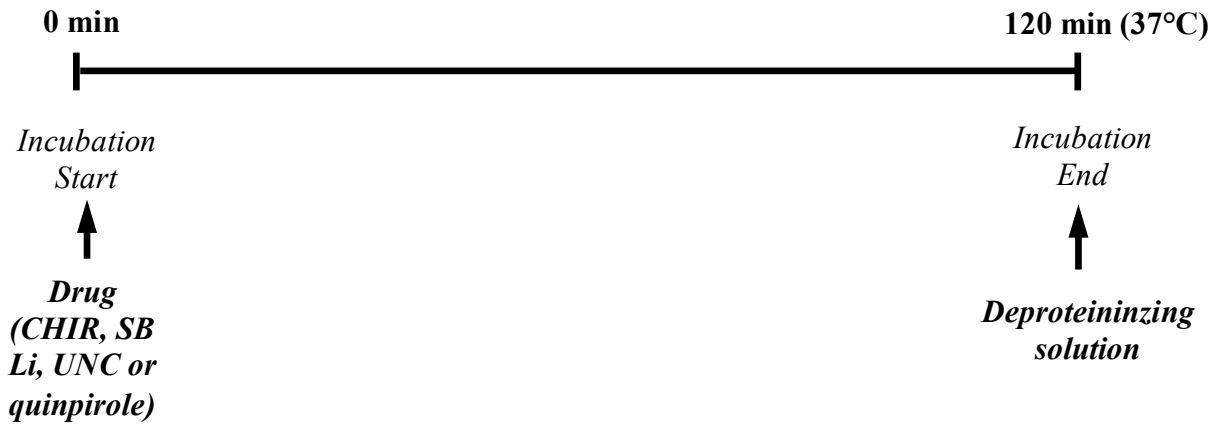

Figure 21. Experimental design of drug incubation time for the determination of DA, DOPAC and L-DOPA accumulation illustrated in a timeline.

Drug treatments and sample incubations for exogenous DA storage

For determination of exogenous DA storage, the method previously explained was used to prepare striatal tissue minces. Basal values were prepared similarly to endogenous DA accumulation as well. However, DA storage was assayed over an incubation period of 1 and 2 hours, and with DA hydrochloride being added during the last 30 minutes or hour (respectively) of incubation. When the incubation period was over, samples were centrifuged (13,000 rpm, 10 min, 4°C) and the supernatants removed to discard any excess DA that was not stored in the minces. 25 microliters of deproteinizing solution of 0.25 M perchloric acid containing 0.25 mM EDTA and 0.1 mM $Na_2S_2O_5$ was then added and mixed with the minces, followed by the addition of Krebs buffer to a final volume of 250 microliters. All samples were then homogenized by 5 second sonications using Dynatech/Sonic Dismembrator (Dynatech Labs, Chantilly, VA). An aliquot was taken for protein quantifications using Pierce BCA protein assay (Thermo Scientific, IL, USA), to quantify the amount of tissue in per sample tubes and adjust the variability between samples. Samples were then centrifuged (13,000 rpm, 5 min, 4°C), supernatants recovered, and concentration of DA was quantified using high-performance liquid chromatography with an electrochemical detector (HPLC-EC).

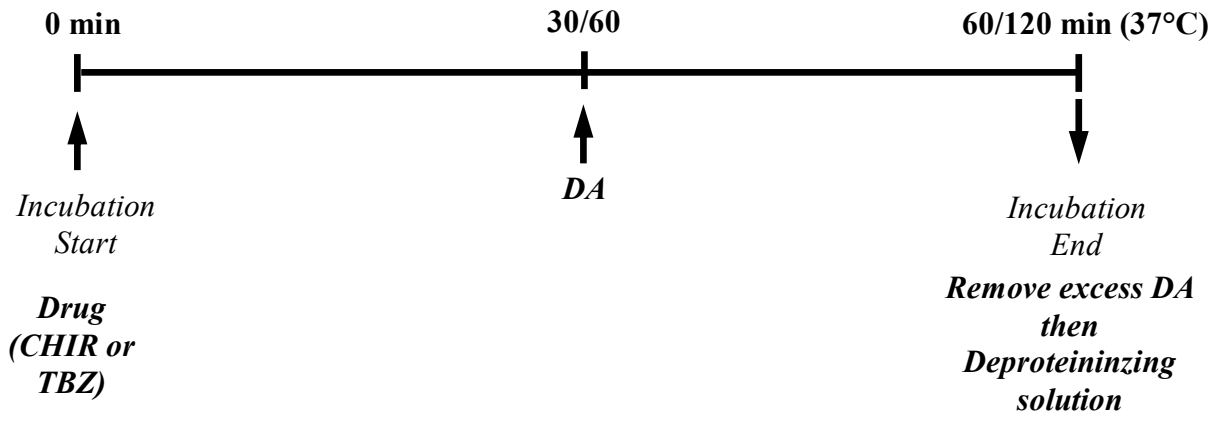

Figure 22. Experimental design of drug incubation time for the determination of DA storage illustrated in a timeline.

Analysis of DA, DOPAC and L-DOPA by HPLC-EC

For determination of DA, DOPAC and L-DOPA using HPLC-EC, the chromatographic system used consists of a reverse-phase C18 column (2.5 µm particle Fortis C18, 10 x 0.46 cm, Sugelabor, Spain) together with an ion-pair mobile phase, consisting of 0.055 M $C_6H_8O_7$, 0.063 mM EDTA, 1.217 mM $CH_3(CH_2)7SO_3$.Na, plus 0.5% (v/v) acetonitrile, pH 2.8 adjusted with triethylamine solution. The flow rate was always 1.5 ml/min. The HPLC system was equipped with Coulochem II (ESA) detector (model 5011 dual-electrode analytical cell with porous graphite electrodes) which simultaneously separates and detects DA, DOPAC and L-DOPA in the samples. Electrodes 1 and 2 had a potential of –0.05V and +0.4V respectively. DA, DOPAC and L-DOPA external standards with concentrations of 0.05-5 pmol/µl were injected in each experiment before samples to quantify concentrations of DA, DOPAC and L-DOPA in the tissue minces. Results were expressed as concentration of DA, DOPAC or L-DOPA versus mg protein in each sample. Relationship between the DOPAC/DA concentrations ratio was presented as a metabolism index linked to either DA release or insufficient uptake into vesicles (Joel Maldonado, Master thesis, 2022).

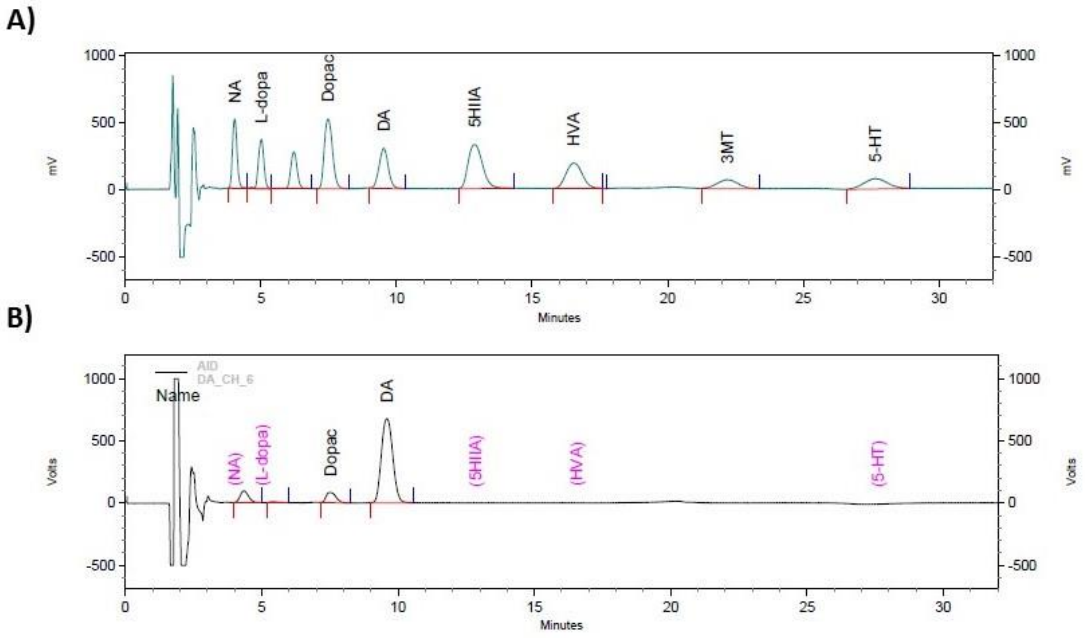

Figure 23. **Typical peaks of a chromatogram obtained from the tissue samples using HPLC-EC.** **A)** The external standards used for quantifications. **B)** DA and DOPAC peaks in a single tissue sample.

Statistical Analysis of HPLC quantifications

Graphics and statistical analysis were performed using the GraphPad Prism Software (version 4) (GraphPad Software Inc, USA). Data were presented as mean ± standard error of the mean (SEM). One-way analysis of variance (ANOVA) was applied with Dunnett´s post-hoc test for comparison against control or Bonferroni post-hoc test for direct comparison between tested groups. Interaction between treatments was assessed by two-way ANOVA followed by Bonferroni´s test for post-hoc comparisons. Other statistical analysis (treated with drug and respective control) was performed by the unpaired Student´s t-test. A difference was considered to be statistically significant if *$p<0.05$, **$p<0.01$ or ***$p<0.001$.

2.5 Western blot

Samples were prepared by dilution in Loading Buffer (BioRad) with 1% (v/v) β-mercaptoethanol and heated at 99ºC for 5 minutes. In the case of TH phosphorylation, samples were incubated as previously explained and homogenization of the sample was with 1% SDS and boiling prior to polyacrylamide gel electrophoresis (PAGE). This ensures that minimum disruption of TH phosphorylation occurs and it also allows to analyze all the TH present in the extracted tissue. In other cases, samples were boiled in

the buffer corresponding to the specific protocol. Protein amount was determined by BCA in all cases. Then equal amounts of protein were separated by SDS-PAGE gel electrophoresis, using a Mini-Protean system (Bio-Rad) and 20-40 μg of sample were loaded per well, following the protocol described by Bio-Rad. Acrylamide concentration for the gel was always 10% except for TH in mitochondria analysis, where a 15% gel was used. Electrophoresis was run at a constant amperage of 36 mA for approximately 1 hour in electrophoresis buffer (25 mM Tris; 192 mM glycine; 0.1% (w/v) SDS).

After electrophoresis, proteins were transferred onto 0.45 μm Immobilon®-FL transfer membranes (Millipore) using a Trans-Blot Turbo Transfer System (Bio-Rad) at 25 V for 30 minutes in transfer buffer (25 mM Tris; 192 mM glycine; 20% (v/v) methanol). Then, membranes were blocked for one hour at room temperature with TBS-Tween buffer (12.5 mM Tris; 75 mM NaCl; 1.5 mM KCl; pH 7.4; 0.1% (v/v) Tween) with 5% (w/v) non-fat milk (blocking buffer). The next step was to incubate the membranes overnight with their respective primary antibodies (Table 4) at 4ºC and in constant agitation. The day after, the membranes were washed three times with TBS-T for 5 minutes and then they were incubated for one hour with the corresponding secondary antibody (Table 5) diluted in blocking buffer. Some of the secondary antibodies were horseradish peroxidase-conjugated. Others were labeled with near-infrared emitters at different wavelengths (IRDye 680RD Anti-rabbit IgG and IRDye 800CW Anti-mouse IgG) in order to perform a clear and accurate imaging of the membranes and, for this reason, the incubation with these secondary antibodies was performed under dark conditions, in order not to lose any signal while developing the membranes. After this incubation, membranes were washed three times with TBS-T for 5 minutes before developing them.

2.6 Western blot signal quantification

In the case of horseradish peroxidase-conjugated secondary antibodies, signals were obtained using a ChemiDoc device (Bio-Rad) and quantitative analysis was performed using the ImageLab software (Bio-Rad). For developing the membranes with near-infrared secondary antibodies, the Odyssey® Fc Imaging System from LI-COR was used. As soon as the secondary antibodies were labeled with near infrared emitters, the membranes were detected at the correspondent near-infrared (NIR) wavelengths. The Odyssey Fc Imager from our department is paired with Image Studio version 5.2 Software, so, for image acquisition and organization this software was used. Finally,

signal quantification was also performed using Image Studio version 5.2 Software and the data collected was treated using Excel (Microsoft Office).

2.7 Calculating phosphorylation signal ratio using near-infrared antibodies

Infrared secondary antibodies and the Odyssey® Fc Imaging System from LI-COR were used to calculate phosphorylation ratio (phosphorylated protein/total protein) changes in TH. In the following example (Figure 24), proteins from striatal minces from rat brain were separated by SDS-PAGE and Western blot. Membranes were incubated, at the same time, with both an antibody against β-catenin phosphorylated in Ser33, Ser37 and Thr41 (phβ-Cat, raised in rabbit, diluted 1:1000) and with an antibody against total β-catenin (β-Cat, raised in mouse, diluted 1:1000). Subsequently, membranes were incubated with two secondary antibodies, an anti-rabbit labeled with a near-infrared emitter at 800 nm and an anti-mouse labeled with a near-infrared emitter at 680 nm. Thus, both phosphorylated and total protein can be assessed in the same band.

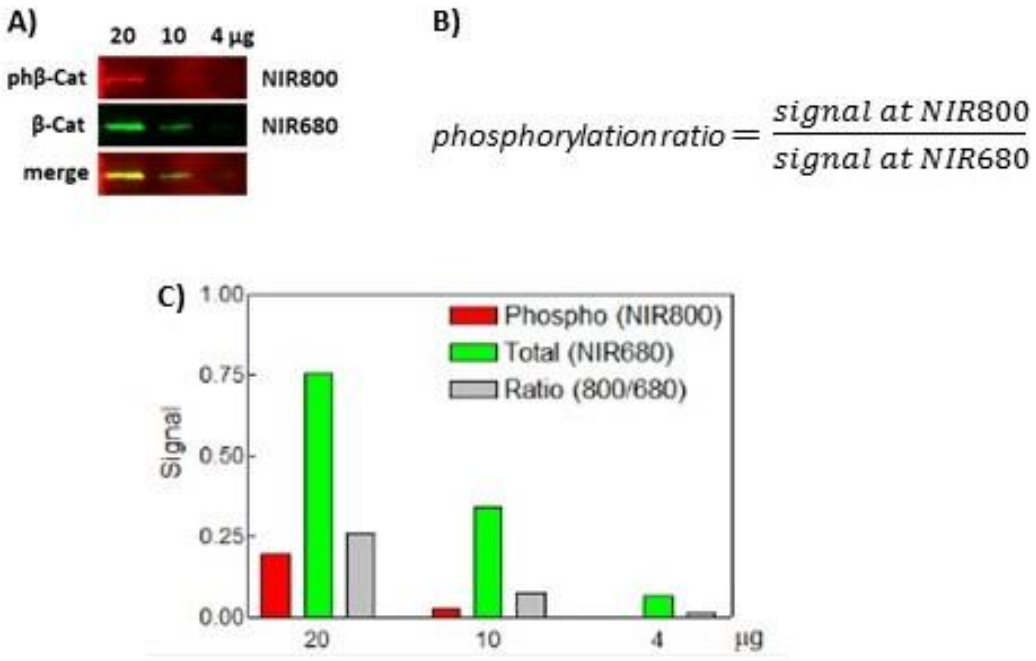

Figure 24. Calculating phosphorylation signal ratio using LI-COR. A) 20, 10 or 4 µg of total protein were loaded. **B)** NIR emissions at 680 nm (green) and at 800 nm (red) were captured and quantified with Odyssey Fc device (LI-COR) and the Image Studio software. In order to determine the level of phosphorylation, the ratio between signal at NIR800 and signal at NIR680 is calculated in every case. **C)** A graphical representation the phosphorylated signal (red), total signal (green) and ratio of phosphorylated/total signal (grey) using 20, 10 and 4 µg of total protein.

2.8 TH activity in homogenates, cytosol and mitochondria

Striatal tissue was extracted and placed in Mitochondrial buffer (220 mM mannitol, 70 mM sucrose, 10 mM KH_2PO_4, 5 mM $MgCl_2$, 1 mM EGTA, 2 mM HEPES, pH adjusted to 7.2 using KOH). Samples were then homogenized using a Potter homogenizer with 15 strokes and rotation at 4 ºC (on ice). To separate into cytosol and mitochondria fractions, homogenates were centrifuged at 900 × g for 10 min at 4°C. The resulting supernatants were further centrifuged at 9,000 × g for 10 min at 4°C, and then separated into supernatants containing cytosol and pellets containing mitochondria, which were resuspended in Mitochondrial buffer. Prior to starting the protocol, eppendorfs were prepared with 100 µM NSD-1015, 30 µM tyrosine and 100 µM tetrahydrobiopterin (BH_4). Then 200 µl of sample (homogenates/cytosol/mitochondria) were distributed into the prepared eppendorfs for a final incubation volume of 250 µl. Samples were incubated for 30 minutes at 37ºC and with low flow carbogen. Incubation was terminated by placing samples on ice and the addition of deproteinizing mixture. Samples were sonicated, BCA was performed, and samples were centrifuged at 10,000 g for 10 min. Finally, supernatants were injected into HPLC-EC to quantify L-DOPA.

2.9 Striatal homogenate separation into cytosol and mitochondria for Western blot

Striatal tissue was dissected and minced in a similar manner to preparation for HPLC and then distributed into a total of 24 eppendorfs (12 control and 12 treated, in this case with CHIR 3 µM) that were incubated in Krebs buffer for 2 hours at 37ºC. Following incubation, samples were then combined after a quick centrifuge, Krebs was removed and tissue was homogenized using a Potter homogenizer with 15 strokes and rotation at 4 ºC (on ice), which contained 500 µl Mitochondrial buffer (prepared as in previous section) and the pH adjusted to 7.2 using KOH. Homogenates were then centrifuged at 900 × g for 10 min at 4°C. The resulting supernatants were further centrifuged at 9,000 × g for 10 min at 4°C, and then separated into supernatants containing cytosol and pellets containing mitochondria, which were resuspended in 500 µl Mitochondrial buffer. Samples were then sonicated and protein concentration determined using the BCA protein assay (Thermo Fisher Sci) for both cytosol and mitochondria and Western blot was performed.

2.10 Lactate dehydrogenase activity assay

In a 1 ml spectrophotometer cuvette, 867 µl of phosphate buffer (0.1 M, pH 7.4) and 66 µl of sample (cytosol or mitochondria) were mixed and incubated at 37°C for 5 minutes. This mixture was used to set the blank in the spectrophotometer at 340 nm. Then 33 µl of NADH (3.5 mM) was added and the reading of this mixture observed on the spectrophotometer. To begin the reaction, 33 µl of sodium pyruvate (final concentration 0.67 mM) was added and mixed, and the cuvette directly placed in the spectrophotometer. The decrease in absorbance was followed and recorded every 20 seconds for 2-3 minutes.

2.11 Peptides used in determining pS31 antibody binding

A mixture of 2 ml of 5% casein in TBS-T and 2 µl pS31 primary antibody (rabbit, 1:500, Table 4) was prepared in 5 separate falcons. 3 µl (30 µg) of each of the 3 peptides/peptide combination (non-phosphorylated peptide, pS31 peptide, pT30 peptide, pS31+pT30 peptides) was added to 4 falcons, while nothing was added to the fifth. The mixtures were left on rotation overnight at 4°C. The following day, an SDS-PAGE gel was prepared and loaded with 20 µl rat liver or rat striatum. Following electrophoresis and transfer, the membrane was stained with Ponceau S and cut into 5 separate membranes. After blocking the membranes in 5% casein in TBS-T, they were each incubated on rotation in one of the 5 previously prepared falcons overnight at 4°C. The next day the membranes were washed 3 times for 5 minutes/wash in TBS-T and incubated for 1 hour with secondary antibody (1:10000, IRDye 680RD anti-rabbit, Table 5) then imaged using the LI-COR as previously explained. The peptide names and corresponding sequences were as follows:

EQ-19P - **pT30:** EQDAKQAEAVtSPRFIGRRQ
EQ-20P - **pS31:** EQDAKQAEAVTsPRFIGRRQ
EQ-20PP - **pT30+pS31:** EQDAKQAEAVtsPRFIGRRQ
EQ-20 - **non-phosphorylated:** EQDAKQAEAVTSPRFIGRRQ

2.12 Striatal and brain stem tissue preparation for immunoprecipitation and coimmunoprecipitation

The striatum and brain stem were dissected from rat brains in a similar manner to that of HPLC tissue preparation. However, following dissection, the tissue was not directly minced, but rather immersed in a homogenizing buffer with the following composition: 250 ml 50 mM TRIS, 1 mM EGTA, 1mM DTT, 2 tablets protease inhibitor, 250 mM

sucrose. The sample was then minced using a Crison tissue tearer, followed by further homogenization with the Bullet Blender Storm 24 (Next Advance BBY24M) and 0.5 mm zirconium oxide beads (Next Advance ZROB05). Next, sample was centrifuged at 500 × g for 10 minutes at 4ºC, and the resulting supernatant was centrifuged again at 100000 × g for 1 hour at 4ºC. The protein concentration was measured by BCA assay, and an aliquot was kept for subsequent confirmation of the immunoprecipitation by western blot.

2.13 Immunoprecipitation and coimmunoprecipitation

Immunoprecipitation of total TH was carried out using the Thermo fisher Pierce Crosslink Magnetic IP/coIP Kit, (88805) and 10 µg of Monoclonal Anti-TH (MAB5280), and according to the procedure specified in the kit, which consists of 3 phases: 1) binding of the antibody to the magnetic beads, 2) crosslinking the bound antibody, and finally 3) immunoprecipitation/coimmunoprecipitation. For immunoprecipitation, incubation of the sample with antibody was carried out overnight at 4ºC. As for coimmunoprecipitation, incubation was for 3 hours at 4ºC and the final washes before elution were replaced with less astringent buffers than the buffers used for immunoprecipitation (2 washes with IP Lysis/Wash Buffer was replaced once with 1 wash with 50 mM TRIS, 300 mM NaCl, and the second time with 50 mM TRIS, 150 mM NaCl, and 1 wash with Milli-Q water was replaced with 50 mM TRIS). In both cases, sample was eluted from the beads using 0.25% trifluoroacetic acid (TFA). Confirmation of the successfully eluted sample was determined by Western blot and silver staining.

2.14 Silver staining and mass spectrometry

Silver staining was performed according to the protocol provided by the laboratory of Proteomics. After proteins were separated by SDS-PAGE gel electrophoresis, the gel was fixed (40% ethanol, 10% acetic acid) for 30 minutes. This was followed by 30 minutes of sensitization (30% ethanol, 0.2% w/v $Na_2S_2O_3$, 6.8% w/v sodium acetate). The gel was then washed 3 times in Milli-Q water and then silver stained for 20 minutes ($AgNO_3$ 2.5 g/L). The gel was then developed (Na_2CO_3 2.5% w/v, HCOH 36.5% w/v) for around 10 minutes (until staining appeared). This was then stopped with (EDTA-$Na_2.2H_2O$ 1.46% w/v) for 10 minutes, followed by final washes in Milli-Q water (3 times). Mass spectrometry analyses was performed by a service (The proteomics laboratory

http://proteomica.uab.cat/index.php?option=com_content&view=frontpage&Itemid=1).

Details of the performed procedures can be found in Annex 1.

Results

Chapter 1: From D_2 receptors to β-arrestin signaling

A Brief Overview

We started this work to search for heterodimerization of D_2 with other receptors. We planned to do this because D_2 receptors are a principal pharmacological target of mental and movement disorders, yet there is a lack of in depth studies surrounding this topic, especially using D_2R antibodies in brain samples. The first step towards this was to validate available antibodies against D_2R using different techniques such as Western blot and Histochemistry.

1.1 Validation of antibodies against D_2R and β-arrestin

Antibodies against D_2R from Alomone and Abcam did not work well with Western blot

The first technique to test the antibodies was Western blot. We used an antibody against D_2R from Alomone, with pig and rat striatum, as well as pig and rat hypophysis (pituitary gland). Pig samples were obtained in collaboration with Joan Tibau laboratory (IRTA-Morells, Girona). D_2 receptors are expressed in almost all cell populations of the hypophysis (Pivonello et al., 2017). We therefore expected to see signal with both tissue (striatum and hypophysis), but we only saw bands at 50 kDa with rat and pig striatum and only in reducing conditions (Figure 25A). The antibody from Abcam did not work well with Western blot as it yielded a very faint band at a molecular weight around 75 kDa.

In order to further validate the antibodies, especially the one from Alomone, we decided to compare the D_2R protein of WT and KO mice, which were provided by the laboratory of Francisco Ciruela (Taura et al., 2018). To our surprise, we saw similar bands in both WT and KO and with both antibodies and again, fainter bands with Abcam. It was possible to incubate a single membrane with both antibodies sequentially as we had previously seen that they give different molecular weights (Figure 25B).

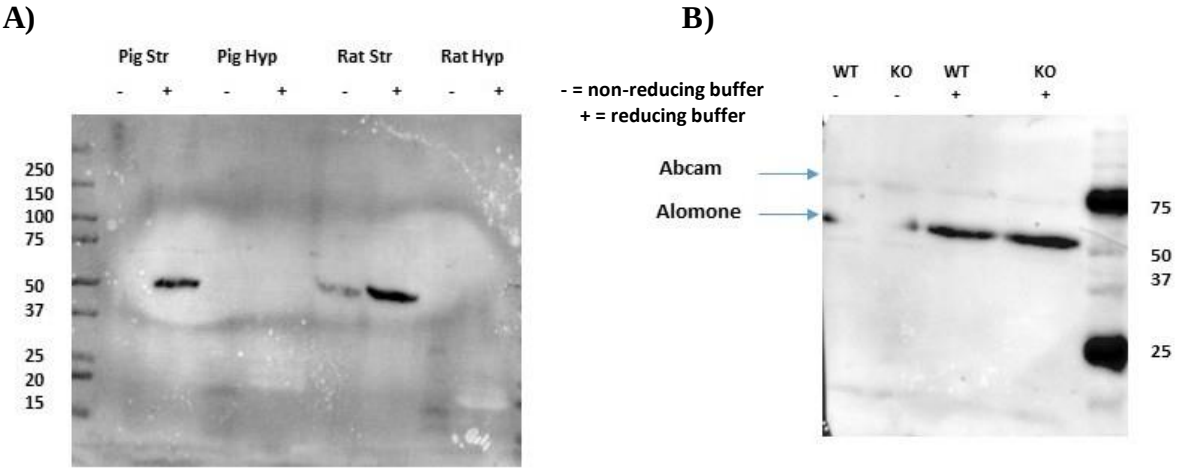

Figure 25. Antibodies against D_2R from Alomone and Abcam with Western blot. A) Western blot using Alomone D_2R primary antibody (raised in rabbit, 1:1000, bands at 50 kDa) with pig striatum and hypophysis, as well as rat striatum and hypophysis, in reducing (+) and non-reducing (-) sample buffer. **B)** Western blot using Abcam D_2R primary antibody (raised in goat, 1:1000, faint bands at 75 kDa) and Alomone D_2R primary antibody (raised in rabbit, 1:1000, bands at 50 kDa) in reducing (+) and non-reducing (-) sample buffer and with WT and KO mouse striatum. Molecular weight markers are shown in kDa, and signals were detected by chemiluminescence with HRP-labeled secondary antibodies.

Both Abcam and Alomone give signal in cortex, a D_2-poor region, as well as in D_2 KO mice using immunostaining

The questionable results with the D_2R WT and KO urged us to further investigate both our tissue samples and antibodies against D_2R. For this purpose, we decided to check the binding of our antibodies to D_2R using another technique. An initial immunostaining was performed with both Alomone and Abcam antibodies; they both seemed to give similar staining and the results with the Abcam antibody are shown in Figure 26.

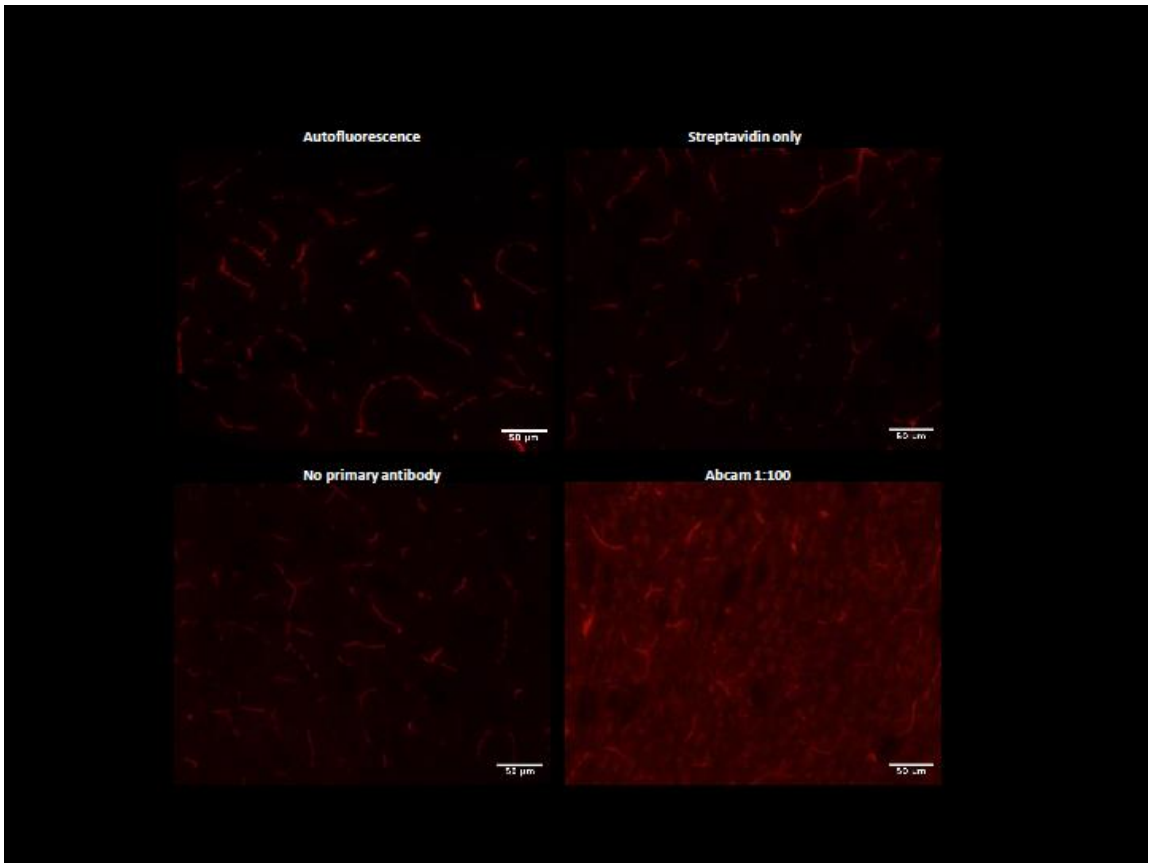

Figure 26. Immunostaining with Abcam D_2R primary antibody using fluorescence microscopy. The striatum from 30 µm sections of a rat brain were fixed by immersion, cryoprotected and incubated with the same Abcam antibody that was previously used in Western blot (Figure 25) at 1:100 (10 µg/ml). Then they were incubated with a secondary antibody (1:1250 biotin-conjugated anti-goat) followed by incubation with Streptavidin Alexa 555 (1:750). Sections were then visualized using fluorescence microscopy. Images show what is supposed to be D_2R staining (red), scale bar represents 50 µm.

After that, we attempted similar staining but of both the striatum and cortex. The cortex was used as the control, because D_2 sites have a much lower density in the cortex as compared to the striatum (Lidow et al., 1989). This was done in both D_2R KO and WT

mice as well as rat slices using the Alomone and Abcam antibodies. The Abcam antibody gave similar staining in rat striatum and cortex. The Alomone antibody also gave similar staining in rat cortex and striatum, and even more staining in mouse KO as compared to WT, which was very surprising, as we were expecting less staining in cortex sections of rat, as well as cortex and striatum sections of KO mice.

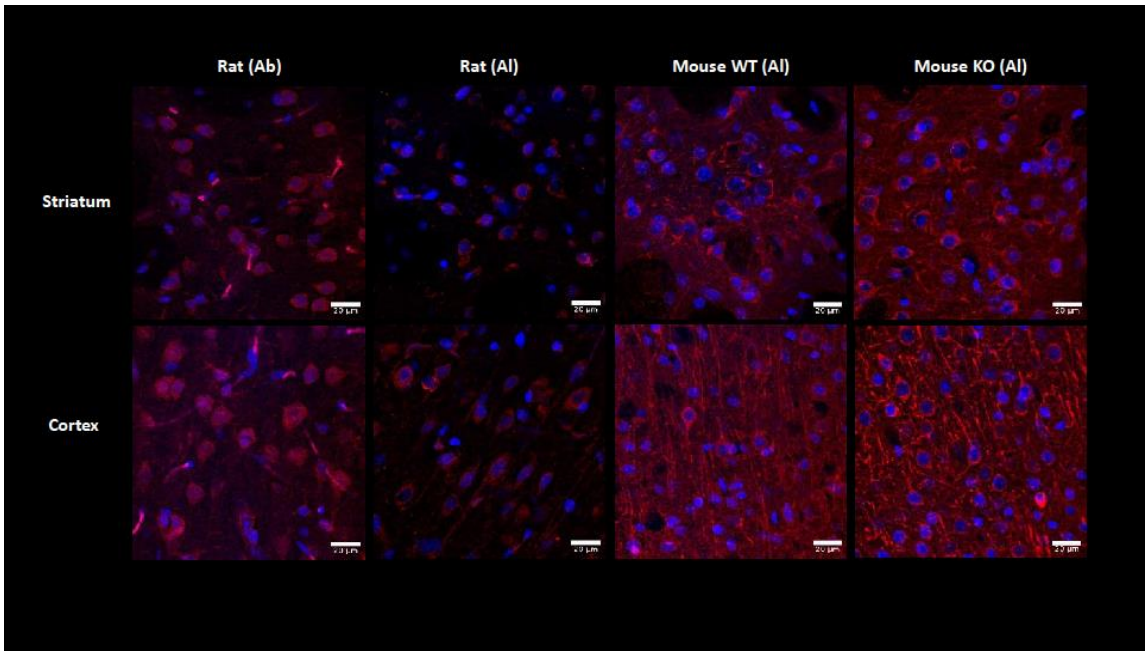

Figure 27. Immunostaining with Alomone and Abcam D_2R primary antibodies using confocal microscopy. The striatum and cortex from 50 µm sections of rat, mouse WT and mouse KO brains were fixed by immersion, cryoprotected and incubated with the same Alomone (Al) and Abcam (Ab) antibodies that were previously used in Western blot (Figure 25) at 1:500. Then they were incubated with secondary antibodies (1:1250 biotin-conjugated anti-rabbit for Alomone and 1:1250 biotin-conjugated anti-goat for Abcam) followed by incubation with Streptavidin Alexa 555 (1:750) and finally counterstained with Hoescht 33258. Sections were then visualized using confocal microscopy. Images show what is supposed to be D_2R staining (red), scale bar represents 20 µm.

β-arrestin antibody does not work well using immunoprecipitation

Since the antibodies against D_2R were not working well, and we were also trying to establish an integration between D_2R and β-arrestin, we also attempted to validate a β-arrestin antibody, so that it can later be used to coimmunoprecipitate D_2R. According to the manufacturer, the antibody gave a band with a molecular weight of 47-50 kDa. When we used it in Western blot, it gave secondary bands at around 22 kDa. The antibody did not work well with immunoprecipitation, as the main band from the eluted sample did not

match that of the raw untreated sample (control). A representative Western blot of several attempts is shown (Figure 28).

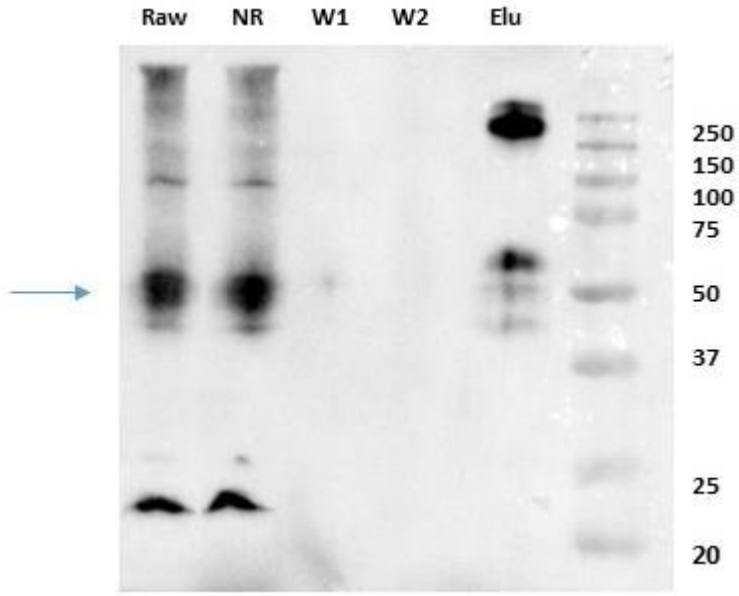

Figure 28. β-arrestin immunoprecipitation and Western blot. Raw: untreated rat striatum, W1: wash 1, W2: wash 2, NR: non-retained sample, Elu: eluted sample. Samples were immunoprecipitated using an antibody against β-arrestin (raised in rabbit, diluted 1:1000 for Western blot). A Western blot was performed to confirm successful immunoprecipitation, which was not the case as the β-arrestin band appears in the non-retained lane and with a different molecular weight in the eluted lane. Molecular weight markers are shown in kDa on the right of the membrane, and signal was detected by chemiluminescence with an HRP-labeled secondary antibody. Arrow indicates β-arrestin band.

1.2 The β-arrestin biased D_2 receptor agonist UNC9994 fully prevents endogenous DA accumulation *ex vivo*

Given that we did not have much success with D_2R and β-arrestin antibodies, we decided to focus on a different approach, which was β-arrestin signaling.

We compared a β-arrestin biased agonist called UNC9994, to a selective D_2R full agonist called Quinpirole. UNC was able to significantly decrease DA accumulation using 1 and 10 μM UNC during a 2 hour incubation period in rat striatal minces *ex vivo,* with an IC_{50} of 1 μM (Figure 29A). The 10 μM concentration even decreased DA accumulation to below the basal (non-incubated) level indicating a very strong action of such ligand with a higher maximal effect than that of quinpirole (MY Omar, PhD thesis). When UNC was tested for a shorter time of 30 minutes and compared alongside a maximal effect of

quinpirole, both compounds also yielded a significant decrease in DA accumulation. Both quinpirole and 1 μM UNC decreased DA accumulation to around 64% of control, while 10 μM UNC produced an even greater decrease to 38% of control, again below the basal level (Figure 29B).

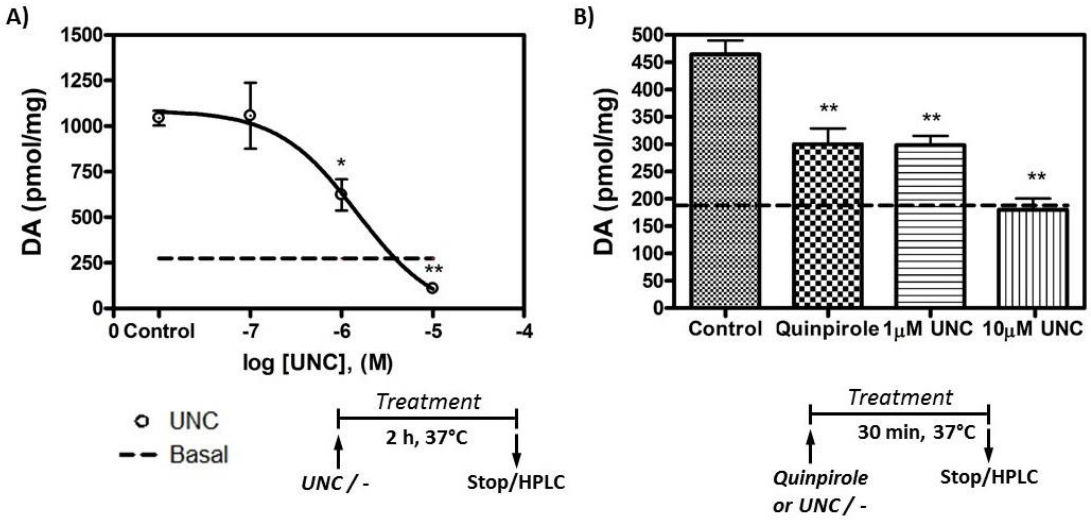

Figure 29. UNC9994 fully prevents endogenous DA accumulation in rat striatal minces *ex vivo*. A) Concentration-response curve of UNC9994 on striatal DA accumulation over an incubation period of 2 hours *ex vivo*, using concentrations of 0.1, 1 and 10 μM UNC (6 incubates per group obtained from a single animal per panel, n=6), control without UNC (6), and basal DA measured same as control samples placed on ice during the 2-hour incubation period (n=6, dashed line). **B)** Bar graph representation of different treatments of 0.1 μM quinpirole, 1 μM UNC, 10 μM UNC, control without treatment and basal (n=6) over a 30 minute incubation period. Data are expressed as mean ± SEM pmol/mg protein for each group. Asterisks indicate *p<0.05, **p<0.01 UNC or quinpirole vs control, one-way ANOVA followed by Dunnett´s post-hoc test. Sigmoidal dose-response curve regression was used to create the adjusted curve.

1.3 UNC9994 increases DOPAC/DA ratio

DOPAC is a metabolite of DA, and the ratio DOPAC/DA is a measure of DA turnover, i.e. the ratio between DA metabolites and DA itself, and therefore a measure of DA metabolism. It is considered to reflect the degree of DA metabolization by MAO and has been used as a biomarker for several diseases such as Parkinson´s (Spina & Cohen, 1989), insulin resistance (Kleinridders et al., 2015) and schizophrenia (McCutcheon et al., 2019). We found that UNC9994 does not affect DOPAC levels (Figure 30A) and significantly increases DA turnover (Figure 30B), and this points to an effect of UNC on DA metabolism. It must be noted that quinpirole treatment decreased both DA and DOPAC levels in parallel (MY Omar, PhD thesis). These effects of UNC may be related to DA release or storage (see Discussion).

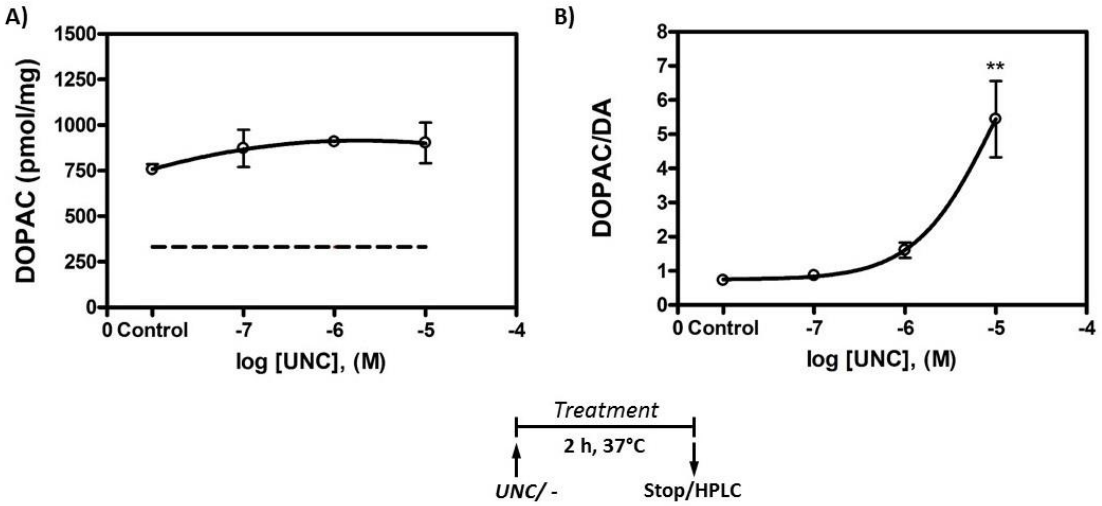

Figure 30. UNC9994 increases DOPAC/DA. A) DOPAC levels of UNC on rat striatal minces *ex vivo* over an incubation period of 2h at 37°C, using concentrations of 0.1, 1 and 10 μM UNC or control without UNC (6 incubates per group obtained from a single animal, n=6) and basal DOPAC measured same as control samples placed on ice during the 2-hour incubation period (n=6, dashed line). **B)** DOPAC/DA ratio of UNC on rat striatal minces *ex vivo* under the same conditions as in A. Data are expressed as mean ± SEM pmol/mg protein for each group. Asterisks indicate **p<0.01 UNC vs control, one-way ANOVA followed by Dunnett´s post-hoc test. Sigmoidal dose-response curve regression was used in every case to create the adjusted curves.

Chapter 2: Effects of GSK3 inhibitors on DA dynamics

A Brief Overview

As previously explained, since we could not validate antibodies against D_2 and β-arrestin, we decided to focus on the β-arrestin signaling pathway instead. And since GSK3 is a downstream target of the β-arrestin pathway, it seemed like a promising target to link UNC9994 effects to TH or other cellular targets. The striking effects of UNC9994 and the lack of published information on GSK3 actions on TH led us to test GSK3 inhibitors on DA dynamics.

In addition, biased ligands that are able to activate the β-arrestin pathway without affecting the G protein pathway present a promising tool to treat DA-related neurological disorders while avoiding the secondary side effects that are associated with typical antipsychotics, as discussed in the Introduction.

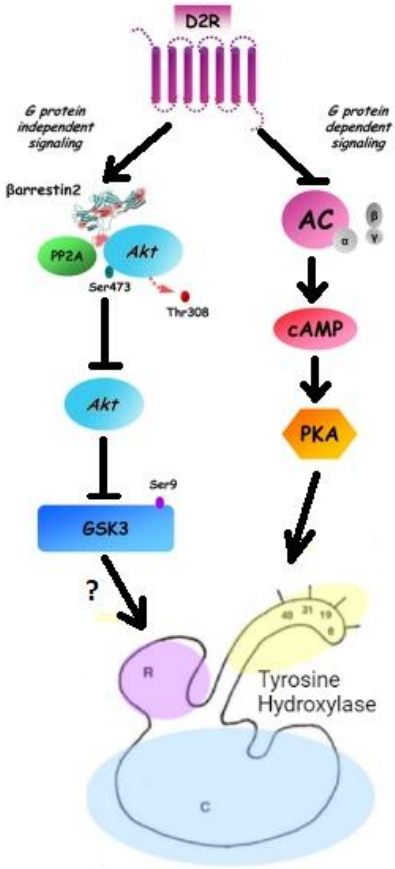

Figure 31. Our hypothesis linking GSK3 to TH and ultimately DA synthesis and/or accumulation (Image is adapted from Beaulieu et al., 2011 and Daubner et al., 2011).

CHIR99021, also known as Laduviglusib or CT99021, is a highly selective GSK3β inhibitor that acts as a Wnt activator, with an IC_{50}~10 nM on GSK3α and ~5 nM on GSK3β (Bennett et al., 2002). It has a molecular formula of $C_{22}H_{19}Cl_3N_8$ and a molecular weight of 501.8 g/mol. CHIR99021 is currently in clinical phase 2b for the restoration of some types of hearing loss (McLean et al., 2021; ClinicalTrials.gov Identifier: NCT05086276) and is a promising molecule that has also been successfully tested in inhibition of adipogenesis (Bennett et al., 2002), coronary and myocardial diseases (Badimon et al., 2019; Drakhlis et al., 2021), cancer (Houben et al., 2022; Lee et al., 2018; Oh et al., 2017;), lung repair therapy (Uhl et al., 2015), stimulation of stem cells (Zhao et al., 2014), and type II diabetes mellitus (Ring et al., 2003). Moreover, CHIR99021 has been proposed as a potential drug for Huntington's disease, acting through off-target effects on calpain inactivation and enhancement of the mitochondrial function (Hu et la., 2021).

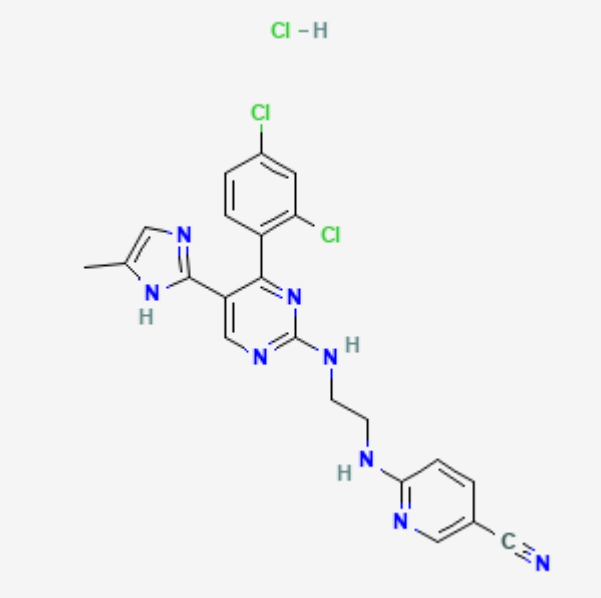

Figure 32. The chemical structure of CHIR99021 HCl. The image is extracted from https://pubchem.ncbi.nlm.nih.gov/compound/CHIR-99021-HCl .

2.1 CHIR99021 strongly decreases endogenous DA accumulation in rat striatal minces *ex vivo*

Treatment of striatal minces with 3 different concentrations of CHIR yielded a significant decrease in DA accumulation with the higher two concentrations (3 µM and 30 µM) but not with 0.3 µM over an incubation period of 2 hours, as determined by HPLC-EC, and

with an IC_{50} of 3 µM (Figure 33A). The 3 µM concentration decreased DA accumulation to 55% of control, while the 30 µM concentration was even able to decrease accumulation below the basal level (to 14% of control). This significant decrease in accumulation was also consistent when minces were incubated for 1, 2 or 4 hours, however, 30 minutes was too short to produce this effect (Figure 33B).

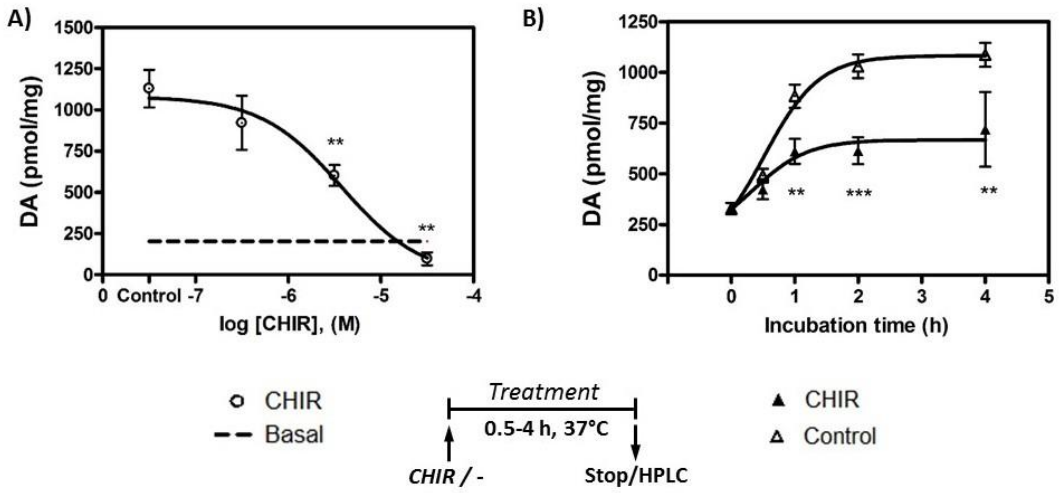

Figure 33. CHIR99021 decreases DA accumulation in rat brain striatal minces. A) Concentration-response curve of CHIR, measuring DA accumulation over an incubation period of 2 hours *ex vivo* at 37°C, using concentrations of 0.3, 3 and 30 µM CHIR or control without CHIR (6 incubates per group obtained from a single animal in panel A, n=6 incubates and 3 animals in panel B). Basal DA was measured as control samples placed on ice during the 2-hour incubation period (6 incubates, dashed line). **B)** Time-response curve on striatal minces *ex vivo* for a CHIR concentration of 3 µM and for 30 minutes, 1 hour, 2 hours, 4 hours and controls for each incubation period, which were treated with the corresponding concentration of DMSO used to dissolve CHIR (n=6) at 37°C, and basal DA measured same as in A) and represented as 0 time (n=6). Data are expressed as mean ± SEM pmol/mg protein for each group, one-way ANOVA followed by Dunnett´s post-hoc test for dose-response graph and two-way ANOVA followed by Bonferroni's post-hoc test for time-response graph. Asterisks indicate **p<0.01, ***p<0.001 CHIR vs control. Sigmoidal dose-response curve regression was used in every case to create the adjusted curves.

2.2 CHIR99021 strongly decreases DA synthesis and inhibits TH activity in rat striatal minces *ex vivo*, but not in striatal homogenates

Since DA accumulation is a result of new DA synthesis and storage, we decided to test its effect on newly synthesized DA using a radioisotopic method to measure [^{3}H]-DA synthesis from [^{3}H]-tyrosine in striatal minces. Using HPLC-UV, we were able to determine that DA synthesis in striatal minces was also significantly reduced in the presence of 0.3 µM, 3 µM and 30 µM CHIR (to 60%, 35% and 15% of control, respectively) (Figure 34A). Given that it was found that CHIR was affecting DA

synthesis, and since DA is synthesized starting from tyrosine and going through L-DOPA as an intermediate product, and this is done with the help of TH and AADC, we used NSD-1015 to block AADC and measured L-DOPA levels as an indicator of TH activity in minces. We saw a significant decrease in L-DOPA accumulation, and therefore of TH activity, with 30 µM CHIR (Figure 34C). To determine whether the mentioned effect was due to a direct interaction of CHIR with TH, the same protocol was performed in striatal homogenates (Figure 34D) and no effect of CHIR was observed. This result suggests that the decrease of L-DOPA levels is not a result from direct interaction between CHIR and TH, but the intact intracellular machinery is needed. Homogenization disrupts the intracellular order leading to loss of CHIR effects.

With this result, as an obvious next question, we had to check if CHIR would affect TH amount and cause TH degradation. This was done by comparing TH amount in control and CHIR-treated incubates. GAPDH was used as a control for protein amount loaded, in addition to a BCA done prior to that. This experiment was performed to show that the decrease in DA synthesis was not due to a decrease in the amount of TH protein. The results show that the amount of TH protein was not altered after any of the CHIR concentrations tested, neither in absolute values nor in relation to GAPDH (Figure 34B). Thus, the abrogation of the TH activity by CHIR is not due to loss of TH protein but to a regulatory mechanism affecting efficiency of the enzyme.

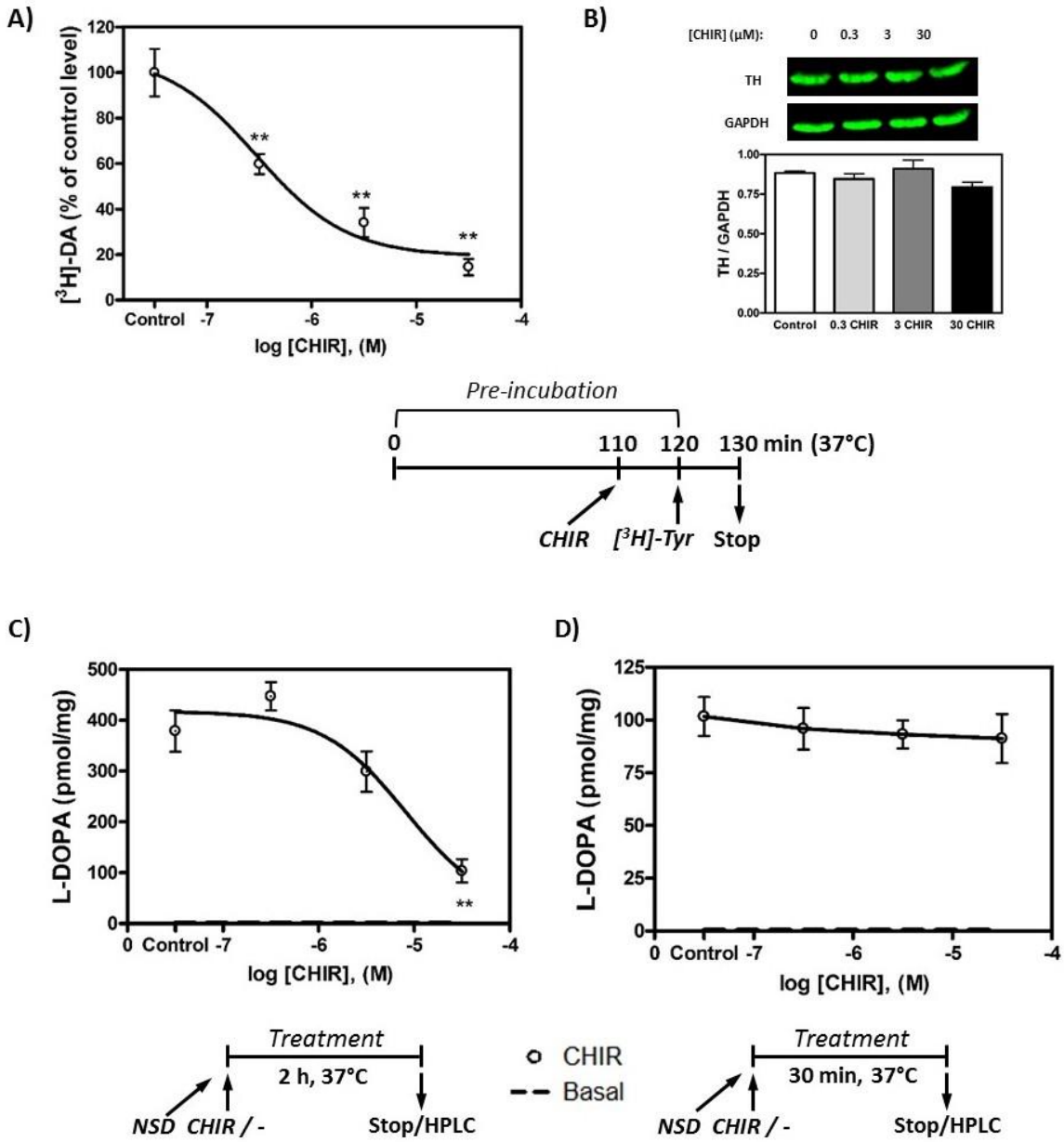

Figure 34. CHIR99021 inhibits TH activity in striatal minces. A) Concentration-response curve of CHIR on striatal [^{3}H]-DA synthesis in minces *ex vivo* over an incubation period of 2 hours at 37°C, using concentrations of 0.3, 3 and 30 μM CHIR (6 incubates per group obtained from a single animal per panel, n=6), control without CHIR (n=6) and basal (n=4) recorded as blank samples and used to correct all results, which were recorded as disintegration per min (DPM) counts. Samples were also corrected by other variables: (1) DA internal standard recovery, (2) amount of protein in each incubated tube, and (3) DPM counts in blank samples as mentioned. The curve is obtained by normalization of the data to percent of control. **B)** TH amount was assessed by Western blot after treatment of minces with 0.3, 3 and 30 μM CHIR or control without CHIR (shown as 0). GAPDH amount was also detected by Western blot and TH / GAPDH ratio was calculated and is represented as a bar graph, which shows means and SEM, after one-way ANOVA analysis with Newman-Keuls post-test, which yielded non-significant in every case. Bands from representative Western blots are also shown. **C)** L-DOPA levels of CHIR concentration-response on striatal minces *ex vivo* over an incubation period of 2h at 37°C, using concentrations of 0.3, 3 and 30 μM

CHIR or control without CHIR (n=6), and basal L-DOPA measured as control samples placed on ice during the 2-hour incubation period (n=6, dashed line near bottom axis), all 30 samples were also treated with 100 μM NSD. **D)** L-DOPA levels of CHIR concentration-response on striatal homogenates over an incubation period of 30 minutes at 37°C, using the same conditions as in C, except that in addition to 100 μM NSD, samples were also treated with 30 μM tyrosine and 100 μM BH4. In all cases, data are expressed as mean ± SEM pmol/mg protein for each group. Asterisks indicate **p<0.01 CHIR vs control, one-way ANOVA followed by Dunnett´s post-hoc test. Sigmoidal dose-response curve regression was used in every case to create the adjusted curves.

2.3 SB216763 and lithium ion decrease DA content with less potency than CHIR99021

To corroborate the role of GSK3 in the decrease of TH activity and DA accumulation, we used another compound called SB216763, which is a potent and selective, ATP-competitive GSK3β inhibitor. SB216763 was able to significantly decrease DA accumulation in rat striatal minces over a 2-hour period, but only at 30 μM, to 75% of control (Figure 35A). When 30 μM SB was attempted again for 2 hours and 4 hours as well, there was no significant decrease in DA accumulation with neither time period (Figure 35B). Given that lithium has antipsychotic properties (Stokes, 1976) and has also been reported to inhibit GSK3 (Galli et al., 2012), its effects on striatal minces were tested, observing that 20 mM was able to significantly decrease DA accumulation to 75% of control over a 2-hour incubation period, whereas no effect was detected at 1 and 5 mM (Figure 35C). This slight but significant decrease in accumulation was increased when minces were incubated for 4 hours (Figure 35D).

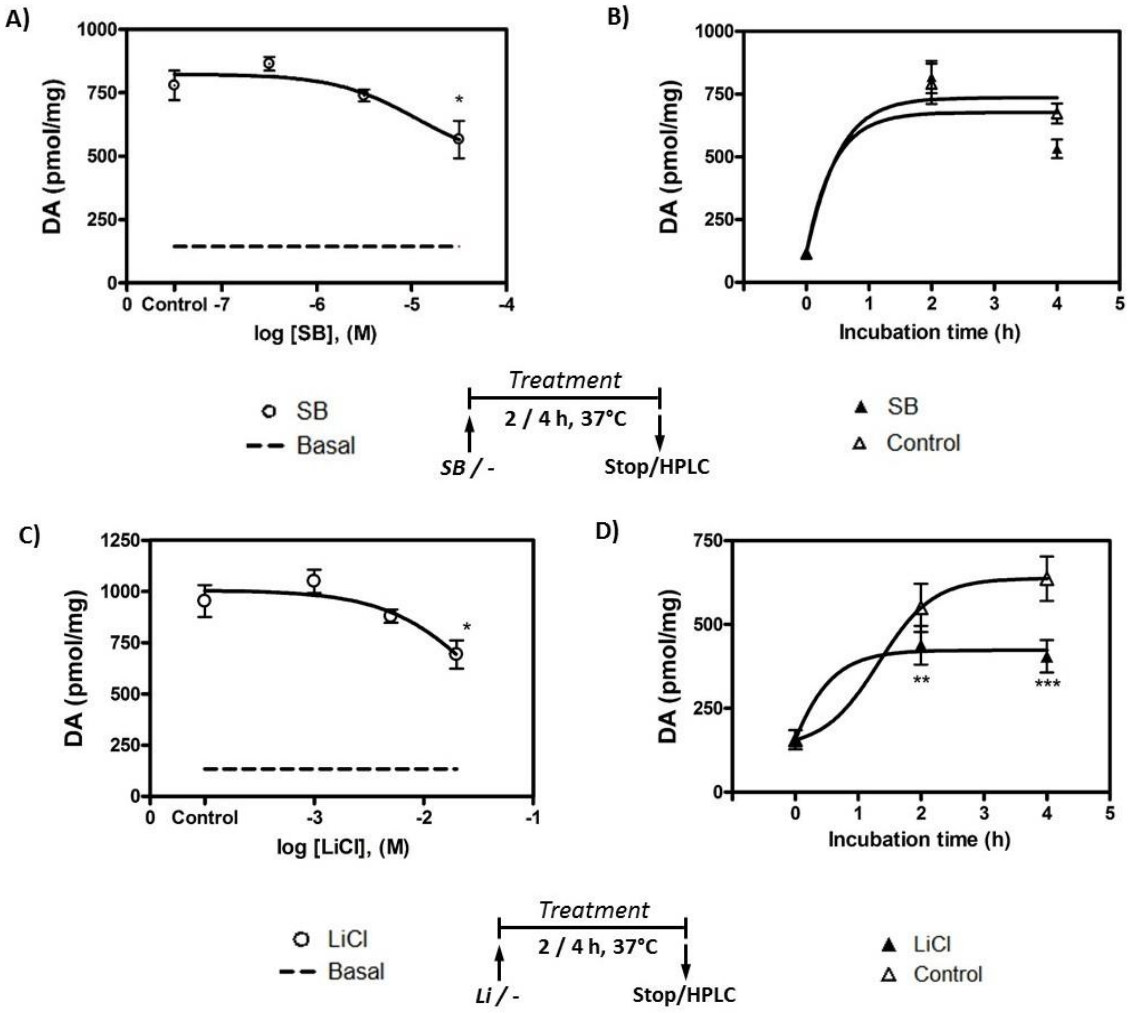

Figure 35. SB216763 and lithium ion decrease DA content with less potency than CHIR99021. A) Concentration-response curve of SB216763 on striatal DA minces *ex vivo* over an incubation period of 2 hours at 37℃ using concentrations of 0.3, 3 and 30 μM SB (6 incubates per group obtained from a single animal per panel, n=6), control without SB (n=6), and basal DA (dashed line) measured as control samples placed on ice during the 2-hour incubation period (n=6). **B)** Time-response curve on striatal minces *ex vivo* for an SB concentration of 30 μM and for 2 and 4 hours and controls for each incubation period (n=6) at 37℃, and basal DA measured same as in A) and represented as 0 time (n=6). **C)** Concentration-response curve of LiCl on striatal DA minces *ex vivo* over an incubation period of 2 hours at 37℃ using concentrations of 1, 5 and 20 mM lithium (n=6), control without lithium (n=6), and basal DA measured same as in A). **D)** Time-response curve on striatal minces *ex vivo* for a LiCl concentration of 20 mM and for 2 and 4 hours and controls for each incubation period (n=6) at 37℃, and basal DA measured same as in A) and represented as 0 time (n=6). Data are expressed as mean ± SEM pmol/mg protein for each group, one-way ANOVA followed by Dunnett´s post-hoc test for dose-response graphs and two-way ANOVA followed by Bonferroni's post-hoc test for time-response graphs. Asterisks indicate *p<0.05, **p<0.01, ***p<0.001 SB or LiCl vs control. Sigmoidal dose-response curve regression was used in every case to create the curves.

2.4 SB216763 and lithium ion decrease DOPAC levels, while CHIR99021 does not

Given that DOPAC is a metabolite of DA, the effects of CHIR, SB and lithium on DOPAC levels was also investigated. Increasing concentrations of SB and lithium both decreased DOPAC levels in parallel to their decrease of DA levels (Figure 36B and 36C) (significant only with the greatest concentration of drug used). On the other hand, DOPAC levels after CHIR treatment remained constant or even tended to increase. (Figure 36A).

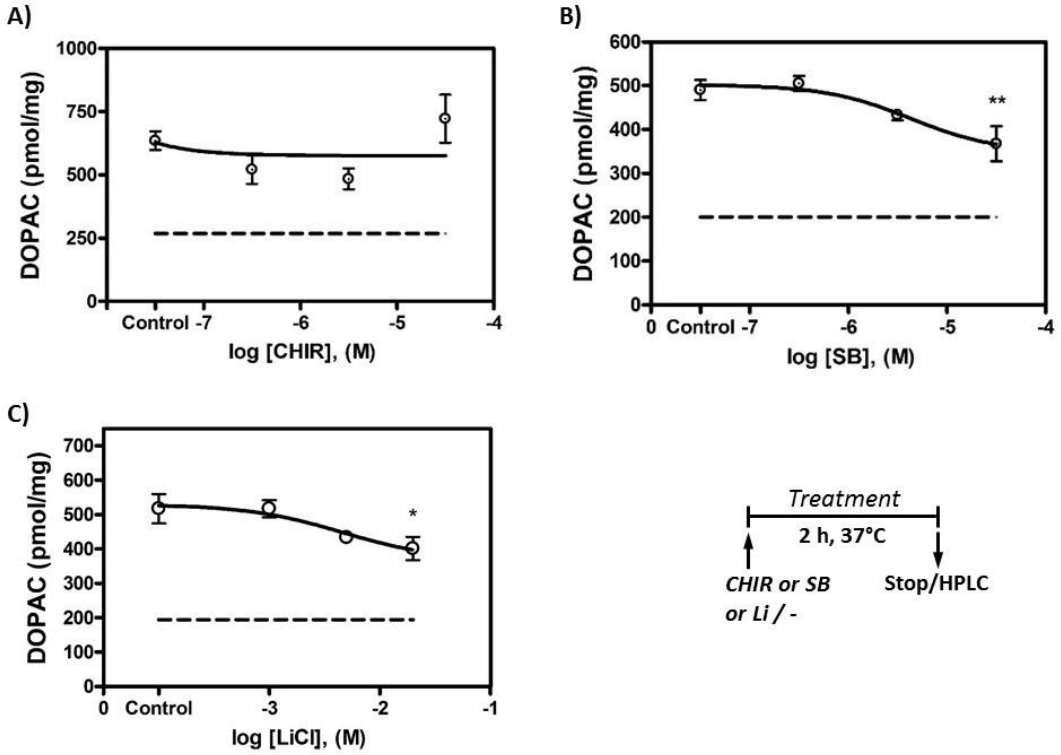

Figure 36. SB216763 and lithium ion decrease DOPAC content while CHIR99021 does not. A) DOPAC levels of CHIR on striatal minces *ex vivo* over an incubation period of 2h at 37ºC, using concentrations of 0.3, 3 and 30 μM CHIR or control without CHIR (n=6 incubations per group obtained from 1 rat per panel), and basal DOPAC measured as control samples placed on ice during the 2-hour incubation period (n=6). **B)** DOPAC levels of SB on striatal minces *ex vivo* over an incubation period of 2h at 37ºC, using concentrations of 0.3, 3 and 30 μM SB or control without SB (n=6), and basal DOPAC measured as in A. **C)** DOPAC levels of lithium on striatal minces *ex vivo* over an incubation period of 2h at 37ºC, using concentrations of 1, 5 and 20 mM lithium or control without lithium (n=6), and basal DOPAC measured as in A. Basal DOPAC (ice control without incubation) is represented by a dashed line in all cases. Data are expressed as mean ± SEM pmol/mg protein for each group. Asterisks indicate *$p<0.05$ or **$p<0.01$ SB or LiCl vs control, one-way ANOVA followed by Dunnett´s post-hoc test. Sigmoidal dose-response curve regression was used in every case to create the adjusted curves.

2.5 CHIR99021 increases DOPAC/DA ratio, whereas SB216763 and lithium ion do not

While CHIR dramatically increases DA turnover at 30 µM (Figure 37A), both SB and lithium have no effect on this ratio at any concentration (Figure 37B and C). This is due to the fact that CHIR dramatically decreases DA at this concentration, while DOPAC remains constant, suggesting that CHIR is promoting DA metabolization.

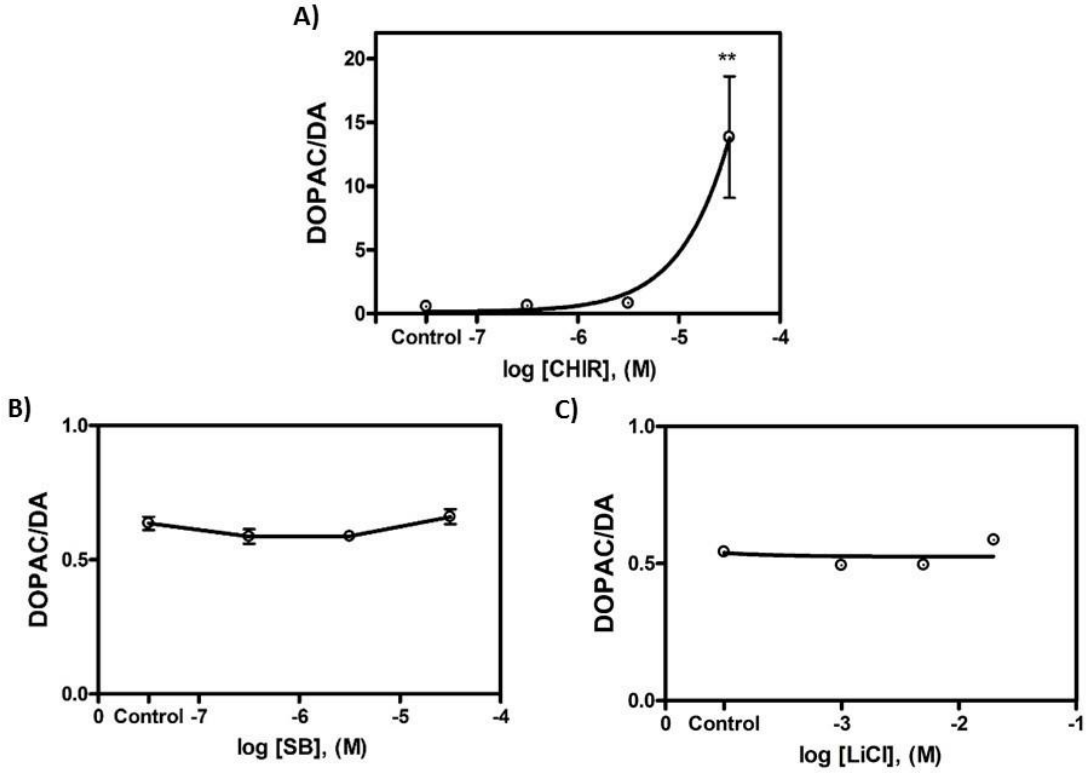

Figure 37. CHIR99021 increases DOPAC/DA while SB216763 and lithium ion do not. A) DOPAC/DA ratio of CHIR on striatal minces *ex vivo* over an incubation period of 2h at 37°C, using concentrations of 0.3, 3 and 30 µM CHIR or control without CHIR (n=6 incubations per group obtained from 1 rat per panel). **B)** DOPAC/DA levels of SB on striatal minces *ex vivo* over an incubation period of 2h at 37°C, using concentrations of 0.3, 3 and 30 µM SB or control without SB (n=6). **C)** DOPAC/DA levels of lithium on striatal minces *ex vivo* over an incubation period of 2h at 37°C, using concentrations of 1, 5 and 20 mM lithium or control without lithium (n=6). Data are expressed as mean ± SEM pmol/mg protein for each group. Asterisks indicate **p<0.01 CHIR vs control, one-way ANOVA followed by Dunnett´s post-hoc test. Sigmoidal dose-response curve regression was used in every case to create the curves.

2.6 SB216763 and lithium ion do not alter TH activity

We have previously shown that CHIR was able to inhibit TH activity in rat striatal minces *ex vivo* (Figure 34C). Given that SB and lithium seemed to be less potent than CHIR, their effect on TH activity was also examined, again, by measuring L-DOPA levels. Neither SB nor lithium were able to decrease L-DOPA accumulation with statistical significance (Figure 38).

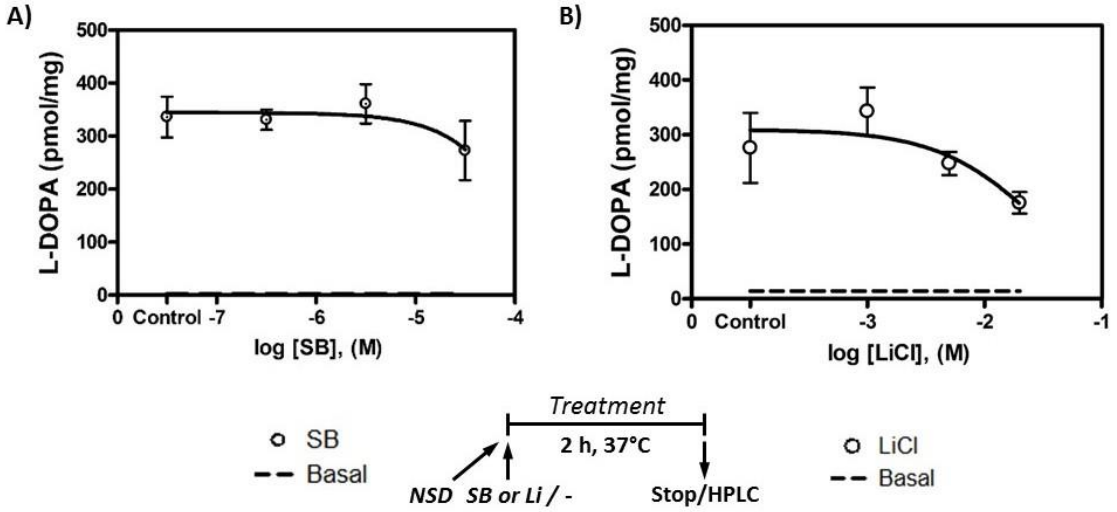

Figure 38. SB216763 and lithium ion do not inhibit TH activity in striatal minces. A) L-DOPA levels of SB on striatal minces *ex vivo* over an incubation period of 2h at 37°C, using concentrations of 0.3, 3 and 30 μM SB or control without SB (n=6 incubations per group obtained from 1 rat per panel), and basal L-DOPA measured as control samples placed on ice during the 2-hour incubation period (n=6, dashed line near bottom axis). All 30 samples were also treated with 100 μM NSD. **B)** L-DOPA levels of LiCl on striatal minces *ex vivo* over an incubation period of 2h at 37°C, using concentrations of 1, 5 and 20 mM LiCl or control without LiCl (n=6), and basal L-DOPA measured as in A. All 30 samples were also treated with 100 μM NSD. In all cases, data are expressed as mean ± SEM pmol/mg protein for each group. One-way ANOVA was performed, followed by Dunnett´s post-hoc test. Sigmoidal dose-response curve regression was used in every case to create the adjusted curves.

2.7 CHIR99021 impairs the incorporation of exogenous DA into striatal minces

We were able to show that CHIR decreases DA accumulation and synthesis in rat striatal minces *ex vivo*, and that this effect was due to decreased TH activity. The purpose of the work that followed this result was to determine how CHIR was affecting TH. In this section, we describe an experiment aimed at testing the effect of CHIR on DA storage, which has a strong influence on TH. Our laboratory had previously shown that the VMAT2 inhibitor tetrabenazine (TBZ) completely impairs [^{3}H]-DA synthesis, and that

non-stored DA negatively feeds-back on the TH enzyme, and DA storage dynamics strongly influence DA biosynthesis (González-Sepúlveda et al., 2022). Given the fact that we have found that CHIR also affects DA synthesis (Figure 34A) and therefore TH activity, we therefore decided to check whether CHIR may also be affecting DA transport and storage into striatal tissue similarly to TBZ. Minces were pre-incubated with 1 µM TBZ or 30 µM CHIR for 1 hour and 5 µM exogenous DA was added for the next hour. Following incubation, excess DA was washed away, and incorporated DA was measured. However, Figure 39A shows that even though CHIR and TBZ were in fact depleting DA, they were doing so to below the control (without DA) level, suggesting that they were not only affecting exogenous DA, but endogenous DA as well (the vesicles were already filled with endogenous DA at 2 hours). We therefore decided to decrease the incubation time to 30 minutes and added 5 µM DA for the next 30 minutes (Figure 39B). In this case, the DA accumulated in the CHIR and the TBZ groups remained greater than the control without DA group, so the two compounds were only affecting exogenous DA. TBZ significantly decreased DA accumulation, as expected, but a similar effect was also seen with CHIR, suggesting that CHIR is also affecting DA storage and transport, possibly by exhibiting a negative feedback inhibition on TH.

DOPAC levels from the same experiments showed that even though CHIR treatment for 2 hours does not affect DOPAC levels (Figure 39C) in a similar manner to Figure 36A where CHIR was also incubated for 2 hours, a 1 hour CHIR treatment (Figure 39D), however, does significantly decrease DOPAC levels.

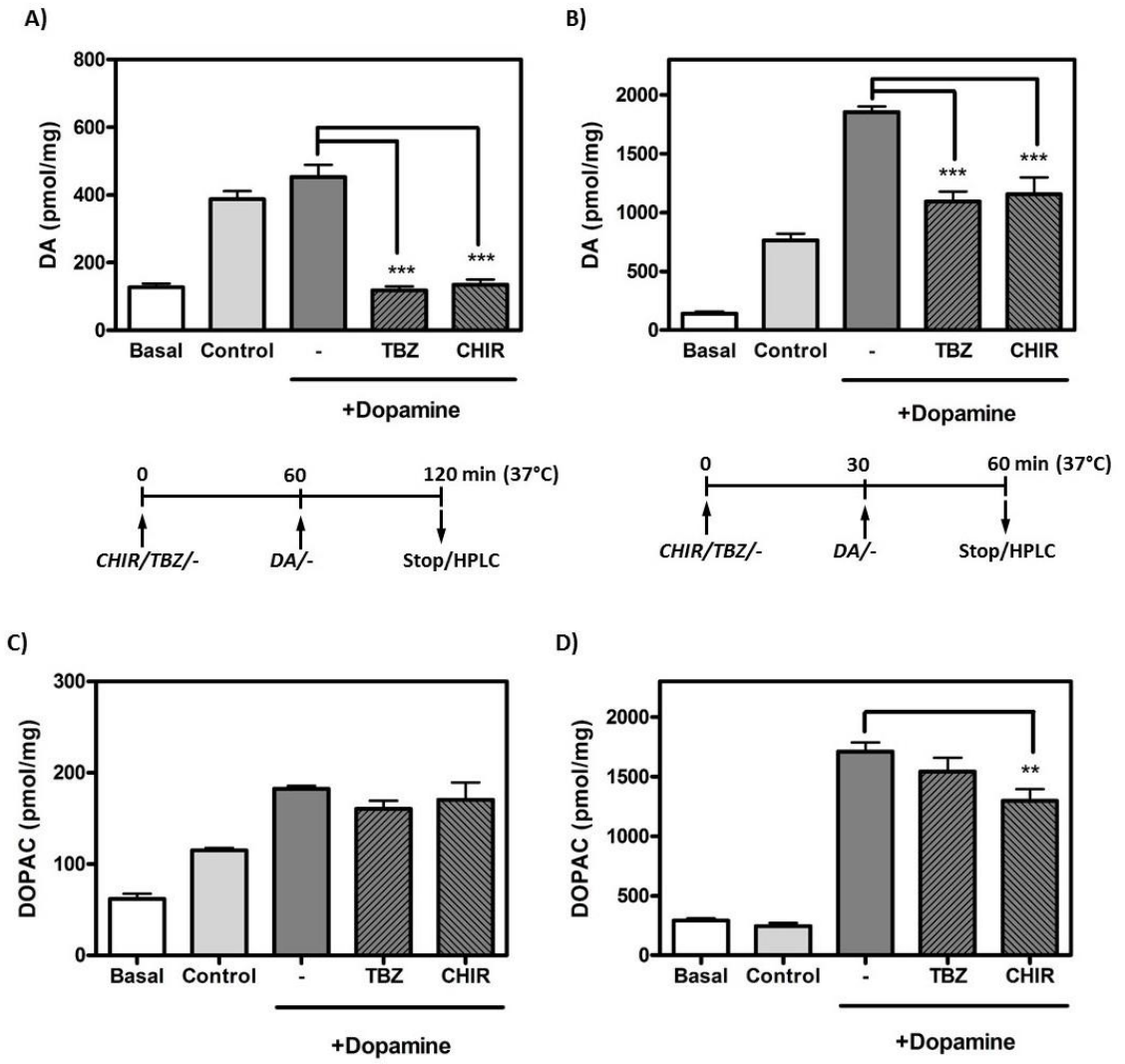

Figure 39. CHIR99021 decreases DA storage in rat brain striatal minces. When indicated, striatal minces were incubated for 2 h (**A**, **C**) or 1 h (**B**, **D**) at 37°C with tetrabenazine 1 µM (TBZ), with CHIR99021 30 µM (CHIR) or with Krebs-Ringer buffer (-). For the last hour (**A**, **C**) or 30 min (**B**, **D**) of incubation 5 µM DA was also added in all the three cases. Basal DA or DOPAC was measured as control samples placed on ice during the 2 or 1 h incubation period, while Control samples were incubated at 37°C without any drug or added DA. Subsequently, minces were recovered by centrifugation and washed once with Krebs-Ringer buffer. The amounts of DA incorporated inside tissue or DOPAC were determined in every case by HPLC (pmol/mg protein, n=6 incubations per group obtained from 1 rat per panel). Data are expressed as mean ± SEM for each group. One-way ANOVA test was performed followed by Newman-Keuls post-test, **p<0.01, ***p<0.001.

Chapter 3: Effect of different treatments on TH phosphorylation

A Brief Overview

The use of GSK3 inhibitors was initially hypothesized to affect TH phosphorylation, although literature does not show such effects. The following Western blots were performed using near-infrared secondary antibodies. As explained in details in Materials and Methods, we used a dual infrared system to determine changes in phosphorylation by quantifying phosphorylated and total signals from the same band. We also used mass spectrometry to confirm changes in TH phosphorylation.

3.1 Western blot analysis of TH phosphorylation with GSK3 inhibitors

Positive control: TH phosphorylation in the presence of PD98059

As previously mentioned, TH can be phosphorylated by protein kinases such as PKA, ERK or CaMKII, and it can be dephosphorylated by PP2A and PP2C protein phosphatases (Dunkley et al., 2004). Since the dual infrared system to determine phosphorylation was never used in our hands before, we decided to first check the reliability of the technique. Thus, we determined the phosphorylation status of TH under the treatment of the MEK inhibitor PD98059. TH phosphorylation in Ser19, Ser31 and in Ser40 vs. total TH was determined in the presence of 25 μM of PD98059 by Western blot, since ERK1/2 affect phosphorylation in Ser31. A positive control of the effectiveness of PD98059 was performed by detection of phosphoERK1/2 in Thr202 and in Tyr204. PD98059 decreased ERK1/2 phosphorylation (see Figure 40) (-74% from control), as expected for a MEK inhibitor, and it also changed pS31 in TH (-37% from control), whereas S19 and S40 remained unaltered, proving that our phosphorylation ratio system was working properly.

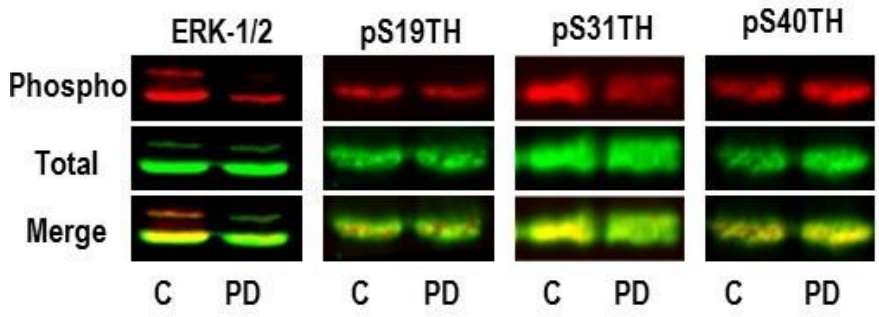

Figure 40. TH phosphorylation after MEK inhibition. Samples from rat striatum were treated with 25 μM PD98059 (PD) or DMSO as control (C) and incubated for 2 hours. Antibodies used were against TH (raised in mouse, diluted 1:1000), pS19-TH (raised in rabbit, diluted 1:500), pS31-TH, (raised in rabbit, diluted 1:500), pS40-TH, (raised in rabbit, diluted 1:1000), pERK1/2, (raised in rabbit, diluted 1:1000), and ERK1/2 (raised in mouse, diluted 1:000). Subsequently, secondary antibodies were anti-mouse NIR680-labeled and anti-rabbit NIR800-labeled, both diluted 1:10000. The Western blot represents ERK or TH phosphorylation with or without PD98059. Red signal corresponds to pERK (lane 1), or tyrosine hydroxylase phosphorylated in S19, S31, or S40 (lanes 2-4); green signal corresponds to total ERK (lane 1) or total tyrosine hydroxylase (lanes 2-4), while merge of both signals appears in yellow.

CHIR99021 and SB216763, but not lithium, inhibit GSK3β activity on β-catenin in striatum minces

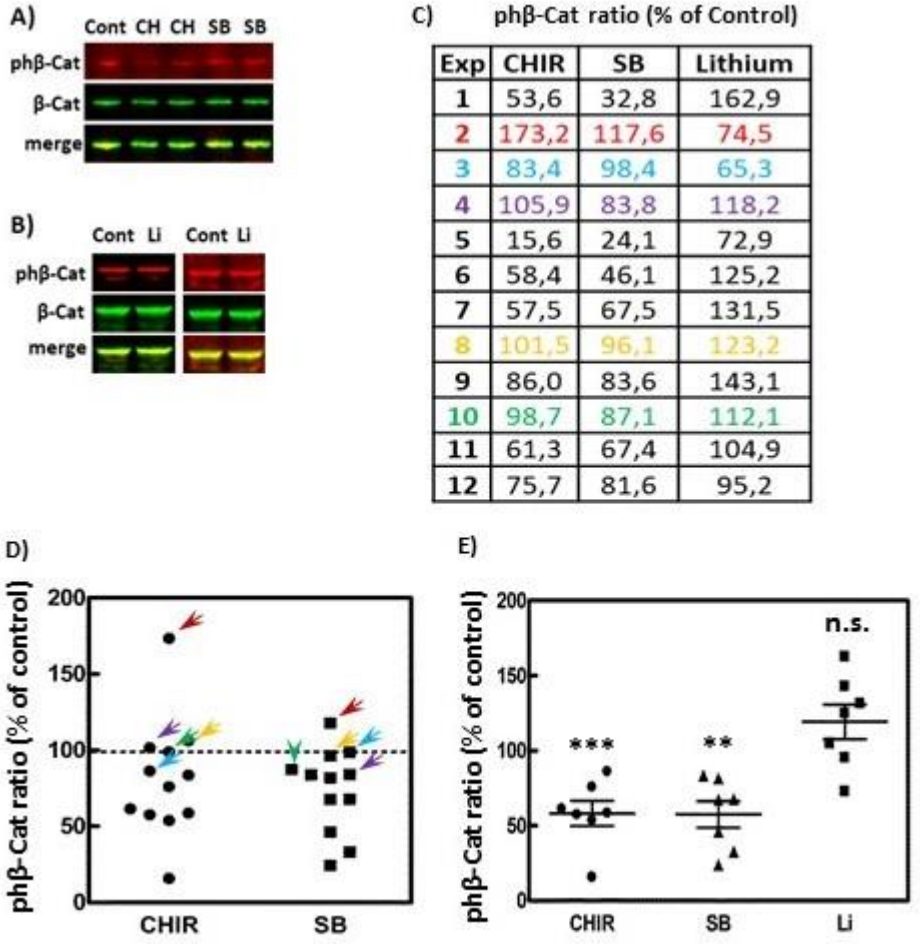

Exp	CHIR	SB	Lithium
1	53,6	32,8	162,9
2	173,2	117,6	74,5
3	83,4	98,4	65,3
4	105,9	83,8	118,2
5	15,6	24,1	72,9
6	58,4	46,1	125,2
7	57,5	67,5	131,5
8	101,5	96,1	123,2
9	86,0	83,6	143,1
10	98,7	87,1	112,1
11	61,3	67,4	104,9
12	75,7	81,6	95,2

Figure 41. Changes in phosphorylation of β-catenin in S33/S37/T41 after treatment with GSK3 inhibitors or lithium ion. Rat striatal minces from 6 animals were treated with GSK3 inhibitors, CHIR99021 (CH, 3 μM) or SB216763 (3 μM), both for 2h. In parallel striatal minces were also treated with lithium ion (Li, 5 mM for 2h). Levels of phosho-βcatenin were assessed with Western blot using Near IR-labeled secondary antibodies, as described in Figure 24 in Materials and Methods. **A)** Representative Western blots are shown after CHIR or SB treatment. Red signal corresponds to β-catenin phosphorylated in S33, S37 and T41, green signal corresponds to total β-catenin, while merge of both signals appears in yellow. **B)** Representative Western blots are shown after lithium treatment. **C)** Twelve experiments were performed, and only those which showed significant decrease of phosphorylation (more than 15% of decrease in both inhibitors) were considered successful and used in future determinations of TH phosphorylation. The eliminated experiments are colored. **D)** Scatter plot of every individual experiment listed in C. Arrows point to the eliminated experiments and the color code corresponds to the same as C. **E)** Scatter plot representation of the β-catenin phosphorylation ratios after treatment with CHIR99021, SB216763 or lithium. These ratios correspond only to the experiments considered as successful, shown in C) and D). Graphics shows means and SEM, after one-way ANOVA analysis with Newman-Keuls post-test. (** $p<0.01$, *** $p<0.001$, n.s. non-significant).

Given the certain heterogeneity of our samples, the striatum minces, we decided to check the effective action of the GSK3 inhibitors prior to determining TH phosphorylation. With this aim, the phosphorylation of β-catenin, a known GSK3 substrate (Kazi et al., 2018), was determined by Western blot and the dual infrared system (Figures 41A and 42B). Once the ratios of each experiment were calculated, only those that showed more than 15% of decrease in phosphorylation for both inhibitors were considered as successful and used for further determinations (Figures 41C and 41D). Samples successfully treated with CHIR and SB showed a significant decrease in the phosphorylation of β-catenin, while there was no significant decrease for those treated with lithium (Figure 41E).

Altogether, these results presented here support the fact that CHIR and SB are capable of reducing GSK3 activity in our samples from rat striatum.

CHIR99021 and SB216763 decrease TH phosphorylation in Ser19, but not in Ser31 and Ser40

TH is known as the rate-limiting enzyme in the synthesis of DA, and the major way of controlling the activity of TH is protein phosphorylation at different serine residues (Ser8, Ser19, Ser31 and Ser40) (Dunkley & Dickson, 2019). So, to explore if GSK3 inhibitors (CHIR and SB) are affecting TH activity, we investigated the phosphorylation at the different serine residues of TH. We used the phosphorylation ratio as an indicator of the degree of TH activation and expected a decrease in this ratio when the sample was treated with both inhibitors. As mentioned in the Introduction, the phosphorylation of TH could be hierarchical. In this model, it is strongly thought that phosphorylation at Ser19 and Ser31 causes the enzyme to be in a more open conformation and allows Ser40 to be phosphorylated easily. Increases in Ser40 and Ser31 phosphorylation increase TH activity (Dunkley et al., 2004).

For this purpose, Western blot experiments were performed in order to detect differences in the phosphorylation of Ser19 from TH (Figure 42A). Samples treated with CHIR and SB showed a modest but significant decrease in phosphorylation at Ser19 (34% and 31% respectively), but treatment with lithium did not decrease the phosphorylation significantly (Figure 42B).

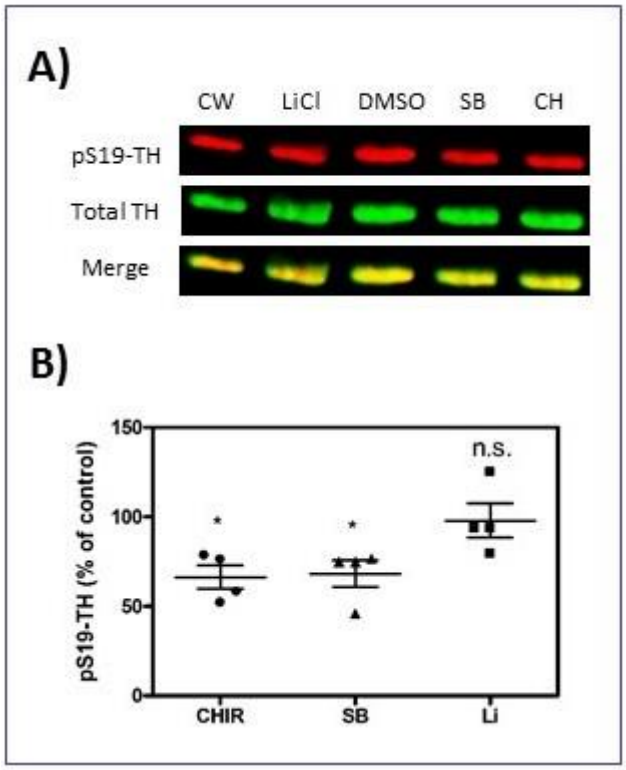

Figure 42. Changes in phosphorylation of TH in Ser19 after treatment with GSK3 inhibitors and lithium ion. Samples from rat striatum were treated with CHIR99021 (CH, 3μM), SB216763 (3μM), Lithium Chloride (LiCl, 5mM), DMSO (control for CH and SB) and water (CW, control for LiCl). Antibodies used were against TH (raised in mouse, diluted 1:1000) and pS19-TH (raised in rabbit, diluted 1:500). Subsequently, secondary antibodies were anti-mouse NIR680-labeled and anti-rabbit NIR800-labeled, both diluted 1:10000. **A)** Representative Western blot after treatment with CH, SB and lithium ion is shown. Red signal corresponds to TH phosphorylated in Ser19; green signal corresponds to total TH, while merge of both signals appears in yellow. **B)** Scatter plot representation of the TH phosphorylation at Ser19 ratios after treatment with CH, SB or lithium. Graphic shows individual incubations (Western blots) from different rats as well as means and SEM, after one-way ANOVA analysis with Newman-Keuls post-test. (* $p<0.05$, n.s. non-significant).

Once we saw a decrease in phosphorylation of Ser19 from TH, the next step was to see if there was also a decrease in phosphorylation of Ser31.

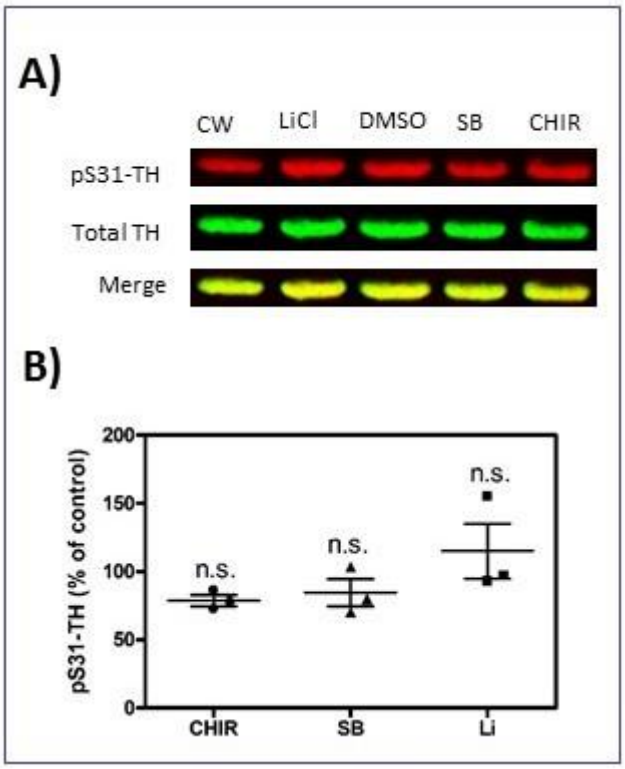

Figure 43. Changes in phosphorylation of TH in Ser31 after treatment with GSK3 inhibitors and lithium ion. Samples from rat striatum were treated with CHIR99021 (CH, 3μM), SB216763 (3μM), Lithium Chloride (LiCl, 5mM), DMSO (control for CH and SB) and water (CW, control for LiCl). Antibodies used were against TH (raised in mouse, diluted 1:1000) and pS31-TH (raised in rabbit, diluted 1:500). Subsequently, secondary antibodies were anti-mouse NIR680-labeled and anti-rabbit NIR800-labeled, both diluted 1:10000. **A)** Representative Western blot after treatment with CH, SB and lithium ion is shown. Red signal corresponds to TH phosphorylated in Ser31; green signal corresponds to total TH, while merge of both signals appears in yellow. **B)** Scatter plot representation of the TH phosphorylation at Ser31 ratios after treatment with CH, SB or lithium. Graphic shows individual incubations (Western blots) from different rats as well as means and SEM, after one-way ANOVA analysis with Newman-Keuls post-test. (n.s. non-significant).

In this case, treatment with both GSK3 inhibitors or with lithium did not decrease the phosphorylation ratio at Ser31 from TH (Figure 43) in respect to the untreated/control samples. This suggested that treatment with GSK3 inhibitors did not have an effect on Ser31 phosphorylation.

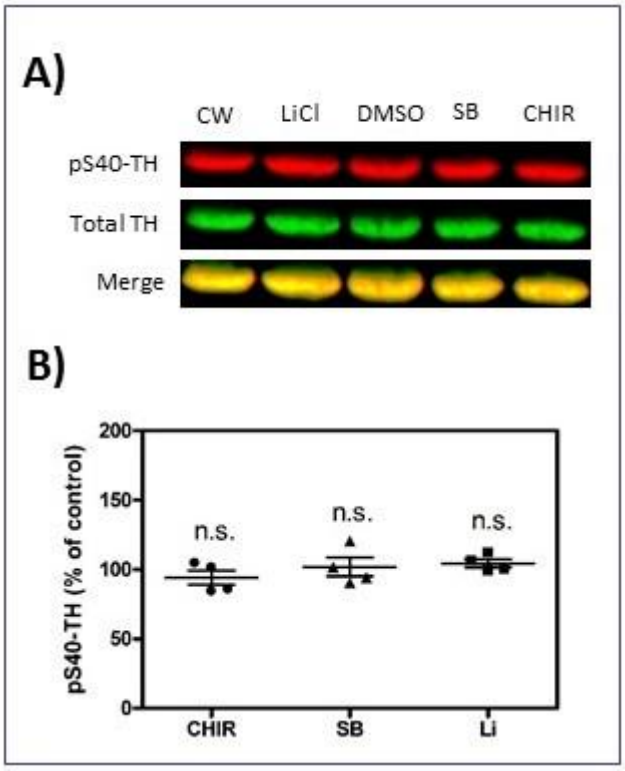

Figure 44. Changes in phosphorylation of TH at Ser40 after treatment with GSK3 inhibitors and lithium ion. Samples from rat striatum were treated with CHIR99021 (CH, 3μM), SB216763 (3μM), Lithium Chloride (LiCl, 5mM), DMSO (control for CH and SB) and water (CW, control for LiCl). Antibodies used were against TH (raised in mouse, diluted 1:1000) and pS40-TH (raised in rabbit, diluted 1:1000). Subsequently, secondary antibodies were anti-mouse NIR680-labeled and anti-rabbit NIR800-labeled, both diluted 1:10000. **A)** Representative Western blot after treatment with CH, SB and lithium ion is shown. Red signal corresponds to TH phosphorylated in Ser40; green signal corresponds to total TH, while merge of both signals appears in yellow. **B)** Scatter plot representation of the TH phosphorylation at Ser40 ratios after treatment with CH, SB or lithium. Graphic shows individual incubations (Western blots) from different rats as well as means and SEM, after one-way ANOVA analysis with Newman-Keuls post-test. (n.s. non-significant).

Western blots were successful because we saw clear bands (Figure 44A) when using the infra-red emitting antibodies, but, after analyzing the bands and calculating the phosphorylation ratio (Figure 44B) no significant changes were detected in phosphorylation levels for all three treatments (CHIR, SB and lithium), and we were expecting a significant decrease at least with CHIR treatment.

Thus, the results presented here support the notion that CHIR and SB might be affecting phosphorylation of Ser19 from TH, but not in Ser31 and Ser40. In consequence, the lack of SB216763 effect on DA metabolism seems to be due to absence of GSK3β action on TH and not to a lack of compound efficacy.

Reliability of an antibody against pS8-TH

In addition to the phosphorylation centers seen in the last section, TH can also be phosphorylated at Ser8. As discussed in the Introduction, there is no evidence that phosphorylation at this serine residue increases TH activity (Dunkley et al., 2004). However, the consensus sequence of the substrates that GSK3 phosphorylates matches that of Ser8, and Ser8 is also an ERK 1/2 target. With this in mind, we thought about the possibility that Ser8 from TH could be a potential target of phosphorylation by GSK3. This also contributed to our decision to check TH activity after we saw that CHIR was affecting DA synthesis (Figure 34A). However, we first performed an experiment in order to check the reliability of a commercially available antibody against pS8-TH.

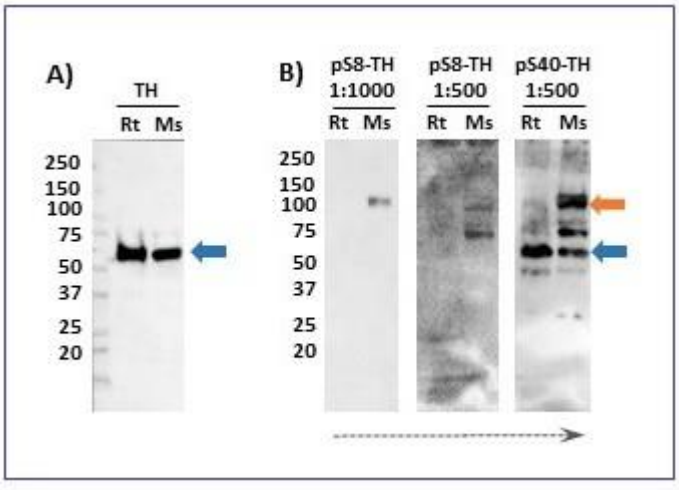

Figure 45. Antibody against pS8-TH test of reliability. A) Western blot of untreated samples from rat or mouse striatum with antibody against TH at 1:1000. Blue arrow indicates TH signal. **B)** Western blots of the same samples as A. The membrane was initially incubated with an antibody against pS8-TH at 1:1000. The same membrane was subsequently reincubated with anti-pS8-TH at 1:500. Next, a third consecutive time the membrane was reincubated with anti-pS40-TH at 1:500. Red arrow indicates the initial signal obtained with pS8-TH at 1:1000 and blue arrow indicates TH signal, according to the MW. Molecular weight markers are shown in kDa on the left in both cases, and signal was detected by chemiluminescence with an HRP-labeled secondary antibody.

As expected, the antibody against total TH worked properly and showed a band between 75 and 50 kDa but closer to 50 kDa in both rat and mouse striatum (Figure 45A). However, the first incubation with an antibody against pS8-TH at 1:1000 did not show any band at the expected height (Figure 45B); it just showed a band around 100kDa, which is not the weight we were expecting to obtain. A second incubation with the same

antibody but at 1:500 showed the same band around 100 kDa and an additional one a little lower than 75 kDa in mouse striatum (Figure 45B). This was not what we were expecting either. Finally, to check if it was an experimental error or if the antibody against pS8-TH was not working, the membrane was incubated a third time with an antibody against pS40-TH at 1:500. As expected, we obtained a band between 75 and 50 kDa but closer to 50 kDa in both rat and mouse striatum channels (Figure 45B). In conclusion, the commercial antibody did not yield, in our hands, the results that the brand claimed to be obtained.

3.2 Western blot analysis of TH phosphorylation with D_2 agonists

In a similar manner to how we tested how our GSK3 inhibitors are affecting TH activity by investigating the phosphorylation at the different serine residues of TH, we again used the phosphorylation ratio as an indicator of the degree of TH activation caused by UNC9994 and quinpirole. For this purpose, Western blot experiments were performed in order to detect differences in the phosphorylation of Ser19 from TH (Figure 46A). Samples treated with quinpirole did not decrease phosphorylation at Ser19 from TH nor did samples treated with UNC (Figure 46B).

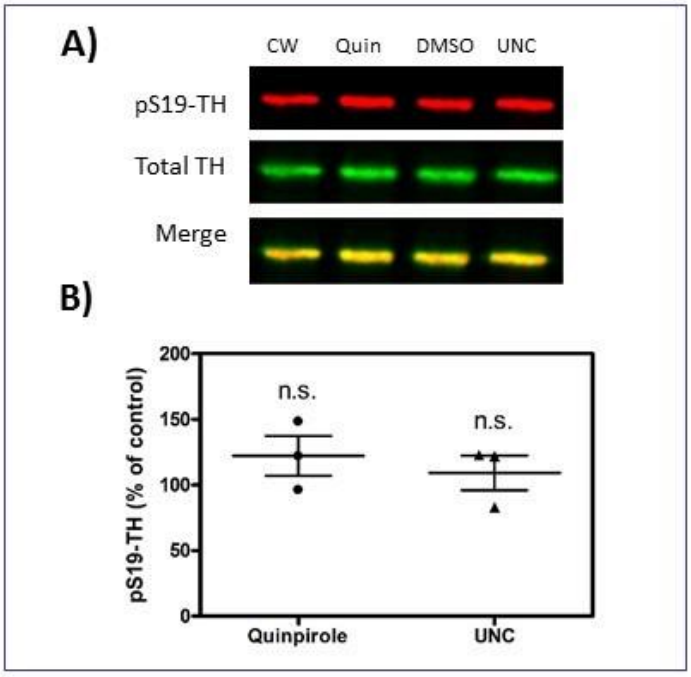

Figure 46. Changes in phosphorylation of TH in Ser19 after treatment with quinpirole and UNC9994. Samples from rat striatum were treated with quinpirole (0.1 μM), UNC (10 μM), DMSO (control for UNC) and water (CW, control for quinpirole). Antibodies used were against TH (raised in mouse, diluted 1:1000) and pS19-TH (raised in rabbit, diluted 1:500). Subsequently, secondary antibodies were anti-mouse NIR680-labeled and anti-rabbit NIR800-labeled, both diluted 1:10000. **A)** Representative Western blot after treatment with quinpirole and UNC is shown. Red signal corresponds to TH phosphorylated in Ser19; green signal corresponds to total TH, while merge of both signals appears in yellow. **B)** Scatter plot representation of the TH phosphorylation at Ser19 ratios after treatment with quinpirole and UNC. Graphic shows individual incubations (Western blots) from different rats as well as means and SEM, after one-way ANOVA analysis with Newman-Keuls post-test. No significant changes were found with quinpirole or UNC. (n.s. non-significant).

The next step was to see if there was a decrease in phosphorylation of Ser31. In this case, treatment with either UNC or quinpirole did not decrease the phosphorylation ratio at Ser31 from TH (Figure 47B) in respect to the untreated/control samples. This suggested that treatment with UNC and quinpirole did not have an effect on Ser31 phosphorylation either.

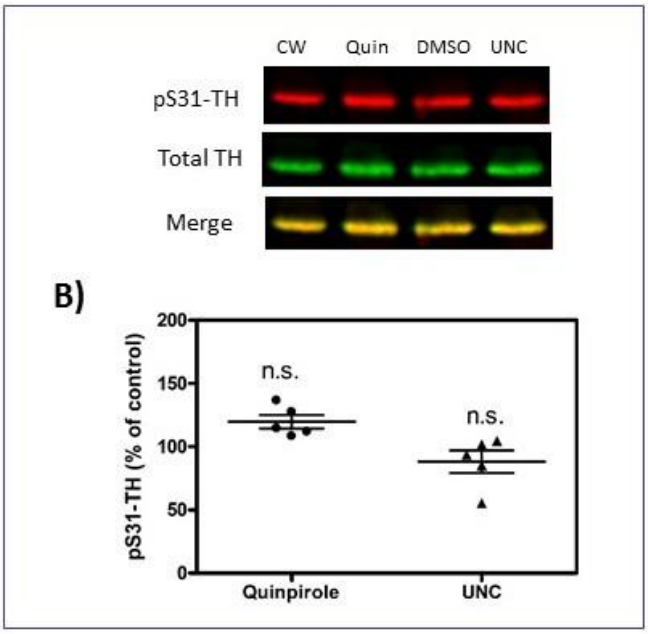

Figure 47. Changes in phosphorylation of TH in Ser31 after treatment with quinpirole and UNC9994. Samples from rat striatum were treated with quinpirole (0.1 μM), UNC (10 μM), DMSO (control for UNC) and water (CW, control for quinpirole). Antibodies used were against TH (raised in mouse, diluted 1:1000) and pS31-TH (raised in rabbit, diluted 1:500). Subsequently, secondary antibodies were anti-mouse NIR680-labeled and anti-rabbit NIR800-labeled, both diluted 1:10000. **A)** Representative Western blot after treatment with quinpirole and UNC is shown. Red signal corresponds to TH phosphorylated in Ser31; green signal corresponds to total TH, while merge of both signals appears in yellow. **B)** Scatter plot representation of the TH phosphorylation at Ser31 ratios after treatment with quinpirole and UNC. Graphic shows individual incubations (Western blots) from different rats as well as means and SEM, after one-way ANOVA analysis with Newman-Keuls post-test. No significant changes were found with quinpirole or UNC. (n.s. non-significant).

The final phosphorylation site to be analyzed by Western blot was Ser40. After analyzing the bands and calculating the phosphorylation ratio (Figure 48B) we again did not detect significant changes in phosphorylation levels with neither compound. It must be noted that basal TH phosphorylation in our samples might be very low (see Discussion) so further decreases in TH phosphorylation triggered by drugs might be difficult to obtain. Thus, the results presented here support the notion that quinpirole and UNC might not be affecting phosphorylation of any serine residue from TH.

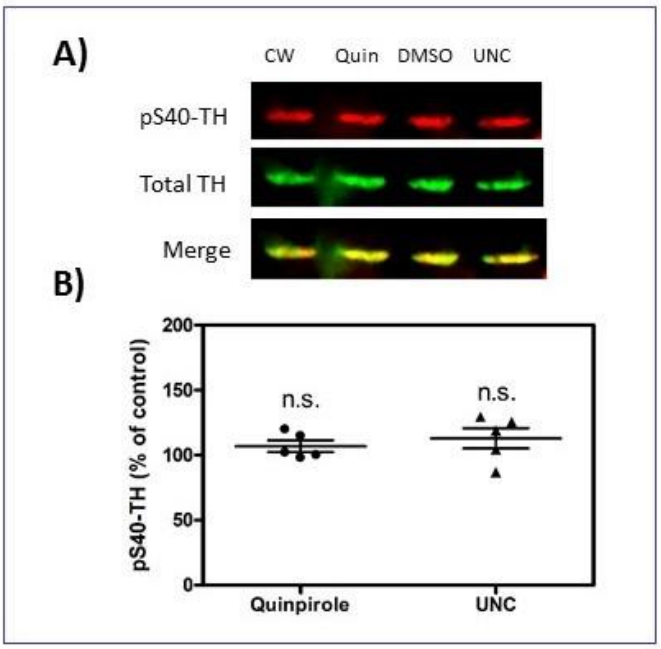

Figure 48. Changes in phosphorylation of TH in Ser40 after treatment with quinpirole and UNC9994. Samples from rat striatum were treated with quinpirole (0.1 μM), UNC (10 μM), DMSO (control for UNC) and water (CW, control for quinpirole). Antibodies used were against TH (raised in mouse, diluted 1:1000) and pS40-TH (raised in rabbit, diluted 1:500). Subsequently, secondary antibodies were anti-mouse NIR680-labeled and anti-rabbit NIR800-labeled, both diluted 1:10000. **A)** Representative Western blot after treatment with quinpirole and UNC is shown. Red signal corresponds to TH phosphorylated in Ser40; green signal corresponds to total TH, while merge of both signals appears in yellow. **B)** Scatter plot representation of the TH phosphorylation at Ser40 ratios after treatment with quinpirole and UNC. Graphic shows individual incubations (Western blots) from different rats as well as means and SEM, after one-way ANOVA analysis with Newman-Keuls post-test. No significant changes were found with quinpirole or UNC. (n.s. non-significant).

3.3 TH immunoprecipitation and mass spectrometry analysis reveal Threonine 30 as a new phosphorylation site

We decided to use mass spectrometry as another method to detect the effects of CHIR on TH phosphorylation. This included a series of steps, as follows.

Identifying Total TH

Before comparing CHIR-treated samples with control, a preliminary control basal experiment was performed with immunoprecipitation and mass spectrometry analysis to confirm that we had correctly immunoprecipitated total TH. This was done with 2 rat striatal cytosol using an IP/coIP kit (details in Materials and Methods) and a monoclonal mouse primary antibody (Figure 49A) and a polyclonal sheep primary antibody (Figure

49B) and according to the kit´s immunoprecipitation protocol. This was followed by silver staining (Figure 49C) using the same eluted samples from Figure 49 (A) and (B).

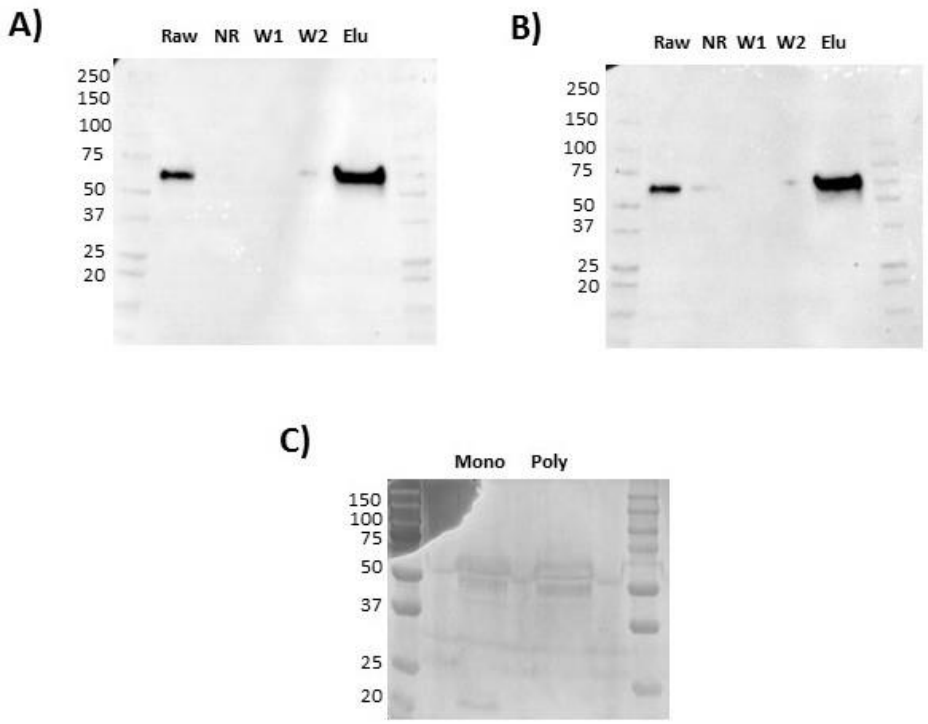

Figure 49. TH immunoprecipitation and silver staining. Raw: untreated rat striatum cytosol, W1: wash 1, W2: wash 2, NR: non-retained sample, Elu: eluted sample**.** Samples were immunoprecipitated using TH **A)** monoclonal and **B)** polyclonal antibodies (Table 4, Materials and Methods). Western blots were performed to confirm successful immunoprecipitation. Antibodies used were against TH (monoclonal was raised in mouse, diluted 1:1000 and polyclonal was raised in sheep, diluted 1:1000). Molecular weight markers are shown in kDa on the left of the membranes, and signal was detected by chemiluminescence with HRP-labeled secondary antibodies. **C)** The 2 protein bands from the eluted samples corresponding to the correct molecular weight were separated by SDS-PAGE then silver staining, followed by in-gel digestion and the bands were excised and analyzed by MALDI-TOF which correctly identified the eluted samples as TH with Mascot scores of 99 and 88 for the monoclonal and polyclonal antibodies respectively (Protein scores greater than 61 are significant ($p<0.05$)).

Moving forward, we decided to use the monoclonal antibody since it gave a higher score and had previously given better results in Western blot. Using Mascot Server, which is a search engine that uses mass spectrometry data to identify proteins from peptide sequence databases, several peptides in the TH sequence were identified that were present in the immunoprecipitated sample using the monoclonal antibody (Figure 50).

Figure 50. Mascot search of TH. Tyrosine hydroxylase sequence with positively identified peptides by Mascot search in colors using the monoclonal TH antibody.

The effect of incubation on TH phosphorylation

Our methodology for measuring DA synthesis and accumulation using HPLC includes an incubation step at 37°C for different periods of time that can reach up to 4 hours. We were able to show using Western blot that these incubation periods have no effect on the phosphorylation levels of pS19, pS31 or pS40, but we wanted to confirm using mass spectrometry as another control experiment to verify that any changes in phosphorylation of TH in CHIR-treated samples will solely be due to CHIR. For this purpose, we decided to compare the phosphorylation levels of Ser19, Ser31 and Ser40 of 2 groups, one which had been incubated for 4 hours and the other which had not been incubated. We also wanted to see if we could quantify phosphorylation of Ser8, since we could not do so using Western blot.

In order to detect specifically the sites of interest (Ser8, Ser19, Ser31 and Ser40) the protein was virtually digested and analyzed by liquid chromatography-mass spectrometry (LC-MS). Although not initially a site of interest, a novel phosphorylation site ´Threonine 30´ was identified. Unfortunately, Ser8 phosphorylation could not be identified due to the technical challenge to obtain a peptide including this residue.

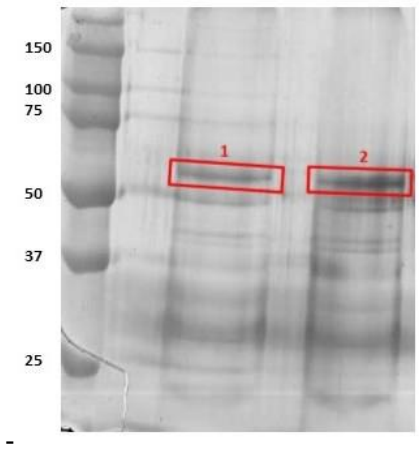

Figure 51. 0h and 4h incubation excised bands for analysis. The striatum of 2 rats were extracted, minced and prepared in a similar manner to our HPLC protocol. 24 incubates were prepared and divided into 2 groups, the first group was incubated for 4 hours, while the second group were kept on ice for the same period of time (non-incubated/0 hours). At the end of the incubation period the samples of each group were combined into a single sample which were then immunoprecipitated. The 2 protein bands from the eluted samples corresponding to the correct molecular weight were separated by SDS-PAGE and in-gel digestion as shown in the figure (where 1= 0 hour incubation and 2 = 4 hour incubation) after silver staining. The bands were then excised and analyzed by MALDI-TOF, which correctly identified them as tyrosine hydroxylase with a score of 83.

A)

B)

Detected p-sites and phosphorylated sequences:

Ser19 -AVsEQDAKQAEAVTSPR

Thr30 -AVSEQDAKQAEAVtSPR/ QAEAVtSPR

Ser31-AVSEQDAKQAEAVTsPR/ QAEAVTsPR

Ser40 -RQsLIEDAR

Figure 52. Sequence of interest from TH. A) UniProt rat TH sequence with tryptic peptides and phosphorylation sites (red) identified. **B)** The phosphorylated sites in red with their corresponding name in bold.

After database search, 7 peptides (276 peptide spectrum matches, PSMs) from TH were detected in sample 1 (0 h incubation) and 7 peptides (218 PSMs) in sample 2 (4 h incubation). Among these peptides were AVSEQDAKQAEAVTSPR (66/43 PSMs sample 1/sample 2), AVSEQDAKQAEAVTsPR (42/43 PSMs),

AVsEQDAKQAEAVTsPR (5/7 PSMs), QAEAVTSPR (49/38 PSMs), QAEAVTsPR (9/9 PSMs) and RQSLIEDAR (13/9 PSMs). So, phosphorylated sites Ser19 and Ser31 were confirmed.

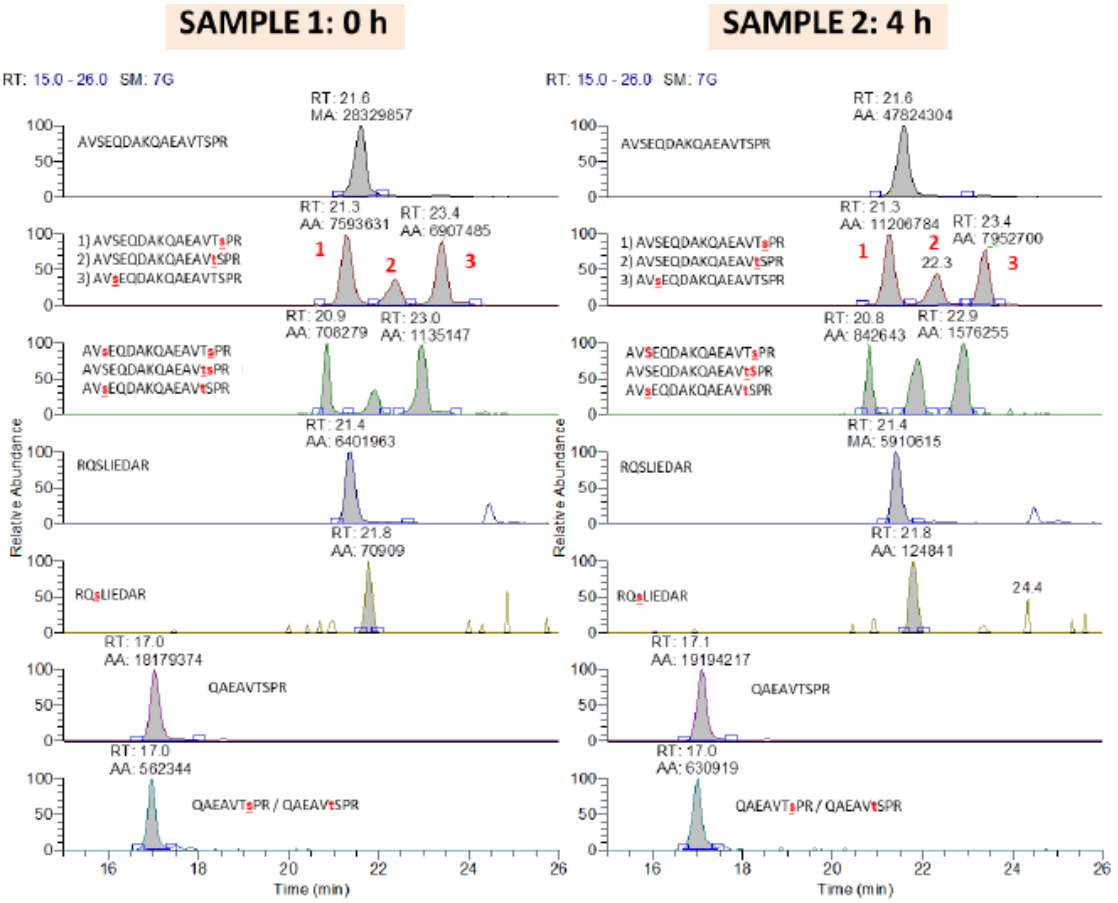

Figure 53. LC-MS assessment of rat TH N-terminal phosphorylation in non-incubated (1) and 4h-incubated striatal samples (2). Rat TH peptide fragments identified by HPLC-MS after TH-immunoprecipitation and tryptic digestion. RT: retention time; MA/AA: Manual or automatic peak area. s: phosphorylated serine; S: non-phosphorylated serine. Ratios of serine phosphorylation signals (s/S) were obtained from peak areas shown, which reflect peptide abundance and ionization efficiency. Threonine30 phosphorylation was observed (t, peak #2; T, non-phosphorylated threonine).

In addition to the database search, the extracted ion chromatograms from each theoretical sequence of interest were plotted (Figure 53). The graph shows that Ser19, Thr30 and Ser31, present in the sequence AVSEQDAKQAEAVTSPR, can be quantified separately (Table 6). However, in the case of double phosphorylation of this peptide, three signals were detected, but it was not possible to assign each signal to its corresponding peptide because no fragmentation data is available. The phosphorylation of Ser40 (RQsLIEDAR) was not identified in database search after applying FDR (false discovery rate) filters due

to the low amount of this peptide, however it was possible to quantify the ratio of phosphorylated to non-phosphorylated peptide by means of the area of extracted ion chromatogram.

Phosphorylation site	Phosphorylation sequence	Phosphorylated signal at 0 h	Phosphorylated signal at 4 h
Ser19	**AVsEQDAKQAEAVTSPR**	25.1	18
Thr30	**AVSEQDAKQAEAVtSPR/ QAEAVtSPR**	11.7	13.6
Ser31	**AVSEQDAKQAEAVTsPR/ QAEAVTsPR**	27.6	25.3
Ser40	**RQsLIEDAR**	1.1	2

Table 6. Percentage ratio of areas of phosphorylated/non-phosphorylated peptides. Percentage ratio of phosphorylated/non-phosphorylated areas obtained from the extracted ion chromatogram from sample 1 (0 h) and sample 2 (4 h) with their corresponding sequence and phosphorylation site name.

The ratio of Ser31 phosphorylated vs. non-phosphorylated peptides was almost unchanged (27.6% in ice control and 25.3% in 4 h incubation). Ser40 phosphorylation was much lower than Ser31, and not decreased by time (1.1% in ice control, 2% after 4 h incubation). Thus, mass spectrometry confirmed the main Western blot results: incubation time did not alter TH phosphorylation in Ser31 and Ser40, and Ser31 was significantly phosphorylated during the whole incubation. In addition, Ser19 phosphorylation could be detected (25.1% in ice control vs. 18% in the 4 h-incubated sample, % relative to the unphosphorylated signal of peptide). Furthermore, Thr30 phosphorylation was also detected (11.7% in ice control vs. 13.6% in 4 h-incubated sample). To our knowledge, this is the first report of TH phosphorylation in Thr30 which we published in (González-Sepúlveda et al, 2022).

The effect of CHIR on TH phosphorylation

Now that we had established that our TH antibody and immunoprecipitation kit were able to successfully immunoprecipitate total TH, and that incubating samples for several hours does not affect the phosphorylation of TH, the next step was to compare CHIR-treated samples with control. Two groups were prepared, ´control´ and ´CHIR´, and following incubation, samples were immunoprecipitated. With the aim of increasing the protein

sequence coverage, two enzymes were used in the digestion process. Therefore, each sample was divided in two aliquots and each one digested with Trypsin or Glu-C.

After digestion was complete, the samples were analysed by LC-MS/MS with two different acquisition modes. In the first run, the samples were acquired in a data dependent acquisition mode from a global list (DDA), all the ions acquired were taken into account for fragmentation. In a second run, in order to detect specifically the sites of interest (phosphorylated sites from positions 1 to 40 in TH), the protein was virtually digested and lists with the theoretical tryptic and Glu-C peptides were generated. In addition to the theoretical peptides (amino acids from 1 to 40), FEVPSGDLAALLSSVR and TGFQLRPVAGLLSAR were also added into Trypsin samples to check the method performance as these two peptides were detected with a high number of PSMs in a previous DDA analysis (control). Only the ions included in the inclusion list were fragmented in this acquisition mode (further details in Annex 1).

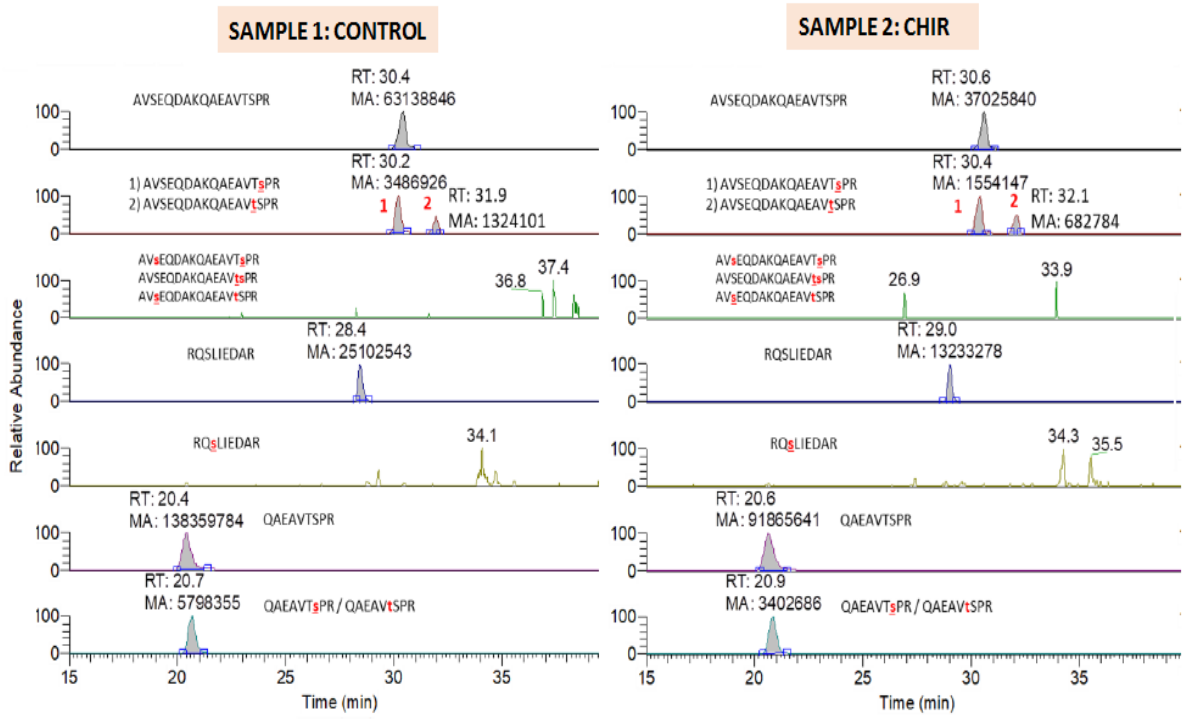

Figure 54. LC-MS assessment of rat TH N-terminal phosphorylation in Control (1) and CHIR-treated striatal samples (2) digested with Trypsin. Rat TH peptide fragments identified by HPLC-MS after TH-immunoprecipitation and tryptic digestion. RT: retention time; MA: Manual peak area. s: phosphorylated serine; S: non-phosphorylated serine. Ratios of serine phosphorylation signals (s/S) were obtained from peak areas shown, which reflect peptide abundance and ionization efficiency. Threonine30 phosphorylation was observed (t, peak #2; T, non-phosphorylated threonine).

After database search of samples digested with Trypsin and acquired in inclusion list mode, only the phosphorylation at Ser31 was confirmed (AVSEQDAKQAEAVTsPR and QAEAVTsPR). In addition to the database search, the extracted ion chromatograms from each theoretical sequence of interest were plotted (Figure 54). Thr30 and Ser31, present in the sequence AVSEQDAKQAEAVTSPR, were quantified separately again (Figure 54). In order to quantify the abundance of the different phosphorylated peptides, the chromatographic peaks were integrated and the areas obtained. With these values the ratios between phosphorylated/non-phosphorylated peptides were obtained (Table 7).

Phosphorylation site	Phosphorylation sequence	Control phosphorylated signal	CHIR phosphorylated signal
Ser19	**AVsEQDAKQAEAVTSPR**	-	-
Thr30	**AVSEQDAKQAEAVtSPR/ QAEAVtSPR**	2.1	1.8
Ser31	**AVSEQDAKQAEAVTsPR/ QAEAVTsPR**	5.5	4.2
Ser40	**RQsLIEDAR**	-	-

Table 7. Percentage ratio of areas of phosphorylated/non-phosphorylated peptides. Percentage ratio of phosphorylated/non-phosphorylated areas obtained from the extracted ion chromatogram from sample 1 (Control) and sample 2 (CHIR) with their corresponding sequence and phosphorylation site name.

The ratio of Ser31 phosphorylated vs. non-phosphorylated peptides decreased but only slightly (5.5% in control and 4.2% in CHIR). Thr30 phosphorylation was also detected again and also slightly decreased in CHIR-treated samples (2.1% in control vs. 1.8% in CHIR). It is however difficult to analyze whether these decreases are significant, given that the phosphorylation level is low. Unfortunately, Ser19 and Ser40 phosphorylations were not detected, even though the experiment was repeated several times.

3.4 Investigating whether phosphorylation of Thr30 is affecting pS31 antibody binding

As previously mentioned, our mass spectrometry analysis of TH revealed a novel phosphorylation site at Thr30. The close proximity of this site to Ser31 led us to investigate whether our pS31 antibody was also binding to Thr30, or even binding to Thr30 instead of Ser31 altogether. For this purpose, a series of peptides mimicking

phosphorylated TH sequences, pS31 and pT30, were used in Western blot analysis (details in Materials and Methods).

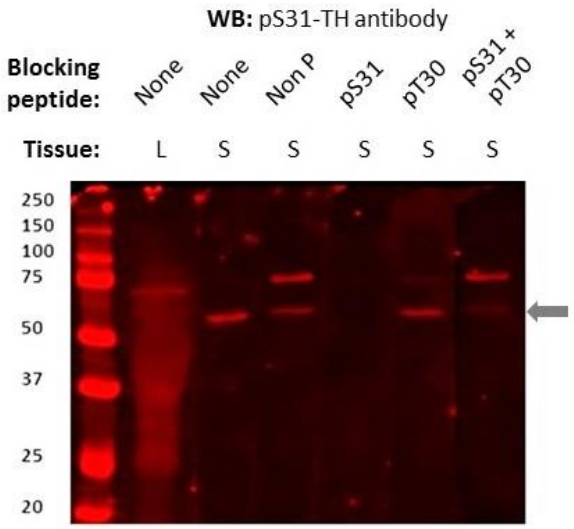

Figure 55. Peptides and tissue used in determining pS31 antibody binding. None: without blocking peptide, Non P: Non-phosphorylated peptide, L: Liver, S: Striatum. 20 µl of tissue (liver or striatum) were loaded per well onto an SDS-gel and subsequently transferred to a membrane. The membrane was cut into 6 parts and parts 1 and 2 (the first two lanes) were incubated in pS31-TH antibody (raised in rabbit, diluted 1:500). The rest were also incubated in pS31-TH antibody, but that had been previously blocked by 30 µg of one of the 4 peptides as mentioned. Subsequently, all membranes were incubated in secondary anti-rabbit NIR800-labeled, diluted 1:10000. Bands around 55 kDa (arrow) correspond to pS31-TH, while bands around 75 kDa are unspecific.

Liver tissue in non-blocked pS31-TH antibody was used as a negative control, whereas striatum in non-blocked pS31-TH was the positive control. The results show that blocking the antibody with a pS31 peptide causes the band to disappear, whereas this does not happen with the pT30 peptide. Although there is a faint band with the pS31 & pT30 peptide, this could be because the peptide is diluted due to the combination of both. Therefore, we determined that the antibody recognizing pS31 is not significantly affected by phosphorylation in Thr30 (Figure 55).

Chapter 4: TH association with mitochondria

A Brief Overview

In order to have a deeper analysis and characterization of TH, we decided to identify the possible proteins in complex with it. We also thought that identifying TH protein partners might give us greater insight on its regulation and activity.

4.1 TH coimmunoprecipitation and mass spectrometry analysis identify 14-3-3 and α-synuclein, as well as a large number of mitochondrial proteins

The brain stem and striatum from one rat were extracted and coimmunoprecipitated with TH antibody. This is because the brain stem has been reported to be rich with TH neurons (Konradi et al., 1988; Pearson et al., 1983). After the coimmunoprecipitated sample was passed through LC-MS/MS, a total number of 131 proteins (958 peptides) were identified (complete list of proteins in Annex 1). We mention here (Table 8) a few of the most important proteins, in terms of score and known association with TH, as well as percentage distribution of all 131 proteins (Figure 56).

Description	Score
Tubulin beta-2A chain OS=Rattus norvegicus OX=10116 GN=Tubb2a PE=1 SV=1 - [TBB2A_RAT]	396.77
Tyrosine 3-monooxygenase OS=Rattus norvegicus OX=10116 GN=Th PE=1 SV=3 - [TY3H_RAT]	369.40
Tubulin beta-4B chain OS=Rattus norvegicus OX=10116 GN=Tubb4b PE=1 SV=1 - [TBB4B_RAT]	356.24
Tubulin beta-5 chain OS=Rattus norvegicus OX=10116 GN=Tubb5 PE=1 SV=1 - [TBB5_RAT]	352.37
Tubulin alpha-1A chain OS=Rattus norvegicus OX=10116 GN=Tuba1a PE=1 SV=1 - [TBA1A_RAT]	279.67
Tubulin beta-3 chain OS=Rattus norvegicus OX=10116 GN=Tubb3 PE=1 SV=1 - [TBB3_RAT]	256.76
Microtubule-associated protein 6 OS=Rattus norvegicus OX=10116 GN=Map6 PE=1 SV=1 - [MAP6_RAT]	240.62
Tubulin alpha-4A chain OS=Rattus norvegicus OX=10116 GN=Tuba4a PE=1 SV=1 - [TBA4A_RAT]	184.11
Alpha-synuclein OS=Rattus norvegicus OX=10116 GN=Snca PE=1 SV=1 - [SYUA_RAT]	76.98
14-3-3 protein zeta/delta OS=Rattus norvegicus OX=10116 GN=Ywhaz PE=1 SV=1 - [1433Z_RAT]	26.38
14-3-3 protein gamma OS=Rattus norvegicus OX=10116 GN=Ywhag PE=1 SV=2 - [1433G_RAT]	19.59
14-3-3 protein epsilon OS=Rattus norvegicus OX=10116 GN=Ywhae PE=1 SV=1 - [1433E_RAT]	16.20
Isoform Short of 14-3-3 protein beta/alpha OS=Rattus norvegicus OX=10116 GN=Ywhab - [1433B_RAT]	16.29

Table 8. Some of the proteins coimmunoprecipitated with TH. A representative list of the proteins with the highest scores (protein scores greater than 61 are significant ($p<0.05$)) as well as a few smaller score proteins that are related to TH as described in the literature. The full list can be found in the Annex.

There was an abundance of tubulin in the coimmunoprecipitate, one of which had an even higher score than TH (396.77). The rest of the microtubule proteins had scores ranging between 184.11 and 356.24. The second most abundant protein was TH (369.4). α-synuclein (76.98) and 14-3-3 (16.29-26.38) were also detected (Table 8), as well as several mitochondrial proteins (Figure 56).

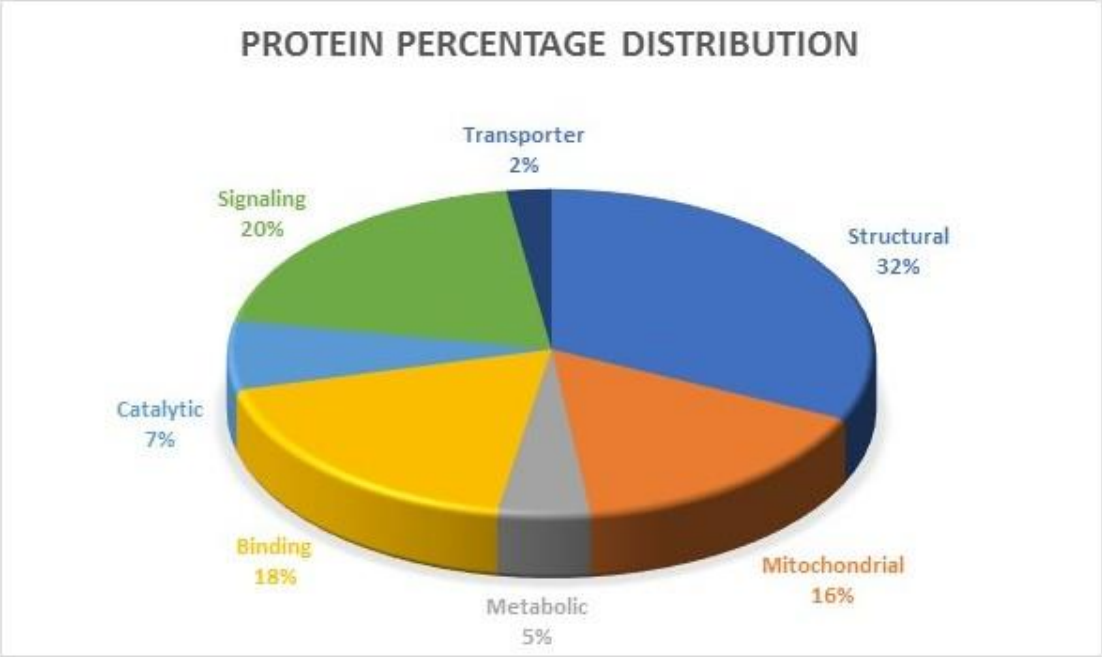

Figure 56. Distribution of all proteins found coimmunoprecipitated with TH. Proteins were divided into 7 groups according to function, and the percentage of the number of proteins per group was calculated.

4.2 Higher TH protein and activity in the mitochondria as compared to the cytosol

Since we saw a high number of mitochondrial proteins in the TH coimmunoprecipitate, we decided to further investigate the potential relationship between TH and mitochondria. There have been a few studies linking TH and mitochondria (Pickel et al., 1975b; Wang et al., 2009) but TH is generally considered to be a cytosolic enzyme.

Presence of TH protein in mitochondrial fraction

Following striatum extraction and homogenization, two methods were used to confirm successful separation into cytosol and mitochondria, as well as the presence of TH in the mitochondrial fraction. The first method was measuring LDH activity, an enzyme exclusive to the cytosol, where we found much higher activity in the cytosol as compared to the mitochondria, confirming correct separation. The second method was Western blot

and an antibody against TOM20, a mitochondrial-specific protein, where a band appeared only in the mitochondrial fraction, again, discarding contamination. And lastly, staining a membrane with Bluesafe dye shows different patterns of protein between cytosol and mitochondria.

In addition to the aforementioned representations, an antibody against α-synuclein was also used, where a higher amount of α-synuclein in the mitochondria as compared to the cytosol was found. α-synuclein has been associated with TH in several ways, such as altering TH phosphorylation (Alerte et al., 2008) and inhibiting TH synthesis (Yu et al., 2004). Similarly to our result, α-synuclein has also been previously found co-immunoprecipitated with TH (Perez et al., 2002).

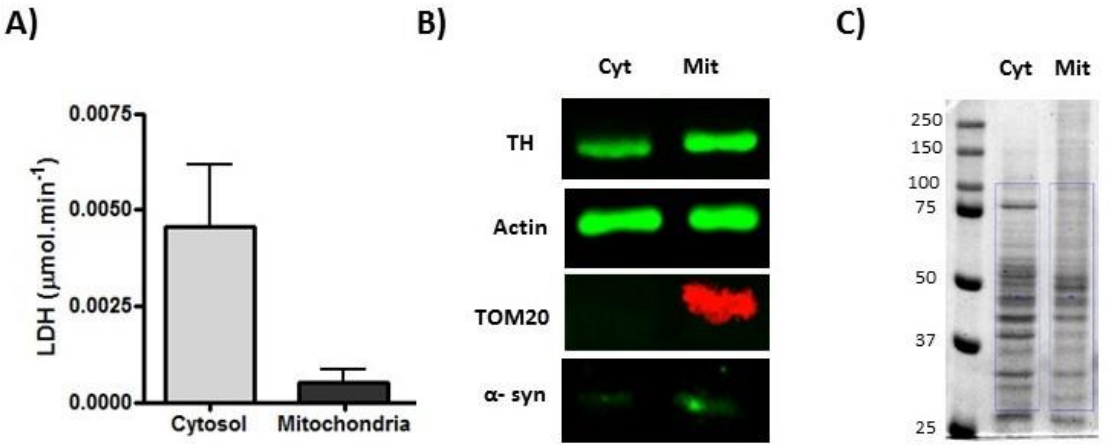

Figure 57. Confirming successful separation of cytosol and mitochondria from rat striatum total homogenate. Striatal homogenate from rat brain was separated into cytosol and mitochondria. **A)** LDH activity was measured as stated in Materials and Methods. The experiment was repeated twice per sample from two different brains and a representative graph is shown. **B)** Proteins were separated by SDS-PAGE and Western blot. Membranes were incubated with antibodies against total TH (raised in mouse, diluted 1:1000), TOM20 (raised in rabbit, diluted 1:1000), actin (raised in mouse, diluted 1:1000) and α-synuclein (raised in mouse, diluted 1:1000). Subsequently, membranes were incubated with secondary antibodies, anti-rabbit labeled with a near-infrared emitter at 800 nm and an anti-mouse labeled with a near-infrared emitter at 680 nm. Cyt: Cytosol, Mit: Mitochondria. **C)** Cytosol and mitochondria fractions separated by SDS-PAGE and subsequently dyed with Bluesafe.

Comparing TH activity in Cytosol and Mitochondria

The next step after confirming successful separation was measuring and comparing TH activity in both fractions, which was done using L-DOPA accumulation in HPLC-EC. Surprisingly, we saw a much higher activity in the mitochondrial fraction as compared to the cytosol. The experiment was repeated 3 times with similar results.

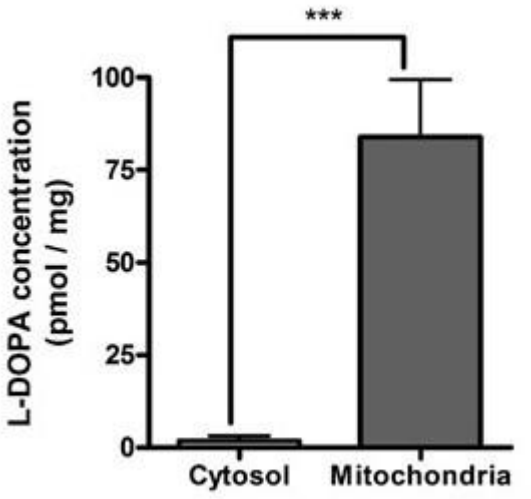

Figure 58. Comparing TH activity in cytosol and mitochondria. Rat striatum homogenate was separated into cytosol and mitochondria. HPLC-EC was used to calculate accumulation of L-DOPA/mg of protein *ex vivo*. 100 µM NSD-1015, 30 µM tyrosine and 100 µM BH_4 were added prior to starting the incubation. Incubation was with low flow carbogen and for 30 minutes. Graphic shows means and SEM, after one-way ANOVA analysis with Newman-Keuls post-test. Asterisks indicate ***$p<0.001$ cytosol vs mitochondria.

Western blot analysis of mitochondria-associated TH

Next, we wanted to compare TH amount in cytosol and mitochondria of control and CHIR-treated samples. There was significantly less TH amount in the cytosol as compared to the mitochondria, which coincides with our HPLC results (Figure 58), and this was true for both control and CHIR-treated samples. However, CHIR treatment non-significantly seems to increase TH in the cytosol and decrease it in the mitochondria.

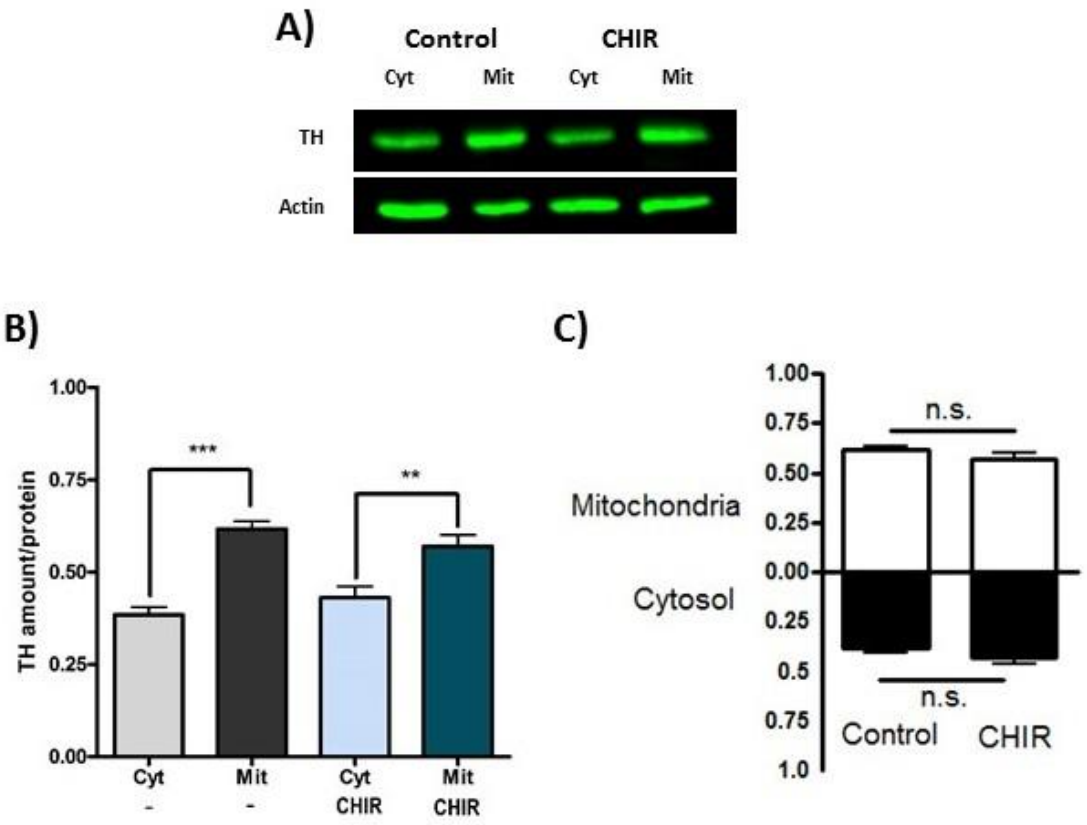

Figure 59. There is a higher TH amount in the mitochondria as compared to the cytosol. Striatal minces were divided into two groups, control group (-) and 3 µM CHIR-treated group incubated for 2 hours. After incubation samples were homogenized and separated into cytosol and mitochondria. **A)** Subsequent Western blots were performed and a representative Western blot is shown. **B)** Bar graph representation of TH amount with or without CHIR in cytosol and mitochondria fractions. TH amount is normalized as a fraction of 1 where cytosol TH and mitochondria TH of control add up to 1, and cytosol TH and mitochondria TH of CHIR also add up to 1. **C)** Floating bar graph representation of the same samples as B). Graphics show means and SEM, after two-way ANOVA analysis with Newman-Keuls post-test. Asterisks indicate **p<0.01, ***p<0.001 and n.s.= non-significant. Cyt=Cytosol, Mit=Mitochondria.

Western blot analysis of TH phosphorylation in cytosol and mitochondria

As previously discussed, TH activity is mediated by phosphorylation at three serine residues; Ser19, Ser31 and Ser40. In a similar manner to how we investigated changes in these phosphoserines in striatal minces, we wanted to replicate the method but in cytosolic and mitochondrial fractions, that is, in control and CHIR-treated fractions.

For this reason, Western blot analysis was used to detect differences in the phosphorylation of Ser19, Ser31 and Ser40 from TH. At this point, our Ser19 and Ser31 antibodies were giving poor signals, and even buying new batches yielded similar results.

For this reason, we were not able to perform replicates and statistics, however the few membranes that did give signal are shown in Figure 60. To our surprise, we saw that phosphorylation in Ser19 is dramatically lower in the mitochondrial fraction of both control and CHIR-treated samples as compared to their respective cytosols, even more so in the control sample, where the band disappears completely (Figure 60A). On the other hand, CHIR had no effect on the phosphorylation levels of Ser31 or Ser40 (Figure 60 B and C).

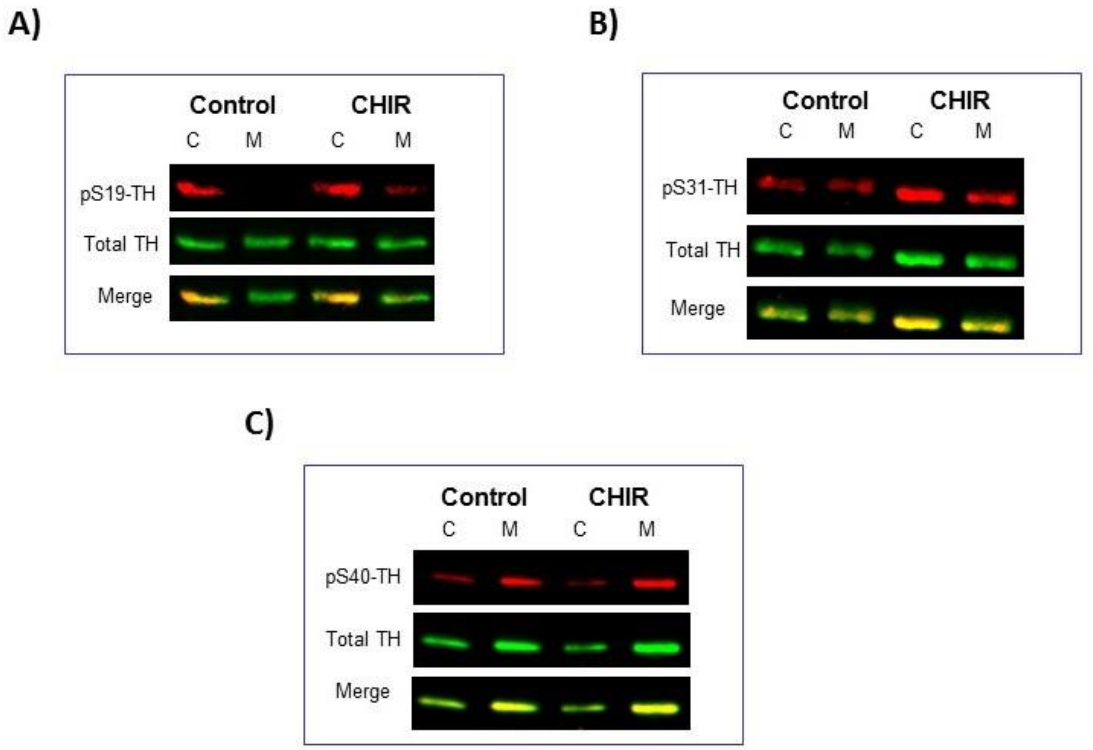

Figure 60. Changes in phosphorylation of TH in cytosol and mitochondria after CHIR99021 treatment. Samples from rat striatum cytosol (C) or mitochondria (M) were treated with 3µM CHIR99021 or DMSO as a control. Western blots after treatment with CHIR are shown. Antibodies used were against TH (raised in mouse, diluted 1:1000), pS19-TH (raised in rabbit, diluted 1:500), pS31-TH (raised in rabbit, diluted 1:500) and pS40-TH (raised in rabbit, diluted 1:1000). Subsequently, secondary antibodies were anti-mouse NIR680-labeled and anti-rabbit NIR800-labeled, both diluted 1:10000. Red signal corresponds to TH phosphorylated in **A)** Ser19, **B)** Ser31, or **C)** Ser40; green signal corresponds to total TH, while merge of both signals appears in yellow.

Discussion

1. General discussion

D_2 antibodies validation

Even though D_2 receptors have been somewhat characterized in the brain (Weiner et al., 1991; Yung & Bolam, 2000), there is a lack of updated studies with properly reported results using antibodies against D_2 receptors (Lin et al., 2016; Matchynski-Franks et al., 2016; May et al., 2013; Sharma et. Al, 2013; Wang et al., 2010). One important problem is that the antibodies yield several bands with different molecular weights in Western blot, which one study claims to be different forms of D_2R (native and denatured forms) with different molecular weights (110, 68 and 47 kDa bands) (Zhen Meng et al., 1998). Another recent study used the same antibody against D_2R from Abcam that we used in this work (Zhang et al., 2022). They wanted to determine the effects of sulpiride and clozapine on the translation levels of functional proteins involved in dopaminergic and serotonergic systems in zebrafish telencephalon. The antibody in their hands also yields two molecular weights (51 and 48 kDa) with no explanation. At one point during our work, we attempted to remove D_2R glycosylation enzymatically with glycosidase PNGase-F, because we thought it could also be a contributing factor to the multiplicity in different forms of D_2R. Unfortunately, the method did not work, and the results are therefore not shown.

D_2 receptors form heterodimers with mu opioid receptor (MOR) (Vasudevan et al., 2019), bradykinin 2 receptor (B_2R) (Niewiarowska-Sendo et al., 2017), D_1 receptor (Grymek et al., 2009), and serotonin 5-HT(2A) receptor (Lukasiewicz et al., 2010). It is therefore possible that D_2R heterodimerization is a contributor to the difficulties of D_2R detection by Western blot. Similarly to our antibodies against D_2R, we also could not validate our antibody against β-arrestin for immunoprecipitation (Figure 28). Had it been possible, it would have provided a new way to test D_2R activation as β-arrestin is known to translocate to membranes by receptor activation. The main issue we faced was insufficient specificity of the antibodies, especially evident in similar staining of the striatum and cortex in Figure 27. The binding of $D_{2/3}$ receptors is much lower in the cortex than in striatum at all ages. Binding is measured with ligands, and the technique therefore does not require antibodies. D_2 receptors have also been thoroughly quantified and studied in the striatum by means of positron emission tomography of the binding of labelled ligands such as N-[^{11}C]-methylspiperone and [^{11}C]-raclopride (Khodaii et al., 2022). Antibodies

and radioligands are the main tools to detect native proteins in tissue, and the use of the latter to detect receptor heteromers is also challenging (Sánchez-Soto et al., 2018).

UNC9994 and Quinpirole

The comparative study conducted between UNC9994 and Quinpirole was aimed at gaining further insight into β-arrestin signaling by comparing a functionally selective β-arrestin-biased D_2R agonist (UNC) with the selective D_2R full agonist (quinpirole). UNC9994, an analogue of Aripiprazole with an EC_{50} <10 nM (a concentration lower than the IC_{50} in this thesis), is simultaneously an antagonist of Gi-regulated cAMP production and a partial agonist for D_2R/β-arrestin-2 interactions. It can be characterized as an extremely β-arrestin–biased D_2R agonist since the antipsychotic-like activity it displays in wild-type mice is completely abolished in β-arrestin-2 knockout mice. Therefore, it is safe to say that β-arrestin signaling and recruitment through functionally selective, β-arrestin–biased D_2R ligands, can be an extremely significant contributor to antipsychotic efficacy while being simultaneously protective against motoric side effects (Allen et al., 2011). On the other hand, Quinpirole is a selective dopamine D_2 receptor full agonist (Inaba et al., 2021; Peczely et al., 2022) with a Ki value of 4.8 nM at D_2 receptors (Seeman & Schaus, 1991). It causes a selective and significant down-regulation of striatal D_2 receptors (Chen et al., 1993). Furthermore, quinpirole reduces the rate of firing in dopaminergic neurons and may have neuroprotective effects against Parkinson´s (Wiemerslage et al., 2013). However, quinpirole induces compulsive behavior symptomatic of obsessive-compulsive disorder in rats (Alkhatib et al., 2013). Its administration in the early life stages of development also leads to late alterations in behavioral parameters of adult zebrafish, such as increased fear and anxiety (Nabinger at al., 2021).

The β-arrestin pathway could be characterized as ´slow signal transduction´, and the G-protein pathway as ´fast signal transduction.´ For example, β-arrestin-dependent ERK 1/2 activation has been characterized as being slower in onset and more sustained in duration as compared to G-protein-dependent ERK 1/2 activation, which is rapid and transient (Ebisuya et al., 2005; Shenoy et al., 2006). For this reason, we decided to conduct our test over a shorter time of 30 minutes (Figure 29B). However, it seemed that 30 minutes was not enough of a short time to see a difference of ‘slow’ and ‘fast’ between UNC and quinpirole, respectively. Nonetheless, the difference in the levels of DA accumulation

between quinpirole and 10 µM UNC suggest that UNC effects are either better, more specific, and more targeted at decreasing DA levels, or that it is acting in a different mechanism than quinpirole, whose mechanism of action is still not quite understood. It is possible that UNC effects are so strong that DA storage is also affected (Figure 29A), similarly to CHIR effects discussed later.

GSK3 inhibitors effect on DA accumulation and synthesis

Another way to test D_2R signaling is to block the steps downstream D_2R activation. D_2R activation of β-arrestin leads to GSK3 disinhibition, as it is inhibited by Akt, which is inhibited by a β-arrestin PP2A complex (Beaulieu et al., 2007). That´s why we thought it could be relevant to test GSK3 inhibitors on DA synthesis.

GSK3β dysregulation has been described as an event involved in various pathologies such as diabetes mellitus, inflammation, tumorigenesis, mental disorders, neurodegenerative diseases or, even, stem cell regeneration (Wada, 2009). Moreover, inhibition of GSK3β has recently emerged as a possible pharmacological target in hyperglycemia (Ring et al., 2003), lung repair (Uhl et al., 2015), tooth repair (Zaugg et al., 2020), glioblastoma treatment (Lee et al., 2018; Oh et al., 2017) or regeneration of cardiomyocytes (Quaife-Ryan et al., 2020).

CHIR99021 is a small organic molecule that potently inhibits GSK3 at concentrations below those found in the present thesis, where GSKα (IC_{50}~10 nM) and GSK3β (IC_{50}~5 nM). Although CHIR penetration into brain minces and intracellular targets could contribute to explain differences in IC_{50}, off-target effects of the drug should also be considered. CHIR is considered the standard activator of the Wnt/β-catenin pathway (Bennett et al., 2002). Moreover, it is a compound that has been tested in a plethora of pathologies (Badimon et al., 2019; Bennett et al., 2002; Drakhlis et al., 2021; Houben et al., 2022; Lee et al., 2018; Oh et al., 2017; Ring et al., 2003; Uhl et al., 2015; Zhao et al., 2014), showing pharmacological potential in some of them. Furthermore, treatment of isolated rat pancreatic islets with CHIR99021 or SB216763, another GSK3β inhibitor used in the present work, increases the rate of beta cell replication (Mussmann et al., 2007) which points to specific inhibitors of GSK3β as promising tools in diabetes therapies. SB216763 has also been used in retinal stem cell proliferation and maintenance of pluripotent stem cell populations (Inoue et al., 2007). Another GSK3β inhibitor,

tideglusib, was tested in clinical trials for Alzheimer's disease, but no clinical benefit was found. Despite that, authors concluded that "further dose finding studies in early disease stages and for longer duration are warranted to examine GSK-3 inhibition in AD patients" (Lovestone et al., 2015). Tideglusib has also been proposed as a drug for Amyotrophic Lateral Sclerosis (Martínez-Gonzalez et al., 2021).

Despite the fact that CHIR99021 is considered the golden standard for GSK3β inhibition, its off-target effects have been demonstrated. A report describes some action of CHIR99021 on more than 20 kinases as well as the existence of more specific GSK3 inhibitors (An et al., 2012). These off-target effects have been highlighted by a recent report that shows that CHIR99021 causes, independently of GSK3, the suppression of the proteasomal degradation of calpastatin (CAST) and of the subsequent calpain activity, leading to a great enhancement of the mitochondrial function by impairing the action of the GTPase dynamin-related protein 1 (Drp1) on mitochondrial fragmentation. The authors hypothesized that CHIR99021 suppresses CAST degradation through inhibition of ubiquitin ligases or activation of deubiquitinases (Hu et al., 2021). Additionally, the promotion by CHIR99021 of mitochondrial biogenesis, oxidative phosphorylation, and the production of reactive oxygen species in human endodermal progenitor cells have also been observed, despite that these effects were attributed to the GSK3/β-catenin pathway and not to off-target effects of CHIR99021 (Ma et al., 2019).

As aforementioned, CHIR99021 decreases the levels of Drp1 and this leads to disruption of mitochondrial fission (Hu et al., 2021), but has also been involved in regulation of endocytosis and synaptic vesicle recycling, since absence of Drp1 or impairment of its interaction with Bcl-xL slows endocytosis, produces abnormal vesicle membranes and contributes to enlargement of a fast-releasing pool (Li et al., 2013). Other authors showed in Drosophila that Drp1-defective synapses fail to maintain normal neurotransmission, caused by the lack of synaptic mitochondria, rather than to effects on exo- or endocytosis, and by defects in the reserve pool (RP) vesicles (Verstreken et al., 2005). In any case, the Drp-1 dysregulation caused by CHIR99021 could lead to imbalance in the synaptic vesicle cycle, alter neurotransmitter uptake and, consequently, affect the levels of DA and its synthesis pathway.

CHIR99021 effects on DA storage

The feedback inhibition of DA on its own synthesis has previously been described, but the mechanism underlying the process is not clear. Computational analyses have indicated its potential importance in dopaminergic neurotransmission (Wallace, 2007), while *ex vivo* experimental studies have recently revealed that spontaneous inhibition in DA synthesis appeared when storage reached saturation, causing DA spillover and end-product feedback-inhibition of TH in tissue *ex vivo* (González-Sepúlveda et al., 2022). *In vitro* studies suggest the existence in TH of two DA binding sites with high and low affinities (K_D 4 nM and 90 nM, respectively) (Dickson and Briggs, 2013; Gordon et al., 2008; Nakashima et al., 2009; Tekin et al., 2014). The TH low-affinity site/conformation could act as a physiological sensor in case that synaptic vesicles were filled with DA at its maximum capacity, since the surplus of the DA inside the cytosol of synaptic terminals would bind to the low-affinity site/conformation, causing inhibition of TH activity. This process would happen regardless of the TH phosphorylation status and would explain a relevant finding of the present work, which is the dramatic increase of the DOPAC/DA ratio caused by CHIR99021 (Figure 37A). This result can be explained by the enhancement of the MAO activity triggered by the accumulation of its substrate, i.e., DA, in the cytosol of the synaptic terminal. This DA accumulation would also lead to the inhibition of TH by a feed-back effect. An accumulation of DA in striatal minces could also be explained by impairment of the VMAT2 transporter, as has also been observed with TBZ in a previous report from our group (González-Sepúlveda et al, 2022), giving rise to the possibility that CHIR99021 exerts an inhibitory effect on VMAT2, besides acting as a GSK3β inhibitor. The comparison of the effects of CHIR99021 and TBZ on the transport of extracellular DA inside striatal minces shows a relevant similarity. Since the main portion of the DA in the nerve terminal resides inside synaptic vesicles, where it is protected from metabolism prior to their synaptic release, we can assume that most of the exogenous DA incorporated into striatal minces directly reflects the amount of DA inside synaptic vesicles (Figure 39B). TBZ is used for the treatment of the motor symptoms in Huntington's disease (HD), a fatal neurodegenerative disorder, and other hyperkinetic disorders (Jankovic, 2009), but it can cause side effects, like nausea, difficulty in speaking, severe muscle stiffness or, even, depression (Jankovic, 2016). In any case, the reduction of DA release in the motor striatum by VMAT2 inhibition is considered a good therapeutic approach to reduce the involuntary hyperkinetic

movements of tardive dyskinesia (Stahl, 2018). In fact, CHIR99021 showed to potently improve mitochondrial function and enhance cell viability in several models of HD (Hu et al., 2021). Thus, an alternative option to TBZ in the hands of the doctors would be a benefit in cases with severe side effects, and CHIR99021 appears as a candidate to be also used in HD or other movement pathologies, such as tardive dyskinesia or Tourette syndrome. Although the exact mechanism of CHIR-mediated TH inhibition has not been fully elucidated, interference with DA storage should be seriously considered in first place.

TH phosphorylation

Regarding the effect of both CHIR99021 and of SB216763 on TH phosphorylation, Ser19 is reported to be phosphorylated in a 14-3-3 dependent-manner and has little effect on the activity of TH *in vitro* (Itagaki et al. 1999; Toska et al. 2002). Phosphorylation of TH in Ser19 is related to enzyme degradation of the enzyme by proteasome (Nakashima et al. 2016). The interaction with 14-3-3 proteins, mainly with the γ isoform (Halskau et al., 2009), reduces the sensitivity of phosphorylated human TH isoform 1 to proteolysis by protecting its N-terminal part (Obsilova et al. 2008). Despite the aforementioned, the dramatic abrogation of TH activity shown in the present work cannot be caused by loss of TH protein, since its levels remain unaltered after CHIR99021 treatment, nor to the relatively small change in pS19-TH.

As for the slight decrease in phosphorylation at Ser31 (24% less than control, Table 7) found by mass spectrometry following CHIR treatment, it has been previously reported that pS31-TH was detected in VMAT2– and α-synuclein–immunoprecipitated mouse brain samples (Jorge-Finnigan et al., 2017). This group claims that Ser31 phosphorylation may regulate TH subcellular localization via its transport along microtubules, which we also found in abundance co-immunoprecipitated with TH (Table 8). They found that the TH microsomal fraction content decreases when cyclin-dependent kinase 5 (Cdk5) and ERK1/2 are inhibited, the two kinases acting on pS31-TH. They also found that the cellular distribution of an overexpressed phospho-null mutant, which they called “TH1-S31A”, was restricted to the soma of neuroblastoma cells, with decreased association with the microsomal fraction. On the other hand, a phospho-mimic mutant, “TH1-S31E”, was distributed throughout the soma and neurites. However, as previously mentioned about

pS19, this small decrease in pS31 cannot be accounted for the dramatic abrogation of TH activity.

In basal physiological conditions less than 5% of TH is phosphorylated in Ser40 (Dunkley & Dickson, 2019; Dunkley et al., 2004). This low value agrees with the 1–2% signal ratio of phosphorylated/unphosphorylated Ser40-TH peptides we found by mass spectrometry (Table 6), as mass spectrometry signals depend both on peptide abundance and ionization efficiency, the latter being lower when peptides are phosphorylated. Ser40-TH phosphorylation has been reported to increase affinity for tetrahydrobiopterin (BH_4) cofactor and to decrease high-affinity DA binding (Daubner et al., 2011; Ramsey & Fitzpatrick, 1998). The low percentage of Ser40-TH phosphorylation suggests DA normally occupies the high-affinity site/conformation, and basal TH activity is supposed to be low. Nevertheless, TH was very active when newly synthesized DA was being stored in vesicles at the beginning of the incubation (González-Sepúlveda et al, 2022). Again, the low percentage of Ser40-TH phosphorylation suggests that cytosolic DA (newly synthesized, leaking from vesicles, or re-uptaken) may exert its inhibitory effect through the low-affinity binding site/conformation of TH. While vesicles are being actively filled, DA may not access this inhibitory site.

The lack of effect of quinpirole on Ser40-TH phosphorylation (Figure 48) may seem surprising, as canonical D_2 signaling is G_i-adenylate cyclase inhibition-PKA. This kinase is known to phosphorylate Ser40-TH. However, it must be noted that basal Ser40-TH phosphorylation is very low (see Table 6), so further decreases on TH phosphorylation by quinpirole seem unlikely. Quinpirole should then have an additional mechanism to inhibit TH and DA accumulation besides decreasing Ser40-TH phosphorylation.

TH phosphorylation in the brain does not seem to undergo major changes during incubation. This includes TH phosphorylation in Thr30 in rat brain assessed by mass spectrometry (Table 6), which to our knowledge is a novel finding, of unknown physiological relevance. Thr30 is conserved in rat and mouse, whereas a methionine is found in human and pig TH sequences, while Ser19, Ser31 and Ser40 are conserved in all four species. The first speculation is that this phosphorylation site (Thr30) contributes to TH regulation, such as activation, degradation or stability. Another possibility is that the proximity of Thr30 to Ser31 causes a ´leaky´ effect where both sites are targeted by the same kinase (ERK1/2) and possess the same role. It is also worth to mention that mass

spectrometry revealed twice (Tables 6 and 7) that the phosphorylation signal at Thr30 is almost half of that at Ser31. Given the fact we were able to show with pS31 and pT30 peptides that our Ser31 antibody was not recognizing Thr30 (Figure 55), it was currently not possible to determine the exact role of Thr30 and further work is necessary in this regard. However, this information has been published by our group (González-Sepúlveda et al, 2022).

Finally, we were not able to check changes in Ser8-TH phosphorylation, although it initially seemed a good candidate for GSK3 action due to its sequence.

Lithium

Lithium has been used for decades to treat manic depression. A thorough review of the Cochrane Collaboration Depression, Anxiety and Neurosis Controlled Trials Register and Cochrane Controlled Clinical Trials on lithium and its effect on mood disorders concluded that lithium had consistent and significant beneficial effects on bipolar disorder in all the trials. In unipolar disorder, lithium yielded an effect but it did not reach statistical significance. Surprisingly, no study reported negative effects of lithium. It is the only treatment that has shown efficacy for treatment of acute mania, acute depression and the prevention of recurrent mania and depression, which is why it is recommended for the treatment of both bipolar and unipolar depressive disorders (Young, 2009).

Bone marrow stem studies showed that lithium affects phosphorylated inositides, which is a major cellular messenger system. Further studies revealed that lithium stimulates and inhibits several phosphokinases and phosphatases, which all seemed to converge to inhibit GSK3β (Young, 2009). Lithium has also been shown to disrupt the β-arrestin-2/Akt/PP2A complex through direct inhibition of GSK3 (O'Brien et al., 2011).

In general, past results on the effect of lithium on brain DA have been quite diverse. It has been demonstrated that while acute lithium chloride treatment in rats does not affect endogenous DA or synthesis of [^{3}H] DA in striatal slices, chronic administration for 14 days does in fact significantly decrease [^{3}H] DA synthesis (Friedman & Gershon, 1973). Corrodi et. al (1969) found that lithium did not influence the brain concentration of DA in lithium-treated rats after 3 weeks, and when administered with the TH inhibitor, H 44/68, DA depletion was somewhat smaller than after administration of the inhibitor

alone, however the difference was not significant. Ho et. al (1970) found no significant change in tissue concentrations of DA in five brain regions of rats after a 4-week treatment with lithium and a dose of the TH inhibitor L-α-methyltyrosine. Another report analyzed HVA, DOPAC, and DA in 3-week lithium-treated rats, which had significantly increased HVA (52 %) and DOPAC (31 %) concentrations in the striatum, but no significant change in DA concentration. They also measured TH activity by quantifying L-DOPA formation, where they saw no effect of lithium on TH (Hesketh et al., 1978). Moreover, one study discuss the transient nature of 2 and 10 meq/kg single doses of lithium, which shortly produced an increase in the DA content of the striatum but disappeared 24 hours later. None of the two doses altered the activity of TH *ex vivo* but rather enhanced the activity of MAO (Otero Losada & Rubio, 1985).

While some report that lithium is used in the treatment of acute manic episodes using concentrations in the range of 0.8-2 mM (Sproule, 2002), others claim that the effective dose range for lithium is 0.6-1.0 mM in serum and >1.5 mM may be toxic, with levels of 1.5-2.0 mM having mild and reversible toxic effects on kidney, liver, heart, and glands (Young, 2009). In any case, the small effect of LiCl in our minces was seen at a greater concentration of 20 mM. This could be explained by our short treatment time in addition to the fact that we have previously seen in our laboratory with other drugs that our method for measuring DA accumulation in minces requires higher concentrations than those reported and recommended in previous studies as the drug need to diffuse across the tissue and membranes. This therefore also applies to CHIR (as previously mentioned) and SB concentrations used in this work as they are supposed to act on intracellular targets.

TH association with other proteins

Tubulin was the most abundant protein (highest scores) coimmunoprecipitated with TH, with several and diverse subtypes of alpha and beta microtubule proteins (Table 8). Vigny et al., (1980) have demonstrated that bovine adrenal medulla TH associates with microtubules during tubulin assembly, possibly through ionic interactions that occur between microtubules and a negatively charged region of the enzyme. Another report shows that treatment of neonatal animals with nerve growth factor (NGF) causes the appearance of several microtubules in electron microscopic pictures, accompanied by a selective induction of TH and dopamine-β-hydroxylase in sympathetic ganglia (Stöckel et al., 1974). From an immunohistochemical point of view, *in situ* hybridization

histochemistry measured changes in the relative levels of neuron-specific type II beta-tubulin and TH mRNA in locus coeruleus neurons of 2, 12, and 24-month-old Fischer 344 rats following intraventricular infusions of 6-hydroxydopamine. The measures revealed that the levels of both these markers simultaneously increased in the younger 2-month-old rats and decreased in the older 24-month-old rats (Unnerstall & Long, 1996). These studies support our result, which is that tubulin and TH are co-associated. However, the question remains whether or not TH-tubulin binding has a defined physiological role, especially for the purpose of regulating DA synthesis. Singh et al., (2020) suggest an interesting role of the acetylation of membrane tubulin and lipid rafts in G protein function. They found that in depressed-suicides and depressed-non-suicides, as compared to controls, membrane localized tubulin maintains a lower acetylation state. This allows increased sequestration of Gαs in lipid-raft domains, where it is less likely to couple to adenyl cyclase for cAMP production. This suggests that TH-tubulin binding could serve as a scaffold for G-protein/cAMP/PKA signaling.

TH association with mitochondria

This work also revealed a clear relationship between TH and mitochondria. TH is widely known to be a cytosolic enzyme and it has been immunohistochemically localized by the peroxidase-antiperoxidase method which gave selective and specific cytoplasmic localization of TH antisera in every tissue examined (Pickel et al., 1975a). The same group also found that in neurons in the nucleus locus coeruleus of rat brain, there was selective peroxidase reaction product in circular dark structures, joined together by cross-bridging and forming a ring around mitochondria (Pickel et al., 1975b). This is one of the few reports that discuss the association of TH with mitochondria. It has also been suggested that the mitochondria may be a site for physiological interactions between TH and α-synuclein, and TH and 14-3-3. This is because TH is associated to mitochondria in MN9D cells along with α-synuclein. Transmission electron microscopy after immunolabeling using a 14-3-3ζ-specific antibody and gold particle labeling revealed that 14-3-3ζ was localized to MN9D cell mitochondria as well. Using 14-3-3ζ siRNA caused a reduction in L-DOPA and DA levels while total TH levels were unchanged, but 14-3-3ζ siRNA significantly reduced the levels of TH phosphorylated at Ser19 and at Ser40 in the mitochondrial fraction. This evidence suggests that 14-3-3ζ may normally interact with TH that is localized to mitochondria in a manner to stimulate TH activity (Wang et

al., 2009). We were able to clearly corroborate this important relationship with the abundance of mitochondrial proteins coimmunoprecipitated with TH (Figure 56) as well as the much higher TH activity in the mitochondria as compared to the cytosol (Figure 58). However, it does not seem that CHIR changes this intracellular localization (Figure 59C) and therefore cannot be entitled as the causative mechanism behind CHIR actions on DA.

Another study discusses how prolonged binding of TH to phospholipid membranes induces misfolding and self-oligomerization of TH over time as seen by circular dichroism and Thioflavin T fluorescence (Baumann et al. 2016). They observe the formation of chain and ring-like protofilaments in monolayer-bound TH by atomic force microscopy, and they accredit this gradual amyloid-like aggregation to cross-β interactions involving aggregation prone motives in the catalytic domains. The same study reports that relatively short exposure of PC12 cells to the neurotoxin 6-hydroxydopamine (6-OHDA) causes an increase of TH content in the mitochondrial fraction. They demonstrate that this re-localization of TH appears to affect the mitochondrial potential by incubating isolated mitochondria with TH, which led to a decrease in the mitochondrial membrane potential (Baumann et al. 2016).

One of the hallmarks of PD is the decrease of TH levels, as well as the loss of dopaminergic neurons that express it in the SNC. This leads to a reduction of DA levels in the striatum. Keeping that in mind, along with the fact that mitochondrial dysfunction appears in the early stages of PD and is the key to the disease, suggest that this TH-mitochondria relationship could be an important contributor to PD pathology (Baumann et al. 2016).

2. Limitations

- In terms of the HPLC methodology, we were limited by the total number of sample incubations per experiment. This is due to the fact that the incubator can hold a maximum of 24 eppendorfs at a time, which is fine for striatum and brain regions of similar size. It is normal that randomly distributed tissue shows variability between groups. However, the number of incubations did limit us to the number of groups that can be tested per animal/experiment.

- The effect of DA levels in *ex-vivo* studies does not represent the pharmacological effect of the activation of the D_2 receptor alone, as several factors (synthesis, storage, metabolism) might be involved that may indirectly modulate DA levels. However, the challenging complexity of rat striatal tissue may offer an attractive model of study of drug action on brain synapses, with future applications to live animal models and human studies.

- As previously discussed, we were limited by the unavailability of reliable antibodies against D_2R and we therefore had to abandon a project that we had started and shift our attention to another path. This was also true for antibodies against pS19-TH and pS31-TH which, although initially working well, were giving very faint bands towards the end of our work.

- Mass spectrometry analysis is a technique which is less sensitive than Western blot and is more affected by interferences. We attempted to optimize the immunoprecipitation by increasing sample quantity, but this also increased the interference and therefore pS19-TH and pS40-TH could not always be quantified. This is because we were working in critical conditions that were difficult to optimize.

- We attempted to search for TH binding to mitochondria using immunolabeling with transmission electron microscopy, however given that there are very few studies that have successfully labeled TH in mitochondria (Wang et al., 2009), we faced difficulties in finding the correct protocol and our images therefore contained very few labeling (results not shown).

3. Future studies

- Sulpiride is an atypical antipsychotic which is used mainly in the treatment of psychosis associated with schizophrenia and major depressive disorder. It acts as a selective antagonist at dopamine D_2, D_3 and 5-HT_{1A} receptors. An experiment which involves a combination of sulpiride and UNC9994 could be designed in order to confirm whether UNC9994 is specific to D_2 receptors.

- Since we have established that CHIR is affecting DA storage, and we saw that it displayed similar results to TBZ (which affects VMAT2), this can be confirmed by quantifying serotonin concentration after CHIR treatment, because VMAT2 also transports serotonin. We attempted to quantify serotonin in the hippocampus with HPLC, as the hippocampus is densely innervated by serotonergic fibers, and it also expresses the majority of serotonin receptor subtypes (Dale et al., 2016). However, the quantifications were too small to be reliable (results not shown). For this reason, we must improve our protocol in order to be able to quantify serotonin as well.

- For the determination of exogenous DA concentration, we were limited by time, due to the fact that it is a new method that has not been attempted in our laboratory before, and I used it to perform the last 2 experiments of my PhD. Therefore, future experiments that involve different concentrations of CHIR and TBZ (dose-response) as well as a combination of both drugs to test additive effects should be performed.

- The physiological relevance of Thr30, if any, should be further examined.

- The relationship between mitochondria and TH should be further investigated by testing other protocols. One example would be to use mass spectrometry to quantify the levels of pS19-TH in the mitochondria and cytosol, as we saw a much lower level of this phosphorylation using Western blot.

Conclusions

Chapter 1: From D_2 receptors to β-arrestin signaling

1. The antibodies against D_2 used are partly unspecific due to failed negative control as bands and signal appear in D_2R KO mice, and also due to failed positive control as intense labeling appears in cortex and not in hypophysis.
2. β-arrestin antibody could also not be validated for immunoprecipitation, and we therefore could not examine the interaction between D_2R and β-arrestin through antibodies.
3. UNC9994, which is a β-arrestin biased agonist, strongly decreases DA accumulation, even more so than the D_2R full agonist quinpirole in fresh rat brain striatal minces. UNC also causes DA metabolization as the DOPAC/DA ratio also appears dramatically increased. This suggests that biased β-arrestin signaling could have a role in D_2R signaling modulation of DA dynamics.

Chapter 2: Effects of GSK3 inhibitors on DA dynamics

4. CHIR99021 strongly decreases DA accumulation and TH activity in fresh rat brain striatal minces, as assessed by HPLC measurements of DA and of L-DOPA. Thus, the depletion of DA inside striatum structures can be attributed to the halt of the DA synthetic pathway and of TH activity.
5. SB216763 and lithium ion do not clearly decrease DA content or alter DA metabolization and TH activity at the expected concentrations. These results point to an alternative way of action of CHIR99021 other than GSK3 inhibition, namely off target effects.
6. CHIR99021 causes DA metabolization, as the DOPAC/DA ratio appears dramatically increased. This metabolization contributes to the DA depletion.
7. CHIR99021 impairs the incorporation of exogenous DA into striatal minces in a strikingly similar way to tetrabenazine (TBZ), a VMAT2 inhibitor used for symptomatic treatment of hyperkinetic disorders. This suggests that CHIR action on DA storage could have released DA to the cytosol where it can have an inhibitory action on TH.

Chapter 3: Effect of different treatments on TH phosphorylation

8. Both CHIR99021 and SB216763, but not lithium, inhibit GSK3β kinase activity on β-catenin in striatal minces. Thus, the absence of action of SB216763 on DA metabolism cannot be attributed to a lack of its accessibility to GSK3 or a malfunction of the molecule.
9. Both CHIR99021 and SB216763 slightly decrease TH phosphorylation in Ser19, but they have no action on Ser31 and Ser40 according to Western blot.
10. TH Ser8 phosphorylation, although initially a promising candidate as a GSK3 substrate, could not be identified by Western blot or mass spectrometry and could therefore not be assessed.
11. Neither UNC9994 nor quinpirole clearly affect TH phosphorylation, and therefore cannot be accredited as the mechanism of action through which either compound is decreasing DA accumulation.
12. TH immunoprecipitation and mass spectrometry analysis reveal Thr30 as new phosphorylation site.
13. Mass spectrometry analysis also reveals a very slight decrease in phosphorylation of Ser31 in CHIR-treated samples. Our conclusion is that changes in TH phosphorylation cannot be claimed as a cause of the great inhibition of TH activity exerted by CHIR99021.

Chapter 4: TH association with mitochondria

14. Mitochondrial proteins are important partners of TH, as evident by the large number of mitochondrial proteins coimmunoprecipitated with TH, as well as the high TH activity found in the mitochondria.
15. This high TH activity seems to be due to a high TH amount in the mitochondria.
16. CHIR does not seem to cause intracellular translocation of TH.
17. There is no difference in TH phosphorylation between cytosol and mitochondria, except for Ser19. However, this result should be replicated, along with CHIR effects on TH phosphorylation in these two fractions.

References

Alerte, T. N., Akinfolarin, A. A., Friedrich, E. E., Mader, S. A., Hong, C., & Perez, R. G. (2008). α-synuclein aggregation alters tyrosine hydroxylase phosphorylation and immunoreactivity: Lessons from viral transduction of knockout mice. Neuroscience Letters, 435(1), 24-29. https://doi.org/10.1016/j.neulet.2008.02.014

Alkhatib, A. H., Dvorkin-Gheva, A., & Szechtman, H. (2013). Quinpirole and 8-OH-DPAT induce compulsive checking behavior in male rats by acting on different functional parts of an OCD neurocircuit. Behavioural pharmacology, 24(1), 65–73. https://doi.org/10.1097/FBP.0b013e32835d5b7a

Allen, J. A., Yost, J. M., Setola, V., Chen, X., Sassano, M. F., Chen, M., Peterson, S., Yadav, P. N., Huang, X. P., Feng, B., Jensen, N. H., Che, X., Bai, X., Frye, S. V., Wetsel, W. C., Caron, M. G., Javitch, J. A., Roth, B. L., & Jin, J. (2011). Discovery of β-arrestin-biased dopamine D2 ligands for probing signal transduction pathways essential for antipsychotic efficacy. Proceedings of the National Academy of Sciences of the United States of America, 108(45), 18488–18493. https://doi.org/10.1073/pnas.1104807108

An WF, Germain AR, Bishop JA, et al. Discovery of Potent and Highly Selective Inhibitors of GSK3β. (2012) In: Probe Reports from the NIH Molecular Libraries Program [Internet]. Bethesda (MD): National Center for Biotechnology Information (US). https://www.ncbi.nlm.nih.gov/books/NBK133436/

Ashok, A. H., Baugh, J., & Yeragani, V. K. (2012). Paul Eugen Bleuler and the origin of the term schizophrenia (SCHIZOPRENIEGRUPPE). Indian journal of psychiatry, 54(1), 95–96. https://doi.org/10.4103/0019-5545.94660

Bachelerie, F., Graham, G. J., Locati, M., Mantovani, A., Murphy, P. M., Nibbs, R., Rot, A., Sozzani, S., & Thelen, M. (2014). New nomenclature for atypical chemokine receptors. Nature Immunology, 15(3), 207-208. https://doi.org/10.1038/ni.2812

Badimon, L., Casaní, L., Camino-Lopez, S., Juan-Babot, O., & Borrell-Pages, M. (2019). GSK3β inhibition and canonical Wnt signaling in mice hearts after myocardial

ischemic damage. PloS one, 14(6), e0218098. https://doi.org/10.1371/journal.pone.0218098

Báez-Mendoza, R., & Schultz, W. (2013). The role of the striatum in social behavior. Frontiers in neuroscience, 7, 233. https://doi.org/10.3389/fnins.2013.00233

Banaschewski, T., Becker, K., Scherag, S., Franke, B., & Coghill, D. (2010). Molecular genetics of attention-deficit/hyperactivity disorder: An overview. European Child & Adolescent Psychiatry, 19(3), 237-257. https://doi.org/10.1007/s00787-010-0090-z

Baumann, A., Jorge-Finnigan, A., Jung-Kc, K., Sauter, A., Horvath, I., Morozova-Roche, L. A., & Martinez, A. (2016). Tyrosine Hydroxylase Binding to Phospholipid Membranes Prompts Its Amyloid Aggregation and Compromises Bilayer Integrity. Scientific reports, 6, 39488. https://doi.org/10.1038/srep39488

Beaulieu, J. M., Gainetdinov, R. R., & Caron, M. G. (2007). The Akt-GSK-3 signaling cascade in the actions of dopamine. Trends in pharmacological sciences, 28(4), 166–172. https://doi.org/10.1016/j.tips.2007.02.006

Beaulieu, J. M., Del'guidice, T., Sotnikova, T. D., Lemasson, M., & Gainetdinov, R. R. (2011). Beyond cAMP: The Regulation of Akt and GSK3 by Dopamine Receptors. Frontiers in molecular neuroscience, 4, 38. https://doi.org/10.3389/fnmol.2011.00038

Beaulieu, J., Gainetdinov, R. R., & Caron, M. G. (2009). Akt/GSK3 signaling in the action of psychotropic drugs. Annual Review of Pharmacology and Toxicology, 49(1), 327-347. https://doi.org/10.1146/annurev.pharmtox.011008.145634

Bennett, C. N., Ross, S. E., Longo, K. A., Bajnok, L., Hemati, N., Johnson, K. W., Harrison, S. D., & MacDougald, O. A. (2002). Regulation of Wnt signaling during adipogenesis. The Journal of biological chemistry, 277(34), 30998–31004. https://doi.org/10.1074/jbc.M204527200

Best, J. A., Nijhout, H. F., & Reed, M. C. (2009). Homeostatic mechanisms in dopamine synthesis and release: a mathematical model. Theoretical biology & medical modelling, 6, 21. https://doi.org/10.1186/1742-4682-6-21

Biederman, J., & Faraone, S. V. (2005). Attention-deficit hyperactivity disorder. The Lancet, 366(9481), 237-248. https://doi.org/10.1016/s0140-6736(05)66915-2

Bologna, Z., Teoh, J., Bayoumi, A. S., Tang, Y., & Kim, I. (2017). Biased G protein-coupled receptor signaling: New player in modulating physiology and pathology. Biomolecules & Therapeutics, 25(1), 12-25. https://doi.org/10.4062/biomolther.2016.165

Braak, H., Alafuzoff, I., Arzberger, T., Kretzschmar, H., & Del Tredici, K. (2006). Staging of Alzheimer disease-associated neurofibrillary pathology using paraffin sections and immunocytochemistry. Acta Neuropathologica, 112(4), 389-404. https://doi.org/10.1007/s00401-006-0127-z

Braak, H., Tredici, K. D., Rüb, U., De Vos, R. A., Jansen Steur, E. N., & Braak, E. (2003). Staging of brain pathology related to sporadic Parkinson's disease. Neurobiology of Aging, 24(2), 197-211. https://doi.org/10.1016/s0197-4580(02)00065-9

Bueno-Carrasco, M. T., Cuéllar, J., Flydal, M. I., Santiago, C., Kråkenes, T., Kleppe, R., López-Blanco, J. R., Marcilla, M., Teigen, K., Alvira, S., Chacón, P., Martinez, A., & Valpuesta, J. M. (2022). Structural mechanism for tyrosine hydroxylase inhibition by dopamine and reactivation by Ser40 phosphorylation. Nature Communications, 13(1). https://doi.org/10.1038/s41467-021-27657-y

Cabello, N., Gandía, J., Bertarelli, D. C., Watanabe, M., Lluís, C., Franco, R., Ferré, S., Luján, R., & Ciruela, F. (2009). Metabotropic glutamate type 5, dopamine D2 and adenosine A2a receptors form higher-order oligomers in living cells. Journal of neurochemistry, 109(5), 1497–1507. https://doi.org/10.1111/j.1471-4159.2009.06078.x

Casanovas, A., Carrascal, M., Abián, J., López-Tejero, M. D., & Llobera, M. (2009). Discovery of lipoprotein lipase Pi isoforms and contributions to their characterization. Journal of Proteomics, 72(6), 1031-1039. https://doi.org/10.1016/j.jprot.2009.06.002

Castellanos, F. X., & Tannock, R. (2002). Neuroscience of attention-deficit/hyperactivity disorder: The search for endophenotypes. Nature Reviews Neuroscience, 3(8), 617-628. https://doi.org/10.1038/nrn896

Chakravorty, D., & Assmann, S. M. (2018). G protein subunit phosphorylation as a regulatory mechanism in heterotrimeric G protein signaling in mammals, yeast, and plants. The Biochemical journal, 475(21), 3331–3357. https://doi.org/10.1042/BCJ20160819

Chen, J. F., Aloyo, V. J., & Weiss, B. (1993). Continuous treatment with the D2 dopamine receptor agonist quinpirole decreases D2 dopamine receptors, D2 dopamine receptor messenger RNA and proenkephalin messenger RNA, and increases mu opioid receptors in mouse striatum. Neuroscience, 54(3), 669–680. https://doi.org/10.1016/0306-4522(93)90238-b

Chen, J., Song, J., Yuan, P., Tian, Q., Ji, Y., Ren-Patterson, R., Liu, G., Sei, Y., & Weinberger, D. R. (2011). Orientation and cellular distribution of membrane-bound catechol-O-methyltransferase in cortical neurons: implications for drug development. The Journal of biological chemistry, 286(40), 34752–34760. https://doi.org/10.1074/jbc.M111.262790

Corrodi, H., Fuxe, K., & Schou, M. (1969). The effect of prolonged lithium administration on cerebral monoamine neurons in the rat. Life sciences, 8(11), 643–651. https://doi.org/10.1016/0024-3205(69)90026-5

Dale, E., Pehrson, A. L., Jeyarajah, T., Li, Y., Leiser, S. C., Smagin, G., Olsen, C. K., & Sanchez, C. (2016). Effects of serotonin in the hippocampus: how SSRIs and multimodal antidepressants might regulate pyramidal cell function. CNS spectrums, 21(2), 143–161. https://doi.org/10.1017/S1092852915000425

Daubner, S. C., Le, T., & Wang, S. (2011). Tyrosine hydroxylase and regulation of dopamine synthesis. Archives of Biochemistry and Biophysics, 508(1), 1-12. https://doi.org/10.1016/j.abb.2010.12.017

Del Campo, N., Chamberlain, S. R., Sahakian, B. J., & Robbins, T. W. (2011). The roles of dopamine and noradrenaline in the pathophysiology and treatment of attention-deficit/hyperactivity disorder. Biological psychiatry, 69(12), e145–e157. https://doi.org/10.1016/j.biopsych.2011.02.036

Delcambre, S., Nonnenmacher, Y., & Hiller, K. (2016). Dopamine metabolism and reactive oxygen species production. Mitochondrial Mechanisms of Degeneration and Repair in Parkinson's Disease, 25-47. https://doi.org/10.1007/978-3-319-42139-1_2

Dickson, P. W., & Briggs, G. D. (2013). Tyrosine hydroxylase: regulation by feedback inhibition and phosphorylation. Advances in pharmacology (San Diego, Calif.), 68, 13–21. https://doi.org/10.1016/B978-0-12-411512-5.00002-6

Drakhlis, L., Devadas, S. B., & Zweigerdt, R. (2021). Generation of heart-forming organoids from human pluripotent stem cells. Nature protocols, 16(12), 5652–5672. https://doi.org/10.1038/s41596-021-00629-8.

Dunkley, P. R., & Dickson, P. W. (2019). Tyrosine hydroxylase phosphorylation in vivo. Journal of Neurochemistry, 149(6), 706-728. https://doi.org/10.1111/jnc.14675

Dunkley, P. R., Bobrovskaya, L., Graham, M. E., von Nagy-Felsobuki, E. I., & Dickson, P. W. (2004). Tyrosine hydroxylase phosphorylation: regulation and consequences. Journal of neurochemistry, 91(5), 1025–1043. https://doi.org/10.1111/j.1471-4159.2004.02797.x

Ebisuya, M., Kondoh, K., & Nishida, E. (2005). The duration, magnitude and compartmentalization of ERK MAP kinase activity: mechanisms for providing signaling specificity. Journal of cell science, 118(Pt 14), 2997–3002. https://doi.org/10.1242/jcs.02505

Eiden, L. E., & Weihe, E. (2011). VMAT2: A dynamic regulator of brain monoaminergic neuronal function interacting with drugs of abuse. Annals of the New York Academy of Sciences, 1216(1), 86-98. https://doi.org/10.1111/j.1749-6632.2010.05906.x

Eisenhofer, G., Kopin, I. J., & Goldstein, D. S. (2004). Catecholamine metabolism: A contemporary view with implications for physiology and medicine. Pharmacological Reviews, 56(3), 331-349. https://doi.org/10.1124/pr.56.3.1

Engert, V., & Pruessner, J. (2008). Dopaminergic and Noradrenergic contributions to functionality in ADHD: The role of methylphenidate. Current Neuropharmacology, 6(4), 322-328. https://doi.org/10.2174/157015908787386069

Eriksen, J., Jørgensen, T. N., & Gether, U. (2010). Regulation of dopamine transporter function by protein-protein interactions: New discoveries and methodological challenges. Journal of Neurochemistry, 113(1), 27-41. https://doi.org/10.1111/j.1471-4159.2010.06599.x

Erspamer, V. (1940). Pharmakologische Studien Uber Enteramin. Naunyn-Schmiedebergs Archiv für Experimentelle Pathologie und Pharmakologie, 196(2-5), 343-365. https://doi.org/10.1007/bf01861121

Fitzpatrick, P. F. (2006). The aromatic amino acid Hydroxylases. Advances in Enzymology - and Related Areas of Molecular Biology, 235-294. https://doi.org/10.1002/9780470123201.ch6

Fleckenstein, A. E., Volz, T. J., Riddle, E. L., Gibb, J. W., & Hanson, G. R. (2007). New insights into the mechanism of action of amphetamines. Annual Review of Pharmacology and Toxicology, 47(1), 681-698. https://doi.org/10.1146/annurev.pharmtox.47.120505.105140

Ford C. P. (2014). The role of D2-autoreceptors in regulating dopamine neuron activity and transmission. Neuroscience, 282, 13–22. https://doi.org/10.1016/j.neuroscience.2014.01.025

Friedman, E., & Gershon, S. (1973). Effect of lithium on brain dopamine. Nature, 243(5409), 520–521. https://doi.org/10.1038/243520a0

Fu, Y., Yuan, Y., Halliday, G., Rusznák, Z., Watson, C., & Paxinos, G. (2011). A cytoarchitectonic and chemoarchitectonic analysis of the dopamine cell groups in the substantia nigra, ventral tegmental area, and retrorubral field in the mouse. Brain Structure and Function, 217(2), 591-612. https://doi.org/10.1007/s00429-011-0349-2

Gainetdinov, R. R. (2008). Dopamine transporter mutant mice in experimental neuropharmacology. Naunyn-Schmiedeberg's Archives of Pharmacology, 377(4-6), 301-313. https://doi.org/10.1007/s00210-007-0216-0

Galli, C., Piemontese, M., Lumetti, S., Manfredi, E., Macaluso, G. M., & Passeri, G. (2012). Gsk3b-inhibitor lithium chloride enhances activation of Wnt canonical signaling and osteoblast differentiation on hydrophilic titanium surfaces. Clinical Oral Implants Research, 24(8), 921-927. https://doi.org/10.1111/j.1600-0501.2012.02488.x

German, C. L., Baladi, M. G., McFadden, L. M., Hanson, G. R., & Fleckenstein, A. E. (2015). Regulation of the Dopamine and Vesicular Monoamine Transporters: Pharmacological Targets and Implications for Disease. Pharmacological reviews, 67(4), 1005–1024. https://doi.org/10.1124/pr.114.010397

González-Sepúlveda, M., Omar, M. Y., Hamdon, S., Ma, G., Rosell-Vilar, S., Raivio, N., Abass, D., Martínez-Rivas, A., Vila, M., Giraldo, J., Carrascal, M., Abián, J., Gil, C., Sabriá, J., Ortiz, J., & Moreno-Delgado, D. (2022). Spontaneous changes in brain striatal dopamine synthesis and storage dynamics ex vivo reveal end-product feedback-inhibition of tyrosine hydroxylase. Neuropharmacology, 212, 109058. https://doi.org/10.1016/j.neuropharm.2022.109058

González-Sepúlveda, M., Rosell, S., Hoffmann, H. M., Castillo-Ruiz, M. D., Mignon, V., Moreno-Delgado, D., Vignes, M., Díaz, J., Sabriá, J., & Ortiz, J. (2013). Cellular distribution of the histamine H3 receptor in the basal ganglia: Functional modulation of dopamine and glutamate neurotransmission. Basal Ganglia, 3(2), 109-121. https://doi.org/10.1016/j.baga.2012.12.001

Goodwill, K. E., Sabatier, C., & Stevens, R. C. (1998). Crystal structure of tyrosine hydroxylase with bound cofactor analogue and iron at 2.3 A resolution: self-hydroxylation of Phe300 and the pterin-binding site. *Biochemistry*, *37*(39), 13437–13445. https://doi.org/10.1021/bi981462g

Goodwill, K. E., Sabatier, C., Marks, C., Raag, R., Fitzpatrick, P. F., & Stevens, R. C. (1997). Crystal structure of tyrosine hydroxylase at 2.3 a and its implications for inherited neurodegenerative diseases. Nature Structural Biology, 4(7), 578-585. https://doi.org/10.1038/nsb0797-578

Gordon, S. L., Quinsey, N. S., Dunkley, P. R., & Dickson, P. W. (2008). Tyrosine hydroxylase activity is regulated by two distinct dopamine-binding sites. Journal of neurochemistry, 106(4), 1614–1623. https://doi.org/10.1111/j.1471-4159.2008.05509.x

Grymek, K., Łukasiewicz, S., Faron-Góreckaa, A., Tworzydlo, M., Polit, A., & Dziedzicka-Wasylewska, M. (2009). Role of silent polymorphisms within the dopamine D1 receptor associated with schizophrenia on D1-D2 receptor hetero-dimerization. Pharmacological reports : PR, 61(6), 1024–1033. https://doi.org/10.1016/s1734-1140(09)70164-1

Halskau, Ø., Jr, Ying, M., Baumann, A., Kleppe, R., Rodriguez-Larrea, D., Almås, B., Haavik, J., & Martínez, A. (2009). Three-way interaction between 14-3-3 proteins, the N-terminal region of tyrosine hydroxylase, and negatively charged membranes. The Journal of biological chemistry, 284(47), 32758–32769. https://doi.org/10.1074/jbc.M109.027706

Hanson, J. E., Birdsall, E., Seferian, K. S., Crosby, M. A., Keefe, K. A., Gibb, J. W., Hanson, G. R., & Fleckenstein, A. E. (2009). Methamphetamine-induced dopaminergic deficits and refractoriness to subsequent treatment. European journal of pharmacology, 607(1-3), 68–73. https://doi.org/10.1016/j.ejphar.2009.01.037

Hesketh, J. E., Nicolaou, N. M., Arbuthnott, G. W., & Wright, A. K. (1978). The effect of chronic lithium administration on dopamine metabolism in rat striatum. Psychopharmacology, 56(2), 163–166. https://doi.org/10.1007/BF00431843

Ho, A., Loh, H., Craves, F., Hitzemann, R., & Gershon, S. (1970). The effect of prolonged lithium treatment on the synthesis rate and turnover of monoamines in brain regions of rats. European Journal of Pharmacology, 10(1), 72-78. https://doi.org/10.1016/0014-2999(70)90159-7

Houben, R., Hesbacher, S., Sarma, B., Schulte, C., Sarosi, E. M., Popp, S., Adam, C., Kervarrec, T., & Schrama, D. (2022). Inhibition of T-antigen expression promoting glycogen synthase kinase 3 impairs merkel cell carcinoma cell growth. Cancer letters, 524, 259–267. https://doi.org/10.1016/j.canlet.2021.10.031

Howes, O. D., & Kapur, S. (2009). The dopamine hypothesis of schizophrenia: version III--the final common pathway. Schizophrenia bulletin, 35(3), 549–562. https://doi.org/10.1093/schbul/sbp006

Hu, D., Sun, X., Magpusao, A., Fedorov, Y., Thompson, M., Wang, B., Lundberg, K., Adams, D. J., & Qi, X. (2021). Small-molecule suppression of calpastatin degradation reduces neuropathology in models of Huntington's disease. Nature communications, 12(1), 5305. https://doi.org/10.1038/s41467-021-25651-y

Hu, G. M., Mai, T. L., & Chen, C. M. (2017). Visualizing the GPCR Network: Classification and Evolution. Scientific reports, 7(1), 15495. https://doi.org/10.1038/s41598-017-15707-9

Hufton, S. E., Jennings, I. G., & Cotton, R. G. (1995). Structure and function of the aromatic amino acid hydroxylases. Biochemical Journal, 311(2), 353-366. https://doi.org/10.1042/bj3110353

Inaba, H., Namba, H., Kida, S., & Nawa, H. (2021). The dopamine D2 agonist quinpirole impairs frontal mismatch responses to sound frequency deviations in freely

moving rats. Neuropsychopharmacology reports, 41(3), 405–415. https://doi.org/10.1002/npr2.12199

Inoue, T., Kawaji, T., Inoue-Mochita, M., Taga, T., & Tanihara, H. (2007). Media conditioned by retinal pigment epithelial cells suppress the canonical Wnt pathway. Neuroscience letters, 424(3), 190–193. https://doi.org/10.1016/j.neulet.2007.07.022

Itagaki, C., Isobe, T., Taoka, M., Natsume, T., Nomura, N., Horigome, T., Omata, S., Ichinose, H., Nagatsu, T., Greene, L. A., & Ichimura, T. (1999). Stimulus-coupled interaction of tyrosine hydroxylase with 14-3-3 proteins. Biochemistry, 38(47), 15673–15680. https://doi.org/10.1021/bi9914255

Jakel, R. J., & Maragos, W. F. (2000). Neuronal cell death in Huntington's disease: A potential role for dopamine. Trends in Neurosciences, 23(6), 239-245. https://doi.org/10.1016/s0166-2236(00)01568-x

Jankovic J. (2009). Treatment of hyperkinetic movement disorders. The Lancet. Neurology, 8(9), 844-856. https://doi.org/10.1016/S1474-4422(09)70183-8

Jankovic J. (2016). Dopamine depleters in the treatment of hyperkinetic movement disorders. Expert opinion on pharmacotherapy, 17(18), 2461–2470. https://doi.org/10.1080/14656566.2016.1258063

Jimenez-Sanchez, M., Licitra, F., Underwood, B. R., & Rubinsztein, D. C. (2017). Huntington's Disease: Mechanisms of Pathogenesis and Therapeutic Strategies. Cold Spring Harbor perspectives in medicine, 7(7), a024240. https://doi.org/10.1101/cshperspect.a024240

Jones, D. R., Moussaud, S., & McLean, P. (2013). Targeting heat shock proteins to modulate α-synuclein toxicity. Therapeutic Advances in Neurological Disorders, 7(1), 33-51. https://doi.org/10.1177/1756285613493469

Jorge-Finnigan, A., Kleppe, R., Jung-KC, K., Ying, M., Marie, M., Rios-Mondragon, I., Salvatore, M. F., Saraste, J., & Martinez, A. (2017). Phosphorylation at serine 31 targets

tyrosine hydroxylase to vesicles for transport along microtubules. Journal of Biological Chemistry, 292(34), 14092-14107. https://doi.org/10.1074/jbc.m116.762344

Juárez Olguín, H., Calderón Guzmán, D., Hernández García, E., & Barragán Mejía, G. (2016). The Role of Dopamine and Its Dysfunction as a Consequence of Oxidative Stress. Oxidative medicine and cellular longevity, 2016, 9730467. https://doi.org/10.1155/2016/9730467

Kapur, S. (2000). Relationship between dopamine D2 occupancy, clinical response, and side effects: A double-blind PET study of first-episode schizophrenia. American Journal of Psychiatry, 157(4), 514-520. https://doi.org/10.1176/appi.ajp.157.4.514

Kazi, A., Xiang, S., Yang, H., Delitto, D., Trevino, J., Jiang, R. H., Ayaz, M., Lawrence, H. R., Kennedy, P., & Sebti, S. M. (2018). GSK3 suppression upregulates β-catenin and C-MyC to abrogate kras-dependent tumors. Nature Communications, 9(1). https://doi.org/10.1038/s41467-018-07644-6

Khodaii, J., Nomura, Y., Chang, N. H. S., Wong, D. F., Møller, A., & Gjedde, A. (2022). Dopamine $D_{2/3}$ Receptor Availabilities in Striatal and Extrastriatal Regions of the Adult Human Brain: Comparison of Four Methods of Analysis. Neurochemical research, 10.1007/s11064-022-03825-4. Advance online publication. https://doi.org/10.1007/s11064-022-03825-4

Klein, M. O., Battagello, D. S., Cardoso, A. R., Hauser, D. N., Bittencourt, J. C., & Correa, R. G. (2019). Dopamine: Functions, Signaling, and Association with Neurological Diseases. Cellular and molecular neurobiology, 39(1), 31–59. https://doi.org/10.1007/s10571-018-0632-3

Klein, P. S., & Melton, D. A. (1996). A molecular mechanism for the effect of lithium on development. Proceedings of the National Academy of Sciences, 93(16), 8455-8459. https://doi.org/10.1073/pnas.93.16.8455

Kleinridders, A., Cai, W., Cappellucci, L., Ghazarian, A., Collins, W. R., Vienberg, S. G., Pothos, E. N., & Kahn, C. R. (2015). Insulin resistance in brain alters

dopamine turnover and causes behavioral disorders. Proceedings of the National Academy of Sciences, 112(11), 3463-3468. https://doi.org/10.1073/pnas.1500877112

Konradi, C., Svoma, E., Jellinger, K., Riederer, P., Denney, R., & Thibault, J. (1988). Topographic immunocytochemical mapping of monoamine oxidase-A, monoamine oxidase-B and tyrosine hydroxylase in human post mortem brain stem. Neuroscience, 26(3), 791-802. https://doi.org/10.1016/0306-4522(88)90099-1

Kumer, S. C., & Vrana, K. E. (2002). Intricate regulation of tyrosine Hydroxylase activity and gene expression. Journal of Neurochemistry, 67(2), 443-462. https://doi.org/10.1046/j.1471-4159.1996.67020443.x

Lee, C., Robinson, M., & Willerth, S. M. (2018). Direct Reprogramming of Glioblastoma Cells into Neurons Using Small Molecules. ACS chemical neuroscience, 9(12), 3175–3185. https://doi.org/10.1021/acschemneuro.8b00365

Li, H., Alavian, K. N., Lazrove, E., Mehta, N., Jones, A., Zhang, P., Licznerski, P., Graham, M., Uo, T., Guo, J., Rahner, C., Duman, R. S., Morrison, R. S., & Jonas, E. A. (2013). A Bcl-xL-Drp1 complex regulates synaptic vesicle membrane dynamics during endocytosis. Nature cell biology, 15(7), 773–785. https://doi.org/10.1038/ncb2791

Lidow, M. S., Goldman-Rakic, P. S., Rakic, P., & Innis, R. B. (1989). Dopamine D2 receptors in the cerebral cortex: Distribution and pharmacological characterization with [3H]raclopride. Proceedings of the National Academy of Sciences, 86(16), 6412-6416. https://doi.org/10.1073/pnas.86.16.6412

Lin, H. C., Pan, H. C., Lin, S. H., Lo, Y. C., Shen, E. T., Liao, L. D., Liao, P. H., Chien, Y. W., Liao, K. D., Jaw, F. S., Chu, K. W., Lai, H. Y., & Chen, Y. Y. (2016). Central Thalamic Deep-Brain Stimulation Alters Striatal-Thalamic Connectivity in Cognitive Neural Behavior. Frontiers in neural circuits, 9, 87. https://doi.org/10.3389/fncir.2015.00087

López-Muñoz, F., Alamo, C., Cuenca, E., Shen, W. W., Clervoy, P., & Rubio, G. (2005). History of the discovery and clinical introduction of chlorpromazine. Annals of

clinical psychiatry : official journal of the American Academy of Clinical Psychiatrists, 17(3), 113–135. https://doi.org/10.1080/10401230591002002

Lovestone, S., Boada, M., Dubois, B., Hüll, M., Rinne, J. O., Huppertz, H. J., Calero, M., Andrés, M. V., Gómez-Carrillo, B., León, T., del Ser, T., & ARGO investigators (2015). A phase II trial of tideglusib in Alzheimer's disease. Journal of Alzheimer's disease: JAD, 45(1), 75–88. https://doi.org/10.3233/JAD-141959

Lukasiewicz, S., Polit, A., Kędracka-Krok, S., Wędzony, K., Maćkowiak, M., & Dziedzicka-Wasylewska, M. (2010). Hetero-dimerization of serotonin 5-HT(2A) and dopamine D(2) receptors. Biochimica et biophysica acta, 1803(12), 1347–1358. https://doi.org/10.1016/j.bbamcr.2010.08.010

Ma, L., & Pei, G. (2007). Beta-arrestin signaling and regulation of transcription. Journal of cell science, 120(Pt 2), 213–218. https://doi.org/10.1242/jcs.03338

Ma, Y., Ma, M., Sun, J., Li, W., Li, Y., Guo, X., & Zhang, H. (2019). CHIR-99021 regulates mitochondrial remodelling via β-catenin signalling and miRNA expression during endodermal differentiation. Journal of cell science, 132(15), jcs229948. https://doi.org/10.1242/jcs.229948

Ma, G. F., Raivio, N., Sabria, J., & Ortiz, J. (2015). Agonist and antagonist effects of aripiprazole on D2-like receptors controlling rat brain dopamine synthesis depend on the Dopaminergic tone. International Journal of Neuropsychopharmacology, 18(4), pyu046-pyu046. https://doi.org/10.1093/ijnp/pyu046

Marshall, F. H., & Foord, S. M. (2010). Heterodimerization of the GABAB receptor-implications for GPCR signaling and drug discovery. Advances in pharmacology (San Diego, Calif.), 58, 63–91. https://doi.org/10.1016/S1054-3589(10)58003-7

Martínez-González, L., Gonzalo-Consuegra, C., Gómez-Almería, M., Porras, G., de Lago, E., Martín-Requero, Á., & Martínez, A. (2021). Tideglusib, a Non-ATP Competitive Inhibitor of GSK-3β as a Drug Candidate for the Treatment of

Amyotrophic Lateral Sclerosis. International journal of molecular sciences, 22(16), 8975. https://doi.org/10.3390/ijms2roth2168975

Matchynski-Franks, J. J., Susick, L. L., Schneider, B. L., Perrine, S. A., & Conti, A. C. (2016). Impaired ethanol-induced sensitization and decreased cannabinoid receptor-1 in a model of posttraumatic stress disorder. PLOS ONE, 11(5), e0155759. https://doi.org/10.1371/journal.pone.0155759

May, S., Andreasson-Ochsner, M., Fu, Z., Low, Y. X., Tan, D., de Hoog, H. P., Ritz, S., Nallani, M., & Sinner, E. K. (2013). In vitro expressed GPCR inserted in polymersome membranes for ligand-binding studies. Angewandte Chemie (International ed. in English), 52(2), 749–753. https://doi.org/10.1002/anie.201204645

McCutcheon, R. A., Abi-Dargham, A., & Howes, O. D. (2019). Schizophrenia, dopamine and the striatum: From biology to symptoms. Trends in Neurosciences, 42(3), 205-220. https://doi.org/10.1016/j.tins.2018.12.004

McLean, W. J., Hinton, A. S., Herby, J. T. J., Salt, A. N., Hartsock, J. J., Wilson, S., Lucchino, D. L., Lenarz, T., Warnecke, A., Prenzler, N., Schmitt, H., King, S., Jackson, L. E., Rosenbloom, J., Atiee, G., Bear, M., Runge, C. L., Gifford, R. H., Rauch, S. D., Lee, D. J., … LeBel, C. (2021). Improved Speech Intelligibility in Subjects With Stable Sensorineural Hearing Loss Following Intratympanic Dosing of FX-322 in a Phase 1b Study. Otology & neurotology : official publication of the American Otological Society, American Neurotology Society [and] European Academy of Otology and Neurotology, 42(7), e849–e857. https://doi.org/10.1097/MAO.0000000000003120

Meiser, J., Weindl, D., & Hiller, K. (2013). Complexity of dopamine metabolism. Cell communication and signaling : CCS, 11(1), 34. https://doi.org/10.1186/1478-811X-11-34

Meltzer, H. Y. (2013). Update on typical and atypical antipsychotic drugs. Annual Review of Medicine, 64(1), 393-406. https://doi.org/10.1146/annurev-med-050911-161504

Milligan, G., & Kostenis, E. (2006). Heterotrimeric G-proteins: a short history. British journal of pharmacology, 147 Suppl 1(Suppl 1), S46–S55. https://doi.org/10.1038/sj.bjp.0706405

Mishra, A., Singh, S., & Shukla, S. (2018). Physiological and functional basis of dopamine receptors and their role in neurogenesis: Possible implication for Parkinson's disease. Journal of Experimental Neuroscience, 12, 117906951877982. https://doi.org/10.1177/1179069518779829

Mogenson, G. J., Jones, D. L., & Yim, C. Y. (1980). From motivation to action: functional interface between the limbic system and the motor system. Progress in neurobiology, 14(2-3), 69–97. https://doi.org/10.1016/0301-0082(80)90018-0

Mussmann, R., Geese, M., Harder, F., Kegel, S., Andag, U., Lomow, A., Burk, U., Onichtchouk, D., Dohrmann, C., & Austen, M. (2007). Inhibition of GSK3 promotes replication and survival of pancreatic beta cells. The Journal of biological chemistry, 282(16), 12030–12037. https://doi.org/10.1074/jbc.M609637200

Nabinger, D. D., Altenhofen, S., Peixoto, J. V., da Silva, J. M. K., & Bonan, C. D. (2021). Long-lasting behavioral effects of quinpirole exposure on zebrafish. Neurotoxicology and teratology, 88, 107034. https://doi.org/10.1016/j.ntt.2021.107034

Nakashima, A., Hayashi, N., Kaneko, Y. S., Mori, K., Sabban, E. L., Nagatsu, T., & Ota, A. (2009). Role of N-terminus of tyrosine hydroxylase in the biosynthesis of catecholamines. Journal of neural transmission (Vienna, Austria: 1996), 116(11), 1355–1362. https://doi.org/10.1007/s00702-009-0227-8

Nakashima, A., Ohnuma, S., Kodani, Y., Kaneko, Y. S., Nagasaki, H., Nagatsu, T., & Ota, A. (2016). Inhibition of deubiquitinating activity of USP14 decreases tyrosine hydroxylase phosphorylated at Ser19 in PC12D cells. Biochemical and biophysical research communications, 472(4), 598–602. https://doi.org/10.1016/j.bbrc.2016.03.022

Nibbs, R. J., & Graham, G. J. (2013). Immune regulation by atypical chemokine receptors. Nature Reviews Immunology, 13(11), 815-829. https://doi.org/10.1038/nri3544

Niewiarowska-Sendo, A., Polit, A., Piwowar, M., Tworzydło, M., Kozik, A., & Guevara-Lora, I. (2017). Bradykinin B2 and dopamine D2 receptors form a functional dimer. Biochimica et biophysica acta. Molecular cell research, 1864(10), 1855–1866. https://doi.org/10.1016/j.bbamcr.2017.07.012

O'Brien, W. T., Huang, J., Buccafusca, R., Garskof, J., Valvezan, A. J., Berry, G. T., & Klein, P. S. (2011). Glycogen synthase kinase-3 is essential for β-arrestin-2 complex formation and lithium-sensitive behaviors in mice. The Journal of clinical investigation, 121(9), 3756–3762. https://doi.org/10.1172/JCI45194

Obsilova, V., Nedbalkova, E., Silhan, J., Boura, E., Herman, P., Vecer, J., Sulc, M., Teisinger, J., Dyda, F., & Obsil, T. (2008). The 14-3-3 protein affects the conformation of the regulatory domain of human tyrosine hydroxylase. Biochemistry, 47(6), 1768–1777. https://doi.org/10.1021/bi7019468

Oh, J., Kim, Y., Che, L., Kim, J. B., Chang, G. E., Cheong, E., Kang, S. G., & Ha, Y. (2017). Regulation of cAMP and GSK3 signaling pathways contributes to the neuronal conversion of glioma. PloS one, 12(11), e0178881. https://doi.org/10.1371/journal.pone.0178881

Oka, K., Ashiba, G., Kiss, B., & Nagatsu, T. (1982). Short-term effect of stress on tyrosine hydroxylase activity. Neurochemistry International, 4(5), 375-382. https://doi.org/10.1016/0197-0186(82)90079-1

Ortiz, J., Gómez, J., Torrent, A., Aldavert, M., & Blanco, I. (2000). Quantitative radioisotopic determination of histidine decarboxylase using high-performance liquid chromatography. Analytical biochemistry, 280(1), 111–117. https://doi.org/10.1006/abio.2000.4494

Osinga, T. E., Links, T. P., Dullaart, R. P., Pacak, K., Horst-Schrivers, A. N., Kerstens, M. N., & Kema, I. P. (2017). Emerging role of dopamine in neovascularization of pheochromocytoma and paraganglioma. The FASEB Journal, 31(6), 2226-2240. https://doi.org/10.1096/fj.201601131r

Otero Losada, M. E., & Rubio, M. C. (1985). Striatal dopamine and motor activity changes observed shortly after lithium administration. Naunyn-Schmiedeberg's archives of pharmacology, 330(3), 169–174. https://doi.org/10.1007/BF00572429

Palczewski, K., Kumasaka, T., Hori, T., Behnke, C. A., Motoshima, H., Fox, B. A., Trong, I. L., Teller, D. C., Okada, T., Stenkamp, R. E., Yamamoto, M., & Miyano, M. (2000). Crystal structure of rhodopsin: A G protein-coupled receptor. Science, 289(5480), 739-745. https://doi.org/10.1126/science.289.5480.739

Pandey, S., Kumari, P., Baidya, M., Kise, R., Cao, Y., Dwivedi-Agnihotri, H., Banerjee, R., Li, X. X., Cui, C. S., Lee, J. D., Kawakami, K., Chaturvedi, M., Ranjan, A., Laporte, S. A., Woodruff, T. M., Inoue, A., & Shukla, A. K. (2021). Intrinsic bias at non-canonical, β-arrestin-coupled seven transmembrane receptors. https://doi.org/10.1101/2021.02.02.429298

Patel, K. R., Cherian, J., Gohil, K., & Atkinson, D. (2014). Schizophrenia: overview and treatment options. P & T : a peer-reviewed journal for formulary management, 39(9), 638–645.

Pearson, J., Goldstein, M., Markey, K., & Brandeis, L. (1983). Human brainstem catecholamine neuronal anatomy as indicated by immunocytochemistry with antibodies to tyrosine hydroxylase. Neuroscience, 8(1), 3-32. https://doi.org/10.1016/0306-4522(83)90023-4

Peczely, L., Ollmann, T., Laszlo, K., Lenard, L., & Grace, A. A. (2022). The D2-like Dopamine Receptor Agonist Quinpirole Microinjected Into the Ventral Pallidum Dose-Dependently Inhibits the VTA and Induces Place Aversion. The international journal of neuropsychopharmacology, 25(7), 590–599. https://doi.org/10.1093/ijnp/pyac024

Perez, R. G., Waymire, J. C., Lin, E., Liu, J. J., Guo, F., & Zigmond, M. J. (2002). A role for α-synuclein in the regulation of dopamine biosynthesis. The Journal of Neuroscience, 22(8), 3090-3099. https://doi.org/10.1523/jneurosci.22-08-03090.2002

Picchioni, M., & Murray, R. (2008). Schizophrenia. Scholarpedia, 3(4), 4132. https://doi.org/10.4249/scholarpedia.4132

Pickel, V. M., Joh, T. H., & Reis, D. J. (1975b). Ultrastructural localization of tyrosine hydroxylase in noradrenergic neurons of brain. Proceedings of the National Academy of Sciences of the United States of America, 72(2), 659–663. https://doi.org/10.1073/pnas.72.2.659

Pickel, V. M., Joh, T. H., Field, P. M., Becker, C. G., & Reis, D. J. (1975a). Cellular localization of tyrosine hydroxylase by immunohistochemistry. Journal of Histochemistry & Cytochemistry, 23(1), 1-12. https://doi.org/10.1177/23.1.234988

Pivonello, R., Waaijers, M., Kros, J. M., Pivonello, C., de Angelis, C., Cozzolino, A., Colao, A., Lamberts, S. W. J., & Hofland, L. J. (2017). Dopamine D2 receptor expression in the corticotroph cells of the human normal pituitary gland. Endocrine, 57(2), 314–325. https://doi.org/10.1007/s12020-016-1107-2

Polanczyk, G., De Lima, M. S., Horta, B. L., Biederman, J., & Rohde, L. A. (2007). The worldwide prevalence of ADHD: A systematic review and Metaregression analysis. American Journal of Psychiatry, 164(6), 942-948. https://doi.org/10.1176/ajp.2007.164.6.942

Pringsheim, T., Wiltshire, K., Day, L., Dykeman, J., Steeves, T., & Jette, N. (2012). The incidence and prevalence of Huntington's disease: A systematic review and meta-analysis. Movement Disorders, 27(9), 1083-1091. https://doi.org/10.1002/mds.25075

Quaife-Ryan, G. A., Mills, R. J., Lavers, G., Voges, H. K., Vivien, C. J., Elliott, D. A., Ramialison, M., Hudson, J. E., & Porrello, E. R. (2020). β-Catenin drives distinct transcriptional networks in proliferative and nonproliferative cardiomyocytes.

Development (Cambridge, England), 147(22), dev193417. https://doi.org/10.1242/dev.193417

Rajagopal, S., Rajagopal, K., & Lefkowitz, R. J. (2010). Teaching old receptors new tricks: Biasing seven-transmembrane receptors. Nature Reviews Drug Discovery, 9(5), 373-386. https://doi.org/10.1038/nrd3024

Ramsey, A. J., & Fitzpatrick, P. F. (1998). Effects of phosphorylation of serine 40 of tyrosine Hydroxylase on binding of Catecholamines: evidence for a novel regulatory mechanism. *Biochemistry*, *37*(25), 8980-8986. https://doi.org/10.1021/bi980582l

Reed, M. C., Lieb, A., & Nijhout, H. F. (2010). The biological significance of substrate inhibition: a mechanism with diverse functions. BioEssays : news and reviews in molecular, cellular and developmental biology, 32(5), 422–429. https://doi.org/10.1002/bies.200900167

Reiter, E., Ahn, S., Shukla, A. K., & Lefkowitz, R. J. (2012). Molecular mechanism of β-arrestin-Biased Agonism at seven-transmembrane receptors. Annual Review of Pharmacology and Toxicology, 52(1), 179-197. https://doi.org/10.1146/annurev.pharmtox.010909.105800

Ring, D. B., Johnson, K. W., Henriksen, E. J., Nuss, J. M., Goff, D., Kinnick, T. R., Ma, S. T., Reeder, J. W., Samuels, I., Slabiak, T., Wagman, A. S., Hammond, M. E., & Harrison, S. D. (2003). Selective glycogen synthase kinase 3 inhibitors potentiate insulin activation of glucose transport and utilization in vitro and in vivo. Diabetes, 52(3), 588–595. https://doi.org/10.2337/diabetes.52.3.588

Rippin, I., & Eldar-Finkelman, H. (2021). Mechanisms and therapeutic implications of GSK-3 in treating Neurodegeneration. Cells, 10(2), 262. https://doi.org/10.3390/cells10020262

Robertson, M. M., & Stern, J. S. (1997). The Gilles de la Tourette syndrome. Critical Reviews™ in Neurobiology, 11(1), 1-19. https://doi.org/10.1615/critrevneurobiol.v11.i1.10

Roos, R. A. (2010). Huntington's disease: A clinical review. Orphanet Journal of Rare Diseases, 5(1). https://doi.org/10.1186/1750-1172-5-40

Rosenbaum, D. M., Rasmussen, S. G., & Kobilka, B. K. (2009). The structure and function of G-protein-coupled receptors. Nature, 459(7245), 356–363. https://doi.org/10.1038/nature08144

Saba, R. A., Maia, D. P., Cardoso, F. E. C., Borges, V., F Andrade, L. A., Ferraz, H. B., Barbosa, E. R., Rieder, C. R. M., da Silva, D. J., Chien, H. F., Capato, T., Rosso, A. L., Souza Lima, C. F., Bezerra, J. M. F., Nicaretta, D., Povoas Barsottini, O. G., Godeiro-Júnior, C., Broseghini Barcelos, L., Cury, R. G., Spitz, M., … Della Colletta, M. V. (2022). Guidelines for Parkinson's disease treatment: consensus from the Movement Disorders Scientific Department of the Brazilian Academy of Neurology - motor symptoms. Arquivos de neuro-psiquiatria, 80(3), 316–329. https://doi.org/10.1590/0004-282X-ANP-2021-0219

Sánchez-Soto, M., Casadó-Anguera, V., Yano, H., Bender, B. J., Cai, N. S., Moreno, E., Canela, E. I., Cortés, A., Meiler, J., Casadó, V., & Ferré, S. (2018). α_{2A}- and α_{2C}-Adrenoceptors as Potential Targets for Dopamine and Dopamine Receptor Ligands. Molecular neurobiology, 55(11), 8438–8454. https://doi.org/10.1007/s12035-018-1004-1

Satake, H., & Sakai, T. (2008). Recent advances and perceptions in studies of heterodimerization between G protein-coupled receptors. Protein and peptide letters, 15(3), 300–308. https://doi.org/10.2174/092986608783744207

Seeman, P. (2011). All roads to schizophrenia lead to dopamine supersensitivity and elevated dopamine D2High receptors. CNS Neuroscience & Therapeutics, 17(2), 118-132. https://doi.org/10.1111/j.1755-5949.2010.00162.x

Seeman, P., & Schaus, J. M. (1991). Dopamine receptors labelled by [3H]quinpirole. European journal of pharmacology, 203(1), 105–109. https://doi.org/10.1016/0014-2999(91)90796-s

Sharma, M., Celver, J., Octeau, J. C., & Kovoor, A. (2013). Plasma membrane compartmentalization of D2 dopamine receptors. The Journal of biological chemistry, 288(18), 12554–12568. https://doi.org/10.1074/jbc.M112.443945

Shenoy, S. K., Drake, M. T., Nelson, C. D., Houtz, D. A., Xiao, K., Madabushi, S., Reiter, E., Premont, R. T., Lichtarge, O., & Lefkowitz, R. J. (2006). beta-arrestin-dependent, G protein-independent ERK1/2 activation by the beta2 adrenergic receptor. The Journal of biological chemistry, 281(2), 1261–1273. https://doi.org/10.1074/jbc.M506576200

Simon, C., Soga, T., Okano, H. J., & Parhar, I. (2021). α-Synuclein-mediated neurodegeneration in Dementia with Lewy bodies: the pathobiology of a paradox. Cell & bioscience, 11(1), 196. https://doi.org/10.1186/s13578-021-00709-y

Singh, H., Chmura, J., Bhaumik, R., Pandey, G. N., & Rasenick, M. M. (2020). Membrane-Associated α-Tubulin Is Less Acetylated in Postmortem Prefrontal Cortex from Depressed Subjects Relative to Controls: Cytoskeletal Dynamics, HDAC6, and Depression. The Journal of neuroscience : the official journal of the Society for Neuroscience, 40(20), 4033–4041. https://doi.org/10.1523/JNEUROSCI.3033-19.2020

Smith, J. S., Lefkowitz, R. J., & Rajagopal, S. (2018). Biased signalling: From simple switches to allosteric microprocessors. Nature Reviews Drug Discovery, 17(4), 243-260. https://doi.org/10.1038/nrd.2017.229

Sojka, A. C., Brennan, K. M., Maizels, E. T., & Young, C. D. (2017). The Science Behind G Protein-Coupled Receptors (GPCRs) and Their Accurate Visual Representation in Scientific Research. The Journal of biocommunication, 41(1), e6. https://doi.org/10.5210/jbc.v41i1.7309

Spina, M. B., & Cohen, G. (1989). Dopamine turnover and glutathione oxidation: Implications for Parkinson disease. Proceedings of the National Academy of Sciences, 86(4), 1398-1400. https://doi.org/10.1073/pnas.86.4.1398

Sproule B. (2002). Lithium in bipolar disorder: can drug concentrations predict therapeutic effect?. Clinical pharmacokinetics, 41(9), 639–660. https://doi.org/10.2165/00003088-200241090-00002

Stahl, S. M. (2018). Mechanism of action of vesicular monoamine transporter 2 (VMAT2) inhibitors in tardive dyskinesia: Reducing dopamine leads to less "go" and more "stop" from the motor striatum for robust therapeutic effects. CNS Spectrums, 23(1), 1-6. https://doi.org/10.1017/s1092852917000621

Stöckel, K., Solomon, F., Paravicini, U., & Thoenen, H. (1974). Dissociation between effects of nerve growth factor on tyrosine hydrolase and tubulin synthesis in sympathetic ganglia. Nature, 250(462), 150–151. https://doi.org/10.1038/250150a0

Stokes, P. E. (1976). Relationship of lithium chloride dose to treatment response in acute mania. Archives of General Psychiatry, 33(9), 1080. https://doi.org/10.1001/archpsyc.1976.01770090070006

Sulzer, D., Sonders, M. S., Poulsen, N. W., & Galli, A. (2005). Mechanisms of neurotransmitter release by amphetamines: A review. Progress in Neurobiology, 75(6), 406-433. https://doi.org/10.1016/j.pneurobio.2005.04.003

Surmeier, D. J., Ding, J., Day, M., Wang, Z., & Shen, W. (2007). D1 and D2 dopamine-receptor modulation of striatal glutamatergic signaling in striatal medium spiny neurons. Trends in Neurosciences, 30(5), 228-235. https://doi.org/10.1016/j.tins.2007.03.008

Szigetvari, P. D., Muruganandam, G., Kallio, J. P., Hallin, E. I., Fossbakk, A., Loris, R., Kursula, I., Møller, L. B., Knappskog, P. M., Kursula, P., & Haavik, J. (2019). The quaternary structure of human tyrosine hydroxylase: effects of dystonia-associated missense variants on oligomeric state and enzyme activity. Journal of neurochemistry, 148(2), 291–306. https://doi.org/10.1111/jnc.14624

Taura, J., Valle-León, M., Sahlholm, K., Watanabe, M., Van Craenenbroeck, K., Fernández-Dueñas, V., Ferré, S., & Ciruela, F. (2018). Behavioral control by striatal

adenosine A_{2A} -dopamine D_2 receptor heteromers. Genes, brain, and behavior, 17(4), e12432. https://doi.org/10.1111/gbb.12432

Tekin, I., Roskoski, R., Carkaci-Salli, N., & Vrana, K. E. (2014). Complex molecular regulation of tyrosine hydroxylase. Journal of Neural Transmission, 121(12), 1451-1481. https://doi.org/10.1007/s00702-014-1238-7

Toska, K., Kleppe, R., Armstrong, C. G., Morrice, N. A., Cohen, P., & Haavik, J. (2002). Regulation of tyrosine hydroxylase by stress-activated protein kinases. Journal of neurochemistry, 83(4), 775–783. https://doi.org/10.1046/j.1471-4159.2002.01172.x

Truong, J. G., Newman, A. H., Hanson, G. R., & Fleckenstein, A. E. (2004). Dopamine D2 receptor activation increases vesicular dopamine uptake and redistributes vesicular monoamine transporter-2 protein. European journal of pharmacology, 504(1-2), 27–32. https://doi.org/10.1016/j.ejphar.2004.09.049

Tuteja N. (2009). Signaling through G protein coupled receptors. Plant signaling & behavior, 4(10), 942–947. https://doi.org/10.4161/psb.4.10.9530

Tysnes, O., & Storstein, A. (2017). Epidemiology of Parkinson's disease. Journal of Neural Transmission, 124(8), 901-905. https://doi.org/10.1007/s00702-017-1686-y

Uçok, A., & Gaebel, W. (2008). Side effects of atypical antipsychotics: a brief overview. World psychiatry : official journal of the World Psychiatric Association (WPA), 7(1), 58–62. https://doi.org/10.1002/j.2051-5545.2008.tb00154.x

Uhl, F. E., Vierkotten, S., Wagner, D. E., Burgstaller, G., Costa, R., Koch, I., Lindner, M., Meiners, S., Eickelberg, O., & Königshoff, M. (2015). Preclinical validation and imaging of Wnt-induced repair in human 3D lung tissue cultures. The European respiratory journal, 46(4), 1150–1166. https://doi.org/10.1183/09031936.00183214

Unnerstall, J. R., & Long, M. M. (1996). Differential effects of the intraventricular administration of 6-hydroxydopamine on the induction of type II beta-tubulin and tyrosine hydroxylase mRNA in the locus coeruleus of the aging Fischer 344 rat. The

Journal of comparative neurology, 364(2), 363–381. https://doi.org/10.1002/(SICI)1096-9861(19960108)364:2<363::AID-CNE12>3.0.CO;2-Q

Usiello, A., Baik, J., Rougé-Pont, F., Picetti, R., Dierich, A., LeMeur, M., Piazza, P. V., & Borrelli, E. (2000). Distinct functions of the two isoforms of dopamine D2 receptors. Nature, 408(6809), 199-203. https://doi.org/10.1038/35041572

Valle, R. (2020). Schizophrenia in ICD-11: Comparison of ICD-10 and DSM-5. Revista de Psiquiatría y Salud Mental (English Edition), 13(2), 95-104. https://doi.org/10.1016/j.rpsmen.2020.01.002

Van Lith, L. H., Oosterom, J., Van Elsas, A., & Zaman, G. J. (2009). C5a-stimulated recruitment of β-arrestin2 to the Nonsignaling 7-Transmembrane decoy receptor C5L2. SLAS Discovery, 14(9), 1067-1075. https://doi.org/10.1177/1087057109341407

Vasudevan, L., Borroto-Escuela, D. O., Huysentruyt, J., Fuxe, K., Saini, D. K., & Stove, C. (2019). Heterodimerization of Mu Opioid Receptor Protomer with Dopamine D_2 Receptor Modulates Agonist-Induced Internalization of Mu Opioid Receptor. Biomolecules, 9(8), 368. https://doi.org/10.3390/biom9080368

Verstreken, P., Ly, C. V., Venken, K. J., Koh, T. W., Zhou, Y., & Bellen, H. J. (2005). Synaptic mitochondria are critical for mobilization of reserve pool vesicles at Drosophila neuromuscular junctions. Neuron, 47(3), 365–378. https://doi.org/10.1016/j.neuron.2005.06.018

Vigny, A., Huitorel, P., Henry, J. P., & Pantaloni, D. (1980). Interaction of tyrosine hydroxylase with tubulin. Biochemical and biophysical research communications, 92(2), 431–439. https://doi.org/10.1016/0006-291x(80)90351-4

Violin, J. D., & Lefkowitz, R. J. (2007). Beta-arrestin-biased ligands at seven-transmembrane receptors. Trends in pharmacological sciences, 28(8), 416–422. https://doi.org/10.1016/j.tips.2007.06.006

Voss, J. H., & Müller, C. E. (2022). Heterotrimeric G Protein α-Subunits - Structures, Peptide-Derived Inhibitors, and Mechanisms. *Current medicinal chemistry*, *29*(42), 6359–6378. https://doi.org/10.2174/0929867329666220308112424

Wada A. (2009). GSK-3 inhibitors and insulin receptor signaling in health, disease, and therapeutics. Frontiers in bioscience (Landmark edition), 14(4), 1558–1570. https://doi.org/10.2741/3324

Wallace L. J. (2007). A small dopamine permeability of storage vesicle membranes and end product inhibition of tyrosine hydroxylase are sufficient to explain changes occurring in dopamine synthesis and storage after inhibition of neuron firing. Synapse (New York, N.Y.), 61(9), 715–723. https://doi.org/10.1002/syn.20408

Wang, J., Lou, H., Pedersen, C. J., Smith, A. D., & Perez, R. G. (2009). 14-3-3zeta contributes to tyrosine hydroxylase activity in MN9D cells: localization of dopamine regulatory proteins to mitochondria. The Journal of biological chemistry, 284(21), 14011–14019. https://doi.org/10.1074/jbc.M901310200

Wang, M., Pei, L., Fletcher, P. J., Kapur, S., Seeman, P., & Liu, F. (2010). Schizophrenia, amphetamine-induced sensitized state and acute amphetamine exposure all show a common alteration: increased dopamine D2 receptor dimerization. Molecular brain, 3, 25. https://doi.org/10.1186/1756-6606-3-25

Weiner, D. M., Levey, A. I., Sunahara, R. K., Niznik, H. B., O'Dowd, B. F., Seeman, P., & Brann, M. R. (1991). D1 and D2 dopamine receptor mRNA in rat brain. Proceedings of the National Academy of Sciences of the United States of America, 88(5), 1859–1863. https://doi.org/10.1073/pnas.88.5.1859

Weis, W. I., & Kobilka, B. K. (2018). The molecular basis of G protein–coupled receptor activation. Annual Review of Biochemistry, 87(1), 897-919. https://doi.org/10.1146/annurev-biochem-060614-033910

Wiemerslage, L., Schultz, B. J., Ganguly, A., & Lee, D. (2013). Selective degeneration of dopaminergic neurons by MPP(+) and its rescue by D2 autoreceptors in Drosophila

primary culture. Journal of neurochemistry, 126(4), 529–540. https://doi.org/10.1111/jnc.12228

Wu, D., & Pan, W. (2010). GSK3: A multifaceted kinase in Wnt signaling. Trends in Biochemical Sciences, 35(3), 161-168. https://doi.org/10.1016/j.tibs.2009.10.002

Youdim, M. B., & Bakhle, Y. S. (2006). Monoamine oxidase: isoforms and inhibitors in Parkinson's disease and depressive illness. British journal of pharmacology, 147 Suppl 1(Suppl 1), S287–S296. https://doi.org/10.1038/sj.bjp.0706464

Young W. (2009). Review of lithium effects on brain and blood. Cell transplantation, 18(9), 951–975. https://doi.org/10.3727/096368909X471251

Yu, S., Zuo, X., Li, Y., Zhang, C., Zhou, M., Zhang, Y. A., Uéda, K., & Chan, P. (2004). Inhibition of tyrosine hydroxylase expression in α-synuclein-transfected dopaminergic neuronal cells. Neuroscience Letters, 367(1), 34-39. https://doi.org/10.1016/j.neulet.2004.05.118

Yung, K. K., & Bolam, J. P. (2000). Localization of dopamine D1 and D2 receptors in the rat neostriatum: synaptic interaction with glutamate- and GABA-containing axonal terminals. Synapse (New York, N.Y.), 38(4), 413–420. https://doi.org/10.1002/1098-2396(20001215)38:4<413::AID-SYN6>3.0.CO;2-V

Zaugg, L. K., Banu, A., Walther, A. R., Chandrasekaran, D., Babb, R. C., Salzlechner, C., Hedegaard, M., Gentleman, E., & Sharpe, P. T. (2020). Translation Approach for Dentine Regeneration Using GSK-3 Antagonists. Journal of dental research, 99(5), 544–551. https://doi.org/10.1177/0022034520908593

Zhang, B., Peng, X., Sun, X., Guo, Y., & Li, T. (2022). Environmentally-relevant concentrations of the antipsychotic drugs sulpiride and clozapine induce abnormal dopamine and serotonin signaling in zebrafish brain. Scientific Reports, 12(1). https://doi.org/10.1038/s41598-022-22169-1

Zhao, J., Li, S., Trilok, S., Tanaka, M., Jokubaitis-Jameson, V., Wang, B., Niwa, H., & Nakayama, N. (2014). Small molecule-directed specification of sclerotome-like chondroprogenitors and induction of a somatic chondrogenesis program from embryonic stem cells. Development (Cambridge, England), 141(20), 3848–3858. https://doi.org/10.1242/dev.105981

Zhen Meng, S., Obonai, T., & Takashima, S. (1998). A developmental study of the dopamine D2R receptors in the human basal ganglia and thalamus. Early Human Development, 51(1), 23-30. https://doi.org/10.1016/s0378-3782(97)00071-6

Annex

Annex 1

1. In-gel digestion and LC-MS/MS analysis

Bands were manually excised and digested with trypsin using a DigestPro MS digestor (Intavis). The process involved reduction with DTT, derivatization with iodoacetamide, and enzymatic digestion with trypsin at 37°C for 8 h (Casanovas et. al, 2009). The resulting peptide mixtures were evaporated to dryness and redissolved in 20 µL 5% MeOH, 0.5% TFA.

Peptides were analyzed by LC-MS/MS using a 1200 HPLC system (Agilent Technologies, Santa Clara, CA, USA) coupled to an LTQ Orbitrap XL mass spectrometer (Thermo Scientific) equipped with a nanoelectrospray source (Proxeon, Odense, Denmark). Samples were separated with a C18 pre-concentration cartridge (Agilent Technologies) connected to a C18 100 µm x 150 mm column (Nikkyo Technos Co, Tokyo, Japan) at 400 nL/min using a 30-min linear gradient from 0 to 35% solvent B (Solvent A: 0.1% (v/v) formic acid; solvent B: ACN 0.1% (v/v) formic acid). The LTQ XL Orbitrap was operated in the positive ion mode with a spray voltage of 1.8 kV. The spectrometric analysis was performed in a data dependent mode, acquiring a full scan followed by 8 MS/MS scans of the 8 most intense signals from the inclusion list (Table 9). If an ion resulting from a neutral loss of phosphate was detected (49, 32.6, 24.5) among the 3 most abundant fragments in the MS/MS spectrum, a MS^3 scan was performed on this ion. The full MS (scan range m/z 400-1650) was acquired in the Orbitrap with a resolution of 60.000 (at m/z 400). The MS/MS spectra were done in the linear ion-trap. For relative quantification, the area of each monitorized peptide was calculated using the Xcalibur software (Thermo Scientific).

modification	sequence	z=1	z=2	z=3
	(K)GFRRAVSEQDAK(Q)	1363.7077	682.35385	455.2359
1Phospho	(K)GFRRAVSEQDAK(Q)	1443.674	722.337	481.891333
	(R)RAVSEQDAK(Q)	1003.5167	502.25835	335.172233
1Phospho	(R)RAVSEQDAK(Q)	1083.483	542.2415	361.827667
	(R)RAVSEQDAKQAEAVTSPR(F)	1942.9941	971.99705	648.331367
1Phospho	(R)RAVSEQDAKQAEAVTSPR(F)	2022.9604	1011.9802	674.9868
2Phospho	(R)RAVSEQDAKQAEAVTSPR(F)	2102.9268	1051.9634	701.642267
3Phospho	(R)RAVSEQDAKQAEAVTSPR(F)	2182.8931	1091.94655	728.2977
	(R)AVSEQDAK(Q)	847.4156	424.2078	283.138533
1Phospho	(R)AVSEQDAK(Q)	927.3819	464.19095	309.793967
	(R)AVSEQDAKQAEAVTSPR(F)	1786.893	893.9465	596.297667

1Phospho	(R)AVSEQDAKQAEAVTSPR(F)	1866.8593	933.92965	622.9531
2Phospho	(R)AVSEQDAKQAEAVTSPR(F)	1946.8256	973.9128	649.608533
3Phospho	(R)AVSEQDAKQAEAVTSPR(F)	2026.792	1013.896	676.264
	(R)AVSEQDAKQAEAVTSPRFIGR(R)	2260.168	1130.584	754.056
1Phospho	(R)AVSEQDAKQAEAVTSPRFIGR(R)	2340.1344	1170.5672	780.711467
2Phospho	(R)AVSEQDAKQAEAVTSPRFIGR(R)	2420.1007	1210.55035	807.3669
3Phospho	(R)AVSEQDAKQAEAVTSPRFIGR(R)	2500.067	1250.5335	834.022333
	(K)QAEAVTSPR(F)	958.4952	479.7476	320.165067
1Phospho	(K)QAEAVTSPR(F)	1038.4616	519.7308	346.820533
2Phospho	(K)QAEAVTSPR(F)	1118.4279	559.71395	373.475967
	(K)QAEAVTSPRFIGR(R)	1431.7703	716.38515	477.923433
1Phospho	(K)QAEAVTSPRFIGR(R)	1511.7366	756.3683	504.578867
2Phospho	(K)QAEAVTSPRFIGR(R)	1591.7029	796.35145	531.2343
	(K)QAEAVTSPRFIGRR(Q)	1587.8714	794.4357	529.957133
1Phospho	(K)QAEAVTSPRFIGRR(Q)	1667.8377	834.41885	556.612567
2Phospho	(K)QAEAVTSPRFIGRR(Q)	1747.8041	874.40205	583.268033
	(R)FIGRRQSLIEDAR(K)	1560.8605	780.93025	520.9535
1Phospho	(R)FIGRRQSLIEDAR(K)	1640.8268	820.9134	547.608933
	(R)RQSLIEDAR(K)	1087.5854	544.2927	363.195133
1Phospho	(R)RQSLIEDAR(K)	1167.5518	584.2759	389.8506
	(R)RQSLIEDARK(E)	1215.6804	608.3402	405.893467
1Phospho	(R)RQSLIEDARK(E)	1295.6467	648.32335	432.5489
	(R)QSLIEDAR(K)	931.4843	466.24215	311.161433
1Phospho	(R)QSLIEDAR(K)	1011.4507	506.22535	337.8169
	(R)QSLIEDARK(E)	1059.5793	530.28965	353.859767
1Phospho	(R)QSLIEDARK(E)	1139.5456	570.2728	380.5152
	(R)FEVPSGDLAALLSSVR(R)	1660.8905	830.94525	554.296833
	(R)TGFQLRPVAGLLSAR(D)	1585.9173	793.45865	529.305767

Table 9. Inclusion list for mass spectrometry method. In order to detect specifically the sites of interest the protein was virtually digested and a list with the theoretical tryptic peptides containing the modification sites was generated.

2. The effect of incubation on TH phosphorylation

2.1 In-gel digestion and Peptide Mass Fingerprinting

Samples were excised and after that digested using an automatic device (DigestPro MS, Intavis). The processing involved reduction with dithiothreitol (DTT), derivatization with iodoacetamide (IAA), and enzymatic digestion with trypsin (37ºC, 8 h). The resulting peptide mixture was spotted on a MALDI plate with CHCA and analysed using a MALDI-TOF/TOF mass spectrometer (4800 AB Sciex). The TOF spectra were interpreted by database search (Mascot, Matrix Science, MA, USA) using the following parameters: peptide mass tolerance, 50 ppm; maximum number of missed cleavages, 2; fixed modification, carbamidomethyl cysteine; variable modification, oxidation of methionine; significance threshold of the MOWSE score, $p<0.05$. The database used for identification was NCBIprot taxonomy Mammalia. All identifications were manually validated.

2.2 LC-MS/MS analysis

The MS system used was an LTQ XL Orbitrap (ThermoFisher) equipped with a nanoESI ion source. Samples were taken to 20 µL with 5% MeOH, 0.5% TFA and loaded into the chromatographic system consisting of a C18 preconcentration cartridge (Agilent Technologies) connected to a 15 cm long, 100 µm i.d. C18 column (Nikkyo Technos Co.). The separation was done at 0.4 µL/min in a 30-min acetonitrile gradient from 0 to 35% (solvent A: 0.1% formic acid, solvent B: acetonitrile 0.1% formic acid). The HPLC system was composed of an Agilent 1200 capillary nano pump, a binary pump, a thermostated micro injector and a micro switch valve. The LTQ XL Orbitrap was operated in the positive ion mode with a spray voltage of 1.8 kV. The spectrometric analysis was performed in a data dependent mode, acquiring a full scan followed by 8 MS/MS scans of the 8 most intense signals from the inclusion list. If a neutral loss of phosphate was detected (49, 32.6, 24.5) a third scan was performed. The full MS (range 400-1650) was acquired in the Orbitrap with a resolution of 60.000. The MS/MS spectra were done in the linear ion-trap. LC-MS/MS spectra were searched using SEQUEST (Proteome Discoverer v1.4, ThermoFisher) with the following parameters for MS2 spectra: peptide mass tolerance 20 ppm, fragment tolerance 0.6 Da, enzyme set as Trypsin and allowance up to 3 missed cleavages, dynamic modification of methionine oxidation

(+16 Da), phosphorylation S,T,Y (+80), and fixed modification of cysteine carbamidomethylation (+57 Da). For MS3 spectra, peptide mass tolerance 2 Da, fragment tolerance 0.6 Da, enzyme set as Trypsin and allowance up to 3 missed cleavages, dynamic modification of methionine oxidation (+16 Da), phosphorylation S,T,Y (+80 Da), dehydrated S,T (18 Da) and fixed modification of cysteine carbamidomethylation (+57 Da). The ptmRS algorithm was used to provide a confidence measure for the localization of phosphorylation and any other modifications in peptide sequences. The database used for searching was Rattus norvegicus (Uniprot 09/19). Final results were filtered by peptide rank 1, peptide confidence high (1% FDR), search engine rank 1.

3 The effect of CHIR on TH phosphorylation

3.1 In-liquid digestion

Reagents:

- DTT 1M diluted 1/10 with ammonium bicarbonate (20 µL to 200 µL).
- Iodoacetamide 0.5 M diluted 1/5 with ammonium bicarbonate (20 µL to 100 µL).
- NH_4HCO_3, 20 mM.
- Glu-C, 0.1 µg/µL in phosphate buffer pH 7.7 (diluted 1/10 with phosphate buffer)
- Trypsin, 0.1 µg/µL in ammonium bicarbonate, (diluted 1/10 with ammonium bicarbonate)
- Phosphate buffer pH 7.7

Procedure:

- Samples were evaporated until dryness. 100 µL of ammonium bicarbonate was added and samples were divided into two, one for Trypsin and other for Glu-C.
- Trypsin samples were diluted to 200 µL with NH_4HCO_3 and Glu-C samples to 200 µL with phosphate buffer.
- DTT was added to a final concentration of 2 mM (4 µL of DTT 0.1 M). Samples were then incubated for 30 minutes at 56°C with agitation.
- Iodoacetamide was added to a final concentration of 7 mM (14.28 µL of iodoacetamide 0.1 M). Samples were incubated for 30 minutes at 25°C in darkness with agitation.
- DTT was added to a final concentration of 2 mM (4.36 µL of DTT 0.1 M).

- Trypsin was diluted 1/10 with ammonium bicarbonate and Glu-C 1/10 with phosphate buffer.
- Trypsin/Glu-C was added to each sample (2% w/w, 2 µL). Samples were incubated at 37°C overnight (for 18 hours).
- Digestion was stopped with TFA, 1% vol/vol (2.2 µL).

3.2 *LC-MS/MS Analysis*

The MS system used was an LTQ XL Orbitrap (ThermoFisher) equipped with a nanoESI ion source. 20% of the sample was loaded into the chromatographic system consisting in a C18 preconcentration cartridge (Agilent Technologies) connected to a 15 cm long, 100 µm i.d. C18 column (Nikkyo Technos Co.). The separation was done at 0.4 µL/min in a 60-min acetonitrile gradient from 3 to 35% (solvent A: 0.1% formic acid, solvent B: acetonitrile 0.1% formic acid). The HPLC system was composed of an Agilent 1200 capillary nano pump, a binary pump, a thermostated micro injector and a micro switch valve. The LTQ XL Orbitrap was operated in the positive ion mode with a spray voltage of 1.8 kV.

The spectrometric analysis DDA from global list was performed in a data dependent mode, acquiring a full scan followed by 10 MS/MS scans of the 10 most intense signals detected in the MS scan from the global list. The full MS (range 400-1650) was acquired in the Orbitrap with a resolution of 60.000. The MS/MS spectra were done in the linear ion-trap. The spectrometric analysis Inclusion list was performed in a data dependent mode, acquiring a full scan followed by 8 MS/MS scans of the 8 most intense signals from the inclusion list. If a neutral loss of phosphate was detected (49, 32.6, 24.5) a third scan was performed. The full MS (range 400-1650) was acquired in the Orbitrap with a resolution of 60.000. The MS/MS spectra were done in the linear ion-trap.

m/z (mi)	modification	start	end	sequence	z=1	z=2	z=3
1148.5946	1Met-loss+Acetyl	1	12	(-)MPTPSAPSPQPK(G)	1148.5946	574.7973	383.531533
1228.5609	1Met-loss+Acetyl 1phospho	1	12	(-)MPTPSAPSPQPK(G)	1228.5609	614.78045	410.186967
1237.6245		1	12	(-)MPTPSAPSPQPK(G)	1237.6245	619.31225	413.208167
1308.5273	1Met-loss+Acetyl 2Phospho	1	12	(-)MPTPSAPSPQPK(G)	1308.5273	654.76365	436.842433
1317.5909	1Phospho	1	12	(-)MPTPSAPSPQPK(G)	1317.5909	659.29545	439.863633
1388.4936	1Met-loss+Acetyl 3Phospho	1	12	(-)MPTPSAPSPQPK(G)	1388.4936	694.7468	463.497867
1397.5572	2Phospho	1	12	(-)MPTPSAPSPQPK(G)	1397.5572	699.2786	466.519067
1477.5235	3Phospho	1	12	(-)MPTPSAPSPQPK(G)	1477.5235	739.26175	493.1745
1508.7856	1Met-loss+Acetyl	1	15	(-)MPTPSAPSPQPKGFR(R)	1508.7856	754.8928	503.5952
1588.7519	1Met-loss+Acetyl 1phospho	1	15	(-)MPTPSAPSPQPKGFR(R)	1588.7519	794.87595	530.250633
1597.8155		1	15	(-)MPTPSAPSPQPKGFR(R)	1597.8155	799.40775	533.271833
1668.7183	1Met-loss+Acetyl 2Phospho	1	15	(-)MPTPSAPSPQPKGFR(R)	1668.7183	834.85915	556.9061
1677.7819	1Phospho	1	15	(-)MPTPSAPSPQPKGFR(R)	1677.7819	839.39095	559.9273
1748.6846	1Met-loss+Acetyl 3Phospho	1	15	(-)MPTPSAPSPQPKGFR(R)	1748.6846	874.8423	583.561533
1757.7482	2Phospho	1	15	(-)MPTPSAPSPQPKGFR(R)	1757.7482	879.3741	586.582733
1837.7145	3Phospho	1	15	(-)MPTPSAPSPQPKGFR(R)	1837.7145	919.35725	613.238167
1003.5167		16	24	(R)RAVSEQDAK(Q)	1003.5167	502.25835	335.172233

1083.483	1Phospho	16	24	(R)RAVSEQDAK(Q)	1083.483	542.2415	361.827667
847.4156		17	24	(R)AVSEQDAK(Q)	847.4156	424.2078	283.138533
927.3819	1Phospho	17	24	(R)AVSEQDAK(Q)	927.3819	464.19095	309.793967
1786.893		17	33	(R)AVSEQDAKQAEAVTSPR(F)	1786.893	893.9465	596.297667
1866.8593	1Phospho	17	33	(R)AVSEQDAKQAEAVTSPR(F)	1866.8593	933.92965	622.9531
1946.8256	2Phospho	17	33	(R)AVSEQDAKQAEAVTSPR(F)	1946.8256	973.9128	649.608533
2026.792	3Phospho	17	33	(R)AVSEQDAKQAEAVTSPR(F)	2026.792	1013.896	676.264
958.4952		25	33	(K)QAEAVTSPR(F)	958.4952	479.7476	320.165067
1038.4616	1Phospho	25	33	(K)QAEAVTSPR(F)	1038.4616	519.7308	346.820533
1118.4279	2Phospho	25	33	(K)QAEAVTSPR(F)	1118.4279	559.71395	373.475967
1431.7703		25	37	(K)QAEAVTSPRFIGR(R)	1431.7703	716.38515	477.923433
1511.7366	1Phospho	25	37	(K)QAEAVTSPRFIGR(R)	1511.7366	756.3683	504.578867
1591.7029	2Phospho	25	37	(K)QAEAVTSPRFIGR(R)	1591.7029	796.35145	531.2343
1087.5854		38	46	(R)RQSLIEDAR(K)	1087.5854	544.2927	363.195133
1167.5518	1Phospho	38	46	(R)RQSLIEDAR(K)	1167.5518	584.2759	389.8506
931.4843		39	46	(R)QSLIEDAR(K)	931.4843	466.24215	311.161433
1011.4507	1Phospho	39	46	(R)QSLIEDAR(K)	1011.4507	506.22535	337.8169
1059.5793		39	47	(R)QSLIEDARK(E)	1059.5793	530.28965	353.859767
1139.5456	1Phospho	39	47	(R)QSLIEDARK(E)	1139.5456	570.2728	380.5152
1660.8905		135	150	(R)FEVPSGDLAALLSSVR(R)	1660.8905	830.94525	554.296833
1585.9173		284	298	(R)TGFQLRPVAGLLSAR(D)	1585.9173	793.45865	529.305767

Table 10. Inclusion list with trypsin.

m/z (mi)	Modifications	Start	End	Sequence	z=1	z=2	z=3
2009.0563	1Met-loss	1	20	(-)MPTPSAPSPQPKGFRRAVSE(Q)	2009.0563	1005.02815	670.3521
2051.0669	1Met-loss+Acetyl	1	20	(-)MPTPSAPSPQPKGFRRAVSE(Q)	2051.0669	1026.03345	684.3556
2089.0226	1Met-loss 1Phospho	1	20	(-)MPTPSAPSPQPKGFRRAVSE(Q)	2089.0226	1045.0113	697.0075
2131.0332	1Met-loss+Acetyl 1Phospho	1	20	(-)MPTPSAPSPQPKGFRRAVSE(Q)	2131.0332	1066.0166	711.0111
2140.0968		1	20	(-)MPTPSAPSPQPKGFRRAVSE(Q)	2140.0968	1070.5484	714.0323
2156.0917	1Oxidation	1	20	(-)MPTPSAPSPQPKGFRRAVSE(Q)	2156.0917	1078.54585	719.3639
2168.989	1Met-loss 2Phospho	1	20	(-)MPTPSAPSPQPKGFRRAVSE(Q)	2168.989	1084.9945	723.6630
2182.1073	1Acetyl	1	20	(-)MPTPSAPSPQPKGFRRAVSE(Q)	2182.1073	1091.55365	728.0358
2210.9995	1Met-loss+Acetyl 2Phospho	1	20	(-)MPTPSAPSPQPKGFRRAVSE(Q)	2210.9995	1105.99975	737.6665
2220.0631	1Phospho	1	20	(-)MPTPSAPSPQPKGFRRAVSE(Q)	2220.0631	1110.53155	740.6877
2236.058	1Oxidation 1Phospho	1	20	(-)MPTPSAPSPQPKGFRRAVSE(Q)	2236.058	1118.529	746.0193
2248.9553	1Met-loss 3Phospho	1	20	(-)MPTPSAPSPQPKGFRRAVSE(Q)	2248.9553	1124.97765	750.3184
2252.1418	1Met-loss	1	22	(-)MPTPSAPSPQPKGFRRAVSEQD(A)	2252.1418	1126.5709	751.3806
2262.0737	1Acetyl 1Phospho	1	20	(-)MPTPSAPSPQPKGFRRAVSE(Q)	2262.0737	1131.53685	754.6912

2290.9659	1Met-loss+Acetyl 3Phospho	1	20	(-)MPTPSAPSPQPKGFRRAVSE(Q)	2290.9659	1145.98295	764.3220
2294.1524	1Met-loss+Acetyl	1	22	(-)MPTPSAPSPQPKGFRRAVSEQD(A)	2294.1524	1147.5762	765.3841
2300.0294	2Phospho	1	20	(-)MPTPSAPSPQPKGFRRAVSE(Q)	2300.0294	1150.5147	767.3431
2316.0244	1Oxidation 2Phospho	1	20	(-)MPTPSAPSPQPKGFRRAVSE(Q)	2316.0244	1158.5122	772.6748
2328.9216	1Met-loss 4Phospho	1	20	(-)MPTPSAPSPQPKGFRRAVSE(Q)	2328.9216	1164.9608	776.9739
2332.1081	1Met-loss 1Phospho	1	22	(-)MPTPSAPSPQPKGFRRAVSEQD(A)	2332.1081	1166.55405	778.0360
2342.04	1Acetyl 2Phospho	1	20	(-)MPTPSAPSPQPKGFRRAVSE(Q)	2342.04	1171.52	781.3467
2370.9322	1Met-loss+Acetyl 4Phospho	1	20	(-)MPTPSAPSPQPKGFRRAVSE(Q)	2370.9322	1185.9661	790.9774
2374.1187	1Met-loss+Acetyl 1Phospho	1	22	(-)MPTPSAPSPQPKGFRRAVSEQD(A)	2374.1187	1187.55935	792.0396
2379.9958	3Phospho	1	20	(-)MPTPSAPSPQPKGFRRAVSE(Q)	2379.9958	1190.4979	793.9986
2383.1823		1	22	(-)MPTPSAPSPQPKGFRRAVSEQD(A)	2383.1823	1192.09115	795.0608
2395.9907	1Oxidation 3Phospho	1	20	(-)MPTPSAPSPQPKGFRRAVSE(Q)	2395.9907	1198.49535	799.3302
2399.1772	1Oxidation	1	22	(-)MPTPSAPSPQPKGFRRAVSEQD(A)	2399.1772	1200.0886	800.3924
2412.0745	1Met-loss 2Phospho	1	22	(-)MPTPSAPSPQPKGFRRAVSEQD(A)	2412.0745	1206.53725	804.6915
2422.0063	1Acetyl 3Phospho	1	20	(-)MPTPSAPSPQPKGFRRAVSE(Q)	2422.0063	1211.50315	808.0021
2425.1929	1Acetyl	1	22	(-)MPTPSAPSPQPKGFRRAVSEQD(A)	2425.1929	1213.09645	809.0643
2454.085	1Met-loss+Acetyl 2Phospho	1	22	(-)MPTPSAPSPQPKGFRRAVSEQD(A)	2454.085	1227.5425	818.6950
2459.9621	4Phospho	1	20	(-)MPTPSAPSPQPKGFRRAVSE(Q)	2459.9621	1230.48105	820.6540
2463.1486	1Phospho	1	22	(-)MPTPSAPSPQPKGFRRAVSEQD(A)	2463.1486	1232.0743	821.7162
2475.957	1Oxidation 4Phospho	1	20	(-)MPTPSAPSPQPKGFRRAVSE(Q)	2475.957	1238.4785	825.9857
2479.1435	1Oxidation 1Phospho	1	22	(-)MPTPSAPSPQPKGFRRAVSEQD(A)	2479.1435	1240.07175	827.0478
2492.0408	1Met-loss 3Phospho	1	22	(-)MPTPSAPSPQPKGFRRAVSEQD(A)	2492.0408	1246.5204	831.3469
2501.9727	1Acetyl 4Phospho	1	20	(-)MPTPSAPSPQPKGFRRAVSE(Q)	2501.9727	1251.48635	834.6576
2505.1592	1Acetyl 1Phospho	1	22	(-)MPTPSAPSPQPKGFRRAVSEQD(A)	2505.1592	1253.0796	835.7197
2517.9676	1Acetyl 1Oxidation 4Phospho	1	20	(-)MPTPSAPSPQPKGFRRAVSE(Q)	2517.9676	1259.4838	839.9892
2534.0514	1Met-loss+Acetyl 3Phospho	1	22	(-)MPTPSAPSPQPKGFRRAVSEQD(A)	2534.0514	1267.5257	845.3505
2543.115	2Phospho	1	22	(-)MPTPSAPSPQPKGFRRAVSEQD(A)	2543.115	1272.0575	848.3717
2559.1099	1Oxidation 2Phospho	1	22	(-)MPTPSAPSPQPKGFRRAVSEQD(A)	2559.1099	1280.05495	853.7033
2572.0071	1Met-loss 4Phospho	1	22	(-)MPTPSAPSPQPKGFRRAVSEQD(A)	2572.0071	1286.50355	858.0024
2585.1255	1Acetyl 2Phospho	1	22	(-)MPTPSAPSPQPKGFRRAVSEQD(A)	2585.1255	1293.06275	862.3752
2614.0177	1Met-loss+Acetyl 4Phospho	1	22	(-)MPTPSAPSPQPKGFRRAVSEQD(A)	2614.0177	1307.50885	872.0059
2623.0813	3Phospho	1	22	(-)MPTPSAPSPQPKGFRRAVSEQD(A)	2623.0813	1312.04065	875.0271

2639.0762	1Oxidation 3Phospho	1	22	(-)MPTPSAPSPQPKGFRRAVSEQD(A)	2639.0762	1320.0381	880.3587
2665.0919	1Acetyl 3Phospho	1	22	(-)MPTPSAPSPQPKGFRRAVSEQD(A)	2665.0919	1333.04595	889.0306
2703.0476	4Phospho	1	22	(-)MPTPSAPSPQPKGFRRAVSEQD(A)	2703.0476	1352.0238	901.6825
2719.0425	1Oxidation 4Phospho	1	22	(-)MPTPSAPSPQPKGFRRAVSEQD(A)	2719.0425	1360.02125	907.0142
2745.0582	1Acetyl 4Phospho	1	22	(-)MPTPSAPSPQPKGFRRAVSEQD(A)	2745.0582	1373.0291	915.6861
2761.0531	1Acetyl 1Oxidation 4Phospho	1	22	(-)MPTPSAPSPQPKGFRRAVSEQD(A)	2761.0531	1381.02655	921.0177
2357.3048		23	43	(D)AKQAEAVTSPRFIGRRQSLIE(D)	2357.3048	1179.1524	786.4349
2437.2711	1Phospho	23	43	(D)AKQAEAVTSPRFIGRRQSLIE(D)	2437.2711	1219.13555	813.0904
2517.2375	2Phospho	23	43	(D)AKQAEAVTSPRFIGRRQSLIE(D)	2517.2375	1259.11875	839.7458
2597.2038	3Phospho	23	43	(D)AKQAEAVTSPRFIGRRQSLIE(D)	2597.2038	1299.1019	866.4013
1830.0344		28	43	(E)AVTSPRFIGRRQSLIE(D)	1830.0344	915.5172	610.6781
1910.0008	1Phospho	28	43	(E)AVTSPRFIGRRQSLIE(D)	1910.0008	955.5004	637.3336
1945.0614		28	44	(E)AVTSPRFIGRRQSLIED(A)	1945.0614	973.0307	649.0205
1989.9671	2Phospho	28	43	(E)AVTSPRFIGRRQSLIE(D)	1989.9671	995.48355	663.9890
2025.0277	1Phospho	28	44	(E)AVTSPRFIGRRQSLIED(A)	2025.0277	1013.01385	675.6759
2069.9334	3Phospho	28	43	(E)AVTSPRFIGRRQSLIE(D)	2069.9334	1035.4667	690.6445
2104.994	2Phospho	28	44	(E)AVTSPRFIGRRQSLIED(A)	2104.994	1052.997	702.3313
2184.9604	3Phospho	28	44	(E)AVTSPRFIGRRQSLIED(A)	2184.9604	1092.9802	728.9868

Table 11. Inclusion list with GluC.

3.3 Inclusion list spectra database search

LC-MS/MS spectra were searched using SEQUEST (Proteome Discoverer v1.4, ThermoFisher) with the following parameters for MS2 spectra: peptide mass tolerance 20 ppm, fragment tolerance 0.6 Da, enzyme set as Trypsin and allowance up to 3 missed cleavages, dynamic modification of methionine oxidation (+16 Da), phosphorylation S,T,Y (+80), and fixed modification of cysteine carbamidomethylation (+57 Da). For MS3 spectra, peptide mass tolerance 2 Da, fragment tolerance 0.6 Da, enzyme set as Trypsin and allowance up to 3 missed cleavages, dynamic modification of methionine oxidation (+16 Da), phosphorylation S,T,Y (+80 Da), dehydrated S,T (18 Da) and fixed modification of cysteine carbamidomethylation (+57 Da). The ptmRS algorithm was used to provide a confidence measure for the localization of phosphorylation and any other modifications in peptide sequences. The database used for searching was Rattus norvegicus (Uniprot 09/19). Final results were filtered by peptide rank 1, peptide confidence high (1% FDR), search engine rank 1.

DDA from global list database search

LC-MS/MS spectra were searched using SEQUEST (Proteome Discoverer v1.4, ThermoFisher) with the following parameters: peptide mass tolerance 20 ppm, fragment tolerance 0.6 Da, enzyme set as Trypsin and allowance up to 3 missed cleavages, dynamic modification of methionine oxidation (+16 Da) , N-terminal acetylation (+42 Da), phosphorylation S,T,Y (+80 Da), and fixed modification of cysteine carbamidomethylation (+57 Da). The ptmRS algorithm was used to provide a confidence measure for the localization of phosphorylation and any other modifications in peptide sequences. The database used for searching was Rattus norvegicus (Uniprot 09/19). Final results were filtered by peptide rank 1, peptide confidence high (1% FDR), search engine rank 1.

DDA for the effect of CHIR on phosphorylation

In samples 1 and 2 (CHIR and control respectively) digested with Trypsin, 48/51 peptides 231/283 PSMs from TH, respectively, were identified. The coverage of the protein sequence was 92.97-92.37% for samples 1 and 2, respectively. Nine peptides from the sequence of interest (amino acids 1 to 40), were detected in both samples, three of them phosphorylated peptides (Ser19, Ser31) with ptmRS site probability higher than 90% (Table 12).

	DDA		Inclusion list	
	# PSMs 1	# PSMs 2	# PSMs 1	# PSMs 2
AVSEQDAKQAEAVTSPR	5	6	31	36
AVSEQDAKQAEAVTsPR	4	6	18	20
QAEAVTSPR	6	10	116	115
QAEAVTsPR	3	1	30	31
RAVSEQDAKQAEAVTSPR	2	3	-	-
RAVsEQDAKQAEAVTSPR	2	3	-	-
RAVSEQDAK	-	-	2	4
RQSLIEDARKER	1	2	-	-
RQSLIEDAR	2	2	13	17
QSLIEDAR	2	6	45	46
QSLIEDARK	-	1	18	8
FEVPSGDLAALLSSVR	-	-	177	172
TGFQLRPVAGLLSAR	-	-	74	112

Table 12. Peptide spectral matches (PSMs) of tryptic peptides identified from the sequence of interest with the two acquisition modes. In the case of inclusion list, the control peptides have been also included.

In samples 1 and 2 digested with GluC, 12/9 peptides 24/24 PSMs from TH, respectively, were identified. The coverage of the protein sequence is 25.30-20.28% for samples 1 and 2, respectively. No peptide from the sequence of interest (aminoacid 1 to 40) was detected.

4 TH coimmunoprecipitation

4.1 In-liquid digestion

Reagents:

- DTT 1M, diluted 1/10 with ammonium bicarbonate (20 µL to 200 µL).
- Iodoacetamide 0.5M, diluted 1/5 with ammonium bicarbonate (20 µL to 100 µL).
- NH_4HCO_3, 20 mM.
- Trypsin, 0.1 µg/µL in ammonium bicarbonate, (diluted 1/10 with ammonium bicarbonate)

Procedure:

- The sample was evaporated until dryness and 200 µL of NH_4HCO_3 were added.
- DTT was added to a final concentration of 2 mM (4 µL of DTT 0.1M). Samples were incubated for 30 minutes at 56°C with agitation.

- Iodoacetamide was added to a final concentration of 7 mM (14.28 µL of iodoacetamide 0.1 M). Samples were incubated for 30 minutes at 25°C in darkness with agitation.
- DTT was added to a final concentration of 2 mM (4.36 µL of DTT 0.1M).
- Trypsin was diluted 1/10 with ammonium bicarbonate (Trypsin to sample at 2% w/w, 3 µg of protein were estimated in sample, so 6 µL of Trypsin 0.01 µg/µL were added).
- Samples were incubated at 37°C overnight (for 18 hours).
- Digestion was stopped with TFA, 1% vol/vol (2.3 µL).

4.2 *LC-MS/MS Analysis*

The MS system used was an LTQ XL Orbitrap (ThermoFisher) equipped with a nanoESI ion source. 20% of the sample was loaded into the chromatographic system consisting in a C18 preconcentration cartridge (Agilent Technologies) connected to a 15 cm long, 100 µm i.d. C18 column (Nikkyo Technos Co.). The separation was done at 0.4 µL/min in a 60-min acetonitrile gradient from 3 to 35% (solvent A: 0.1% formic acid, solvent B: acetonitrile 0.1% formic acid). The HPLC system was composed of an Agilent 1200 capillary nano pump, a binary pump, a thermostated micro injector and a micro switch valve. The LTQ XL Orbitrap was operated in the positive ion mode with a spray voltage of 1.8 kV. The spectrometric analysis was performed in a data dependent mode, acquiring a full scan followed by 10 MS/MS scans of the 10 most intense signals detected in the MS scan from the global list. The full MS (range 400-1650) was acquired in the Orbitrap with a resolution of 60.000. The MS/MS spectra were done in the linear ion-trap. LC-MS/MS spectra were searched using SEQUEST (Proteome Discoverer v1.4, ThermoFisher) with the following parameters: peptide mass tolerance 20 ppm, fragment tolerance 0.6 Da, enzyme set as Trypsin and allowance up to 3 missed cleavages, dynamic modification of methionine oxidation (+16 Da), N-terminal acetylation (+42 Da), and fixed modification of cysteine carbamidomethylation (+57 Da). The database used for searching was Rattus norvegicus (Uniprot 09/19). Final results were filtered by peptide rank 1, peptide confidence high (1% FDR), search engine rank 1 and two peptides per protein.

4.3 Complete list of proteins coimmunoprecipitated with TH

Description	Score
Tubulin beta-2A chain OS=Rattus norvegicus OX=10116 GN=Tubb2a PE=1 SV=1 - [TBB2A_RAT]	396.77
Tyrosine 3-monooxygenase OS=Rattus norvegicus OX=10116 GN=Th PE=1 SV=3 - [TY3H_RAT]	369.40
Tubulin beta-4B chain OS=Rattus norvegicus OX=10116 GN=Tubb4b PE=1 SV=1 - [TBB4B_RAT]	356.24
Tubulin beta-5 chain OS=Rattus norvegicus OX=10116 GN=Tubb5 PE=1 SV=1 - [TBB5_RAT]	352.37
Tubulin alpha-1A chain OS=Rattus norvegicus OX=10116 GN=Tuba1a PE=1 SV=1 - [TBA1A_RAT]	279.67
Tubulin beta-3 chain OS=Rattus norvegicus OX=10116 GN=Tubb3 PE=1 SV=1 - [TBB3_RAT]	256.76
Microtubule-associated protein 6 OS=Rattus norvegicus OX=10116 GN=Map6 PE=1 SV=1 - [MAP6_RAT]	240.62
Tubulin alpha-4A chain OS=Rattus norvegicus OX=10116 GN=Tuba4a PE=1 SV=1 - [TBA4A_RAT]	184.11
Actin, cytoplasmic 1 OS=Rattus norvegicus OX=10116 GN=Actb PE=1 SV=1 - [ACTB_RAT]	166.27
Heat shock cognate 71 kDa protein OS=Rattus norvegicus OX=10116 GN=Hspa8 PE=1 SV=1 - [HSP7C_RAT]	149.99
Glyceraldehyde-3-phosphate dehydrogenase OS=Rattus norvegicus OX=10116 GN=Gapdh PE=1 SV=3 - [G3P_RAT]	145.52
Ig gamma-2A chain C region OS=Rattus norvegicus OX=10116 GN=Igg-2a PE=1 SV=1 - [IGG2A_RAT]	138.51
Isoform 2 of Microtubule-associated protein 2 OS=Rattus norvegicus OX=10116 GN=Map2 - [MTAP2_RAT]	130.86
Ig gamma-2B chain C region OS=Rattus norvegicus OX=10116 GN=Igh-1a PE=1 SV=1 - [IGG2B_RAT]	129.96
ATP synthase subunit alpha, mitochondrial OS=Rattus norvegicus OX=10116 GN=Atp5f1a PE=1 SV=2 - [ATPA_RAT]	126.95
60 kDa heat shock protein, mitochondrial OS=Rattus norvegicus OX=10116 GN=Hspd1 PE=1 SV=1 - [CH60_RAT]	120.19
Neurofilament medium polypeptide OS=Rattus norvegicus OX=10116 GN=Nefm PE=1 SV=4 - [NFM_RAT]	114.24
Beta-synuclein OS=Rattus norvegicus OX=10116 GN=Sncb PE=1 SV=1 - [SYUB_RAT]	101.07
Dihydropyrimidinase-related protein 2 OS=Rattus norvegicus OX=10116 GN=Dpysl2 PE=1 SV=1 - [DPYL2_RAT]	100.17
Ig kappa chain C region, B allele OS=Rattus norvegicus OX=10116 PE=1 SV=1 - [KACB_RAT]	97.37
Ig gamma-2C chain C region OS=Rattus norvegicus OX=10116 PE=2 SV=1 - [IGG2C_RAT]	91.32
Ig gamma-1 chain C region OS=Rattus norvegicus OX=10116 PE=1 SV=1 - [IGHG1_RAT]	88.54
Neurofilament light polypeptide OS=Rattus norvegicus OX=10116 GN=Nefl PE=1 SV=3 - [NFL_RAT]	87.38
Alpha-synuclein OS=Rattus norvegicus OX=10116 GN=Snca PE=1 SV=1 - [SYUA_RAT]	76.98
Ig kappa chain C region, A allele OS=Rattus norvegicus OX=10116 PE=1 SV=1 - [KACA_RAT]	76.63
Hemoglobin subunit beta-1 OS=Rattus norvegicus OX=10116 GN=Hbb PE=1 SV=3 - [HBB1_RAT]	74.09
Isocitrate dehydrogenase [NAD] subunit gamma 1, mitochondrial OS=Rattus norvegicus OX=10116 GN=Idh3g PE=1 SV=2 - [IDHG1_RAT]	65.40
Isoform 2 of Glial fibrillary acidic protein OS=Rattus norvegicus OX=10116 GN=Gfap - [GFAP_RAT]	65.27
Isocitrate dehydrogenase [NAD] subunit alpha, mitochondrial OS=Rattus norvegicus OX=10116 GN=Idh3a PE=1 SV=1 - [IDH3A_RAT]	61.35
Spectrin alpha chain, non-erythrocytic 1 OS=Rattus norvegicus OX=10116 GN=Sptan1 PE=1 SV=2 - [SPTN1_RAT]	56.76
Hemoglobin subunit alpha-1/2 OS=Rattus norvegicus OX=10116 GN=Hba1 PE=1 SV=3 - [HBA_RAT]	52.16
Ig lambda-2 chain C region OS=Rattus norvegicus OX=10116 PE=4 SV=1 - [LAC2_RAT]	50.58
Protein phosphatase 1 regulatory subunit 1B OS=Rattus norvegicus OX=10116 GN=Ppp1r1b PE=1 SV=1 - [PPR1B_RAT]	50.56
Elongation factor 1-alpha 1 OS=Rattus norvegicus OX=10116 GN=Eef1a1 PE=2 SV=1 - [EF1A1_RAT]	47.96
ATP synthase subunit beta, mitochondrial OS=Rattus norvegicus OX=10116 GN=Atp5f1b PE=1 SV=2 - [ATPB_RAT]	46.84
Isoform IB of Synapsin-1 OS=Rattus norvegicus OX=10116 GN=Syn1 - [SYN1_RAT]	46.16
ProSAAS OS=Rattus norvegicus OX=10116 GN=Pcsk1n PE=1 SV=1 - [PCSK1_RAT]	44.63
Isocitrate dehydrogenase [NAD] subunit beta, mitochondrial OS=Rattus norvegicus OX=10116 GN=Idh3B PE=2 SV=1 - [IDH3B_RAT]	40.57
Keratin, type II cytoskeletal 5 OS=Rattus norvegicus OX=10116 GN=Krt5 PE=1 SV=1 - [K2C5_RAT]	40.53

Elongation factor 1-alpha 2 OS=Rattus norvegicus OX=10116 GN=Eef1a2 PE=1 SV=1 - [EF1A2_RAT]	38.90
Keratin, type II cytoskeletal 1 OS=Rattus norvegicus OX=10116 GN=Krt1 PE=2 SV=1 - [K2C1_RAT]	38.70
Isoform 5 of Myelin basic protein OS=Rattus norvegicus OX=10116 GN=Mbp - [MBP_RAT]	38.21
4-aminobutyrate aminotransferase, mitochondrial OS=Rattus norvegicus OX=10116 GN=Abat PE=1 SV=3 - [GABT_RAT]	37.86
Stress-70 protein, mitochondrial OS=Rattus norvegicus OX=10116 GN=Hspa9 PE=1 SV=3 - [GRP75_RAT]	33.69
ATP synthase subunit O, mitochondrial OS=Rattus norvegicus OX=10116 GN=Atp5po PE=1 SV=1 - [ATPO_RAT]	32.12
Alpha-internexin OS=Rattus norvegicus OX=10116 GN=Ina PE=1 SV=2 - [AINX_RAT]	31.12
Isoform Tau-C of Microtubule-associated protein tau OS=Rattus norvegicus OX=10116 GN=Mapt - [TAU_RAT]	30.39
Endoplasmic reticulum chaperone BiP OS=Rattus norvegicus OX=10116 GN=Hspa5 PE=1 SV=1 - [BIP_RAT]	29.44
14-3-3 protein zeta/delta OS=Rattus norvegicus OX=10116 GN=Ywhaz PE=1 SV=1 - [1433Z_RAT]	26.38
60S acidic ribosomal protein P2 OS=Rattus norvegicus OX=10116 GN=Rplp2 PE=1 SV=2 - [RLA2_RAT]	26.36
Calmodulin-2 OS=Rattus norvegicus OX=10116 GN=Calm2 PE=1 SV=1 - [CALM2_RAT]	24.72
Ras-related protein Rab-14 OS=Rattus norvegicus OX=10116 GN=Rab14 PE=1 SV=3 - [RAB14_RAT]	24.55
Synapsin-2 OS=Rattus norvegicus OX=10116 GN=Syn2 PE=1 SV=1 - [SYN2_RAT]	24.35
Keratin, type I cytoskeletal 10 OS=Rattus norvegicus OX=10116 GN=Krt10 PE=3 SV=1 - [K1C10_RAT]	23.71
Serum albumin OS=Rattus norvegicus OX=10116 GN=Alb PE=1 SV=2 - [ALBU_RAT]	23.66
Keratin, type I cytoskeletal 17 OS=Rattus norvegicus OX=10116 GN=Krt17 PE=1 SV=1 - [K1C17_RAT]	23.33
V-type proton ATPase subunit E 1 OS=Rattus norvegicus OX=10116 GN=Atp6v1e1 PE=1 SV=1 - [VATE1_RAT]	22.28
3-hydroxyacyl-CoA dehydrogenase type-2 OS=Rattus norvegicus OX=10116 GN=Hsd17b10 PE=1 SV=3 - [HCD2_RAT]	22.09
Ras-related protein Rab-3A OS=Rattus norvegicus OX=10116 GN=Rab3a PE=1 SV=1 - [RAB3A_RAT]	21.55
Transcriptional activator protein Pur-alpha (Fragments) OS=Rattus norvegicus OX=10116 GN=Pura PE=1 SV=1 - [PURA_RAT]	20.26
Brain acid soluble protein 1 OS=Rattus norvegicus OX=10116 GN=Basp1 PE=1 SV=2 - [BASP1_RAT]	20.20
Heat shock protein HSP 90-alpha OS=Rattus norvegicus OX=10116 GN=Hsp90aa1 PE=1 SV=3 - [HS90A_RAT]	19.98
14-3-3 protein gamma OS=Rattus norvegicus OX=10116 GN=Ywhag PE=1 SV=2 - [1433G_RAT]	19.59
Succinate dehydrogenase [ubiquinone] flavoprotein subunit, mitochondrial OS=Rattus norvegicus OX=10116 GN=Sdha PE=1 SV=1 - [SDHA_RAT]	18.82
Adenylate kinase isoenzyme 1 OS=Rattus norvegicus OX=10116 GN=Ak1 PE=1 SV=3 - [KAD1_RAT]	18.55
Transitional endoplasmic reticulum ATPase OS=Rattus norvegicus OX=10116 GN=Vcp PE=1 SV=3 - [TERA_RAT]	18.25
Fructose-bisphosphate aldolase A OS=Rattus norvegicus OX=10116 GN=Aldoa PE=1 SV=2 - [ALDOA_RAT]	17.28
Far upstream element-binding protein 2 OS=Rattus norvegicus OX=10116 GN=Khsrp PE=1 SV=1 - [FUBP2_RAT]	16.96
Complexin-1 OS=Rattus norvegicus OX=10116 GN=Cplx1 PE=1 SV=1 - [CPLX1_RAT]	16.75
Short coiled-coil protein OS=Rattus norvegicus OX=10116 GN=Scoc PE=2 SV=1 - [SCOC_RAT]	16.74
Isoform Short of 14-3-3 protein beta/alpha OS=Rattus norvegicus OX=10116 GN=Ywhab - [1433B_RAT]	16.29
Peroxiredoxin-2 OS=Rattus norvegicus OX=10116 GN=Prdx2 PE=1 SV=3 - [PRDX2_RAT]	16.23
14-3-3 protein epsilon OS=Rattus norvegicus OX=10116 GN=Ywhae PE=1 SV=1 - [1433E_RAT]	16.20
Keratin, type II cytoskeletal 2 epidermal OS=Rattus norvegicus OX=10116 GN=Krt2 PE=3 SV=1 - [K22E_RAT]	16.17
Creatine kinase B-type OS=Rattus norvegicus OX=10116 GN=Ckb PE=1 SV=2 - [KCRB_RAT]	15.46
Histone H2A.J OS=Rattus norvegicus OX=10116 GN=H2afj PE=2 SV=1 - [H2AJ_RAT]	15.17
Complexin-2 OS=Rattus norvegicus OX=10116 GN=Cplx2 PE=1 SV=1 - [CPLX2_RAT]	15.09
Vimentin OS=Rattus norvegicus OX=10116 GN=Vim PE=1 SV=2 - [VIME_RAT]	15.00
Ras-related protein Rab-7a OS=Rattus norvegicus OX=10116 GN=Rab7a PE=1 SV=2 - [RAB7A_RAT]	14.91
Cofilin-1 OS=Rattus norvegicus OX=10116 GN=Cfl1 PE=1 SV=3 - [COF1_RAT]	14.79
Phosphoglycerate mutase 1 OS=Rattus norvegicus OX=10116 GN=Pgam1 PE=1 SV=4 - [PGAM1_RAT]	14.49
V-type proton ATPase subunit B, brain isoform OS=Rattus norvegicus OX=10116 GN=Atp6v1b2 PE=1 SV=1 - [VATB2_RAT]	14.49
Neurofilament heavy polypeptide OS=Rattus norvegicus OX=10116 GN=Nefh PE=1 SV=4 - [NFH_RAT]	14.22
Ras-related protein Rab-11B OS=Rattus norvegicus OX=10116 GN=Rab11b PE=1 SV=4 - [RB11B_RAT]	14.15

Neuroendocrine protein 7B2 OS=Rattus norvegicus OX=10116 GN=Scg5 PE=1 SV=1 - [7B2_RAT]	13.53
Mitochondrial import inner membrane translocase subunit Tim8 A OS=Rattus norvegicus OX=10116 GN=Timm8a PE=1 SV=1 - [TIM8A_RAT]	13.48
Guanine nucleotide-binding protein subunit beta-4 OS=Rattus norvegicus OX=10116 GN=Gnb4 PE=2 SV=4 - [GBB4_RAT]	13.18
10 kDa heat shock protein, mitochondrial OS=Rattus norvegicus OX=10116 GN=Hspe1 PE=1 SV=3 - [CH10_RAT]	13.10
Protein kinase C and casein kinase substrate in neurons protein 1 OS=Rattus norvegicus OX=10116 GN=Pacsin1 PE=1 SV=1 - [PACN1_RAT]	12.51
Peroxiredoxin-1 OS=Rattus norvegicus OX=10116 GN=Prdx1 PE=1 SV=1 - [PRDX1_RAT]	12.47
Thioredoxin-dependent peroxide reductase, mitochondrial OS=Rattus norvegicus OX=10116 GN=Prdx3 PE=1 SV=2 - [PRDX3_RAT]	12.38
ATP synthase subunit delta, mitochondrial OS=Rattus norvegicus OX=10116 GN=Atp5f1d PE=1 SV=2 - [ATPD_RAT]	12.12
Electron transfer flavoprotein subunit beta OS=Rattus norvegicus OX=10116 GN=Etfb PE=1 SV=3 - [ETFB_RAT]	11.11
NSFL1 cofactor p47 OS=Rattus norvegicus OX=10116 GN=Nsfl1c PE=1 SV=1 - [NSF1C_RAT]	10.97
Elongation factor Tu, mitochondrial OS=Rattus norvegicus OX=10116 GN=Tufm PE=1 SV=1 - [EFTU_RAT]	10.64
Isoform 5 of Tropomyosin alpha-1 chain OS=Rattus norvegicus OX=10116 GN=Tpm1 - [TPM1_RAT]	10.26
Protein-L-isoaspartate(D-aspartate) O-methyltransferase OS=Rattus norvegicus OX=10116 GN=Pcmt1 PE=1 SV=2 - [PIMT_RAT]	10.03
mRNA cap guanine-N7 methyltransferase OS=Rattus norvegicus OX=10116 GN=Rnmt PE=1 SV=1 - [MCES_RAT]	9.78
Alpha-centractin OS=Rattus norvegicus OX=10116 GN=Actr1a PE=1 SV=1 - [ACTZ_RAT]	9.39
Microtubule-associated protein 1A OS=Rattus norvegicus OX=10116 GN=Map1a PE=1 SV=1 - [MAP1A_RAT]	8.49
Progranulin OS=Rattus norvegicus OX=10116 GN=Grn PE=1 SV=3 - [GRN_RAT]	8.49
Heterogeneous nuclear ribonucleoprotein K OS=Rattus norvegicus OX=10116 GN=Hnrnpk PE=1 SV=1 - [HNRPK_RAT]	7.92
Dihydrolipoyllysine-residue acetyltransferase component of pyruvate dehydrogenase complex, mitochondrial OS=Rattus norvegicus OX=10116 GN=Dlat PE=1 SV=3 - [ODP2_RAT]	7.63
Isoform 3 of Heterogeneous nuclear ribonucleoprotein H OS=Rattus norvegicus OX=10116 GN=Hnrnph1 - [HNRH1_RAT]	7.19
Adenosine deaminase OS=Rattus norvegicus OX=10116 GN=Ada PE=1 SV=3 - [ADA_RAT]	6.99
Gamma-enolase OS=Rattus norvegicus OX=10116 GN=Eno2 PE=1 SV=2 - [ENOG_RAT]	6.88
Isoform 3 of Tropomyosin alpha-3 chain OS=Rattus norvegicus OX=10116 GN=Tpm3 - [TPM3_RAT]	6.53
Serine/threonine-protein phosphatase 2B catalytic subunit alpha isoform OS=Rattus norvegicus OX=10116 GN=Ppp3ca PE=1 SV=1 - [PP2BA_RAT]	6.35
Peroxiredoxin-6 OS=Rattus norvegicus OX=10116 GN=Prdx6 PE=1 SV=3 - [PRDX6_RAT]	5.98
Isoform Cytoplasmic of Cysteine desulfurase, mitochondrial OS=Rattus norvegicus OX=10116 GN=Nfs1 - [NFS1_RAT]	5.93
Isoform 1 of Cytosolic acyl coenzyme A thioester hydrolase OS=Rattus norvegicus OX=10116 GN=Acot7 - [BACH_RAT]	5.88
Isoform 2 of Microtubule-associated protein 4 OS=Rattus norvegicus OX=10116 GN=Map4 - [MAP4_RAT]	5.88
26S proteasome non-ATPase regulatory subunit 2 OS=Rattus norvegicus OX=10116 GN=Psmd2 PE=1 SV=1 - [PSMD2_RAT]	5.74
Apolipoprotein E OS=Rattus norvegicus OX=10116 GN=Apoe PE=1 SV=2 - [APOE_RAT]	5.69
Ras-related protein Rab-2A OS=Rattus norvegicus OX=10116 GN=Rab2a PE=2 SV=1 - [RAB2A_RAT]	5.68
Ubiquitin carboxyl-terminal hydrolase isozyme L1 OS=Rattus norvegicus OX=10116 GN=Uchl1 PE=1 SV=2 - [UCHL1_RAT]	5.53
Dynactin subunit 2 OS=Rattus norvegicus OX=10116 GN=Dctn2 PE=1 SV=1 - [DCTN2_RAT]	5.06
Electron transfer flavoprotein subunit alpha, mitochondrial OS=Rattus norvegicus OX=10116 GN=Etfa PE=1 SV=4 - [ETFA_RAT]	5.03
Polyadenylate-binding protein 1 OS=Rattus norvegicus OX=10116 GN=Pabpc1 PE=1 SV=1 - [PABP1_RAT]	4.80
Ras-related C3 botulinum toxin substrate 1 OS=Rattus norvegicus OX=10116 GN=Rac1 PE=1 SV=1 - [RAC1_RAT]	4.77
Thioredoxin OS=Rattus norvegicus OX=10116 GN=Txn PE=1 SV=2 - [THIO_RAT]	4.57
Ubiquitin-like modifier-activating enzyme 1 OS=Rattus norvegicus OX=10116 GN=Uba1 PE=1 SV=1 - [UBA1_RAT]	4.53
Malate dehydrogenase, mitochondrial OS=Rattus norvegicus OX=10116 GN=Mdh2 PE=1 SV=2 - [MDHM_RAT]	4.51

Ig heavy chain V region IR2 OS=Rattus norvegicus OX=10116 PE=4 SV=1 - [HVR01_RAT]	4.25
Isoform Cytoplasmic+peroxisomal of Peroxiredoxin-5, mitochondrial OS=Rattus norvegicus OX=10116 GN=Prdx5 - [PRDX5_RAT]	4.16
Histone H4 OS=Rattus norvegicus OX=10116 GN=Hist1h4b PE=1 SV=2 - [H4_RAT]	4.02
Beta-adducin OS=Rattus norvegicus OX=10116 GN=Add2 PE=1 SV=4 - [ADDB_RAT]	3.81
Neuromodulin OS=Rattus norvegicus OX=10116 GN=Gap43 PE=1 SV=1 - [NEUM_RAT]	3.67
Calretinin OS=Rattus norvegicus OX=10116 GN=Calb2 PE=1 SV=1 - [CALB2_RAT]	2.19
Neurolysin, mitochondrial OS=Rattus norvegicus OX=10116 GN=Nln PE=1 SV=1 - [NEUL_RAT]	1.83
Heterogeneous nuclear ribonucleoprotein M OS=Rattus norvegicus OX=10116 GN=Hnrnpm PE=1 SV=4 - [HNRPM_RAT]	0.00

Annex 2

Neuropharmacology 212 (2022) 109058

Contents lists available at ScienceDirect

Neuropharmacology

journal homepage: www.elsevier.com/locate/neuropharm

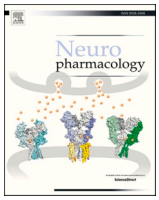

Spontaneous changes in brain striatal dopamine synthesis and storage dynamics *ex vivo* reveal end-product feedback-inhibition of tyrosine hydroxylase

Marta González-Sepúlveda [a,b,f], Muhammad Yusof Omar [a,b], Sally Hamdon [a,b], Guofen Ma [a,b], Santi Rosell-Vilar [a], Noora Raivio [a], Doaa Abass [a], Anna Martínez-Rivas [a,b], Miquel Vila [a,f,g], Jesús Giraldo [a,c,e], Montserrat Carrascal [d], Joaquín Abián [d], Carles Gil [a,b,1], Josefa Sabriá [a,b,1], Jordi Ortiz [a,b,e,*,1], David Moreno-Delgado [a,b,1]

[a] *Neuroscience Institute, School of Medicine, Universitat Autònoma de Barcelona, Spain*
[b] *Department of Biochemistry and Molecular Biology, Universitat Autònoma de Barcelona, Spain*
[c] *Biostatistics Unit, Universitat Autònoma de Barcelona, Spain*
[d] *Biological and Environmental Proteomics, IIBB-CSIC/IDIBAPS, Barcelona, Spain*
[e] *Centro Investigación Biomédica en Red de Salud Mental, CIBERSAM, and Translational Neuroscience Unit, Parc Taulí University Hospital and Universitat Autònoma de Barcelona, Spain*
[f] *Neurodegenerative Diseases Research Group, Vall d'Hebron Research Institute (VHIR)-Network Center for Biomedical Research in Neurodegenerative Diseases (CIBERNED), Spain*
[g] *Catalan Institution for Research and Advanced Studies (ICREA), Spain*

ARTICLE INFO

Keywords:
Striatum
HPLC
VMAT2
Tetrabenazine
Quinpirole

ABSTRACT

Synaptic events are important to define treatment strategies for brain disorders. In the present paper, freshly obtained rat brain striatal minces were incubated under different times and conditions to determine dopamine biosynthesis, storage, and tyrosine hydroxylase phosphorylation. Remarkably, we found that endogenous dopamine spontaneously accumulated during tissue incubation at 37 °C *ex vivo* while dopamine synthesis simultaneously decreased. We analyzed whether these changes in brain dopamine biosynthesis and storage were linked to dopamine feedback inhibition of its synthesis-limiting enzyme tyrosine hydroxylase. The aromatic-L-amino-acid decarboxylase inhibitor NSD-1015 prevented both effects. As expected, dopamine accumulation was increased with L-DOPA addition or VMAT2-overexpression, and dopamine synthesis decreased further with added dopamine, the VMAT2 inhibitor tetrabenazine or D_2 auto-receptor activation with quinpirole, accordingly to the known synaptic effects of these treatments. Phosphorylation activation and inhibition of tyrosine hydroxylase on Ser31 and Ser40 with okadaic acid, Sp-cAMP and PD98059 also exerted the expected effects. However, no clear-cut association was found between dopamine feedback inhibition of its own biosynthesis and changes of tyrosine hydroxylase phosphorylation, assessed by Western blot and mass spectrometry. The later technique also revealed a new Thr30 phosphorylation in rat tyrosine hydroxylase. Our methodological assessment of brain dopamine synthesis and storage dynamics *ex vivo* could be applied to predict the *in vivo* effects of pharmacological interventions in animal models of dopamine-related disorders.

1. Introduction

Excessive dopaminergic neurotransmission contributes to hyperkinetic movement disorders and psychotic episodes, and these conditions are currently treated with dopamine (DA)-interfering drugs. Because DA storage determines stimulus-dependent DA release, drugs

Abbreviations: DA, dopamine; L-DOPA, levodopa; Okadaic acid, Ok; TH, tyrosine hydroxylase; VMAT2, vesicular monoamine transporter 2; 5-HT, serotonin.

* Corresponding author. Neuroscience Institute and Department of Biochemistry and Molecular Biology, School of Medicine, Room M2-110, Universitat Autonoma de Barcelona, 08193, Bellaterra (Cerdanyola del Vallès, Catalonia), Spain.
E-mail address: jordi.ortiz@uab.cat (J. Ortiz).

[1] Contributed equally.

https://doi.org/10.1016/j.neuropharm.2022.109058
Received 16 November 2021; Received in revised form 9 March 2022; Accepted 5 April 2022
Available online 13 April 2022

reducing DA storage by inhibiting VMAT2 transporters have become first-line treatments for Huntington's disease, tardive dyskinesia and Tourette syndrome (Jankovic, 2016). However, VMAT2 inhibition also produces very common side-effects that require medical attention, partly related to the fact that VMAT2 is not DA-selective, and therefore its inhibition reduces neurotransmission mediated by other monoamines. Catecholamine synthesis inhibition could -putatively- maintain the clinical benefits and avoid some unwanted effects of VMAT2 inhibition (Ankenman and Salvatore, 2007). For these reasons, an experimental model to simultaneously assess DA synthesis and storage under the influence of different combinations of drugs could be of interest.

Tyrosine hydroxylase (TH; tyrosine 3-monooxygenase; E.C. 1.14.16.2) is the first and rate-limiting enzyme in dopamine biosynthesis. Regulatory mechanisms of TH activity involve gene expression, phosphorylation and end-product feedback inhibition by catecholamines (Spector et al., 1967). The TH protein has been proposed to be a homotetramer where each monomer contains a phosphorylatable N-terminal domain that enhances cofactor affinity and enzymatic activity (Dunkley et al., 2004; Dunkley and Dickson, 2019; Haycock and Haycock, 1991; Lindgren et al., 2000; Zhang et al., 2014). TH phosphorylation has been extensively investigated, as changes in TH phosphorylation state are generally considered to be critical in the short-term regulation of DA biosynthesis (Haycock and Haycock, 1991). In particular, phosphorylations in Ser40, Ser31 and Ser19 of TH by several kinases including PKA, ERK and CaMKII enhance its enzymatic activity, thereby stimulating the synthesis of the neurotransmitter (Dunkley and Dickson, 2019; Harada et al., 1996; Lindgren et al., 2000). In addition, phosphorylation can also modulate TH action by stabilization of the protein (Nakashima et al., 2013) or affect TH binding to partners, such as 14-3-3 isoforms (Ghorbani et al., 2020). On the other hand, the mechanisms of end-product feedback inhibition are less clear. It is currently accepted that catecholamines bind to TH with high affinity (K_D 4 nM for DA) and that phosphorylation increases K_D for DA to 78–208 nM, relieving feedback inhibition (McCulloch et al., 2001; Ramsey and Fitzpatrick, 1998; Sura et al., 2004). *In vitro* studies using recombinant TH suggested that each TH dimer of the homotetramer could present a second DA binding site of low affinity (K_D 90 nM) (Briggs et al., 2011, 2014; Dickson and Briggs, 2013; Dunkley and Dickson, 2019; Gordon et al., 2008, 2009). This would imply simultaneous DA binding to high- and low-affinity sites inhibiting TH. However, these results could also be explained by distinct TH conformations in the homotetramer where a single DA binding site presents different K_D values in each monomer (Tekin et al., 2014).

Computational analysis have indicated the potential importance of feedback inhibition for dopaminergic neurotransmission (Justice et al., 1988; Wallace, 2007). Its experimental study is difficult due to the presence of indeterminate amounts of endogenous DA bound to TH *in vivo*. Furthermore, methods to estimate TH activity in brain usually block DA formation by inhibiting aromatic-L-amino-acid decarboxylase to accumulate L-DOPA (Lindgren et al., 2000), preventing to estimate DA feedback. To overcome this limitation, in this paper we modified the L-DOPA accumulation method and compared it to a radioisotopic method that accurately determines [^{3}H]-DA synthesis from [^{3}H]-tyrosine in rat striatal minces (Ma et al., 2014). By using both methods we were surprised to clearly observe that incubating brain tissue *ex vivo* at 37 °C was sufficient to induce an initially high DA synthesis and storage in vesicles. When storage approached saturation, end-product feedback inhibition of TH became the main factor limiting new DA biosynthesis.

2. Materials and methods

2.1. Chemicals

Opti-Phase HiSafe-3 liquid scintillation cocktail (Cat. No. 1200.437) and [3, 5-^{3}H]-L-tyrosine (^{3}H-Tyr, 50 Ci/mmol NET127005MC) were supplied by PerkinElmer Wallac (Turku, Finland). cAMP-Sp, PD98059 (1213), TBZ (2175) and okadaic acid (1136) were obtained from Tocris Bioscience (Bristol, United Kingdom). 3-hydroxybenzylhydrazine (NSD-1015, Cat. No. 54880), EDTA, HPLC standards, and other reagents were purchased from Sigma/RBI (Sigma-Aldrich Co.).

2.2. Animals

Animal experiments were conducted with 48 male Sprague-Dawley rats of 8 weeks of age, weighing 200–300 g (Animal Service, Universitat Autònoma de Barcelona, Spain or Charles River). Animals were housed two or three per cage with *ad libitum* access to food and water during a 12-h light/dark cycle. Protocols for animal handling were approved by the Ethics Committee for Human and Animal Research (Universitat Autònoma de Barcelona) in accordance with guidelines established by the Ethical Committee for the use of Laboratory Animals in Spain (53/2013) and the European Ethical Committee (2010/63/EU) and approved by the Vall d'Hebron Research Institute (VHIR) Ethical Experimentation Committee. All experiments were conducted in compliance with the ARRIVE guidelines. Surgical procedures were performed under general anesthesia using isoflurane (5% for the induction phase and 2% for the maintenance phase) (Baxter) due to its fast induction and recovery, negligible metabolism and relative sparing effect on cardiovascular function and cerebral blood flow autoregulation (Ludders, 1992). To increase DA storage, an AAV-hVMAT2 vector was injected in the morning to 8 male Charles River rats as previously stated (Carballo-Carbajal et al., 2019). No randomization was performed to allocate subjects in the study. In brief, a 10 μL Hamilton syringe with a glass capillary was used to inject 2 μL at a rate of 0.4 μL/min of the viral vector unilaterally on the right side (R) of the brain right above the substantia nigra pars compacta at the following coordinates (flat skull position), antero-posterior: −5.2 mm; medio-lateral: −2 mm, dorso-ventral: −7.6 mm, calculated relative to bregma according to the stereotaxic atlas of Paxinos and Watson (Paxinos and Watson, 1982). Then the needle was left in place for an additional 4 min period before it was slowly retracted. Rats received meloxicam 2 mg/kg after stereotaxic surgery. Continuation of analgesic treatment was decided by trained specialists who supervised animals daily to prevent and minimize any possibility of suffering, according to EU directive 2010/63/EU annex III 3.1. b. Rats were euthanized and brain tissue used 4 weeks after surgery, according to the time-line diagram shown.

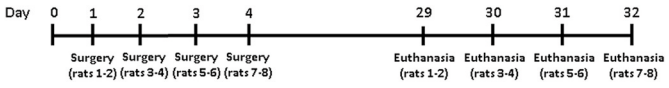

2.3. Preparation of striatal minces

Rats were euthanized by CO_2 and decapitation and brains were chilled immediately in modified Krebs-Ringer-bicarbonate medium with the following composition: 120 mM NaCl, 0.8 mM KCl, 2.6 mM $CaCl_2$, 0.67 mM $MgSO_4$, 1.2 mM KH_2PO_4, 27.5 mM $NaHCO_3$, and 10 mM glucose, pH 7.4 bubbled with 95% O_2/5% CO_2. In a 4 °C room, dorsal/medial striata from both hemispheres were dissected and sliced using a McIlwain tissue chopper obtaining tissue minces of 0.3 × 0.3 mm/side. Tissue minces were suspended in ice-cold Krebs Ringer bicarbonate medium, and washed twice by centrifugation (1000×*g*, 1 min, 4 °C) and resuspension in order to remove debris of damaged cells. Striatal tissue from a single rat yielded up to 28 aliquots of 25 ml each of the settled minces suspension - corresponding to 24 tissue incubations and 4 blank samples - which were randomly distributed into 2 ml polypropylene tubes containing 225 ml of ice-cold Krebs Ringer bicarbonate medium. Blank tubes were kept on ice and the rest were incubated at 37 °C and 350 rpm in an Eppendorf Thermomixer (5 Prime, Inc., Boulder, CO) under 95% O_2/5% CO_2 atmosphere. Because striatal tissue is heterogeneous, various tissue samples incubated under the same conditions

cannot be considered true "replicates", and the use of this term has been avoided. Variability between tissue incubates is due, in part, to striatal heterogeneity. Control groups comprising a minimum of 4 tissue incubations were included in every experiment. The number of tissue incubations per group is indicated in Figure legends.

2.4. Estimation of tyrosine hydroxylase activity by l-DOPA accumulation and determination of endogenous DA, DOPAC levels by HPLC-EC

The method used by Lindgren for L-DOPA accumulation in slices (Lindgren et al., 2000) was slightly modified as follows. L-DOPA was measured in two different sets of experiments depending on the presence (Fig. 1A) or absence (Fig. 1B) of a "pre-incubation" time at 37 °C before the inhibition of aromatic-L-amino-acid decarboxylase with 100 mM 3-hydroxybenzylhydrazine (NSD-1015) (properly named "incubation" where L-DOPA accumulates at a rate that is quantified in pmol mg protein^{-1} h^{-1} in Fig. 1A–B). In experiments without pre-incubation, NSD-1015 was added at the beginning of the 30-, 60- or 120-min incubation to allow the synthesis of L-DOPA. In contrast, in experiments with pre-incubation (lasting 15, 30, 60 or 120 min) DA was synthesized before NSD-1015 addition and samples were incubated for 30 min for L-DOPA synthesis rate measurement. The accumulation of L-DOPA was quantified by HPLC with coulometric detection (HPLC-EC) (Bolea et al., 2014). A technician blinded to sample groups quantified HPLC peaks.

Tissue minces were sonicated in 0.25 M perchloric acid containing 0.25 mM EDTA and 0.1 mM sodium metabisulphite. Samples were spun in an Eppendorf microcentrifuge for 10 min, and 20 μL of supernatant were injected directly into the HPLC. The chromatography system consisted of a reversed-phase C18 column (2.5 mm particle Fortis C18, 10 × 0.46 cm, Sugelabor, Spain) and an ion-pair mobile phase, made up of 100 mM sodium phosphate buffer, 1 mM EDTA, 5 mM octanesulfonic acid (pH 2.5) plus 1% (v/v) methanol. The flow rate was 1 ml/min. This HPLC system completely separated standards of L-DOPA and DA that were detected with a Coulochem II (ESA) detector with a model 5011 dual-electrode analytical cell with porous graphite electrodes. The potential of electrodes 1 and 2 was set at −0.05 V and +0.4 V respectively.

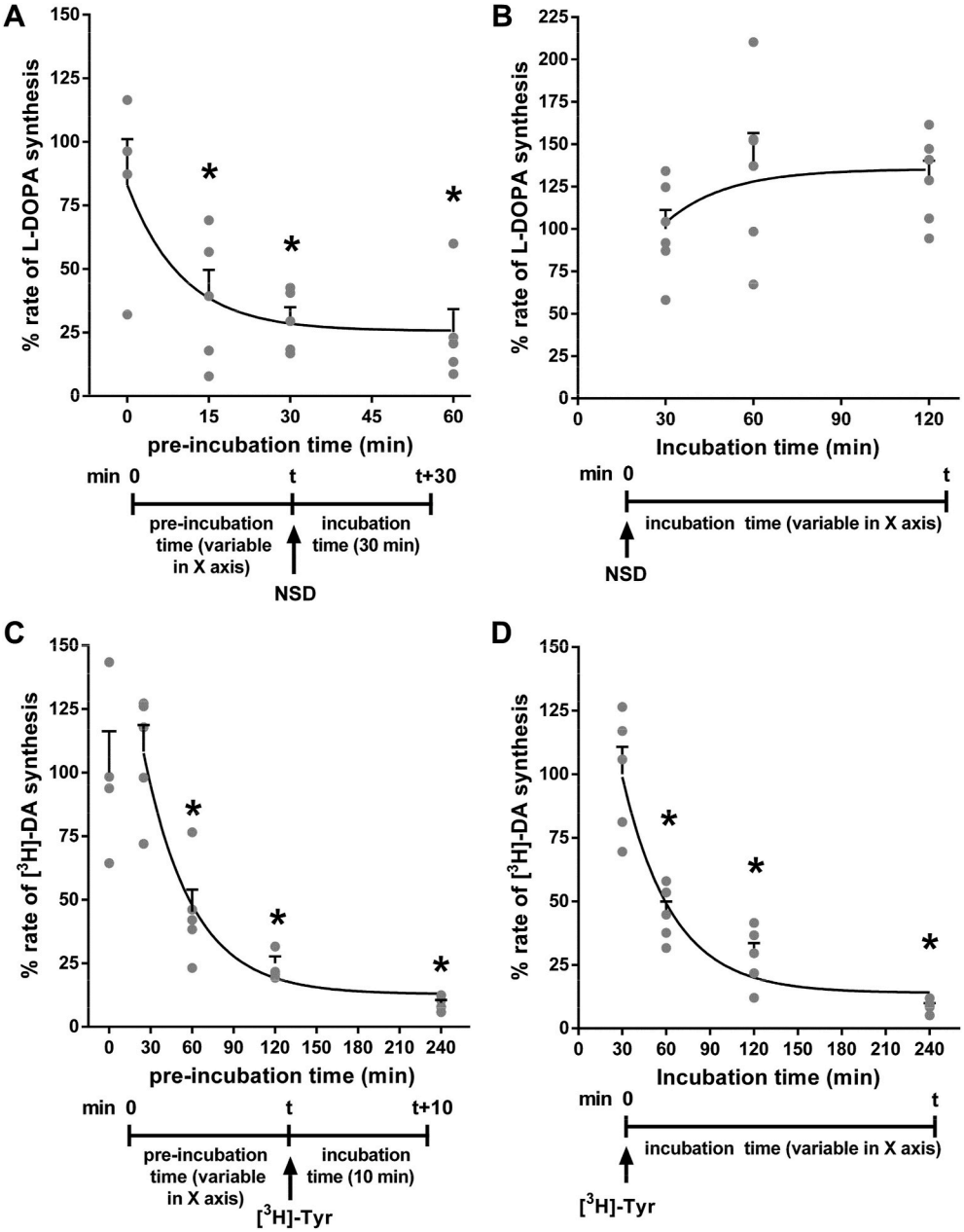

Fig. 1. Initially high L-DOPA and [^{3}H]-DA synthesis rates decrease when DA is produced. Brain striatal minces were allowed DA synthesis (A) or not (B) by the timely addition of 100 mM NSD-1015, the decarboxylase inhibitor used to measure L-DOPA synthesis rate (A, B). The results in A were validated using a second method, where minces were incubated with [^{3}H]-tyrosine after a pre-incubation time (C) or from the beginning of the experiment (D) to measure [^{3}H]-DA synthesis rate. Experimental designs are shown as timelines, where "incubation" properly refers to the time period where L-DOPA synthesis from endogenous tyrosine is measured (30 min in A, x axis variable in B) or alternatively [^{3}H]-DA synthesis from 0.12 mM [^{3}H]-tyrosine (10 min in C, x axis variable in D). "Preincubation" refers to the previous time without NSD or [^{3}H]-tyrosine under the same conditions. Data points and the mean ± SEM of 4–5 (A), 6 (B), 4–5 (C) or 5 (D) brain striatal tissue incubations are represented. 100% corresponds to a mean ± SEM of A) 187 ± 17; B) 10 ± 1 pmol L-DOPA/mg h; C) 257,787 ± 42,097 and D) 362,297 ± 38,857 dpm [^{3}H]-DA/mg h. Data in (A, C and D) adjusted well to a one phase exponential decay regression curve (r^2 0.91; 0.98 and 0.97 respectively). *$p < 0.05$, vs. respective control: A, C) 0 min; B) 30 min, ANOVA plus Dunnett's multiple comparisons test.

Detection limit was 0.2 pmol for L-DOPA. Standards of L-DOPA at different concentrations (4–400 pmol) were injected in every experiment to quantify L-DOPA by the external standard method. Sample values outside the standard range were reanalyzed or excluded. Pmols of L-DOPA were corrected by pmols present in blank samples and protein content in each sample. Results were expressed as a percentage versus control samples in each experiment. Endogenous levels of DA and DOPAC were determined in striatal mince samples with the same method. DOPAC values are shown in Fig. S1.

2.5. Purification of [^{3}H]-tyrosine

Ring-labeled [3,5-^{3}H]-L-tyrosine (40–60 Ci/mmol) decomposes at a rate of 1–3% per month. The main goal of this purification is to maintain a high degree of purity of commercial [^{3}H]-tyrosine after storage. The system used for HPLC purification consisted of a reversed-phase C18 column (Tracer Extrasil ODS2, 5 mm particle size, 25 × 0.46 cm; Teknokroma, Spain) and a mobile phase with the following composition: 100 mM sodium phosphate buffer, 1 mM EDTA, 0.75 mM octanesulfonic acid (pH 3.4) and 1% (v/v) methanol. The flow rate was 1 ml/min. Under these conditions, tyrosine eluted at 9–10 min. In each purification, 0.4 mCi of [3, 5-^{3}H]-L-tyrosine were injected into the HPLC and the whole tyrosine fraction (0.5–1 ml) was collected. The amount of [^{3}H]-tyrosine was quantified against an external standard calibration curve of non-radiolabeled tyrosine detected by UV absorbance at 285 nm.

2.6. Purification of newly-synthesized [^{3}H]-DA by HPLC-UV

The rate of [^{3}H]-DA formation from 0.12 μM purified [^{3}H]-tyrosine was measured with two experimental designs differing on the presence or absence of a pre-incubation period at 37 °C (Fig. 1C–D). In experiments without pre-incubation, purified [^{3}H]-tyrosine was added at the beginning of the incubation for several periods of time to quantify the [^{3}H]-DA synthesis rate. In experiments with pre-incubation, at the end of the desired pre-incubation time (usually 25, 60, 120 or 240 min at 37 °C) purified [^{3}H]-tyrosine was added, and samples were then incubated for 10 min. "Incubation" here refers to the time when [^{3}H]-tyrosine is transformed into [^{3}H]-DA to quantify the synthesis rate (dpm mg prot^{-1} h^{-1}). In experiments where drugs were assayed, the timing of their addition to the incubates is indicated in the graph timelines. In all experiments, [^{3}H]-DA synthesis was stopped by the addition of 35 ml of a deproteinizing mixture containing trichloroacetic acid (0.5% w/v), 1 mM ascorbic acid and 25 nmol non-radiolabeled DA (internal standard). Samples were homogenized in a Dynatech/Sonic Dismembrator (Dynatech Labs, Chantilly, VA). A 10 ml aliquot was taken for protein quantification by the Lowry method. Tissue homogenates were then centrifuged (12,000×g, 10 min, 4 °C), and all supernatants were processed for [^{3}H]-DA purification by HPLC-UV. [^{3}H]-DA formed during the incubation reaction was separated from [^{3}H]-tyrosine by a modification of previous HPLC purification procedures used in our lab for other neurotransmitters (Ortiz et al., 2000). The chromatography system consisted of a reversed-phase C18 column (Tracer Extrasil ODS2, 5 μm particle size, 25 × 0.46 cm; Teknokroma, Spain) and an ion-pair mobile phase, made up of 100 mM sodium phosphate buffer, 1 mM EDTA, 0.75 mM octanesulfonic acid (pH 5) plus 12% (v/v) methanol. The flow rate was 1 ml/min. This HPLC system completely separates standards of tyrosine and DA detected by UV 285 nm (ring absorbance). Samples contained extremely low levels of radiolabeled tyrosine and DA that were undetectable by UV absorbance. Similarly, endogenous tyrosine and DA were negligible as compared to the amounts of internal standard DA, used to trigger [^{3}H]-DA purification and to quantify recovery. The recovery of the internal standard in each sample (internal/external standard peak area) was quantified from internal standard DA HPLC-UV peak areas. Two ml fractions corresponding to the DA peak were recovered in scintillation vials, mixed with 6 ml Optiphase HiSafe III cocktail, and quantified in a liquid scintillation counter (PerkinElmer Tri-Carb 2810 TR, USA) to quantify [^{3}H]-DA. Disintegrations per minute (dpm) obtained in HPLC-purified [^{3}H]-DA fractions were corrected by DA internal standard recovery and dpm in blank samples. Rate of [^{3}H]-DA synthesis was estimated as the ratio of corrected dpm divided by protein content in each incubate and the incubation time in the presence of [^{3}H]-tyrosine (dpmmg prot^{-1} h^{-1}). Results were expressed as a percentage with respect to the mean of control samples run in each experiment in order to combine data from different experiments.

2.7. Phosphorylation of tyrosine hydroxylase by Western blot

After incubation of striatal minces as described above, the Krebs-Ringer buffer was removed by centrifugation and samples were immediately frozen (−80 °C). After thawing samples were homogenized in 100 μl of ice-cold lysis buffer (1 mM orthovanadate, 50 mM Tris-HCl pH 7.5, 25 mM sodium pyrophosphate, 50 mM NaCl, 1% Triton X100, 50 mM sodium fluoride, 5 μM zinc chloride, 2 mM DTT, phosphatase inhibitor cocktail 1 (Sigma) and protease inhibitor cocktail 1 (Sigma). Equal amounts of protein were separated by SDS-PAGE electrophoresis followed by transference in polyvinylidene fluoride membrane at 100 V for 1 h. The blotting buffer used contained 25 mM Tris, 200 mM glycine and 10% methanol (v/v). Membranes were blocked for 1 h with Tris-buffered saline, supplemented with 0.1% Tween 20 and 5% (w/v) defatted milk powder. Then, the membranes were incubated overnight with the indicated antibody diluted in blocking buffer. The primary antibodies against tyrosine hydroxylase (1:2500, AB5280), phosphoSer31-TH (1:1000, AB5423) and phosphoSer40-TH (1:1000, AB5935) were obtained from Millipore. Monoclonal antibody against β-actin was from Sigma-Aldrich (1:4000, clone AC-74). Cell Signaling Technology antibodies against ERK-1/2 (1:1000, 9102) and against dually phosphorylated (Thr202/Tyr204) ERK-1/2 (1:1000, 9101) were used. The secondary horseradish peroxidase-conjugated antibodies used were goat anti-mouse (1:1000, 172–1011) from Bio-Rad and goat anti-rabbit (1:1000, 31460) from Pierce. Signals were obtained using a ChemiDoc device (Bio-Rad) and quantitative analysis was performed using the ImageLab software (Bio-Rad). Results were expressed as pTH/TH ratio of standardized optical density determined within each blot.

2.8. Tyrosine hydroxylase immunoprecipitation, in-gel peptide digestion and LC-MS/MS analysis

TH was immunoprecipitated using 10 μg anti TH antibody (Millipore AB5280) and Pierce Crosslink Magnetic IP/Co-IP Kit (Thermo Fischer 8885) from 4 h-incubated striatal minces and non-incubated ice controls from two animal brains. SDS-PAGE bands revealed with Coomasie blue were manually excised and digested with trypsin using a DigestPro MS digestor (Intavis). The process involved reduction with DTT, derivatization with iodoacetamide, and enzymatic digestion with trypsin at 37 °C for 8 h (Casanovas et al., 2009). The resulting peptide mixtures were evaporated to dryness and redissolved in 20 μL 5% MeOH, 0.5% TFA. Peptides were analyzed by LC-MS/MS using a 1200 HPLC system (Agilent Technologies, Santa Clara, CA, USA) coupled to an LTQ Orbitrap XL mass spectrometer (Thermo Scientific) equipped with a nano-electrospray source (Proxeon, Odense, Denmark). Samples were separated with a C18 pre-concentration cartridge (Agilent Technologies) connected to a C18 100 μm × 150 mm column (Nikkyo Technos Co, Tokyo, Japan) at 400 nL/min using a 30-min linear gradient from 0 to 35% solvent B (Solvent A: water, 0.1% (v/v) formic acid; solvent B: acetonitrile, 0.1% (v/v) formic acid). The LTQ XL Orbitrap was operated in the positive ion mode with a spray voltage of 1.8 kV. The spectrometric analysis was performed in a data-dependent mode, acquiring a full scan followed by 8 MS/MS scans of the 8 most intense signals from the inclusion list (see Supplementary Table S1). If an ion resulting from a neutral loss of phosphate from the precursor ion (loss of 49, 32.6, 24.5 uma) was detected among the 3 most abundant fragments in the MS/MS spectrum, a MS3 scan was performed on this ion. The full scan spectra

(scan range m/z 400–1650) were acquired in the Orbitrap with a resolution of 60.000 (at m/z 400). The MS/MS spectra were acquired in the linear ion-trap. For relative quantification, the area of each monitored peptide was calculated using the Xcalibur software (Thermo Scientific).

2.9. Experimental Design and Statistical Analysis

The study was not pre-registered. No sample calculation or blinding was performed. No animals were excluded, but undetectable protein levels in samples was considered an exclusion criterion. Control groups with a balanced number of brain striatal tissue incubations (at least 4) were included in every experiment. In [^{3}H]-DA and L-DOPA synthesis rate experiments, raw data of control incubations are given in each figure legend. Once normalized to 100% of basal synthesis in each experiment, data were pooled to increase the total number of incubations represented in graphs and used for statistics. Thus graphs represent incubation samples that may be obtained from different animals, which is important due to the limited amount of brain striatal tissue per animal and its inherent heterogeneity. As stated before, the use of the term "replicates" has been avoided to stress the heterogeneity of tissue minces randomly assigned to each treatment group. Statistical analysis was carried out with GraphPad Prism software (v6, GraphPad Software Inc, USA). Normality was assessed with the Shapiro-Wilk normality test. The ROUT test (Q = 1%) was used to detect those data points that can be considered statistical outliers and that should be excluded from analysis. Two-way ANOVA was used to analyze the interaction between different factors on synthesis rate (e.g., time, treatment or concentration of DA as factors). Statistical significance of differences vs. control group was assessed by Dunnett's multiple comparisons test while Sidak's was used to evaluate differences between treatments. Differences were considered statistically significant if the probability of error was less than 5%.

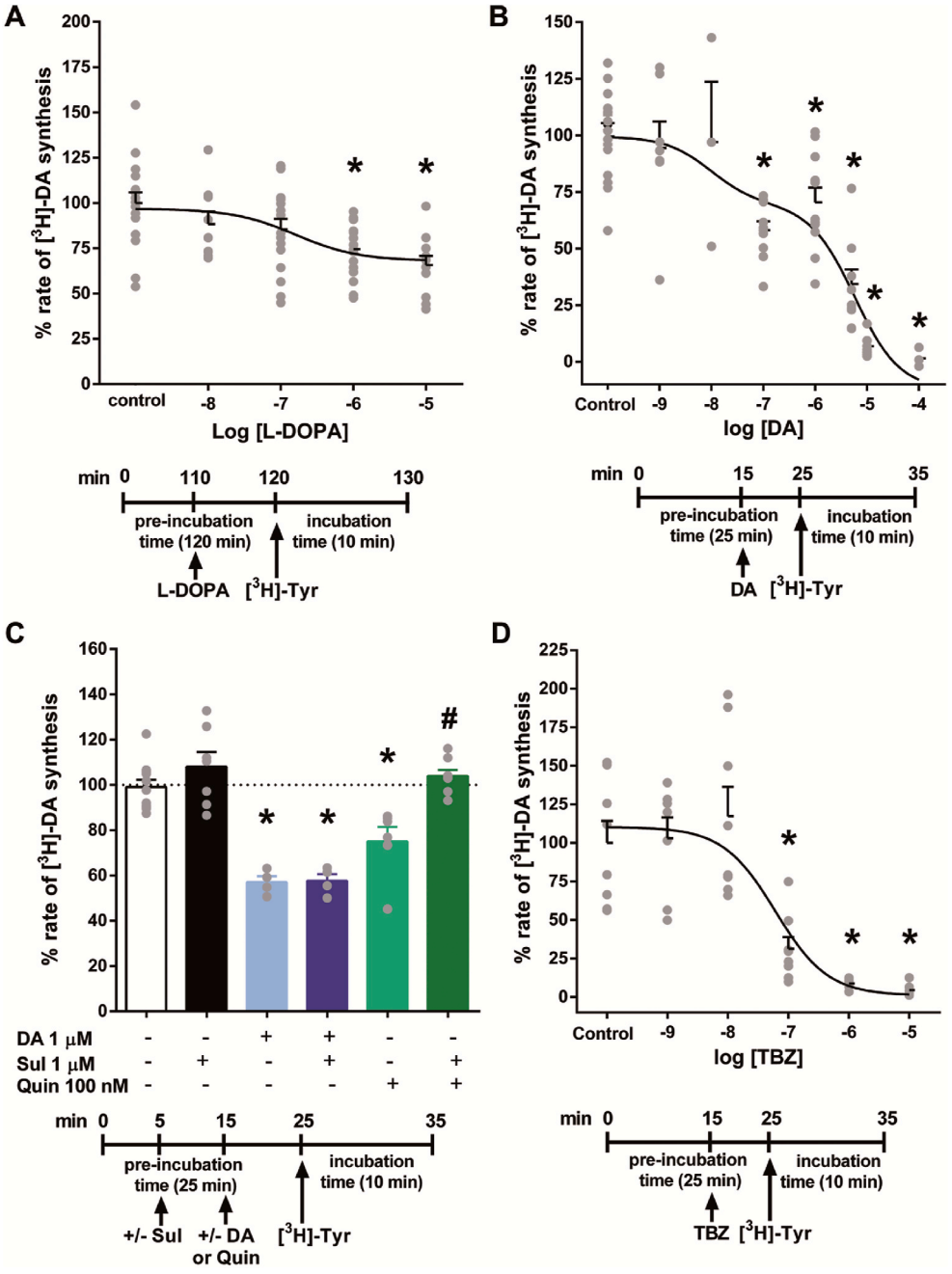

Fig. 2. [^{3}H]-DA synthesis rate is controlled by non-stored DA as well as by D_2-like receptor dependent mechanisms. Increases in intracellular DA were sought by adding increasing concentrations of L-DOPA (A), DA (B) or the VMAT2 inhibitor TBZ (D) to brain striatal minces. In C, either 1 µM DA or the D_2-like receptor agonist quinpirole were applied, but only quinpirole effects were blocked by the D_2-like receptor antagonist sulpiride. Experimental designs until measurement are shown as timelines below each graph. Data points and the mean ± SEM of 9–17 (A), 3–18 (B), 4–11(C) and 6–8 (D) brain striatal tissue incubations are represented. In B) 4 incubations were excluded from the analysis after values were considered outliers by the ROUT test. Dose-response curves adjusted to one site competition (A, IC_{50} $1.6x10^{-7}$ M; r^2 0.95), two-site competition (B, IC_{50} $9.3x10^{-9}$ M and $5.8x10^{-6}$ M; r^2 0.97; $p < 0.005$ vs. one-site competition) and one-site competition (D, IC_{50} $6.1x10^{-8}$ M; r^2 0.96) respectively. 100% corresponds to a mean ± SEM of A) 60,151 ± 4784; B) 295,539 ± 17,413; C) 62,946 ± 2684 and D) 617,245 ± 99,937 dpm [^{3}H]-DA/mg.h. A, B, D). *, $p < 0.05$, vs. respective control; ANOVA plus Dunnett's multiple comparisons test. C) Two-way ANOVA showed a significant effect of treatment ($F(2,34) = 42.2$; $p < 0.0001$) and Sulpiride presence ($F(1,34) = 10.4$; $p < 0.005$), and a significant interaction between these two factors ($F(2,34) = 4.4$ $p < 0.05$); *, $p < 0.05$, vs. group without treatment; #, $p < 0.05$ vs. Quin 100 nM, Two way ANOVA plus Sidak's multiple comparisons test.

3. Results

3.1. De novo DA synthesis is necessary and sufficient to trigger spontaneous end-product inhibition of TH

With the aim of analyzing DA feedback-inhibition of TH activity, we modified the method of L-DOPA accumulation after decarboxylase inhibition with 100 mM NSD-1015 applied to slices (Lindgren et al., 2000) (Fig. 1A–B). To allow *de novo* DA synthesis we pre-incubated tissue for up to 60 min at 37 °C before NSD-1015 addition. We observed a decrease of L-DOPA synthesis rate with pre-incubation time (Fig. 1A) fitting to a one-phase exponential decay regression curve (maximal decrease 80%). The presence of NSD-1015 from the beginning of the incubation prevented decreases in the rate of L-DOPA

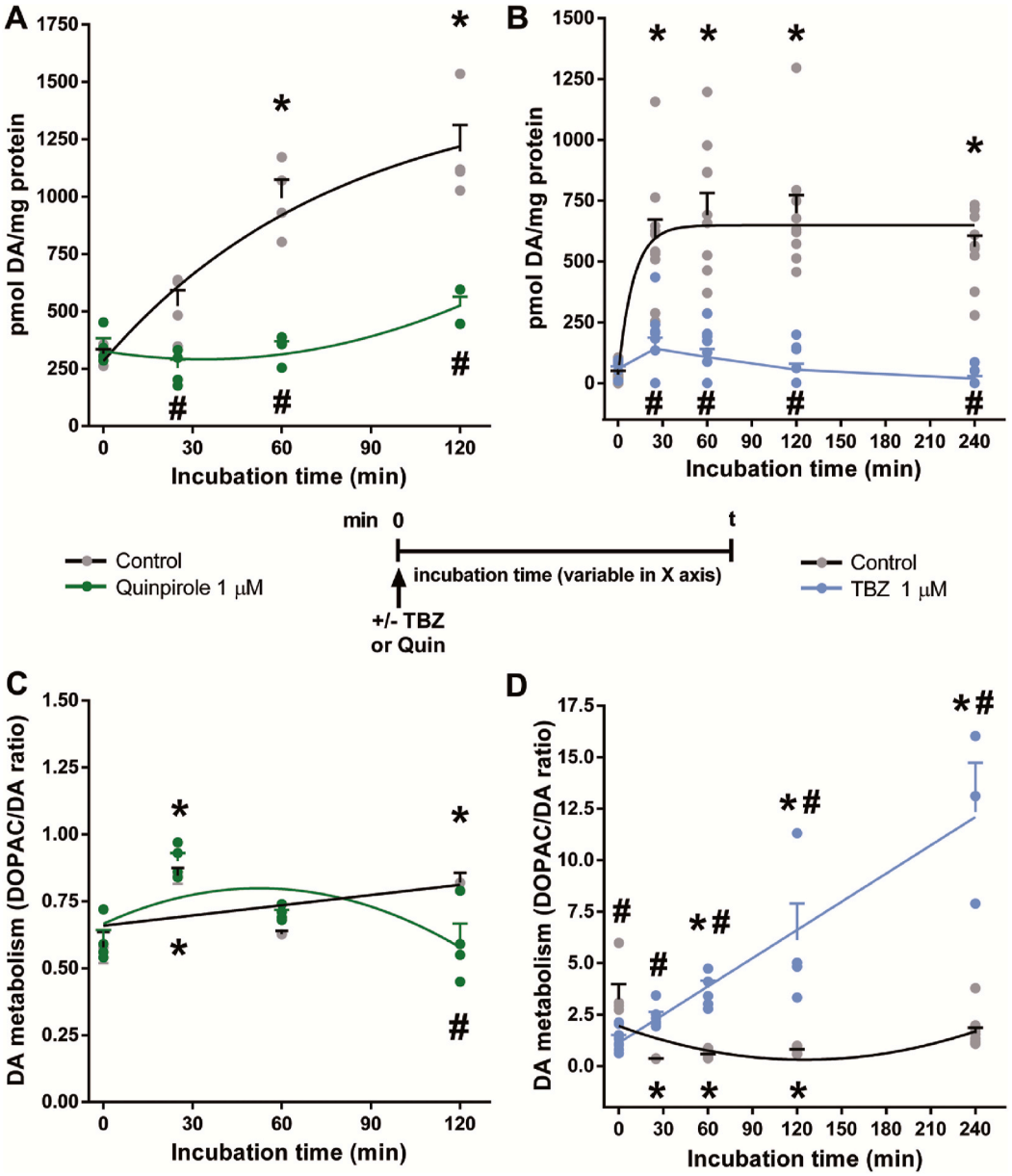

Fig. 3. Endogenous DA concentrations increase spontaneously with incubation time if DA synthesis and storage are not impaired. DA accumulated during the incubation of brain striatal minces (A, B, black lines) unless D_2-like autoreceptors were stimulated with 1 μM quinpirole (A, green line) or the VMAT2 inhibitor TBZ 1 μM (B, blue line) was present. The DOPAC/DA ratio index of DA metabolism increased with TBZ (D), but not with quinpirole (C) treatments or in control conditions (C, D, black lines). The experimental design is shown in the timeline. Data and the means ± SEM of N equal to A) 4 (control), 4 (Quin); B) 6–10 (control), 9–10 (TBZ); C) 3–4 (control), 4 (Quin); D) 5–10 (control), 3–8 (TBZ) brain striatal tissue incubations are represented. In B) 1 and D) 4 incubations were excluded from the analysis after values were considered outliers by the ROUT test. Control curves of DA accumulation (A, B) adjusted to a one-phase association curve (r^2 0.96 and 0.95, respectively) while those of DOPAC/DA ratio (C, D) fit to a linear (r^2 0.81) and a second order polynomial (r^2 0.97) equations, respectively. This latter regression was also followed by Quin in both A) and C) (r^2 0.92 and 0.85, respectively). TBZ effects on D) followed a linear regression (r^2 0.97). Two-way ANOVA showed in A) a significant effect of Treatment ($F(1,24) = 81.6$; $p < 0.0001$) and Time ($F(3,24) = 32.3$; $p < 0.0001$), and a significant interaction between these two factors ($F(3,24) = 15.3$ $p < 0.0001$); in B) a significant effect of Treatment ($F(1,85) = 161.3$; $p < 0.0001$) and Time ($F(4,85) = 11.8$; $p < 0.0001$), and a significant interaction between these two factors ($F(4,85) = 10.1$ $p < 0.0001$); in C) a significant effect of Time ($F(3,23) = 16.1$; $p < 0.0001$), and a significant interaction between time and treatment ($F(3,23) = 5.5$ $p < 0.005$) and in D) a significant effect of Treatment ($F(1,60) = 141.5$; $p < 0.0001$) and Time ($F(4,60) = 36.3$; $p < 0.0001$), and a significant interaction between these two factors ($F(4,60) = 40.4$ $p < 0.0001$); *$p < 0.05$, vs. 0 min, ANOVA plus Dunnett's multiple comparisons test; $^{\#}p < 0.05$, vs. data in control curve, ANOVA plus Sidak's multiple comparisons test.

accumulation with incubation time (Fig. 1B). As NSD-1015 blocks the aromatic-L-amino-acid decarboxylase, preventing new DA production, this result likely indicated that DA feedback-inhibition was responsible for the decay of TH activity. To confirm this result, we used a second method to determine DA synthesis without NSD-1015, based on the HPLC purification of [^{3}H]-DA after incubation of tissue minces with [^{3}H]-tyrosine. Again, a time-dependent decay in [^{3}H]-DA synthesis rate was observed consistent with new DA formation. The decrease adjusted to a one phase exponential decay regression curve either with or without pre-incubation before [^{3}H]-Tyr was added with similar results (Fig. 1C and D). [^{3}H]-DA synthesis rate appeared maximal between the initial 0 and 25 min of pre-incubation time.

Next, we studied the effects of exogenous L-DOPA or DA. The addition of L-DOPA further reduced the rate of [^{3}H]-DA synthesis in a concentration-dependent manner (Fig. 2A). The addition of DA also decreased [^{3}H]-DA synthesis rate in a concentration-dependent manner

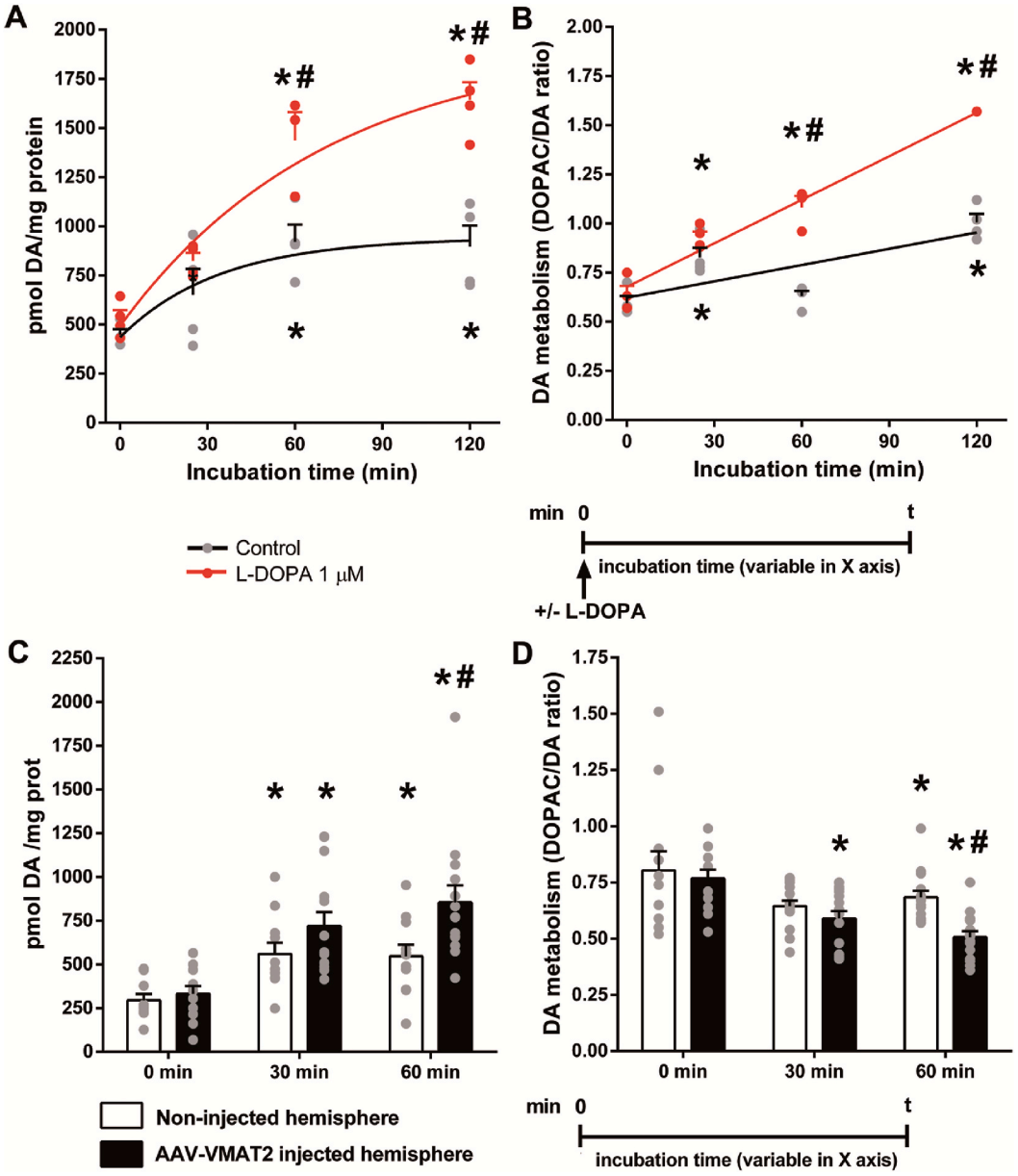

Fig. 4. Endogenous DA vesicular storage and metabolism is altered by exogenous L-DOPA and VMAT2 overexpression. L-DOPA addition to brain striatal minces increased DA concentrations (A) and metabolism (B) while VMAT2 overexpression increased DA storage (C) but decreased DA metabolism (D). Incubation designs are shown as timelines: In A, B) variable incubation times with addition of 1 μM L-DOPA at the beginning of incubation; C-D) no incubation, 30- or 60-min incubation of left or right striatum one month after the injection of AAV-hVMAT2 viral vector unilaterally in the right substantia nigra. Data represent the endogenous DA values and DOPAC/DA ratio and the means ± SEM of N equal to A, B) 4 (control), 3–4 (L-DOPA); C) 13–14 (non-injected), 13–16 (injected); D) 12–15 (non-injected), 12–15 (injected) brain striatal tissue incubations. In B) 1 and C) 5 incubations were excluded from the analysis after values were considered outliers by the ROUT test. Control and L-DOPA curves adjusted to A) a one-phase association curve (r^2 0.89 and 0.97, respectively) and B) linear regression (r^2 0.89 and 0.98, respectively). Two-way ANOVA showed in A) a significant effect of Treatment ($F(1,23) = 35.5$; $p < 0.0001$) and Time ($F(3,23) = 34.2$; $p < 0.0001$), and a significant interaction between these two factors ($F(3,23) = 6.1$ $p < 0.0001$); in B) a significant effect of Treatment ($F(1,22) = 112.5$; $p < 0.0001$) and Time ($F(3,22) = 99.8$; $p < 0.0001$), and a significant interaction between these two factors ($F(3,22) = 21.3$ $p < 0.0001$); in C) a significant effect of Treatment ($F(1,65) = 7.8$; $p < 0.01$) and Time ($F(2,65) = 15.1$; $p < 0.0001$) without a significant interaction between these factors and in D) a significant effect of Treatment ($F(1,78) = 7.1$; $p < 0.01$) and Time ($F(2,78) = 11.8$; $p < 0.0001$), without a significant interaction between these factors; *$p < 0.05$, vs. 0 min, ANOVA plus Dunnett's multiple comparisons test. #$p < 0.05$, vs. respective control: A, B) data in control curve; C-D) non-injected hemisphere, ANOVA plus Sidak's multiple comparisons test.

(Fig. 2B). DA effect adjusted well to a two-site competition curve (IC_{50} $9.3x10^{-9}$ M and $5.8x10^{-6}$ M; r^2 0.97; $p < 0.005$ vs. one-site competition). 100 μM DA completely abolished [^{3}H]-DA synthesis rate. D_2 receptor stimulation did not explain the effects of 1 μM DA, as DA effects were not blocked by the D_2-like receptor antagonist sulpiride (Fig. 2C). Nevertheless, as a positive control we checked whether D_2-like receptors were functional in our brain minces. Indeed, the agonist quinpirole (100 nM) did produce a significant reduction in [^{3}H]-DA synthesis rate (Fig. 2C) that was completely antagonized by pre-incubation with 1 μM sulpiride (Fig. 2C). Next, we tested whether intracellular DA was involved in the [^{3}H]-DA synthesis decrease through manipulating DA storage with the VMAT2 inhibitor tetrabenazine (TBZ). As expected, TBZ produced a concentration-dependent decrease of [^{3}H]-DA synthesis rate (IC_{50} $6.1x10^{-8}$ M; one-site competition, r^2 0.96) (Fig. 2D). 1 μM TBZ completely impaired DA synthesis. These findings indicate that non-stored DA negatively feeds-back on the TH enzyme, and DA storage dynamics strongly influence DA biosynthesis.

3.2. DA storage dynamics

The striking dependence of DA synthesis rate on incubation time *ex vivo* led us to evaluate endogenous DA levels on the same time frame. Unexpectedly, we found that endogenous DA levels in brain striatum markedly and spontaneously increased during incubation, approaching a plateau after 60 min (Fig. 3A and B). The kinetics of this spontaneous DA accumulation in tissue *ex vivo* led us to hypothesize that the initially high rate of DA synthesis becomes more moderate as DA storage in vesicles approached saturation. To test this hypothesis, we conducted several experiments interfering with DA synthesis or storage and determining endogenous DA levels. First, as expected, addition of the aromatic-L-amino-acid decarboxylase inhibitor NSD-1015 (100 mM) completely prevented the time-dependent increase in DA levels, or even decreased them (ice control: 244 ± 69 pmol DA/mg protein; 2 h incubated in the presence of NSD-1015: 144 ± 32 pmol DA/mg protein, mean ± S.D., N = 6/group). Second, incubation time-dependent dopamine accumulation *ex vivo* was greatly reduced by the presence of the D_2 receptor agonist quinpirole (1 μM) during the 2 h incubation (Fig. 3A, green line). Third, the VMAT2 inhibitor tetrabenazine (1 μM) completely impaired DA accumulation (Fig. 3B, blue line) as expected by blockade of DA storage. However, differences in the mechanisms of action of quinpirole and TBZ were evident by their differential modulation of the DOPAC/DA ratio. Quinpirole did not increase the DOPAC/DA ratio (Fig. 3C, green line) suggesting the drug slowed down new DA biosynthesis, while TBZ resulted in a clear time-dependent increase DOPAC/DA ratio (Fig. 3D, blue line) revealing increased metabolism of non-stored DA.

Treatments increasing DA storage were also used. The presence of 1 μM L-DOPA during incubation increased both DA accumulation (Fig. 4A) and the DOPAC/DA ratio (Fig. 4B) time-dependently. On the other hand, enhancement of VMAT2 expression by the previous unilateral injection of the hVMAT2 viral vector in the right substantia nigra increased ipsilateral striatal DA concentration (Fig. 4C) and decreased DOPAC/DA ratio (Fig. 4D) when compared with the contralateral side. These effects were only evident after a 60 min incubation, as both hemispheres showed incubation time-dependent effects. Thus, VMAT2 overexpression also increased DA storage but, differently to L-DOPA addition, it decreased DA metabolism. All these results support the hypothesis that the accumulation of newly formed DA in the cytosol is responsible of the observed decay of [^{3}H]-DA biosynthesis with time. Moreover, the spontaneous increase in endogenous DA levels (Fig. 3A–B, black line) without a concomitant alteration of the DOPAC/DA ratio (Fig. 3C–D, black line) indicated us that this tissue preparation was actively synthesizing and storing DA, likely until maximal storage was reached. Thus, we asked if this phenomenon could be generalized to another neurotransmitter. Serotonin (5-HT) levels showed also a clear pattern of incubation time-dependent accumulation *ex vivo*, both in the striatum and hippocampus (Fig. 5). New biosynthesis of DA and 5-HT seems then to nearly fill vesicular stores during the first 2 h of tissue slice incubation *ex vivo*.

3.3. TH phosphorylation status

TH activity is known to be regulated in the short-term by changes in its phosphorylation state (Haycock and Haycock, 1991). TH can be phosphorylated at several serine residues by protein kinases such as PKA, ERK or CaMKII, and it can be dephosphorylated by PP2A and PP2C protein phosphatases (for review see (Dunkley et al., 2004)). A 25 min incubation with the MEK inhibitor PD98059 50 μM decreased [^{3}H]-DA synthesis, while increased [^{3}H]-DA synthesis resulted from PKA activation with 1 mM cAMP-Sp or Ser/Thr protein phosphatases inhibition with Ok 1 μM (Fig. 6A). Interestingly, a time-dependent decay of [^{3}H]-DA synthesis rate was still observed during all these treatments. Either endogenous (Fig. 6A, time effect) or exogenous DA (Fig. 6B) were able to decrease [^{3}H]-DA synthesis under the influence of agents able to alter TH phosphorylation.

TH phosphorylation and TH protein amounts were also monitored. In separate experiments, TH phosphorylation in Ser31 and in Ser40 vs. total TH was determined by Western blot at different incubation time points up to 240 min. β-actin was used as an additional loading control of total TH levels. No clear effects of incubation time on TH phosphorylation were apparent (Fig. 7A, B and C). In contrast, treatment with 1 μM Ok induced a transient two-fold increase in phosphoSer31-TH, reaching the highest point at 120 min (Fig. 7B), and a delayed effect in phosphoSer40-TH, reaching the highest point at the longest time analyzed (240 min, Fig. 7C). Importantly, total TH protein was not decreased during the overall incubation time (Fig. 7A and D and S3). Thus, although Ok increased both [^{3}H]-DA synthesis rate and TH phosphorylation as expected, TH levels or phosphorylation status did not decay time-dependently either in the absence or presence of Ok. In addition, the ratio between TH and actin was also measured, showing no changes at any time of incubation with or without Ok (Supplementary Fig. S3).

25 μM PD98059 did not change phosphoSer31 in TH at the shortest incubation times (Fig. 7E) despite 50 μM decreased [^{3}H]-DA synthesis as soon as 25 min of incubation (Fig. 6A). A positive control of the effectiveness of 25 μM PD98059 was performed by detection of phosphoERK-1/2 in Thr202 and in Tyr204 by Western blot. 25 μM PD98059 decreased ERK-1/2 phosphorylation ratio vs. total ERK-1/2, as expected for a MEK inhibitor, but only after 60 min of incubation (Fig. 7D). Since Ser31-TH phosphorylation in brain does not seem to undergo major changes during incubation (Fig. 7E), the DA feedback on TH we observe also seems unrelated to Ser31- TH phosphorylation.

In order to further search possible changes of the TH phosphorylation status on Ser31 and Ser40 due to brain tissue incubation *ex vivo*, we used mass spectrometry (Fig. 8). Total TH was immunoprecipitated in parallel from 4 h-incubated striatal minces (Fig. 8B) and ice controls (Fig. 8A, not incubated) obtained from the same animal brain. Trypsin digestion of TH immunoprecipitated samples yielded peptides unequivocally recognized as TH fragments. The ratio of Ser31 phosphorylated vs. non-phosphorylated peptides was almost unchanged (28% in ice control and 25% in 4 h incubation). Ser40 phosphorylation was much lower than Ser31, and not decreased by time (1.1% in ice control, 2% after 4 h incubation). Thus, mass spectrometry confirmed the main Western blot results: incubation time did not alter TH phosphorylation in Ser31 and Ser40, and Ser31 was significantly phosphorylated during the whole incubation. In addition, Ser19 phosphorylation could be detected (25% in ice control vs. 18% in the 4 h-incubated sample, % relative to the unphosphorylated peptide). Furthermore, Thr30 phosphorylation was also detected (12% in ice control vs. 14% in 4 h-incubated sample). To our knowledge, this is the first report of TH phosphorylation in Thr30.

In conclusion, the time-dependent decay of [^{3}H]-DA synthesis rate

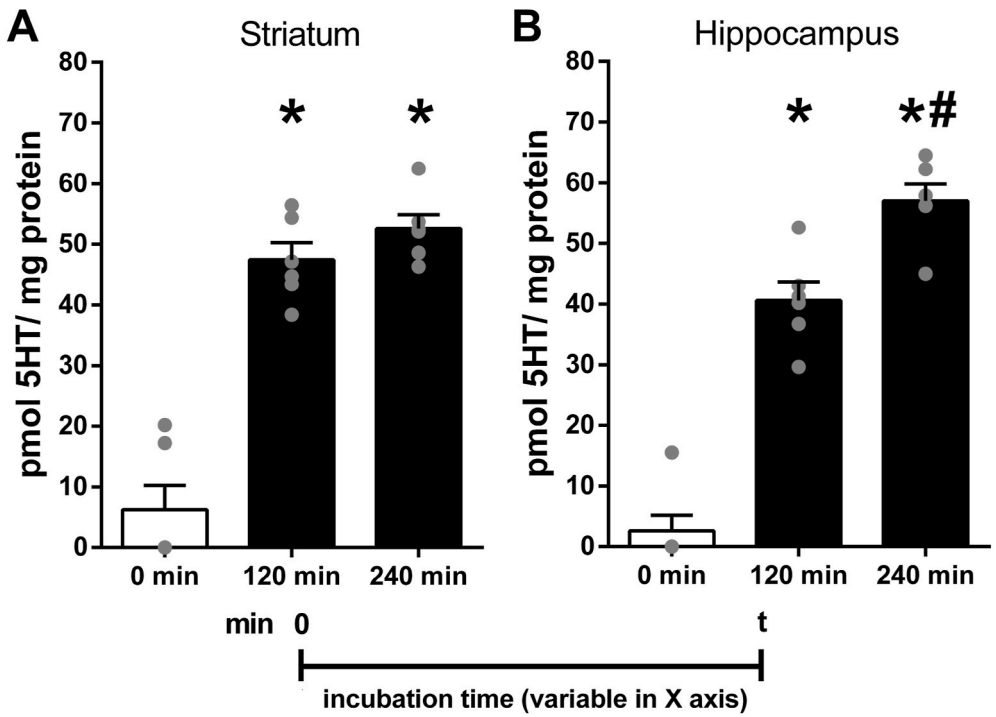

Fig. 5. Like DA, endogenous serotonin (5-HT) concentrations also increase spontaneously with incubation time. 5-HT levels in the striatum (A) and hippocampus (B) showed a clear pattern of incubation time-dependent accumulation *ex vivo*. 0 min bars show non-incubated ice controls. Data represent the endogenous 5-HT values and the means ± SEM of N = 6 brain tissue incubations/group. *$p < 0.05$, vs. 0 min, $^{\#}p < 0.05$, vs. 120 min; one-way ANOVA plus Tukey's multiple comparisons test.

was not due to TH degradation or to a loss of Ser31-or Ser40-TH phosphorylation over time. Agents altering Ser31-or Ser40-TH phosphorylation modified the pattern - but did not prevent - of the time-dependent decay of TH activity. Inability to further store DA is the main factor involved in the decrease of TH activity with incubation time.

4. Discussion

We report that DA inhibition of brain TH activity is strongly dependent on DA storage, and it is measurable in fresh brain *ex vivo*, by using a simple approach to assess dopamine synthesis and storage dynamics.

TH inhibition by DA feedback has long been known, but often overlooked. The popularity of methods to determine brain TH activity based in L-DOPA accumulation should have contributed to its neglection, as pharmacological blockade of aromatic-L-amino-acid decarboxylase prevents DA formation and thus feedback. During the set-up of this technique, we found a time-dependent decrease of brain TH activity (Figs. 1–2) associated to a pattern of spontaneous DA accumulation (Figs. 3 and 4) clearly indicating new DA formation and storage. When DA storage eventually approached saturation of vesicles, non-stored DA was likely free to inhibit TH in the cytosol, decreasing TH activity. Although these findings could be rationally expected, we did not anticipate observing them so clearly by using our simple methodology. Tissue manipulation was limited to chop a fresh brain striatum, wash and incubate it in non-depolarizing Krebs buffer. Hence striatal minces maintained most structure and functionality after probably losing part of its dopamine content during CO_2 euthanasia and tissue chopping. Brain incubation at 37 °C restored a -transiently- hyperactive DA synthesis in catecholaminergic pre-synaptic varicosities or terminals until storage in vesicles reached its maximal capacity. A straightforward HPLC purification of [^{3}H]-DA, or the quantification of endogenous DA, L-DOPA and DOPAC, completed the procedures. In our non-depolarizing conditions (2 mM K^+) the release of newly formed [^{3}H]-DA to the extracellular medium is very low (approximately 1% of total [^{3}H]-DA synthesis (Ma et al., 2014)) and at least 90% of newly formed DA may be stored in vesicles (Eisenhofer et al., 2004). The DA increase with time under non-depolarizing conditions agrees with previous reports of increased TH activity after cessation of neuronal firing (Aghajanian and Roth, 1970; Andén et al., 1973; Walters et al., 1973). Using computer simulations, Wallace (2007) predicted that DA negative feedback on TH would not occur in the presence of efficient DA storage and the absence of release and reuptake, explaining transiently hyperactive dopamine biosynthesis at the beginning of the incubation. When vesicles approach saturation, storage becomes less efficient and DA spillover may happen, leading to the decay in TH activity. Accordingly, the decrease of TH activity was dependent on new DA synthesis (Fig. 1) and storage (Figs. 2–4), and we ruled out other alternatives. Firstly, we discarded the possibility of a depletion of endogenous tyrosine levels, as [^{3}H]-tyrosine was provided for [^{3}H]-DA synthesis at different times (Fig. 1C–D and 2). In addition, a depletion of endogenous tyrosine cannot explain the time-dependent DA accumulation (Figs. 3 and 4). Secondly, we rejected the possible activation of DA degradation pathways because the DOPAC/DA ratio remained stable (Fig. 3C–D, black line). Finally, we also rejected the hypothesis that time dependent changes obeyed to a loss of TH phosphorylation (Figs. 7 and 8) or D_2 autoreceptor activation (Fig. 2C).

Impairment of vesicular uptake with TBZ prevented TH activity presumably by enhancing cytosolic DA. Dopamine D_2 activation by quinpirole prevented TH activity through signal transduction mechanisms. Although in both cases DA accumulation was impaired (Fig. 3), only TBZ increased DOPAC levels showing increased DA metabolism. These results support the involvement of new DA synthesis and storage on DA accumulation. Traditionally, the DOPAC/DA ratio has been considered to reflect metabolism by monoamine oxidase (MAO). We found clear increases of DOPAC/DA ratio with TBZ and L-DOPA (Figs. 3–4), which shows that insufficient DA storage leads to metabolism. In the presence of L-DOPA, DA storage could reach a higher maximum as it can also involve non-dopaminergic cells in brain striatum able to decarboxylate L-DOPA and store DA. Accordingly, VMAT2

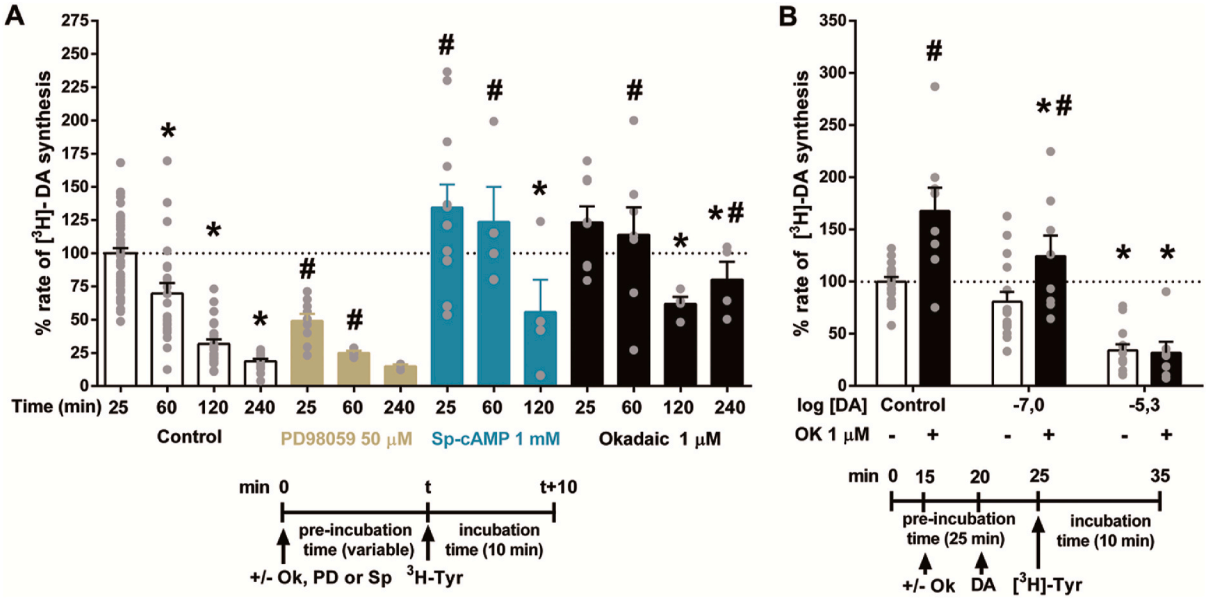

Fig. 6. DA and phosphorylation agents modulate TH activity. The decay of [^{3}H]-DA synthesis rate with time (A) was evaluated in brain striatal minces under the effects of agents that modify TH phosphorylation state such as PD98059, a MEK/ERK pathway inhibitor; Sp-cAMP, a PKA activator; and okadaic acid (Ok), a phosphatase inhibitor. Drugs were added at the beginning of the pre-incubation time indicated in the x-axis and timeline, plus 10 min incubation with [^{3}H]-Tyr properly used to measure [^{3}H]-DA synthesis rate. The effects of 1 μM Ok (B) were further evaluated in combination with 0.1 and 5 μM DA. Addition of the compounds to brain striatal tissue is indicated in timelines. Data represent individual incubation values and mean ± SEM % of control [^{3}H]-DA synthesis at 25 min (A) of N equal to 14–50 (control), 3–9 (PD98059), 4–12 (Sp-AMPc) and 4–8 (Ok) tissue incubations or (B) mean ± SEM of N equal to 16–18 (control) and 7–8 (OK) tissue incubations. 1 incubation in (A) was excluded from the analysis after the value was considered outlier by the ROUT test. In control groups 100% corresponds to a mean ± SEM of 632,898 ± 87,744 (A) and 295,539 ± 17,413 (B) dpm [^{3}H]-DA/mg.h. Two-way ANOVA showed in A) a significant effect of Treatment ($F(1,96) = 16.4$; $p < 0.0001$) and Time ($F(2,96) = 18.4$; $p < 0.0001$), without a significant interaction between these factors for PD98059; a significant effect of Treatment ($F(1,111) = 15.9$; $p < 0.0001$) and Time ($F(2,111) = 23.7$; $p < 0.0001$ without a significant interaction between these factors for Sp-cAMP; and a significant effect of Treatment ($F(1,126) = 32.6$; $p < 0.0001$) and Time ($F(3,126) = 22.8$; $p < 0.0001$) without a significant interaction between these factors for Ok. In B) two-way ANOVA showed a significant effect of Treatment ($F(1,67) = 15.5$; $p < 0.0005$) and DA concentration ($F(2,67) = 40.8$; $p < 0.0001$), and a significant interaction between these two factors ($F(2,67) = 4.9$ $p < 0.05$). A) *$p < 0.05$ vs. respective 25 min pre-incubation, ANOVA plus Dunnett's multiple comparisons test. #$p < 0.05$ vs. control group, ANOVA plus Sidak's multiple comparisons test. B) *$p < 0.05$vs. respective control, ANOVA plus Dunnett's multiple comparisons test. #$p < 0.05$ vs. non-treated groups, ANOVA plus Sidak's multiple comparisons test.

overexpression raised DA storage and decreased the DOPAC/DA ratio (Fig. 4C–D). DA metabolism to DOPAC increased modestly with time when maximal storage was reached, as DA levels in the cytoplasm likely approached the high μM MAO Km (Best et al., 2009). However, the increase of DA metabolism must have been limited by DA feedback on TH. It is of note that 5-HT also accumulated time-dependently even more clearly than DA (Fig. 5), which may be due to the lack of a negative feedback of 5-HT on tryptophan hydroxylase.

Inhibition of [^{3}H]-DA synthesis by exogenous DA fits with a two-site competition regression, with approximate IC_{50} of 20 nM and 4 μM for high- and low-affinities respectively (Fig. 2B). These results support previous *in vitro* studies (Dickson and Briggs, 2013; Gordon et al., 2008) suggesting the existence of two DA binding sites or TH conformations with high and low affinities (K_D 4 nM and 90 nM respectively) (Gordon et al., 2009; Nakashima et al., 2009; Tekin et al., 2014) although we cannot discard additional explanations, especially for the low DA affinity. Quantitative differences between our results and previous publications could be due to the need for exogenous DA to enter the tissue (i.e., through the DA or other transporters) and to the inherent complexity and heterogeneity of brain slices. Without an actual measure of cytosolic DA -difficult to obtain experimentally-it would be speculative to suggest which of the DA binding sites/conformations were occupied by DA in each condition assayed. Nevertheless, if we consider that cytosolic DA concentration may be lower than 100 nM (Mosharov et al., 2006), the high-affinity binding site/conformation might be almost completely occupied by DA. In contrast, the low-affinity binding site/conformation would putatively be the one able to respond to a further increase in cytosolic DA concentrations due to inefficient vesicle storage. Further work could better address this issue, e.g. by using mutant TH insensitive to feedback inhibition by dopamine (Mor et al., 2017). Cell cultures where intracellular amperometric recordings measure dopamine vesicular content would also be helpful to better understand dopamine dynamics (Gu and Ewing, 2021) under non-depolarizing (this work) or depolarizing conditions.

In basal physiological conditions less than 5% of TH is phosphorylated in Ser40 (Dunkley et al., 2004; Dunkley and Dickson, 2019). This low value agrees with the 1–2% signal ratio of phosphorylated/unphosphorylated Ser40-TH peptides we find by mass spectrometry (Fig. 8), as mass spectrometry signals depend both on peptide abundance and ionization efficiency, the latter being lower when peptides are phosphorylated. Ser40-TH phosphorylation has been reported to increase affinity for tetrahydrobiopterin (BH_4) cofactor and to decrease high-affinity DA binding (Daubner et al., 2011; Ramsey and Fitzpatrick, 1998). The low percentage of Ser40-TH phosphorylation suggests DA normally occupies the high-affinity site/conformation, and basal TH activity is supposed to be low. Nevertheless, TH was very active when newly synthesized DA was being stored in vesicles at the beginning of the incubation. Again, the low percentage of Ser40-TH phosphorylation suggests that cytosolic DA (newly synthesized, leaking from vesicles, or exogenously added and re-uptaken) may exert its inhibitory effect through the low-affinity binding site/conformation of TH. In accordance with previous reports (Haycock and Haycock, 1991; Lindgren et al., 2002), our results showed an increase of TH activity rate by PKA-mediated Ser40 phosphorylation and by inhibition of protein phosphatases with Ok (Figs. 6–7). Despite this agrees with literature, we still observed modified time- and concentration-dependent decays of

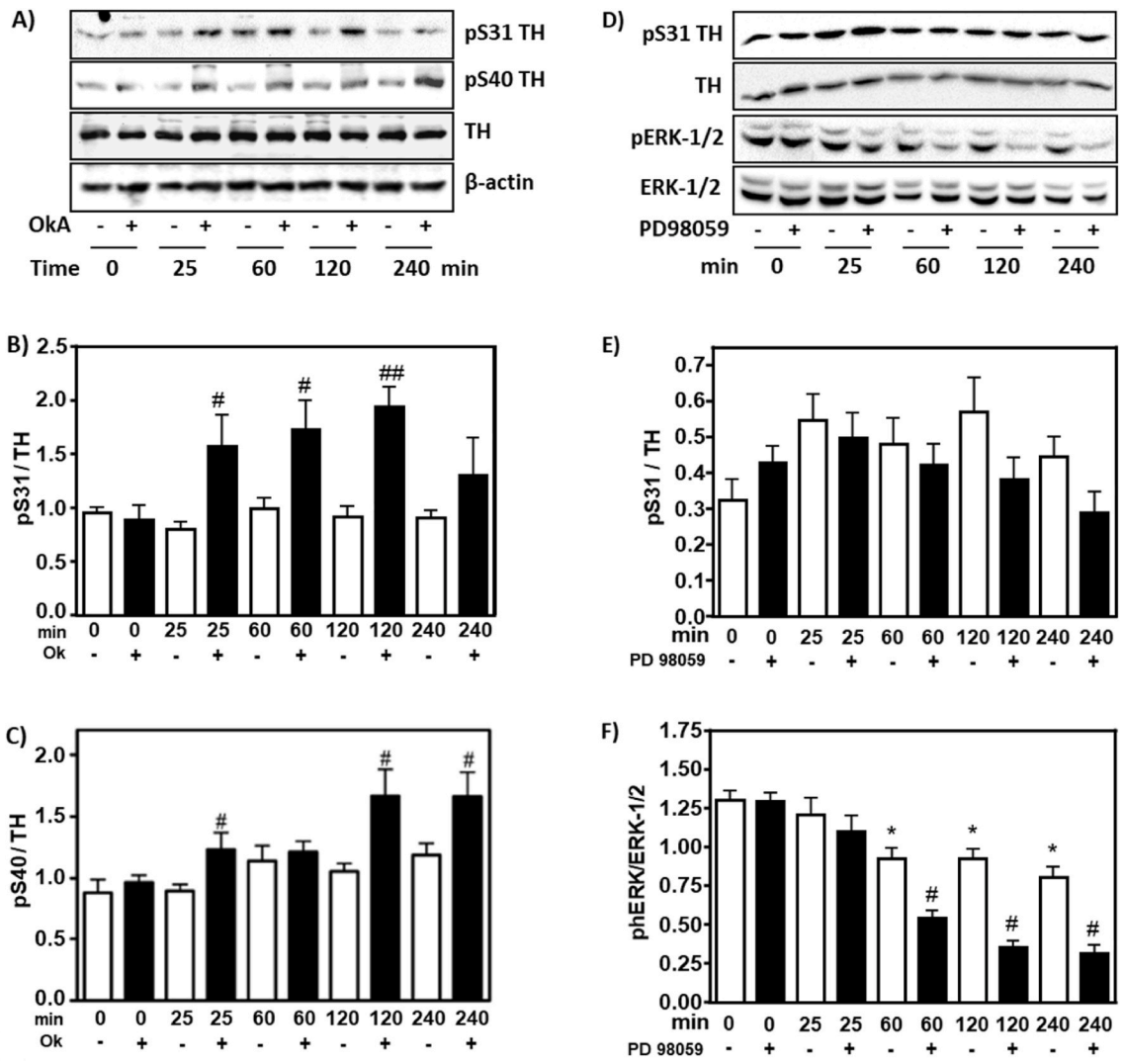

Fig. 7. TH phosphorylation changes in response to okadaic acid and to PD98059 at different times. A) TH phosphorylation at Ser31 and at Ser40 was determined by Western blot after different incubation times with or without 1 μM okadaic acid (Ok, added at time 0). In addition to total TH, β-actin (A) was also assessed as loading control. Mean optical density of the 55 kDa bands in A) were standardized to arbitrary units in each blot and results are expressed as pTH/TH ratio for Ser31 (B) and Ser40 (C). D) TH phosphorylation at Ser31 was determined with or without 25 μM PD98059 at different incubation times by Western blot. Dually phosphorylated ERK-1/2 in Thr202/Tyr204 was also determined as a control of PD98059 action. E) Results from D) are expressed as pS31 TH/TH ratio of standardized optical density of the 55 kDa bands. F) Graph showing phosphoERK/ERK-1/2 ratio of standardized optical density of the 42–44 kDa dimer from D). Data represent the means ± SEM of N equal to 4–5 brain striatal tissue incubations in all graphs. 0 min samples were not incubated. B–C) $^{\#}p < 0.05$, $^{\#\#}p < 0.01$ vs. 0 min incubation with Ok. F) $^{\#}p < 0.01$ vs. 0 min incubation without PD98059 (white bars); $^{*}p < 0.0001$ vs. 0 min incubation with PD98059 (black bars), ANOVA plus Sidak's multiple comparisons test.

[^{3}H]-DA synthesis in brain tissue (Fig. 6) that are not apparently related to a loss of phosphorylation during the incubation (Figs. 7 and 8). Therefore, it is possible that binding of newly-formed DA to the TH low-affinity binding site/conformation may act as a physiological DA sensor (Dickson and Briggs, 2013; Gordon et al., 2008, 2009) indicating that synaptic vesicles are nearly filled in brain. Additionally, no changes in TH protein levels were observed during Ok treatment after 4 h (Figs. 7 and S3). This lack of effect agrees with results observed in PC12D cells, where the TH protein levels remains unaltered even after 24h of incubation with Ok (Kawahata et al., 2009).

TH phosphorylation in Ser31 is more frequent than Ser40 (Fig. 8 and Dunkley and Dickson, 2019). Ser31 is considered an ERK target site. We showed that ERK is active at the beginning of our incubation (Fig. 7F), and ERK pathway inhibition with PD98059 decreased TH activity (Fig. 6A). However, an incubation time-dependent decay of TH activity was observed even in the presence of PD98059 (Fig. 6A). Since Ser31-TH phosphorylation in brain does not seem to undergo major changes during incubation (Figs. 7E and 8), the DA feedback on TH we observe also seems unrelated to Ser31- TH phosphorylation.

We found TH phosphorylation in Thr30 in rat brain by mass spectrometry (Fig. 8). To our knowledge this is a novel finding, of unknown physiological relevance. Thr30 is conserved in rat and mouse, but not in human TH sequences, while Ser31 and Ser40 are in all three species. Further work is necessary in this regard.

Our simple methodology can be replicated in many HPLC-equipped labs and become relevant to understand and refine treatments for DA-related disorders. The spontaneous endogenous DA accumulation allows to compare synaptic drug effects in fresh brain tissue without animal handing. A vesicular storage disorder may contribute to the etiopathogenesis of Parkinson's disease (Pifl et al., 2014). Accordingly, VMAT2 overexpression and L-DOPA raised DA storage. However, L-DOPA and TBZ treatments to human subjects should increase cytosolic DA (Fasano and Bentivoglio, 2009; Mosharov et al., 2009; Qi et al., 2008) as they increase DOPAC (Figs. 3 and 4). TBZ is FDA-approved for

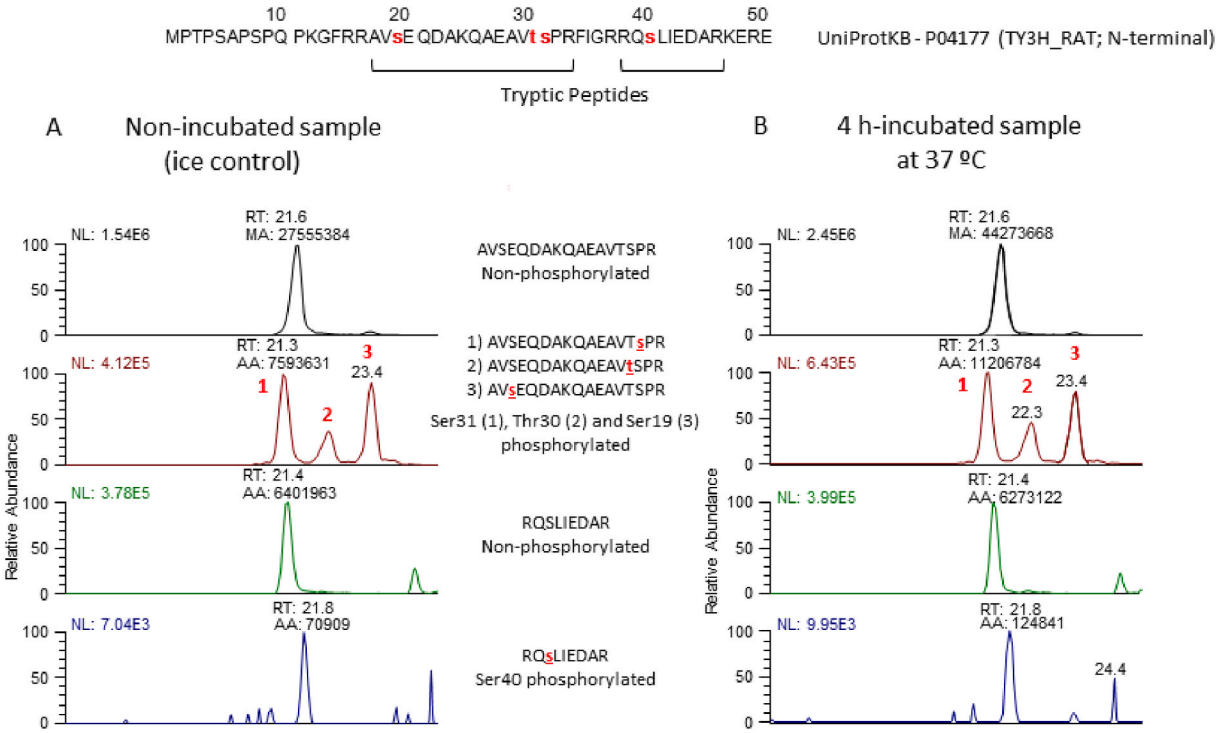

Fig. 8. LC-MS assessment of rat TH N-terminal phosphorylation in non-incubated (A) and 4h-incubated striatal samples (B). Top: UniProt rat TH sequence with tryptic peptides and phosphorylation sites (red) identified. Center: Rat TH peptide fragments identified by HPLC-MS after TH-immunoprecipitation and tryptic digestion. RT: retention time; NL: intensity; MA/AA: Manual or automatic peak area. s: phosphorylated serine; S: non-phosphorylated serine. Ratios of serine phosphorylation signals (s/S) were obtained from peak areas shown, which reflect peptide abundance and ionization efficiency. Threonine30 phosphorylation was observed (t, peak #2; T, non-phosphorylated threonine). The spectrometric analysis was performed in a data dependent mode, acquiring a full scan followed by 8 MS/MS scans of the 8 most intense signals from the inclusion list (see Supplementary Table S1).

Huntington's disease (Scott, 2011). VMAT2 inhibition by TBZ should increase cytosolic DA that produces a strong feedback on TH, which in turn could contribute to its antihyperkinetic benefits. VMAT2 and TH inhibition have been a target for the treatment of psychoses and addictions (Carlsson et al., 1972; Qi et al., 2008; Wimalasena, 2011): the non-selective VMAT inhibitor reserpine was used as antipsychotic. Of note, cytoplasmic DA accumulation can induce the formation of quinones and tetrahydroisoquinolines which have been involved in the degeneration of dopaminergic neurons (Goldstein et al., 2012) and interfere with DA synthesis (Scholz et al., 2008). Thus, it is worth considering the relevance of TH inhibition together with vesicular storage when understanding drug effects in these disorders. Mathematical models could be developed that consider TH inhibition as a factor to optimize drug doses and their combinations, together with experimental testing in brain *ex vivo* before animal and clinical research is carried out. Accordingly, understanding the inhibition of DA synthesis through TH feedback control offers real alternative possibilities for pharmacological intervention that could lead to new treatment strategies for DA-related disorders.

CRediT authorship contribution statement

Marta González-Sepúlveda: Conceptualization, Methodology, Formal analysis, Investigation, Writing, Visualization. **Muhammad Yusof Omar:** Investigation, Visualization. **Sally Hamdon:** Investigation. **Guofen Ma:** Investigation. **Santi Rosell-Vilar:** Methodology, Investigation. **Noora Raivio:** Validation, Investigation. **Doaa Abass:** Validation, Investigation. **Anna Martínez-Rivas:** Validation, Investigation. **Miquel Vila:** Methodology, Funding acquisition. **Jesús Giraldo:** Formal analysis, Funding acquisition. **Montserrat Carrascal:** Methodology, Investigation, Writing, Visualization. **Joaquín Abián:** Methodology, Writing, Funding acquisition. **Carles Gil:** Investigation, Writing, Visualization. **Josefa Sabriá:** Conceptualization, Writing. **Jordi Ortiz:** Conceptualization, Methodology, Writing, Funding acquisition. **David Moreno-Delgado:** Conceptualization, Methodology, Formal analysis, Investigation.

Acknowledgements

This work was supported by Spanish Government grants SAF2006-08240 (J.O.), SAF2009-12510 (J.O.), SAF2014-58396 (J.G, J.O.), SAF2017-87199-R (J.G, J.O.), SAF2016-77541-R (M.V.), The Michael J. Fox Foundation (ID15291, M.V.), "la Caixa" Foundation (ID 100010434), under the agreement LCF/PR/HR17/52150003 (M.V.). The Biological and Environmental Proteomics laboratory is a member of Proteored-PRB3 and is supported by grant PT17/0019/0008 of the PE I + D + i 2013–2016, funded by ISCIII and FEDER. M.G.S. enjoyed a Spanish government FPI fellowship. G.M received a fellowship from the China Scholarship Council. We thank the skillful technical assistance of Susana Benítez.

Appendix A. Supplementary data

Supplementary data to this article can be found online at https://doi.org/10.1016/j.neuropharm.2022.109058.

References

Aghajanian, G.K., Roth, R.H., 1970. Gamma-hydroxybutyrate-induced increase in brain dopamine: localization by fluorescence microscopy. J. Pharmacol. Exp. Therapeut. 175, 131–138. https://jpet.aspetjournals.org/content/175/1/131.

Andén, N.E., Magnusson, T., Stock, G., 1973. Effects of drugs influencing monoamine mechanisms on the increase in brain dopamine produced by axotomy or treatment with gammahydroxybutyric acid. Naunyn-Schmiedeberg's Arch. Pharmacol. 278, 363–372. https://doi.org/10.1007/BF00501480.

Ankenman, R., Salvatore, M.F., 2007. Low dose alpha-methyl-para-tyrosine (AMPT) in the treatment of dystonia and dyskinesia. J. Neuropsychiatry Clin. Neurosci. 19, 65–69. https://doi.org/10.1176/jnp.2007.19.1.65.

Best, J.A., Nijhout, H.F., Reed, M.C., 2009. Homeostatic mechanisms in dopamine synthesis and release: a mathematical model. Theor. Biol. Med. Model. 6, 21. https://doi.org/10.1186/1742-4682-6-21.

Bolea, I., Colivicchi, M.A., Ballini, C., Marco-Contelles, J., Tipton, K.F., Unzeta, M., Della Corte, L., 2014. Neuroprotective effects of the MAO-B inhibitor, PF9601N, in an in vivo model of excitotoxicity. CNS Neurosci. Ther. 20, 641–650. https://doi.org/10.1111/cns.12271.

Briggs, G.D., Bulley, J., Dickson, P.W., 2014. Catalytic domain surface residues mediating catecholamine inhibition in tyrosine hydroxylase. J. Biochem. 155, 183–193. https://doi.org/10.1093/jb/mvt110.

Briggs, G.D., Gordon, S.L., Dickson, P.W., 2011. Mutational analysis of catecholamine binding in tyrosine hydroxylase. Biochemistry 50, 1545–1555. https://doi.org/10.1021/bi101455b.

Carballo-Carbajal, I., Laguna, A., Romero-Giménez, J., Cuadros, T., Bové, J., Martinez-Vicente, M., Parent, A., Gonzalez-Sepulveda, M., Peñuelas, N., Torra, A., Rodríguez-Galván, B., Ballabio, A., Hasegawa, T., Bortolozzi, A., Gelpi, E., Vila, M., 2019. Brain tyrosinase overexpression implicates age-dependent neuromelanin production in Parkinson's disease pathogenesis. Nat. Commun. 10 https://doi.org/10.1038/s41467-019-08858-y.

Carlsson, A., Persson, T., Roos, B.E., Wålinder, J., 1972. Potentiation of phenothiazines by α-methyltyrosine in treatment of chronic schizophrenia. J. Neural. Transm. 33, 83–90. https://doi.org/10.1007/BF01260898.

Casanovas, A., Carrascal, M., Abián, J., López-Tejero, M.D., Llobera, M., 2009. Discovery of lipoprotein lipase pI isoforms and contributions to their characterization. J. Proteonomics 72, 1031–1039. https://doi.org/10.1016/j.jprot.2009.06.002.

Daubner, S.C., Le, T., Wang, S., 2011. Tyrosine hydroxylase and regulation of dopamine synthesis. Arch. Biochem. Biophys. 508, 1–12. https://doi.org/10.1016/j.abb.2010.12.017.

Dickson, P.W., Briggs, G.D., 2013. In: Tyrosine Hydroxylase. Regulation by Feedback Inhibition and Phosphorylation, first ed. Elsevier Inc. https://doi.org/10.1016/B978-0-12-411512-5.00002-6. Advances in Pharmacology.

Dunkley, P.R., Bobrovskaya, L., Graham, M.E., Von Nagy-Felsobuki, E.I., Dickson, P.W., 2004. Tyrosine hydroxylase phosphorylation: regulation and consequences. J. Neurochem. 91, 1025–1043. https://doi.org/10.1111/j.1471-4159.2004.02797.x.

Dunkley, P.R., Dickson, P.W., 2019. Tyrosine hydroxylase phosphorylation in vivo. J. Neurochem. 149, 706–728. https://doi.org/10.1111/jnc.14675.

Eisenhofer, G., Kopin, I.J., Goldstein, D.S., 2004. Leaky catecholamine stores: undue waste or a stress response coping mechanism? Ann. N. Y. Acad. Sci. 1018, 224–230. https://doi.org/10.1196/annals.1296.027.

Fasano, A., Bentivoglio, A.R., 2009. Tetrabenazine. Expert Opin. Pharmacother. 10, 2883–2896. https://doi.org/10.1517/14656560903386292.

Ghorbani, S., Szigetvari, P.D., Haavik, J., Kleppe, R., 2020. Serine 19 phosphorylation and 14-3-3 binding regulate phosphorylation and dephosphorylation of tyrosine hydroxylase on serine 31 and serine 40. J. Neurochem. 152, 29–47. https://doi.org/10.1111/JNC.14872.

Goldstein, D.S., Sullivan, P., Cooney, A., Jinsmaa, Y., Sullivan, R., Gross, D.J., Holmes, C., Kopin, I.J., Sharabi, Y., 2012. Vesicular uptake blockade generates the toxic dopamine metabolite 3,4-dihydroxyphenylacetaldehyde in PC12 cells: relevance to the pathogenesis of Parkinson's disease. J. Neurochem. 123, 932–943. https://doi.org/10.1111/j.1471-4159.2012.07924.x.

Gordon, S.L., Quinsey, N.S., Dunkley, P.R., Dickson, P.W., 2008. Tyrosine hydroxylase activity is regulated by two distinct dopamine-binding sites. J. Neurochem. 106, 1614–1623. https://doi.org/10.1111/j.1471-4159.2008.05509.x.

Gordon, S.L., Webb, J.K., Shehadeh, J., Dunkley, P.R., Dickson, P.W., 2009. The low affinity dopamine binding site on tyrosine hydroxylase: the role of the N-terminus and in situ regulation of enzyme activity. Neurochem. Res. 34, 1830–1837. https://doi.org/10.1007/s11064-009-9989-5.

Gu, C., Ewing, A.G., 2021. Simultaneous detection of vesicular content and exocytotic release with two electrodes in and at a single cell. Chem. Sci. 12, 7393–7400. https://doi.org/10.1039/D1SC01190A.

Harada, Wu, J., Haycock, J.W., Goldstein, M., 1996. Regulation of L-DOPA biosynthesis by site-specific phosphorylation of tyrosine hydroxylase in AtT-20 cells expressing wild-type and serine 40-substituted enzyme. J. Neurochem. 67, 629–635. https://onlinelibrary.wiley.com/doi/full/10.1046/j.1471-4159.1996.67020629.x.

Haycock, J.W., Haycock, D.A., 1991. Tyrosine hydroxylase in rat brain dopaminergic nerve terminals. Multiple-site phosphorylation in vivo and in synaptosomes. J. Biol. Chem. 266, 5650–5657. https://linkinghub.elsevier.com/retrieve/pii/S0021-9258(19)67644-1.

Jankovic, J., 2016. Dopamine depleters in the treatment of hyperkinetic movement disorders, Expert Opinion on Pharmacotherapy. Taylor & Francis. https://doi.org/10.1080/14656566.2016.1258063.

Justice, J.B., Nicolaysen, L.C., Michael, A.C., 1988. Modeling the dopaminergic nerve terminal. J. Neurosci. Methods 22, 239–252. https://doi.org/10.1016/0165-0270(88)90045-3.

Kawahata, I., Tokuoka, H., Parvez, H., Ichinose, H., 2009. Accumulation of phosphorylated tyrosine hydroxylase into insoluble protein aggregates by inhibition of an ubiquitin-proteasome system in PC12D cells. J. Neural. Transm. 116, 1571–1578. https://doi.org/10.1007/S00702-009-0304-Z.

Lindgren, N., Goiny, M., Herrera-Marschitz, M., Haycock, J.W., Hökfelt, T., Fisone, G., Hokfelt, T., Fisone, G., 2002. Activation of extracellular signal-regulated kinases 1 and 2 by depolarization stimulates tyrosine hydroxylase phosphorylation and dopamine synthesis in rat brain. Eur. J. Neurosci. 15, 769–773. https://doi.org/10.1046/j.1460-9568.2002.01901.x.

Lindgren, N., Xu, Z.Q.D., Lindskog, M., Herrera-Marschitz, M., Goiny, M., Haycock, J., Goldstein, M., Hökfelt, T., Fisone, G., 2000. Regulation of tyrosine hydroxylase activity and phosphorylation at Ser19 and Ser40 via activation of glutamate NMDA receptors in rat striatum. J. Neurochem. 74, 2470–2477. https://doi.org/10.1046/j.1471-4159.2000.0742470.x.

Ludders, J.W., 1992. Advantages and guidelines for using isoflurane. In: Veterinary Clinics of North America - Small Animal Practice, pp. 328–331. https://doi.org/10.1016/S0195-5616(92)50626-X.

Ma, G.F., Raivio, N., Sabrià, J., Ortiz, J., 2014. Agonist and antagonist effects of aripiprazole on D2-like receptors controlling rat brain dopamine synthesis depend on the dopaminergic tone. Int. J. Neuropsychopharmacol. pyu046 https://doi.org/10.1093/ijnp/pyu046.

McCulloch, R.I., Daubner, S.C., Fitzpatrick, P.F., 2001. Effects of substitution at serine 40 of tyrosine hydroxylase on catecholamine binding. Biochemistry 40, 7273–7278. https://doi.org/10.1021/bi010546d.

Mor, D.E., Tsika, E., Mazzulli, J.R., Gould, N.S., Kim, H., Daniels, M.J., Doshi, S., Gupta, P., Grossman, J.L., Tan, V.X., Kalb, R.G., Caldwell, K.A., Caldwell, G.A., Wolfe, J.H., Ischiropoulos, H., 2017. Dopamine induces soluble α-synuclein oligomers and nigrostriatal degeneration. Nat. Neurosci. 20, 1560–1568. https://doi.org/10.1038/nn.4641.

Mosharov, E.V., Larsen, K.E., Kanter, E., Phillips, K.A., Wilson, K., Schmitz, Y., Krantz, D. E., Kobayashi, K., Edwards, R.H., Sulzer, D., 2009. Interplay between cytosolic dopamine, calcium, and alpha-synuclein causes selective death of substantia nigra neurons. Neuron 62, 218–229. https://doi.org/10.1016/j.neuron.2009.01.033.

Mosharov, E.V., Staal, R.G.W., Bové, J., Prou, D., Hananiya, A., Markov, D., Poulsen, N., Larsen, K.E., Moore, C.M.H., Troyer, M.D., Edwards, R.H., Przedborski, S., Sulzer, D., 2006. Alpha-synuclein overexpression increases cytosolic catecholamine concentration. J. Neurosci. 26, 9304–9311. https://doi.org/10.1523/JNEUROSCI.0519-06.2006.

Nakashima, A., Hayashi, N., Kaneko, Y.S., Mori, K., Sabban, E.L., Nagatsu, T., Ota, A., 2009. Role of N-terminus of tyrosine hydroxylase in the biosynthesis of catecholamines. J. Neural. Transm. 116, 1355–1362. https://doi.org/10.1007/s00702-009-0227-8.

Nakashima, A., Kaneko, Y.S., Kodani, Y., Mori, K., Nagasaki, H., Nagatsu, T., Ota, A., 2013. Intracellular stability of tyrosine hydroxylase: phosphorylation and proteasomal digestion of the enzyme. Adv. Pharmacol. 68, 3–11. https://doi.org/10.1016/B978-0-12-411512-5.00001-4.

Ortiz, J., Gómez, J., Torrent, A., Aldavert, M., Blanco, I., 2000. Quantitative radioisotopic determination of histidine decarboxylase using high-performance liquid chromatography. Anal. Biochem. 280, 111–117. https://doi.org/10.1006/abio.2000.4494.

Paxinos, G., Watson, C., 1982. The Rat Brain in Stereotaxic Coordinates. Acad. Press. United States Am.

Pifl, C., Rajput, A.H.A., Reither, H., Blesa, J., Cavada, C., Obeso, J.A., Rajput, A.H.A., Hornykiewicz, O., 2014. Is Parkinson's disease a vesicular dopamine storage disorder? Evidence from a study in isolated synaptic vesicles of human and nonhuman primate striatum. J. Neurosci. 34, 8210–8218. https://doi.org/10.1523/JNEUROSCI.5456-13.2014.

Qi, Zhen, Miller, G.W., Voit, E.O., 2008. Computational systems analysis of dopamine metabolism. PLoS One 3, e2444. https://doi.org/10.1371/journal.pone.0002444.

Qi, Z., Miller, G.W., Voit, E.O., 2008. A mathematical model of presynaptic dopamine homeostasis: implications for schizophrenia. Pharmacopsychiatry 41 (Suppl. 1), S89–S98. https://doi.org/10.1055/s-2008-1080936.

Ramsey, A.J., Fitzpatrick, P.F., 1998. Effects of phosphorylation of serine 40 of tyrosine hydroxylase on binding of catecholamnines: evidence for a novel regulatory mechanism. Biochemsitry 37, 8980–8986. https://doi.org/10.1021/bi980582l.

Scholz, J., Toska, K., Luborzewski, A., Maass, A., Schünemann, V., Haavik, J., Moser, A., 2008. Endogenous tetrahydroisoquinolines associated with Parkinson's disease mimic the feedback inhibition of tyrosine hydroxylase by catecholamines. FEBS J. 275, 2109–2121. https://doi.org/10.1111/j.1742-4658.2008.06365.x.

Scott, L.J., 2011. Tetrabenazine: for chorea associated with Huntington's disease. CNS Drugs 25, 1073–1085. https://doi.org/10.2165/11208330-000000000-00000.

Spector, S., Gordon, R., Sjoerdsma, A., Udenfriend, S., 1967. End-product inhibition of tyrosine hydroxylase as a possible mechanism for regulation of norepinephrine synthesis. Mol. Pharmacol. 3, 549–555. http://molpharm.aspetjournals.org/cgi/pmidlookup?view=long&pmid=6075244.

Sura, G.R., Daubner, S.C., Fitzpatrick, P.F., 2004. Effects of phosphorylation by protein kinase A on binding of catecholamines to the human tyrosine hydroxylase isoforms. J. Neurochem. 90, 970–978. https://doi.org/10.1111/j.1471-4159.2004.02566.x.

Tekin, I., Roskoski, R., Carkaci-Salli, N., Vrana, K.E., 2014. Complex molecular regulation of tyrosine hydroxylase. J. Neural. Transm. https://doi.org/10.1007/s00702-014-1238-7.

Wallace, L.J., 2007. A small dopamine permeability of storage vesicle membranes and end product inhibition of tyrosine hydroxylase are sufficient to explain changes occurring in dopamine synthesis and storage after inhibition of neuron firing. Synapse 61, 715–723. https://doi.org/10.1002/syn.20408.

Walters, J.R., Roth, R.H., Aghajanian, G.K., 1973. Dopaminergic neurons: similar biochemical and histochemical effects of gamma-hydroxybutyrate and acute lesions of the nigro-neostriatal pathway. J. Pharmacol. Exp. Therapeut. 186, 630–639. https://jpet.aspetjournals.org/content/186/3/630.

Wimalasena, K., 2011. Vesicular monoamine transporters: structure-function, pharmacology, and medicinal chemistry. Med. Res. Rev. 31, 483–519. https://doi.org/10.1002/med.20187.

Zhang, S., Huang, T., Ilangovan, U., Hinck, A.P., Fitzpatrick, P.F., 2014. The solution structure of the regulatory domain of tyrosine hydroxylase. J. Mol. Biol. 426, 1483–1497. https://doi.org/10.1016/j.jmb.2013.12.015.

Annex 3

CHIR99021 decreases dopamine content in rat brain striatum through inactivation of Tyrosine Hydroxylase

Sally Hamdon[1,2], Pol Fernandez-Gonzalez[2], Muhammad Yusof Omar[1,2], Jordi Ortiz[1,2,3,4], Carles Gil[1,2,4,5]

[1] Institut de Neurociències, Universitat Autònoma de Barcelona, Spain.

[2] Department of Biochemistry and Molecular Biology, Universitat Autònoma de Barcelona, Spain.

[3] Centro Investigación Biomédica en Red de Salud Mental, CIBERSAM, and Translational Neuroscience Unit, Parc Taulí University Hospital and Universitat Autònoma de Barcelona, Spain.

[4] Contributed equally.

[5]To whom correspondence should be addressed: Carles Gil, Institut de Neurociències and Department of Biochemistry and Molecular Biology, School of Medicine, Room M2-122, Universitat Autònoma de Barcelona, 08193 Bellaterra (Cerdanyola del Vallès, Catalonia), Spain, Tel.: +34 935 81 1524, Fax: +34 93 581 1574, E-mail: carles.gil@uab.cat

Category: Neuropharmacology

Running title: CHIR99021 inhibits TH activity in brain striatum.

ABSTRACT

CHIR99021, also known as laduviglusib or CT99021, is a Glycogen-synthase kinase 3 α/β inhibitor, which has been reported as a promising drug for cardiomyocyte regeneration or treatment of sensorial hearing loss, among other pathologies. Since the activation of dopamine (DA) receptors regulate dopamine synthesis itself and use glycogen-synthase kinase 3β (GSK3β) as an element in the β-arrestin pathway, we decided to check the effect of GSK3β inhibitors (CHIR99021, SB216763 and lithium ion) in the control of DA synthesis. Using *ex vivo* experiments with minces from rat brain striatum, we observed that CHIR99021, but not SB216763 nor lithium, causes a complete abrogation of DA synthesis and accumulation, pointing to off-target effects of CHIR99021. This decrease can be attributed to tyrosine hydroxylase (TH) inhibition since the accumulation of L-DOPA in the presence of a DOPA decarboxylase inhibitor was similarly decreased. On the other hand, CHIR99021 caused an exponential increase in the DOPAC / DA ratio, an indicator of DA metabolization, and decreased the incorporation of extracellular DA into striatum minces. In addition, CHIR99021 or SB216763, but not lithium, decreased TH phosphorylation in Ser19. These results demonstrate that CHIR99021 can lead to TH inactivation and DA decrease in brain striatum, opening the possibility of its use in DA-related disorders, and shows effects to be considered in future clinical trials.

1. INTRODUCTION

Dopamine (DA) transmission is described as essential in the control of behavior through natural rewards, such as food, sex, and nurture, but also by a variety of drugs (Spanagel and Weiss, 1999). Moreover, dysregulation of DA metabolism is a key event in neurodegenerative diseases, such as Parkinson's disease (PD) (Johnson et al., 2018) or in mental disorders, such as schizophrenia (Dahoun et al., 2017). DA acts by neurotransmitter circuits localized in the midbrain, originated in the ventral tegmental area (VTA) and the substantia nigra (SN) and projecting to other brain structures, most prominently the nucleus accumbens shell region, the prefrontal cortex and the striatum (Alcaro et al., 2007). DA levels are the result of its biosynthesis, which is regulated by the first enzyme of the pathway, i.e., Tyrosine hydroxylase (TH; tyrosine 3-monooxygenase; E.C. 1.14.16.2), and of its degradation resulting in 3,4-dihydroxyphenylacetic acid (DOPAC) as its main metabolite. After its synthesis, DA must be internalized into synaptic vesicles by means of the vesicular monoamine transporter 2 (VMAT2) to be released (Meiser et al., 2013). Impairment of the control of these mechanisms may provoke inadequate levels of DA in particular brain areas, which may contribute to behavioral psychiatric pathologies, such as psychosis, addiction (Salamone et al., 2016) or depression (Duda et al., 2020). Moreover, due to the role of DA in the control of coordinated movements, alterations in the dopaminergic system also contribute to diseases causing locomotion impairment (Smith-Dijak et al., 2019). Short-term modulation of TH activity includes phosphorylation (Dunkley et al., 2019) and/or end-product feedback inhibition, i.e., by DA itself (González-Sepúlveda et al., 2022). TH is phosphorylated

at serine residues Ser8, Ser19, Ser31 and Ser40, according to the rat and mouse sequences, while humans show a Thr in position 8. Humans express four TH isoforms (hTH1-4), derived from a single gene, while most species, including rat, express only one isoform (Lewis et al., 1993). Several studies showed that increased phosphorylation at Ser40 positively correlated with TH activity (Bobrovskaya et al. 2007), while phosphorylation of Ser19 and Ser31 increases the rate of phosphorylation of Ser40 and potentiates TH activation (Lehmann et al., 2006).

DA exerts its functions through membrane receptors coupled to G proteins (Thal et al., 2018). DA receptors comprise two classes: the D1-like class (D1 and D5) and the D2-like class (D2, D3 and D4) (Xin et al., 2019). Both classes of receptors can act by two pathways, one inhibits intracellular cAMP via protein G_i (Bonifazi et al., 2019) while the other can initiate a cAMP-independent pathway by promoting a scaffolding complex that leads to the activation of both ERK1/2 and GSK3β signals, through the recruitment of β-arrestin (Jiang et al., 2022). These two pathways are differently turned-on depending on the ligand, in a phenomenon known as biased agonism (Beaulieu & Gainetdinov, 2011). Several evidence link GSK3β with neuropsychiatric disorders, mainly psychosis and schizophrenia (Lovestone et al., 2007; Jope, 2011; Koros and Dorner-Ciossek, 2007; O'Leary and Nolan, 2015). Moreover, inhibition of GSK3β has recently emerged as a possible pharmacological target in a plethora of pathologies, such as hyperglycemia (Ring et al., 2003), lung repair (Uhl et al., 2015), tooth repair (Zaugg et al., 2020), glioblastoma treatment (Oh et al., 2017; Lee et al., 2018) or regeneration of cardiomyocytes (Quaife-Ryan et al., 2020).

A GSK3β inhibitor, CHIR99021 (also known as laduviglusib or CT99021) is currently in clinical phase 2b for the restoration of some types of hearing loss (McLean et al., 2021; ClinicalTrials.gov Identifier: NCT05086276) and is a promising molecule that has also been successfully tested in inhibition of adipogenesis (Bennett et al., 2002), coronary and myocardial diseases (Drakhlis et al., 2021; Badimon et al., 2019), cancer (Oh et al., 2017; Lee et al., 2018; Houben et al., 2022), lung repair therapy (Uhl et al., 2015), stimulation of stem cells (Zhao et al., 2014), and type II diabetes mellitus (Ring et al., 2003). Moreover, CHIR99021 has been proposed as a potential drug for Huntington's disease, acting through off-target effects suppressing the proteasomal degradation of calpastatin (CAST) and enhancing the mitochondrial function (Hu et la., 2021).

In the present work we used *ex vivo* assays with rat brain striatum tissue to study the effects of three GSK3β inhibitors (CHIR99021, SB216763 and lithium) on DA metabolism, since the activation of DA receptors regulate DA synthesis itself and use GSK3β as an element in the β-arrestin pathway. The obtained results demonstrate that CHIR99021 indirectly inhibits TH in brain striatum and should be considered as a potential drug for the treatment of disorders caused by overproduction of DA. The exact mechanism by which CHIR99021 impairs TH activity is still unknown.

2. Materials and methods

2.1. Animals.

Experiments were conducted with male Sprague-Dawley rats weighing 200-250 g (from the Animal Service, Universitat Autònoma de Barcelona or from Charles River). Animals were housed five per cage with ad libitum access to food and water during a 12-hour light/dark cycle. Protocols for animal use were approved by the Ethics Committee for Human and Animal Research (Universitat Autònoma de Barcelona) in accordance with guidelines established by the Ethical Committee for the use of Laboratory Animals in Spain (53/2013) and the European Ethical Committee (2010/63/EU).

2.2. Preparation of striatal minces.

Freshly obtained rat brains were chilled immediately in modified Krebs-Ringer-bicarbonate medium with the following composition: 120 mM NaCl, 0.8 mM KCl, 2.6 mM $CaCl_2$, 0.67 mM $MgSO_4$, 1.2 mM KH_2PO_4, 27.5 mM $NaHCO_3$, and 10 mM glucose, saturated with 95% O_2 / 5% CO_2 and adjusted to pH 7.4. Dorsal / medial striata from both hemispheres were dissected and sliced in a 4°C room using a McIlwain tissue chopper obtaining tissue minces of 0.3 x 0.3 mm / side. Tissue minces were suspended in ice-cold Krebs Ringer bicarbonate medium, and washed three times by centrifugation (1,000 g, 1 min, 4°C), to remove debris of damaged cells, and resuspended. Striatal tissue from a single rat yielded up to 30 aliquots of 25 µL each of the settled minces suspension corresponding to 24 incubation samples and 6 blank samples (0.3 - 0.7 mg protein each). Typically, samples were distributed into 2 mL polypropylene tubes containing 225 µL of ice-cold Krebs Ringer bicarbonate medium. Blank tubes were kept on ice and the rest were incubated at

37°C in soft agitation in an Eppendorf Thermomixer (5 Prime, Inc., Boulder, CO) under 95% O_2 / 5% CO_2 atmosphere.

2.3. Determination of endogenous L-DOPA, DA and DOPAC levels by HPLC-EC.

Levels of L-DOPA, DA and DOPAC were determined in striatal minces. After different incubation times, tissue minces were sonicated in 0.25 M perchloric acid containing 0.25 mM EDTA and 0.1 mM sodium metabisulphite. A 10 µL aliquot was taken for protein quantification by the BCA method (Thermo Fisher Scientific). Samples were spun in an Eppendorf microcentrifuge at 12,000 g for 10 min, and 20 µL of supernatant were used for quantification. The accumulation of L-DOPA in the presence of the decarboxylase inhibitor NSD-1015 100 mM and of DA in the absence of NSD-1015 (Fig. 1B) was quantified by HPLC with coulometric detection (HPLC-EC) as previously described (González-Sepúlveda et al., 2022). The chromatography system consisted of a reverse-phase C18 column (2.5 µm particle Fortis C18, 10 x 0.46 cm, Sugelabor, Spain) and an ion-pair mobile phase, made up of 100 mM sodium phosphate buffer, 1 mM EDTA, 5 mM octanesulfonic acid (pH 2.5) plus 1 % (v/v) methanol. The flow rate was 1 mL / min. Concentrations of L-DOPA, DA and DOPAC were detected with a Coulochem II (ESA) detector with a model 5011 dual-electrode analytical cell with porous graphite electrodes. The potential of electrodes 1 and 2 was set at -0.05 V and +0.4 V respectively. Standards of L-DOPA, DA and DOPAC at different concentrations (4 - 40 nmol) were injected in every experiment to quantify the three metabolites by the external standard method. The obtained concentrations were corrected by protein content in each

sample. Statistical analysis was carried out with GraphPad Prism software (v6, GraphPad Software Inc, USA).

2.4. Newly-synthesized [^{3}H]-DA determination by HPLC-UV.

[^{3}H]-Tyrosine was purified as described previously (González-Sepúlveda et al., 2022). Concentration-response curve of CHIR99021 on striatal [^{3}H]-DA synthesis in minces *ex vivo* was measured after a preincubation period (as in *Preparation of striatal minces* section). CHIR was added using concentrations of 0.3, 3 and 30 µM (n = 6 per concentration) or control without CHIR (n = 6) 10 minutes before the end of preincubation. Then, 0.12 µM purified [^{3}H]-tyrosine was added and incubated for 10 additional minutes. In all experiments, [^{3}H]-DA synthesis was stopped by the addition of 25 µL of a deproteinizing mixture containing trichloroacetic acid (0.5 % w/v), 1 mM ascorbic acid and 25 nmol DA (internal standard). Samples were homogenized in a Dynatech / Sonic Dismembrator (Dynatech Labs, Chantilly, VA). A 10 µL aliquot was taken for protein quantification by the BCA method (Thermo Fisher Scientific). Tissue homogenates were then centrifuged (12,000 g, 10 min, 4°C), and all supernatants were processed for [^{3}H]-DA purification by HPLC-UV. [^{3}H]-DA formed during the incubation reaction was separated from [^{3}H]-tyrosine by HPLC purification by a modification of previous procedures used in our lab for other neurotransmitters (Ortiz et al., 2000). The chromatography system consisted of a reverse-phase C18 column (Tracer Extrasil ODS2, 5 µm particle size, 25 x 0.46 cm; Teknokroma, Spain) and an ion-pair mobile phase, made up of 100 mM sodium phosphate buffer, 1 mM EDTA, 0.75 mM octanesulfonic acid (pH 5) plus 12 % (v/v)

methanol. The flow rate was 1 mL / min. This HPLC system completely separates standards of tyrosine and DA detected by UV 285 nm (ring absorbance). Samples contained extremely low levels of radiolabeled tyrosine and DA that were undetectable by UV absorbance. Similarly, endogenous tyrosine and DA were negligible as compared to the amounts of internal standard DA used. The recovery of the internal standard in each sample (internal / external standard peak area) was quantified from internal standard DA HPLC-UV peak areas. 2 mL fractions corresponding to the DA peak were recovered in scintillation vials, mixed with 6 mL Optiphase HiSafe III cocktail, and quantified in a liquid scintillation counter (Perkin Elmer Tri-Carb 2810TR, USA) to determine [^{3}H]-DA. Disintegrations per minute (dpm) obtained in HPLC-purified [^{3}H]-DA fractions were corrected by DA internal standard recovery and dpm in blank samples. Rate of [^{3}H]-DA synthesis was estimated as the ratio of corrected dpm divided by protein content in each incubate and the incubation time in the presence of [^{3}H]-tyrosine. Results were expressed as a percentage with respect to control samples run in the same experiment.

2.5. Tyrosine Hydroxylase activity in homogenates obtained from striatal striatum.

Striata were extracted and placed in 5-6 mL of cold sodium phosphate buffer 10 mM pH 7.4 and homogenized using a glass Potter homogenizer. 200 µL of homogenates were distributed in incubation tubes in the absence or presence of increasing concentrations of CHIR99021. 100 µM NSD-1015, 30 µM tyrosine and 100 µM tetrahydrobiopterin (BH_4) were added. After 30 min of incubation at 37°C samples were placed in an ice block and 25 µL of a deproteinizing mixture (containing 0.5%

w/v trichloroacetic acid) were added. Samples were centrifuged at 10,000 g for 10 minutes and supernatants are injected into HPLC-ECD to quantify L-DOPA and expressed as L-DOPA pmols / mg protein.

2.6. Western blot.

After incubation of striatal minces as described above, Krebs-Ringer buffer was removed by centrifugation and tissue was homogenized in 1% SDS. Protein amount was determined by BCA. Equal amounts of protein were separated by SDS-PAGE electrophoresis followed by transference in polyvinylidene fluoride membrane in a Trans-Blot Turbo Transfer System (Bio-Rad). Blotting buffer contained 25 mM Tris, 200 mM glycine and 10% methanol (v/v). Membranes were blocked for 1 h with Tris-buffered saline, supplemented with 0.1% Tween 20 and 5% (w/v) defatted powdered milk. Then, the membranes were incubated overnight with the indicated antibody diluted in blocking buffer. The primary antibody from rabbit against β-catenin with triple phosphorylation in the residues Ser33, Ser37 and Thr41 was from Invitrogen (PA5-67518, used at 1:1,000), while the mouse antibody against total β-catenin was from Transduction Laboratories (BD610154, used at 1:1,000). The primary antibodies against TH (AB5280, used at 1:2,500), TH phosphorylated at serine 31 (AB5423, used at 1:1,000) and TH phosphorylated at serine 40 (AB5935, used at 1:1,000) were obtained from Millipore. The antibody against TH phosphorylated at serine 19 (AB5935, used at 1:1,000) was obtained from Thermo Fisher Scientific. The secondary antibodies were IRDye 800CW donkey anti-mouse and IRDye 680RD donkey anti-rabbit (Li-Cor) and were used at 1:10,000 in blocking buffer

supplemented with 0.01% SDS, for 1 h at room temperature in the dark. Infra-red signals were visualized using an Odyssey Fc Infrared Imaging System (Li-Cor). Total and phosphorylated forms were evaluated on the same membrane and the signals were acquired and quantified with Image Studio Lite software. The ratios of phosphorylated to total protein were calculated respect to controls, which were arbitrarily set to 100%.

3. Results.

3.1. CHIR99021 strongly decreases dopamine accumulation and TH activity in rat striatal minces.

Treatment of striatal minces with 3 different concentrations of CHIR99021 yielded a significant decrease in DA accumulation with the two higher concentrations used (3 µM and 30 µM), but not with 0.3 µM, over an incubation period of 2 hours, as determined by HPLC-EC (Figure 1A). The 30 µM concentration was even able to decrease accumulation below the basal level. The IC_{50} of CHIR99021 on DA accumulation was approximately 3 µM. This significant decrease in accumulation was also consistent when minces were incubated for 1, 2 or 4 hours, but not for 30 minutes (Figure 1B). Next, L-DOPA was quantified to assess the effect of CHIR99021 on TH activity. The L-aromatic amino acid decarboxylase that metabolizes L-DOPA was blocked with NSD-1015. Thus, using HPLC-EC we were able to determine that DA synthesis in striatal minces was also significantly reduced in the presence of 0.3 µM, 3 µM and 30 µM CHIR99021 (Figure 1C). To further

investigate the DA metabolism, the levels of DOPAC were also measured, and no significant changes were found at any of the CHIR99021 concentrations tested (Figure 1D), but a dramatic increase in the DOPAC / DA ratio at 30 µM CHIR99021 was detected (Figure 1E). The DOPAC / DA ratio is considered to reflect the degree of DA metabolization by monoamine oxidase (MAO). To determine whether the mentioned effect was due to a direct interaction between CHIR99021 and TH, we also performed the same protocol in homogenates from striatal minces (Figure 1F) and no effect of CHIR99021 was observed. This result suggests that the decrease of L-DOPA levels is not a result from direct interaction of CHIR99021 with TH and therefore the intact intracellular machinery is required.

Since DA accumulation is a result of new DA synthesis and storage, we decided to test its effect on newly synthesized DA using a radioisotopic method to measure [^{3}H]-DA synthesis from [^{3}H]-tyrosine in striatal minces. CHIR99021 decreased [^{3}H]-DA synthesis concentration-dependently (Figure 2A), as in the case of DA accumulation. Western blots against TH were performed, to determine whether the decrease in DA synthesis was due to a decrease in the amount of TH protein. This was not altered after any of the CHIR concentrations tested, either in absolute values or in relation to GAPDH (Figure 2B). Thus, the abrogation of the TH activity by CHIR is not due to loss of TH protein but to a regulatory mechanism affecting efficiency of the enzyme.

3.2. SB216763 and lithium ion do not decrease dopamine content or alter DA metabolization.

To corroborate a role of GSK3β in the decrease of TH activity and DA accumulation, another GSK3β inhibitor such as SB216763 was also tested. SB216763 was able to slightly decrease dopamine accumulation in rat striatal minces over a 2-hour period, but only at 30 µM (Figure 3A) and had no effect at 3 µM or 0.3 µM, even after 4 hours of incubation (Figure 3B). The assessment of TH activity by L-DOPA quantification showed a lack of action by SB216763 at every concentration tested (Figure 3C). Quantification of DOPAC levels at increasing concentrations of SB216763 showed a similar profile than that of DA accumulation shown in 3A, with only a slight decrease of DOPAC amount at 30 µM (Figure 3D), thus yielding a DOPAC / DA ratio unaltered respect to control at any SB216763 concentration (Figure 3E). Given that lithium chloride has antipsychotic properties and has also been reported to inhibit GSK3, the effects of lithium ion on DA metabolism in striatal minces were tested. We observed that 20 mM LiCl yielded a slight but significant decrease in DA accumulation over a 2-hour or 4-hour incubation periods, whereas no effect was detected at 1 or 5 mM (Figure 4A).

3.3. CHIR99021 and SB216763, but not lithium, inhibit GSK3β activity on β-catenin in striatum minces.

GSK3β phosphorylates β-catenin in the residues S33, S37 and T41. Thus, to directly test the inhibitory effect of CHIR99021, SB216763 and of lithium on the GSK3β activity in our system, the amount of triple phosphorylated β-catenin was assessed by western blot. Near infrared-labeled secondary antibodies were used, thus

phosphorylated and total protein levels could be assessed in the same membrane, giving rise to reliable signal quantifications. Treatment with CHIR99021 at 3 µM and with SB216763 at 3 µM for 2h decreased GSK3β-phosphorylated β-catenin by half approximately, whereas lithium at 5 mM for 2h did not show any effect on β-catenin phosphorylation (Figures 5A and 5B). These results corroborate that CHIR99021 and SB216763 cause inhibition of GSK3β in our striatal minces. In consequence, the lack of SB216763 effect on DA metabolism is due to absence of GSK3β action on TH and not to a lack of compound efficiency.

3.4. CHIR99021 and SB216763 decrease TH phosphorylation in serine 19, but not in serines 31 and 40.

Since phosphorylation in serine residues have been described as a regulatory event of TH activity, we explored the effect of CHIR99021 on TH phosphorylation. Western blots with phosphospecific antibodies showed that GSK3β inhibition cause significant decrease of TH phosphorylation in serine 19, approximately 30% after CHIR99021 or SB216763 treatment for 2h (Figure 6A). On the other hand, no changes in phosphorylation were detected neither in serine 31 nor in serine 40 (Figure 6B and 6C). Treatment with LiCl (5 mM for 2h) did not yield change in any of the tested phosphosites (Figure 6A, 6B and 6C).

3.5. CHIR99021 impairs the accumulation of exogenous DA into striatal minces.

To further explore the mechanisms that lead to the dramatic action of CHIR99021 on DA accumulation, we tested the effect of CHIR99021 on DA transport into striatal tissue. Striatal minces were incubated with DA 5 µM in the absence or presence of CHIR99021 30 µM or of tetrabenazine (TBZ) 1 µM, a VMAT2 inhibitor, and the amount of DA incorporated inside tissue was determined by HPLC. Both CHIR99021 and TBZ caused a clear and similar decrease in the amount of DA found inside striatal minces (40% reduction approximately). This result opens the possibility to an effect of CHIR99021 on some component of the DA transport or storage inside cells.

4. Discussion.

GSK3β dysregulation has been described as an event involved in various pathologies, arising as a potential pharmacological target for diseases such as diabetes mellitus, inflammation, tumorigenesis, mental disorders, neurodegenerative diseases or, even, stem cell regeneration (Wada, 2009). CHIR99021 is a small organic molecule that potently inhibits GSK3α (IC_{50}~10 nM) and GSK3β (IC_{50}~5 nM) with high selectivity and is considered the standard activator of the Wnt/β-catenin pathway (Benet et al., 2002). Moreover, it is a compound that has been tested in a plethora of pathologies (Bennett et al., 2002; Drakhlis et al., 2021; Badimon et al., 2019; Oh et al., 2017; Lee et al., 2018; Houben et al., 2022; Uhl et al., 2015; Zhao et al., 2014; Ring et al., 2003), showing pharmacological potential in some of them. Furthermore, treatment of isolated rat pancreatic islets with CHIR99021 or SB216763, another GSK3β inhibitor used in the present work,

increases the rate of beta cell replication (Mussmann et al., 2007). These results point to specific inhibitors of GSK3β as promising tools in diabetes therapies, among others. SB216763 has also been used in retinal stem cell proliferation and maintenance of pluripotent stem cell populations (Inoue et al., 2007). Another GSK3β inhibitor, tideglusib, was tested in clinical trials for Alzheimer's disease, but no clinical benefit was found. Despite that, authors concluded that "further dose finding studies in early disease stages and for longer duration are warranted to examine GSK-3 inhibition in AD patients" (Lovestone et al., 2015). The inhibition of GSK3β as a therapeutical approach is reinforced by the fact that tideglusib has also been proposed as a drug for Amyotrophic Lateral Sclerosis (Martínez-Gonzalez et al., 2021).

Even though CHIR99021 is considered the gold standard for GSK3β inhibition, its off-target effects have been demonstrated. A report describes some action of CHIR99021 on more than 20 kinases as well as the existence of more specific GSK3 inhibitors (An et al., 2012). These off-target effects have been highlighted by a recent report showing that CHIR99021 causes, independently of GSK3, the suppression of the proteasomal degradation of CAST and of the related calpain activity. This leads to a great enhancement of the mitochondrial function by impairing the action of the GTPase dynamin-related protein 1 (Drp1) on mitochondrial fragmentation. The authors hypothesized that CHIR99021 suppresses CAST degradation through inhibition of ubiquitin ligases or activation of deubiquitinases (Hu et al., 2021). Additionally, the promotion by CHIR99021 of mitochondrial biogenesis, oxidative phosphorylation, and the production of reactive oxygen species in human

endodermal progenitor cells have also been observed, in spite that these effects were attributed to the GSK3 / β-catenin pathway and not to off-target effects of CHIR99021 (Ma et al., 2019).

Drp1 has also been involved in regulation of endocytosis and synaptic vesicle recycling, since absence of Drp1 or decrease of its interaction with Bcl-x_L slows endocytosis, produces anormal vesicle membranes and contributes to augmentation of the fast-releasing vesicle pool (Li et al., 2013). Other authors showed that Drp1-defective synapses in *Drosophila* fail to maintain normal neurotransmission, due to the lack of synaptic mitochondria and to defects in the reserve pool vesicles rather than to effects on vesicle recycling (Verstreken et al., 2005). In any case, the action of CHIR99021 on Drp1 could lead to a dysregulation in the synaptic vesicle cycle, altering neurotransmitter uptake and, consequently, affecting the levels of DA in the synaptic terminal and its synthesis pathway.

The feedback inhibition of DA synthesis has previously been described, but the mechanism underlying the process is not clear. Computational analyses have indicated its potential importance in dopaminergic neurotransmission (Wallace, 2007), while *ex vivo* experimental studies have recently revealed that spontaneous inhibition in DA synthesis appeared when storage reached saturation, causing DA spillover and end-product feedback-inhibition of TH in living tissue (González-Sepúlveda et al., 2022). *In vitro* studies suggest the existence in TH of two DA binding sites with high and low affinities (K_D 4 nM and 90 nM, respectively) (Gordon et al., 2008; Nakashima et al., 2009; Dickson and Briggs, 2013; Tekin et al., 2014). The TH low-affinity site / conformation could act as a physiological sensor in case

that synaptic vesicles were filled with DA at its maximum capacity, since the surplus of the DA inside the cytosol of synaptic terminals would bind to the low-affinity site / conformation, causing inhibition of TH activity. This process would happen regardless of the TH phosphorylation status.

Regarding the effect of both CHIR99021 and of SB216763 on TH phosphorylation, Ser19 is reported to be phosphorylated in a 14-3-3 dependent-manner and has little effect on the activity of TH in vitro (Itagaki et al. 1999; Toska et al. 2002). Phosphorylation of TH in Ser19 is related to enzyme degradation of the enzyme by proteasome (Nakashima et al. 2016). The interaction with 14-3-3 proteins, mainly with the γ isoform (Halksau et al., 2009), reduces the sensitivity of phosphorylated human TH isoform 1 to proteolysis by protecting its N-terminal part (Obsilova et al. 2008). Despite the afore mentioned, the dramatic abrogation of TH activity shown in the present work cannot be caused by loss of TH protein, since its levels remain unaltered after CHIR99021 treatment, nor to the relatively small change in phosphoSer19.

One relevant finding of the present work is the dramatic increase of the DOPAC / DA ratio caused by CHIR99021 (Figure 1E). This result can be explained by the enhancement of the MAO activity triggered by the accumulation of its substrate, i.e., DA in the cytosol of the synaptic terminal. This DA accumulation would lead to the inhibition of TH by a feed-back effect, as has been described by our group (González-Sepúlveda et al, 2022) and previously mentioned. An accumulation of DA in striatal minces could also be explained by impairment of the VMAT2 transporter, as has also been observed with TBZ in a previous report from our group (González-

Sepúlveda et al, 2022), giving rise to the possibility that CHIR99021 exerts an off-target inhibitory effect on VMAT2, besides acting as a GSK3β inhibitor. The comparison of the effects of CHIR99021 and TBZ on the transport of extracellular DA inside striatal minces shows a relevant similarity (Figure 7). Since the main portion of the DA in the nerve terminal resides inside synaptic vesicles, where it is protected from metabolism prior to their synaptic release, we can assume that most of the DA incorporated into striatal minces directly reflects the amount of DA inside synaptic vesicles. TBZ is used for the treatment of the motor symptoms in Huntington's disease (HD), a fatal neurodegenerative disorder, and other hyperkinetic disorders (Jankovic, 2009), but it can cause side effects, like nausea, difficulty in speaking, severe muscle stiffness or, even, depression (Jankovic, 2016). In any case, the reduction of DA release in the motor striatum by VMAT2 inhibition is considered a good therapeutic approach to reduce the involuntary hyperkinetic movements of tardive dyskinesia (Stahl, 2018). In fact, CHIR99021 showed to potently improve mitochondrial function and enhance cell viability in several models of HD (Hu et al., 2021). Thus, an available option to TBZ in the hands of the doctors would be a benefit in cases with severe side effects, and CHIR99021 appears as a candidate to be also used in HD or other movement pathologies, such as tardive dyskinesia or Tourette syndrome. Although the exact mechanism of CHIR-mediated TH inhibition has not been fully elucidated, interference with DA storage should be seriously considered.

FIGURE LEGENDS

Figure 1. Effects of CHIR99021 on dopamine accumulation and metabolism in rat brain striatal minces. (A) Concentration-response curve of CHIR99021 in striatal minces *ex vivo*, measuring dopamine (DA) accumulation over an incubation period of 2 hours, using concentrations of 0.3, 3 and 30 µM CHIR99021 or control without CHIR99021 (6 incubates per group obtained from a single animal, n = 6). Basal DA was measured as control samples placed on ice during the 2-hour incubation period (6 incubates, dashed line). **(B)** Time-response curve of DA accumulation in striatal minces *ex vivo* with 3 µM CHIR99021 for 30 minutes, 1 hour, 2 hours, 4 hours (black triangles) and controls (white triangles) for each incubation period. Controls were treated with the corresponding concentration of DMSO used to dissolve CHIR99021 (n = 6), and basal dopamine measured same as in A) and represented as 0 time (n = 6). The same protocol as in A was used in striatal minces to determine L-DOPA **(C)** and DOPAC levels **(D)**. **(E)** The DOPAC / DA ratio was also measured. **(F)** L-DOPA levels after CHIR99021 treatment were measured in homogenates from striatal minces. Data are expressed as mean ± SEM for each group, CHIR99021 vs control, one-way ANOVA followed by Dunnett´s post-hoc test for dose-response graphs and two-way ANOVA followed by Bonferroni's post-hoc test for time-response graph. **p<0.01, ***p<0.001. Sigmoidal dose-response curve regression was used in every case to create the adjusted curves.

Figure 2. CHIR99021 inhibits tyrosine hydroxylase enzymatic activity. (A) Concentration-response curve of CHIR99021 on striatal [^{3}H]-DA synthesis in minces *ex vivo* was measured after a preincubation period of 2 hours. CHIR99021 was

added using concentrations of 0.3, 3 and 30 µM (n = 6 per concentration) or control without CHIR (n = 6) 10 minutes before the end of preincubation. Then, [^{3}H]-tyrosine was added and incubated for 10 additional minutes. The curve is obtained by normalization of the data to percent of control. In all cases, data are expressed as mean ± SEM for each group. Asterisks indicate **p<0.01 CHIR99021 vs control, one-way ANOVA followed by Dunnett´s post-hoc test. The curve was adjusted to sigmoidal dose-response regression. **(B)** TH amount was assessed by western blot after treatment of minces with 0.3, 3 and 30 µM CHIR99021 or control without CHIR99021 (shown as 0), as in A. GAPDH amount was also detected by western blot and TH / GAPDH ratio was calculated and is represented as a bar graph, which shows means and SEM, after One-way ANOVA analysis with Newman-Keuls post-test, which yielded non-significant in every case. Bands from representative western blots are also shown.

Figure 3. Effect of SB216763 on dopamine accumulation and metabolism in rat brain striatal minces. (A) Concentration-response curve of SB216763, measuring dopamine (DA) accumulation over an incubation period of 2 hours ex vivo, using concentrations of 0.3, 3 and 30 µM SB216763 or control without SB217663 (6 incubates per group obtained from a single animal, n = 6). Basal dopamine was measured as control samples placed on ice during the 2-hour incubation period (6 incubates, dashed line). **(B)** Time-response curve on striatal minces ex vivo for a SB216763 concentration of 3 µM and for 30 minutes, 1 hour, 2 hours, 4 hours, and controls for each incubation period, which were treated with the corresponding concentration of DMSO used to dissolve SB216763 (n = 6), and basal dopamine

measured same as in (A) and represented as 0 time (n = 6). The same protocol as in A was used in striatal minces to determine L-DOPA **(C)** and DOPAC levels **(D)**. **(E)** The DOPAC / DA ratio was also measured. Data are expressed as mean ± SEM for each group, SB216763 vs control, one-way ANOVA followed by Dunnett´s post-hoc test for dose-response graph and two-way ANOVA followed by Bonferroni's post-hoc test for time-response graph. *p<0.5, **p<0.01. Sigmoidal dose-response curve regression was used in every case to create the adjusted curves.

Figure 4. Effect of lithium ion on dopamine accumulation and metabolism in rat brain striatal minces. (A) Concentration-response curve of lithium, measuring DA accumulation over an incubation period of 2 hours *ex vivo*, using concentrations of 1, 5 and 20 mM LiCl or control without lithium (6 incubates per group obtained from a single animal, n = 6). Basal DA was measured as control samples placed on ice during the 2-hour incubation period (6 incubates, dashed line). **(B)** Time-response curve on striatal minces *ex vivo* for a lithium concentration of 20 mM for 30 minutes, 1 hour, 2 hours, 4 hours (n = 6), and basal DA measured same as in (A) and represented as 0 time (n = 6). The same protocol as in A was used in striatal minces to determine L-DOPA **(C)** and DOPAC levels **(D)**. **(E)** The DOPAC / DA ratio was also measured. Data are expressed as mean ± SEM for each group, lithium vs control, one-way ANOVA followed by Dunnett´s post-hoc test for dose-response graph and two-way ANOVA followed by Bonferroni's post-hoc test for time-response graph. *p<0.5, **p<0.01, ***p<0.001. Sigmoidal dose-response curve regression was used in every case to create the adjusted curves.

Figure 5. GSK3β inhibitors CHIR99021 and SB216763, but not lithium, cause decrease in phosphorylation of β-catenin in rat striatal minces. Tissue samples were treated with two GSK3 inhibitors, CHIR99021 (CH, 3 μM) or SB216763 (SB, 3 μM), both for 2h. In parallel, striatal minces were also treated with lithium ion (Li, 5 mM for 2h). Levels of phosho-β-catenin were assessed with western blot using NearIR-labeled secondary antibodies, as described in Materials and Methods section. **A)** Representative western blots are shown after CHIR99021, SB216763 or lithium treatment. Red signal corresponds to β-catenin triple phosphorylated in S33, S37 and T41, green signal corresponds to total β-catenin, while merge of both signals appears in yellow. **B)** Scatter plot representation of the β-catenin phosphorylation ratios (phoshorylated over total) after treatment with CHIR99021, SB216763 or lithium. Each point corresponds to the percentage of the ratio respect to its control, DMSO in the case of CHIR99021 and SB216763 (CD), as vehicle, and water as vehicle in the case of lithium (CW). Graphics shows means ± SEM, after One-way ANOVA analysis with Newman-Keuls post-test. (** $p<0.01$, *** $p<0.001$, n.s. non-significant).

Figure 6. GSK3 inhibitors decrease phosphorylation of Tyrosine Hydroxylase in Ser19, but not in Ser31 or Ser40. Samples from rat striatal minces were treated for 2 hours with CHIR99021 (CH, 3μM), SB216763 (SB, 3μM), lithium chloride (Li, 5mM), DMSO (control for CH99021 and SB216763, shown as CD) and water (control for LiCl, shown as CW). Phosphorylation in every case was assessed by western blot and NIR-labeled secondary antibodies. Red signal corresponds to phosphorylated TH, green signal corresponds to total TH, while merge of both

signals appears in yellow. Representative western blots of phosphorylated TH in Ser19 **(A)**, Ser31 **(B)** and Ser40 **(C)**, after treatment with CHIR99021, SB216763 and lithium ion are shown. Next to each group of western blots, the corresponding Scatter plot representations of every phosphorylation ratio are shown, in every case. Graphics show mean ± SEM, after One-way ANOVA analysis with Newman-Keuls post-test. (*p<0.5, n.s. non-significant).

Figure 7. CHIR99021 decreases dopamine storage inside rat brain striatal minces. When indicated, striatal minces were incubated for 1 h at 37°C with tetrabenazine 1 µM (TBZ), with CHIR99021 30 µM (CHIR) or with Krebs-Ringer buffer (-). For the last 30 min of incubation 5 µM DA was also added in all the three cases. Basal DA was measured as control samples placed on ice during the 1 h incubation period, while Control samples were incubated at 37°C without any drug or DA. Subsequently, minces were recovered by centrifugation and washed once with Krebs-Ringer buffer. The amount of DA incorporated inside tissue was determined in every case by HPLC (pmol DA / mg protein, 6 incubates per group obtained from a single animal). Data are expressed as mean ± SEM for each group. One-way ANOVA test was performed followed by Newman-Keuls post-test, ***p<0.001. Experimental design is shown as a time-line.

CRediT authorship contribution statement

Sally Hamdon: Methodology, Investigation, Formal analysis, Writing - Original Draft, Visualization. **Pol Fernández:** Methodology, Investigation, Formal analysis.

Mohammed Yusof Omar: Methodology, Investigation, Formal analysis. **Jordi Ortiz:** Conceptualization, Validation, Formal analysis, Writing - Original Draft, Visualization, Supervision, Project administration, Funding acquisition. **Carles Gil:** Conceptualization, Validation, Formal analysis, Writing - Original Draft, Visualization, Supervision, Project administration, Funding acquisition.

Declaration of Competing Interest

The authors declare that they have no known competing financial interests or personal relationships that could have appeared to influence the work reported in this paper.

Acknowledgements

This work was supported by Spanish Government grant SAF2017-87199-R. S.H. received a predoctoral fellowship from the Universitat Autònoma de Barcelona. We thank the skillful technical assistance of Susana Benítez

References

Alcaro, A., Huber, R., & Panksepp, J. (2007). Behavioral functions of the mesolimbic dopaminergic system: an affective neuroethological perspective. Brain research reviews, 56(2), 283–321. https://doi.org/10.1016/j.brainresrev.2007.07.014

An WF, Germain AR, Bishop JA, et al. Discovery of Potent and Highly Selective Inhibitors of GSK3β. (2012) In: Probe Reports from the NIH Molecular Libraries

Program [Internet]. Bethesda (MD): National Center for Biotechnology Information (US). https://www.ncbi.nlm.nih.gov/books/NBK133436/

Badimon, L., Casaní, L., Camino-Lopez, S., Juan-Babot, O., & Borrell-Pages, M. (2019). GSK3β inhibition and canonical Wnt signaling in mice hearts after myocardial ischemic damage. PloS one, 14(6), e0218098. https://doi.org/10.1371/journal.pone.0218098

Beaulieu, J. M., & Gainetdinov, R. R. (2011). The physiology, signaling, and pharmacology of dopamine receptors. Pharmacological reviews, 63(1), 182–217. https://doi.org/10.1124/pr.110.002642

Bennett, C. N., Ross, S. E., Longo, K. A., Bajnok, L., Hemati, N., Johnson, K. W., Harrison, S. D., & MacDougald, O. A. (2002). Regulation of Wnt signaling during adipogenesis. The Journal of biological chemistry, 277(34), 30998–31004. https://doi.org/10.1074/jbc.M204527200

Bobrovskaya, L., Gilligan, C., Bolster, E. K., Flaherty, J. J., Dickson, P. W., & Dunkley, P. R. (2007). Sustained phosphorylation of tyrosine hydroxylase at serine 40: a novel mechanism for maintenance of catecholamine synthesis. Journal of neurochemistry, 100(2), 479–489. https://doi.org/10.1111/j.1471-4159.2006.04213.x

Bonifazi, A., Yano, H., Guerrero, A. M., Kumar, V., Hoffman, A. F., Lupica, C. R., Shi, L., & Newman, A. H. (2019). Novel and Potent Dopamine D2 Receptor Go-Protein Biased Agonists. ACS pharmacology & translational science, 2(1), 52–65. https://doi.org/10.1021/acsptsci.8b00060

Dahoun, T., Trossbach, S. V., Brandon, N. J., Korth, C., & Howes, O. D. (2017). The impact of Disrupted-in-Schizophrenia 1 (DISC1) on the dopaminergic system: a systematic review. Translational psychiatry, 7(1), e1015. https://doi.org/10.1038/tp.2016.282

Dickson, P. W., & Briggs, G. D. (2013). Tyrosine hydroxylase: regulation by feedback inhibition and phosphorylation. Advances in pharmacology (San Diego, Calif.), 68, 13–21. https://doi.org/10.1016/B978-0-12-411512-5.00002-6

Drakhlis, L., Devadas, S. B., & Zweigerdt, R. (2021). Generation of heart-forming organoids from human pluripotent stem cells. Nature protocols, 16(12), 5652–5672. https://doi.org/10.1038/s41596-021-00629-8.

Duda, P., Hajka, D., Wójcicka, O., Rakus, D., & Gizak, A. (2020). GSK3β: A Master Player in Depressive Disorder Pathogenesis and Treatment Responsiveness. Cells, 9(3), 727. https://doi.org/10.3390/cells9030727

Dunkley, P. R., & Dickson, P. W. (2019). Tyrosine hydroxylase phosphorylation in vivo. Journal of neurochemistry, 149(6), 706–728. https://doi.org/10.1111/jnc.14675

González-Sepúlveda, M., Omar, M. Y., Hamdon, S., Ma, G., Rosell-Vilar, S., Raivio, N., Abass, D., Martínez-Rivas, A., Vila, M., Giraldo, J., Carrascal, M., Abián, J., Gil, C., Sabriá, J., Ortiz, J., & Moreno-Delgado, D. (2022). Spontaneous changes in brain striatal dopamine synthesis and storage dynamics ex vivo reveal end-product feedback-inhibition of tyrosine hydroxylase. Neuropharmacology, 212, 109058. https://doi.org/10.1016/j.neuropharm.2022.109058

Gordon, S. L., Quinsey, N. S., Dunkley, P. R., & Dickson, P. W. (2008). Tyrosine hydroxylase activity is regulated by two distinct dopamine-binding sites. Journal of neurochemistry, 106(4), 1614–1623. https://doi.org/10.1111/j.1471-4159.2008.05509.x

Halskau, Ø., Jr, Ying, M., Baumann, A., Kleppe, R., Rodriguez-Larrea, D., Almås, B., Haavik, J., & Martínez, A. (2009). Three-way interaction between 14-3-3 proteins, the N-terminal region of tyrosine hydroxylase, and negatively charged membranes. The Journal of biological chemistry, 284(47), 32758–32769. https://doi.org/10.1074/jbc.M109.027706

Houben, R., Hesbacher, S., Sarma, B., Schulte, C., Sarosi, E. M., Popp, S., Adam, C., Kervarrec, T., & Schrama, D. (2022). Inhibition of T-antigen expression promoting glycogen synthase kinase 3 impairs merkel cell carcinoma cell growth. Cancer letters, 524, 259–267. https://doi.org/10.1016/j.canlet.2021.10.031

Hu, D., Sun, X., Magpusao, A., Fedorov, Y., Thompson, M., Wang, B., Lundberg, K., Adams, D. J., & Qi, X. (2021). Small-molecule suppression of calpastatin degradation reduces neuropathology in models of Huntington's disease. Nature communications, 12(1), 5305. https://doi.org/10.1038/s41467-021-25651-y

Inoue, T., Kawaji, T., Inoue-Mochita, M., Taga, T., & Tanihara, H. (2007). Media conditioned by retinal pigment epithelial cells suppress the canonical Wnt pathway. Neuroscience letters, 424(3), 190–193. https://doi.org/10.1016/j.neulet.2007.07.022

Itagaki, C., Isobe, T., Taoka, M., Natsume, T., Nomura, N., Horigome, T., Omata, S., Ichinose, H., Nagatsu, T., Greene, L. A., & Ichimura, T. (1999). Stimulus-coupled interaction of tyrosine hydroxylase with 14-3-3 proteins. Biochemistry, 38(47), 15673–15680. https://doi.org/10.1021/bi9914255

Jankovic J. (2009). Treatment of hyperkinetic movement disorders. The Lancet. Neurology, 8(9), 844-856. https://doi.org/10.1016/S1474-4422(09)70183-8

Jankovic J. (2016). Dopamine depleters in the treatment of hyperkinetic movement disorders. Expert opinion on pharmacotherapy, 17(18), 2461–2470. https://doi.org/10.1080/14656566.2016.1258063

Jiang, H., Galtes, D., Wang, J., & Rockman, H. A. (2022). G protein-coupled receptor signaling: transducers and effectors. American journal of physiology. Cell physiology, 323(3), C731–C748. https://doi.org/10.1152/ajpcell.00210.2022

Johnson, M. E., Salvatore, M. F., Maiolo, S. A., & Bobrovskaya, L. (2018). Tyrosine hydroxylase as a sentinel for central and peripheral tissue responses in Parkinson's progression: Evidence from clinical studies and neurotoxin models. Progress in neurobiology, 165-167, 1–25. https://doi.org/10.1016/j.pneurobio.2018.01.002

Jope R. S. (2011). Glycogen synthase kinase-3 in the etiology and treatment of mood disorders. Frontiers in molecular neuroscience, 4, 16. https://doi.org/10.3389/fnmol.2011.00016

Koros, E., & Dorner-Ciossek, C. (2007). The role of glycogen synthase kinase-3beta in schizophrenia. Drug news & perspectives, 20(7), 437–445. https://doi.org/10.1358/dnp.2007.20.7.1149632

Lee, C., Robinson, M., & Willerth, S. M. (2018). Direct Reprogramming of Glioblastoma Cells into Neurons Using Small Molecules. ACS chemical neuroscience, 9(12), 3175–3185. https://doi.org/10.1021/acschemneuro.8b00365

Lehmann, I. T., Bobrovskaya, L., Gordon, S. L., Dunkley, P. R., & Dickson, P. W. (2006). Differential regulation of the human tyrosine hydroxylase isoforms via hierarchical phosphorylation. Journal of Biological Chemistry, 281(26), 17644-17651. https://doi.org/10.1074/jbc.M512194200

Lewis, D.A, Melchitzky, D.S., Haycock, J.W. (1993). Four isoforms of tyrosine hydroxylase are expressed in human brain. Neuroscience, 54(2) 477-492. https://doi.org/10.1016/0306-4522(93)90267-J.

Li, H., Alavian, K. N., Lazrove, E., Mehta, N., Jones, A., Zhang, P., Licznerski, P., Graham, M., Uo, T., Guo, J., Rahner, C., Duman, R. S., Morrison, R. S., & Jonas, E. A. (2013). A Bcl-xL-Drp1 complex regulates synaptic vesicle membrane dynamics during endocytosis. Nature cell biology, 15(7), 773–785. https://doi.org/10.1038/ncb2791

Lovestone, S., Boada, M., Dubois, B., Hüll, M., Rinne, J. O., Huppertz, H. J., Calero, M., Andrés, M. V., Gómez-Carrillo, B., León, T., del Ser, T., & ARGO investigators (2015). A phase II trial of tideglusib in Alzheimer's disease. Journal of Alzheimer's disease: JAD, 45(1), 75–88. https://doi.org/10.3233/JAD-141959

Lovestone, S., Killick, R., Di Forti, M., & Murray, R. (2007). Schizophrenia as a GSK-3 dysregulation disorder. Trends in neurosciences, 30(4), 142–149. https://doi.org/10.1016/j.tins.2007.02.002

Ma, Y., Ma, M., Sun, J., Li, W., Li, Y., Guo, X., & Zhang, H. (2019). CHIR-99021 regulates mitochondrial remodelling via β-catenin signalling and miRNA expression during endodermal differentiation. Journal of cell science, 132(15), jcs229948. https://doi.org/10.1242/jcs.229948

Martínez-González, L., Gonzalo-Consuegra, C., Gómez-Almería, M., Porras, G., de Lago, E., Martín-Requero, Á., & Martínez, A. (2021). Tideglusib, a Non-ATP

Competitive Inhibitor of GSK-3β as a Drug Candidate for the Treatment of Amyotrophic Lateral Sclerosis. International journal of molecular sciences, 22(16), 8975. https://doi.org/10.3390/ijms2roth2168975

McLean, W. J., Hinton, A. S., Herby, J., Salt, A. N., Hartsock, J. J., Wilson, S., Lucchino, D. L., Lenarz, T., Warnecke, A., Prenzler, N., Schmitt, H., King, S., Jackson, L. E., Rosenbloom, J., Atiee, G., Bear, M., Runge, C. L., Gifford, R. H., Rauch, S. D., Lee, D. J., R. Langer, J.M. Karp, C. Loose, LeBel, C. (2021). Improved Speech Intelligibility in Subjects with Stable Sensorineural Hearing Loss Following Intratympanic Dosing of FX-322 in a Phase 1b Study. Otology & neurotology: official publication of the American Otological Society, American Neurotology Society [and] European Academy of Otology and Neurotology, 42(7), e849–e857. https://doi.org/10.1097/MAO.0000000000003120

Meiser, J., Weindl, D. & Hiller, K. (2013). Complexity of dopamine metabolism. Cell Commun Signal 11, 34 https://doi.org/10.1186/1478-811X-11-34

Mussmann, R., Geese, M., Harder, F., Kegel, S., Andag, U., Lomow, A., Burk, U., Onichtchouk, D., Dohrmann, C., & Austen, M. (2007). Inhibition of GSK3 promotes replication and survival of pancreatic beta cells. The Journal of biological chemistry, 282(16), 12030–12037. https://doi.org/10.1074/jbc.M609637200

Nakashima, A., Hayashi, N., Kaneko, Y. S., Mori, K., Sabban, E. L., Nagatsu, T., & Ota, A. (2009). Role of N-terminus of tyrosine hydroxylase in the biosynthesis of catecholamines. Journal of neural transmission (Vienna, Austria: 1996), 116(11), 1355–1362. https://doi.org/10.1007/s00702-009-0227-8

Nakashima, A., Ohnuma, S., Kodani, Y., Kaneko, Y. S., Nagasaki, H., Nagatsu, T., & Ota, A. (2016). Inhibition of deubiquitinating activity of USP14 decreases tyrosine hydroxylase phosphorylated at Ser19 in PC12D cells. Biochemical and biophysical research communications, 472(4), 598–602. https://doi.org/10.1016/j.bbrc.2016.03.022

Obsilova, V., Nedbalkova, E., Silhan, J., Boura, E., Herman, P., Vecer, J., Sulc, M., Teisinger, J., Dyda, F., & Obsil, T. (2008). The 14-3-3 protein affects the conformation of the regulatory domain of human tyrosine hydroxylase. Biochemistry, 47(6), 1768–1777. https://doi.org/10.1021/bi7019468

Oh, J., Kim, Y., Che, L., Kim, J. B., Chang, G. E., Cheong, E., Kang, S. G., & Ha, Y. (2017). Regulation of cAMP and GSK3 signaling pathways contributes to the neuronal conversion of glioma. PloS one, 12(11), e0178881. https://doi.org/10.1371/journal.pone.0178881

O'Leary, O., & Nolan, Y. (2015). Glycogen synthase kinase-3 as a therapeutic target for cognitive dysfunction in neuropsychiatric disorders. CNS drugs, 29(1), 1–15. https://doi.org/10.1007/s40263-014-0213-z

Ortiz, J., Gómez, J., Torrent, A., Aldavert, M., & Blanco, I. (2000). Quantitative radioisotopic determination of histidine decarboxylase using high-performance liquid chromatography. Analytical biochemistry, 280(1), 111–117. https://doi.org/10.1006/abio.2000.4494

Quaife-Ryan, G. A., Mills, R. J., Lavers, G., Voges, H. K., Vivien, C. J., Elliott, D. A., Ramialison, M., Hudson, J. E., & Porrello, E. R. (2020). β-Catenin drives distinct transcriptional networks in proliferative and nonproliferative cardiomyocytes. Development (Cambridge, England), 147(22), dev193417. https://doi.org/10.1242/dev.193417

Ring, D. B., Johnson, K. W., Henriksen, E. J., Nuss, J. M., Goff, D., Kinnick, T. R., Ma, S. T., Reeder, J. W., Samuels, I., Slabiak, T., Wagman, A. S., Hammond, M. E., & Harrison, S. D. (2003). Selective glycogen synthase kinase 3 inhibitors potentiate insulin activation of glucose transport and utilization in vitro and in vivo. Diabetes, 52(3), 588–595. https://doi.org/10.2337/diabetes.52.3.588

Salamone, J. D., Yohn, S. E., López-Cruz, L., San Miguel, N., & Correa, M. (2016). Activational and effort-related aspects of motivation: neural mechanisms and implications for psychopathology. Brain: a journal of neurology, 139(Pt 5), 1325–1347. https://doi.org/10.1093/brain/aww050

Smith-Dijak, A. I., Sepers, M. D., & Raymond, L. A. (2019). Alterations in synaptic function and plasticity in Huntington disease. Journal of neurochemistry, 150(4), 346–365. https://doi.org/10.1111/jnc.14723

Spanagel, R., & Weiss, F. (1999). The dopamine hypothesis of reward: past and current status. Trends in neurosciences, 22(11), 521–527. https://doi.org/10.1016/s0166-2236(99)01447-2

Stahl, S. (2018). Mechanism of action of vesicular monoamine transporter 2 (VMAT2) inhibitors in tardive dyskinesia: Reducing dopamine leads to less “go” and more “stop” from the motor striatum for robust therapeutic effects. CNS Spectrums, 23(1), 1-6. doi:10.1017/S1092852917000621

Tekin, I., Roskoski, R., Jr, Carkaci-Salli, N., & Vrana, K. E. (2014). Complex molecular regulation of tyrosine hydroxylase. Journal of neural transmission (Vienna, Austria: 1996), 121(12), 1451–1481. https://doi.org/10.1007/s00702-014-1238-7

Thal, D. M., Glukhova, A., Sexton, P. M., & Christopoulos, A. (2018). Structural insights into G-protein-coupled receptor allostery. Nature, 559(7712), 45–53. https://doi.org/10.1038/s41586-018-0259-z

Toska, K., Kleppe, R., Armstrong, C. G., Morrice, N. A., Cohen, P., & Haavik, J. (2002). Regulation of tyrosine hydroxylase by stress-activated protein kinases. Journal of neurochemistry, 83(4), 775–783. https://doi.org/10.1046/j.1471-4159.2002.01172.x

Uhl, F. E., Vierkotten, S., Wagner, D. E., Burgstaller, G., Costa, R., Koch, I., Lindner, M., Meiners, S., Eickelberg, O., & Königshoff, M. (2015). Preclinical validation and imaging of Wnt-induced repair in human 3D lung tissue cultures. The European respiratory journal, 46(4), 1150–1166. https://doi.org/10.1183/09031936.00183214

Verstreken, P., Ly, C. V., Venken, K. J., Koh, T. W., Zhou, Y., & Bellen, H. J. (2005). Synaptic mitochondria are critical for mobilization of reserve pool vesicles at Drosophila neuromuscular junctions. Neuron, 47(3), 365–378. https://doi.org/10.1016/j.neuron.2005.06.018

Wada A. (2009). GSK-3 inhibitors and insulin receptor signaling in health, disease, and therapeutics. Frontiers in bioscience (Landmark edition), 14(4), 1558–1570. https://doi.org/10.2741/3324

Wallace L. J. (2007). A small dopamine permeability of storage vesicle membranes and end product inhibition of tyrosine hydroxylase are sufficient to explain changes occurring in dopamine synthesis and storage after inhibition of neuron firing. Synapse (New York, N.Y.), 61(9), 715–723. https://doi.org/10.1002/syn.20408

Xin, J., Fan, T., Guo, P., & Wang, J. (2019). Identification of functional divergence sites in dopamine receptors of vertebrates. Computational biology and chemistry, 83, 107140. https://doi.org/10.1016/j.compbiolchem.2019.107140

Zaugg, L. K., Banu, A., Walther, A. R., Chandrasekaran, D., Babb, R. C., Salzlechner, C., Hedegaard, M., Gentleman, E., & Sharpe, P. T. (2020). Translation Approach for Dentine Regeneration Using GSK-3 Antagonists. Journal of dental research, 99(5), 544–551. https://doi.org/10.1177/0022034520908593

Zhao, J., Li, S., Trilok, S., Tanaka, M., Jokubaitis-Jameson, V., Wang, B., Niwa, H., & Nakayama, N. (2014). Small molecule-directed specification of sclerotome-like chondroprogenitors and induction of a somatic chondrogenesis program from embryonic stem cells. Development (Cambridge, England), 141(20), 3848–3858. https://doi.org/10.1242/dev.105981

Figure 1

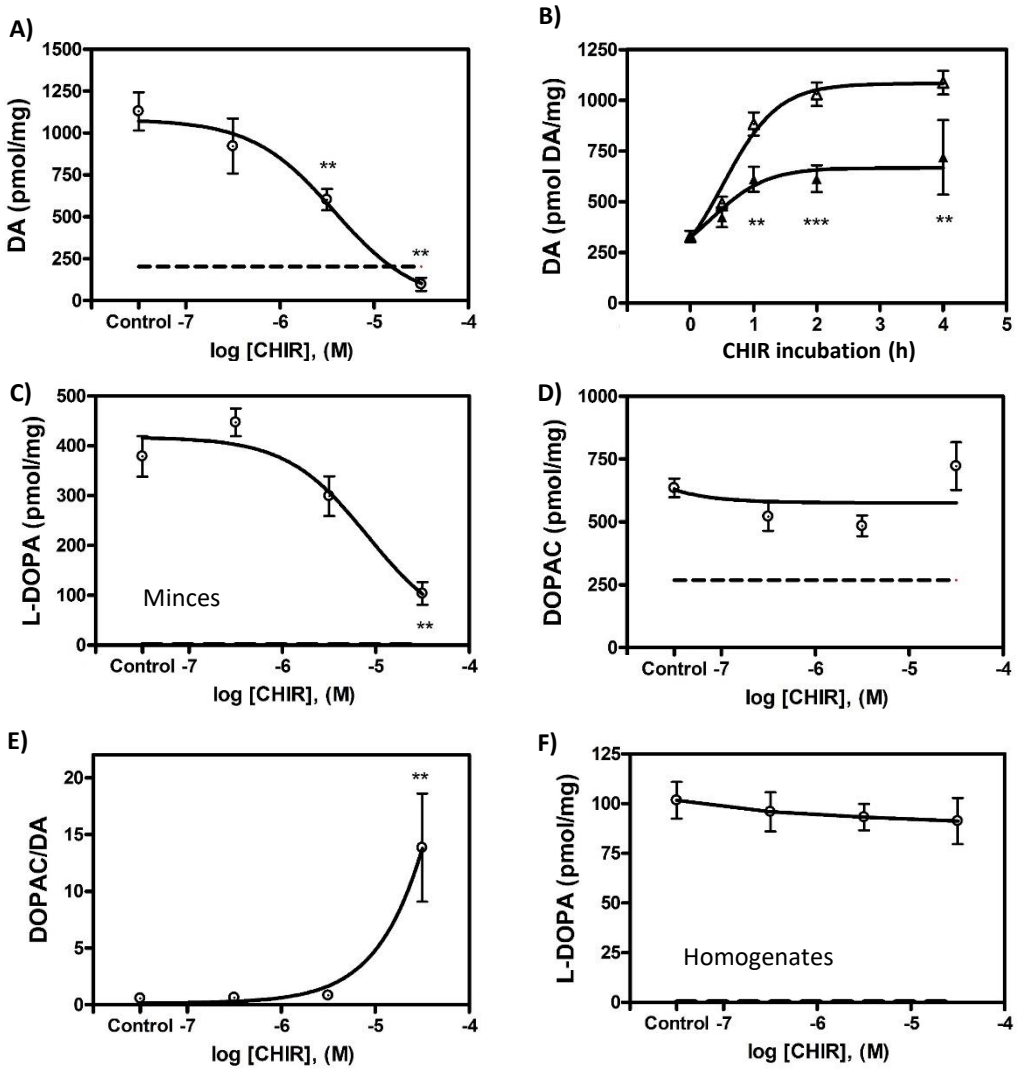

Figure 2

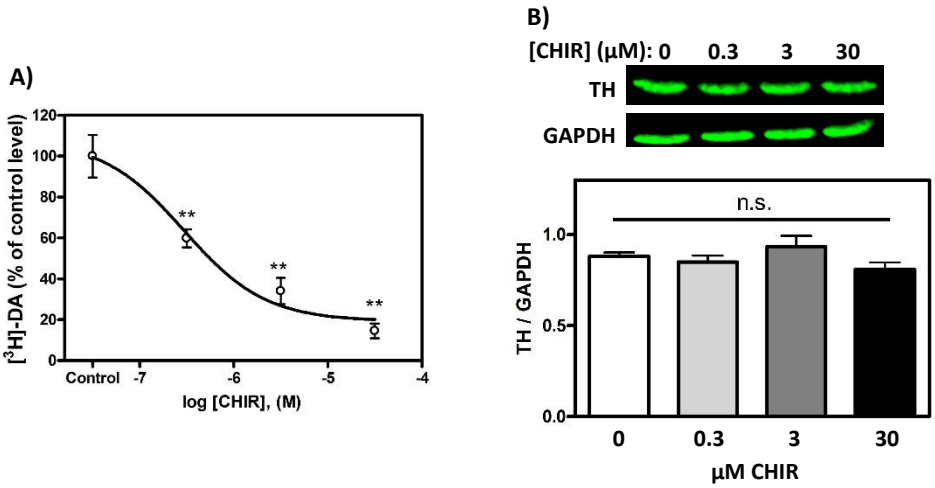

Figure 3

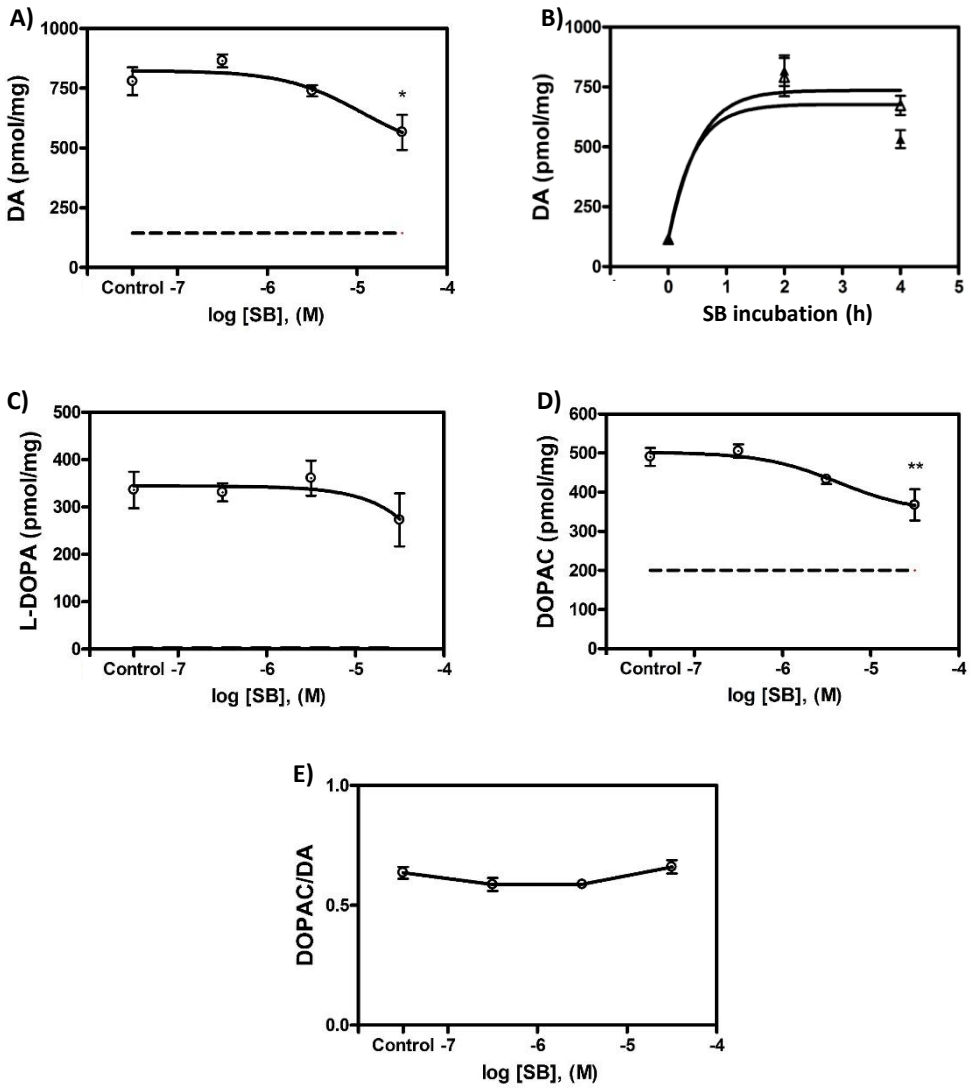

Figure 4

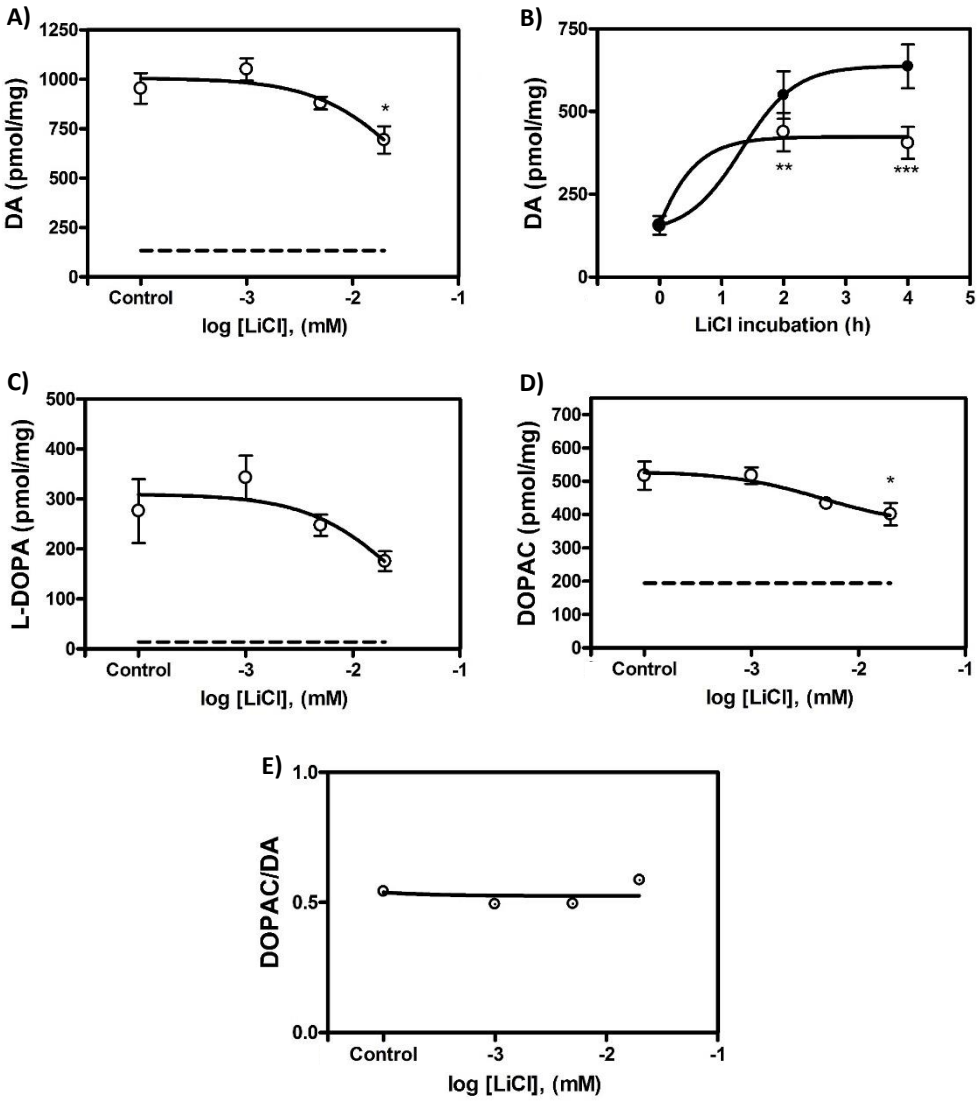

Figure 5

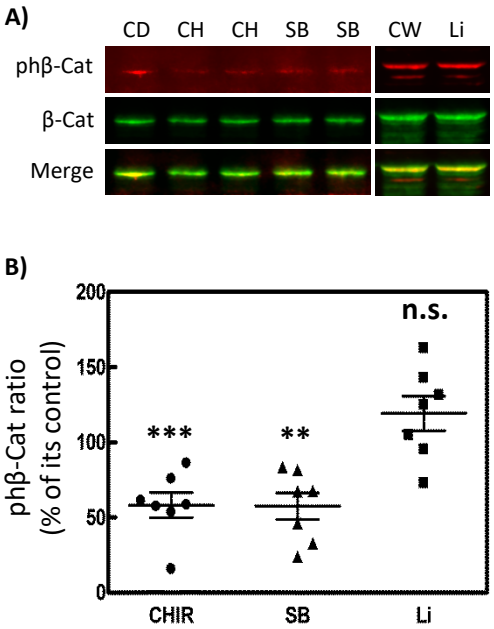

Figure 6

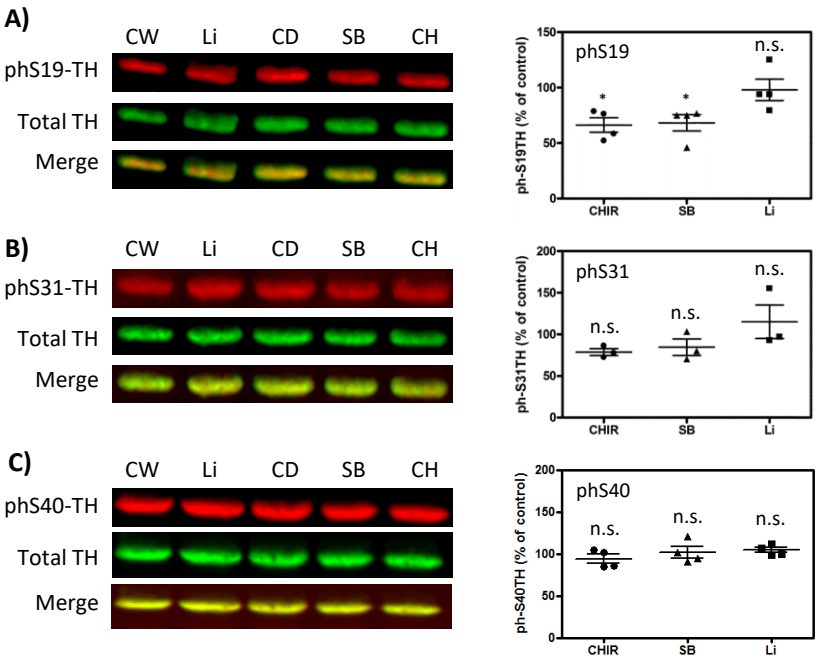

Figure 7